

Investigations into Brain-Computer Interfacing for Stroke Rehabilitation



Darren J. Leamy

Department of Electronic Engineering

Maynooth University

A thesis submitted for the degree of

Philosophiæ Doctor (PhD)

February 2015

Declaration

I, Darren Leamy, declare that this thesis titled 'Investigations into Brain-Computer Interfacing for Stroke Rehabilitation' and the work presented in it are my own. I confirm that:

- This work was done wholly or mainly while in candidature for a research degree at this University.
- Where any part of this thesis has previously been submitted for a degree or any other qualification at this University or any other institution, this has been clearly stated.
- Where I have consulted the published work of others, this is always clearly attributed.
- Where I have quoted from the work of others, the source is always given. With the exception of such quotations, this thesis is entirely my own work.
- I have acknowledged all main sources of help.
- Where the thesis is based on work done by myself jointly with others, I have made clear exactly what was done by others and what I have contributed myself.

Signed:

Date:

This thesis is gift to my parents, John and Mairéad.

For the life of encouragement, support and love they have given me to
make it possible.

Abstract

A stroke is the loss of brain function following the cessation of blood supply to a region of the brain caused by either a blockage or haemorrhage in the vasculature. It is a leading cause of death worldwide but survival rates have increased significantly in the past 25 years with recent estimates putting the number of worldwide stroke survivors at 33 million. Stroke survivors live with lasting effects such as limb weakness, limb paralysis, loss of speech, loss of comprehension and other neurological disorders. The purpose of stroke rehabilitation is to return the sufferer to as normal a life as possible. Traditional methods for this involve mass practice of the affected function to provoke improvement, acquisition of compensatory skills and adaptation to residual post-stroke disability. Recently, however, brain computer interfaces (BCI) have emerged as a technology which may have impact in augmenting traditional approaches, particularly for motor deficits. In this context, BCI provides a means for closing the sensorimotor loop and driving neuroplastic processes to enhance recovery.

A BCI is a system for translating measured brain activity into control signals for an external device, such as a computer or machine. Rehabilitation BCI attempts to use such a device to encourage positive neurorehabilitation in the stroke survivor, to return or strengthen lost or diminished function. This thesis describes concerted work to improve the current state and future prospects of rehabilitation BCI. In particular, BCIs which use electroencephalography (EEG) and functional near-infrared spectroscopy (fNIRS) to measure brain activity are the focus of these efforts. EEG and fNIRS are relatively inexpensive, easy-to-use and portable brain measurement/imaging systems compared to other brain imaging methods commonly found in hospital settings, such as functional magnetic resonance imaging

(fMRI), positron emission tomography (PET) or magnetoencephalography (MEG). These advantages motivate this research in the hope that at-home stroke rehabilitation becomes widespread and the accepted method of stroke rehabilitation.

Investigations described here include the design and development of a novel fNIRS imaging method, a novel fNIRS synthetic data generation algorithm, a novel hybrid fNIRS/EEG measurement system, a novel portable EEG biofeedback BCI, a substantial investigation into the effect of stroke on EEG BCI operation and performance, and an investigation into potential biomarkers for neurorehabilitation based on BCI parameters and scalp EEG. These investigations, based on measurements of both healthy and stroke-affected brain activity, have led to the advancement of EEG and fNIRS-based rehabilitation BCI technology.

Acknowledgements

My greatest thanks go to my supervisor, Dr. Tomas Ward, for his guidance, encouragement, support, advice and friendship. My time as a PhD student, a significant portion of my life, could never have been so enjoyable if it wasn't for Tomas and I'm eternally grateful to him for that.

There are a large number of people who have helped me through this journey and they have helped me in countless ways that they recognise and countless ways that they probably don't. The support I received from my friends means everything to me. I'd particularly like to thank Seamus, Fran, Tom, Gabhan, Brendan and John for their friendship, their help and their endless encouragement.

I'd like to thank the other postgrads of the department who made coming in to the office so enjoyable and with whom I shared some great experiences at home and abroad, particularly Kevin, Aodhan, Anthea, Shane, Damian, Lorcan, Damien and Gerard. The staff at the department has been instrumental in making this journey as smooth as possible and helping me whenever I needed it, so my thanks go to Ronan, Ann, Joanne, Denis, John and all of the academic staff for their advice and assistance. Thank you to my colleagues and co-authors for their contributions to our papers and for their significant guidance. I owe a huge debt of gratitude to Dr. Cuntai Guan for inviting me to spend 6 months working with his research group in Singapore and giving me the such a unique experience. Thank you to everybody I met in Singapore for making me feel so welcome.

My family have always been great supporters of me, cheering me on at every stage. Thank you to John and Mairéad, Níamh, Kevin, Aóife, Fíona, John and all of my aunties, uncles, cousins, grandparents and friends of my family.

There are a significant amount of other friends who have helped and supported me through this. I wish I could name them all but it would be the names of everyone I've ever met. They have all had their part in encouraging me in my work and I thank them.

Finally, I must admit that this thesis is truly a joint effort between me and one other person. My girlfriend Emma has sacrificed and endured more than anyone else during her unwavering support of me. Emma's resilience, love and encouragement are the reason this thesis is here today as she kept me on the right track to completion, even when it was very difficult to keep going. With all of my heart, Emma, thank you.

Contents

List of Figures	xiii
List of Tables	xvii
1 Introduction	1
1.1 Preface	1
1.2 Objective	3
1.3 Contributions	3
1.4 Publications	4
1.5 Outline	5
2 The Stroke-Affected Brain	7
2.1 Introduction	7
2.2 Anatomy and Function of the Healthy Human Brain	8
2.2.1 The Nervous System	8
2.2.2 The Neuron	11
2.2.2.1 The Action Potential	11
2.2.2.2 The Synapse	13
2.2.3 The Vascular System of the Brain	15
2.3 Pathophysiology, Effects and Treatment of Stroke	17
2.3.1 Haemorrhagic Stroke	17
2.3.2 Ischaemic Stroke	17
2.3.3 Transient Ischaemic Attack	19
2.3.4 Effects of a Stroke	19

2.3.5	Treatment and Therapy	21
2.4	Neuroplasticity	21
2.4.1	Cortical Plasticity	22
2.4.1.1	Short-Term Synaptic Plasticity	22
2.4.1.2	Long-Term Synaptic Plasticity	22
2.4.1.3	Representational Plasticity	23
2.4.2	Neurogenesis	25
2.4.3	Stroke Rehabilitation Through Neuroplasticity	25
2.4.4	Constraint-Induced Movement Therapy	27
2.4.5	Other Stroke Rehabilitation Therapies	28
2.5	Summary	28
3	Brain-Computer Interfacing for Stroke Rehabilitation	30
3.1	Introduction	30
3.2	Electroencephalography	31
3.2.1	Recording	31
3.2.2	Source	33
3.2.3	EEG Signals	34
3.2.4	Movement-Related EEG	35
3.3	Functional Near-Infrared Spectroscopy	36
3.3.1	Cortical Haemodynamic Response	37
3.3.2	fNIRS measurement	38
3.3.3	Propagation of light in tissue	38
3.3.4	Transmission Medium Optical Properties	41
3.3.5	Derivation of Haemodynamic Activity	42
3.3.6	fNIRS Signal Components	44
3.4	Brain-Computer Interfacing	44
3.4.1	Components of a BCI	44
3.4.2	Mental Efforts for BCI Operation	45
3.4.3	Signal Acquisition	46
3.4.4	Signal Processing	46
3.4.4.1	Preprocessing	47
3.4.4.2	Feature Extraction	47

3.4.4.3	Classification	48
3.4.5	Output	48
3.4.6	Communication and Control BCI	48
3.4.7	Motor Substitution BCI	49
3.4.8	Entertainment BCI	49
3.4.9	Rehabilitation BCI	49
3.4.9.1	Motor Imagery in Place of Motor Execution	50
3.4.9.2	Closing the Sensorimotor Loop: Biofeedback BCI	51
3.5	Other Imaging Methods	53
3.5.1	fMRI	53
3.5.2	PET	54
3.5.3	MEG	54
3.6	Current Challenges Facing Rehabilitation BCI	56
3.6.1	Patient Experience	56
3.6.2	Financial Cost of Research	58
3.6.3	Signal Acquisition Alternatives	58
3.6.4	Non-Standardised fNIRS	59
3.6.5	Effects of Stroke on BCI Parameters	60
3.7	Summary	60
4	Progressing Rehabilitation BCI	61
4.1	Introduction	61
4.2	Early fNIRS BCI	62
4.3	Additional fNIRS Channels with EEG Incorporation	62
4.3.1	Novel Hybrid fNIRS/EEG Module Design	63
4.3.2	Experimental Tests	63
4.3.2.1	Subjects	65
4.3.2.2	Experimental Protocol	65
4.3.2.3	Signal Processing	65
4.3.2.4	Classification	67
4.3.2.5	Results	67
4.3.3	Discussion	68
4.4	Novel Spatial Imaging for Multichannel fNIRS	74

4.4.1	The Gaussian Process Model	74
4.4.2	GP Model fNIRS Imaging	76
4.4.3	HomER fNIRS Imaging	77
4.4.4	fNIRS Data Source	77
4.4.5	Analysis	78
4.4.6	Results	79
4.4.7	Discussion	81
4.5	Accommodating fNIRS Research and Development	82
4.5.1	Real fNIRS Data	83
4.5.2	Synthetic Data Process	84
4.5.2.1	Balloon Model Simulation	85
4.5.2.2	Conversion to Raw Intensity Signals	86
4.5.2.3	Cardiac Interference	87
4.5.2.4	Mayer Wave Interference	88
4.5.2.5	Noise Interference	89
4.5.2.6	Offset	90
4.5.3	Generating Synthetic Data	90
4.5.4	Results	91
4.5.5	Discussion	92
4.6	Summary	95
5	Healthy and Stroke-Affected Brain Activity	96
5.1	Introduction	96
5.2	Effects of Stroke on Brain Activity	97
5.3	Brain Networks and Connectivity	100
5.4	Effects of Stroke on Brain Connectivity	102
5.5	Recording of Healthy and Stroke-affected EEG	104
5.5.1	Subjects	105
5.5.2	Experimental set-up and motor paradigm	108
5.5.3	EEG data acquisition	109
5.6	Qualitative differences between healthy and stroke-affected EEG	109
5.6.1	Spectral Components	110
5.6.2	Independent Component Analysis	110

5.7 The Need for Further Analysis 117

5.8 Summary 117

6 Stroke Effects and Neuroplastic Change Observed Through Machine

Learning 119

6.1 Introduction 119

6.2 Study Objectives 120

 6.2.1 Choice of Rehabilitation BCI Training Data 120

 6.2.2 Effect of Stroke on BCI Performance 121

 6.2.3 A Biomarker for Post-Stroke Neurorehabilitation 121

6.3 Offline BCI Analysis 122

 6.3.1 Pre-processing 124

 6.3.2 Temporal Filtering 124

 6.3.3 Common Spatial Patterns 124

 6.3.3.1 The CSP algorithm 125

 6.3.3.2 Feature extraction 126

 6.3.3.3 CSP with multiple frequency ranges 127

 6.3.4 Marginal Relevance 129

 6.3.5 Gaussian Process classification 130

 6.3.6 Analyses 131

 6.3.6.1 Single dataset 10-fold cross validation 131

 6.3.6.2 Individual healthy dataset models applied to all data . 132

 6.3.6.3 Grouped healthy dataset model applied to stroke data . 132

 6.3.6.4 Leave-one-out cross-validation of healthy datasets . . . 132

 6.3.6.5 Early Stroke datasets used to classify corresponding
Late Stroke datasets 133

 6.3.6.6 Frequency ranges of selected CSP features 133

6.4 Results 133

 6.4.1 Single dataset 10-fold cross validation 133

 6.4.2 Individual healthy dataset models applied to all data 134

 6.4.3 Grouped healthy dataset model applied to stroke data 134

 6.4.4 Leave-one-out cross-validation of healthy datasets 136

6.4.5	Early Stroke datasets used to classify corresponding Late Stroke datasets	137
6.4.6	Comparison of all BCI training methods for stroke	138
6.4.7	Frequency ranges of selected CSP features	138
6.5	Discussion	142
6.5.1	Effect of Stroke	142
6.5.2	Rehabilitation BCI Training Data	143
6.5.3	CSP Plots	144
6.5.4	Biomarker for Neurorehabilitation	145
6.6	Summary	149
7	Post-Stroke Connectivity Analysis and a Portable Stroke Rehabilitation BCI	150
7.1	Introduction	150
7.2	Connectivity Measurement	151
7.2.1	Granger Causality	152
7.2.2	Phase Slope Index	152
7.3	Connectivity Analysis of Acquired Dataset with PSI	154
7.3.1	PSI with Common Average Referencing	155
7.3.1.1	Processing Steps	155
7.3.1.2	Statistical Analysis	156
7.3.1.3	Results	157
7.3.1.4	Validation	158
7.3.2	Latest EEG Connectivity Analysis Knowledge	162
7.4	Future Stroke Connectivity Analysis	167
7.5	Portable and Inexpensive Biofeedback BCI	168
7.5.1	Pneumatic Glove	169
7.5.2	EEG Brain-Computer Interface	170
7.5.3	Subjects	172
7.5.4	Experimental Protocol	172
7.5.5	Results	173
7.5.6	Discussion	174
7.6	Summary	175

CONTENTS

8 Conclusion	177
8.1 Summary and Discussion	177
8.2 Concluding Remarks	180
References	181

List of Figures

2.1	Main parts of the human brain. <i>Source: Brain parts (cropped and edited) licensed under CC BY-NC 2.0.</i>	9
2.2	Lobes of the cerebral cortex. <i>Source: Public domain</i>	9
2.3	Motor cortex highlighted in red. <i>Source: Brodmann area 4 lateral.jpg licensed under CC BY-SA 2.1 JP.</i>	10
2.4	Structure of a myelinated neuron. <i>Source: Neuron.svg licensed under CC BY 3.0.</i>	11
2.5	Evolution of the action potential. <i>Source: 1222 Action Potential Labels.jpg licensed under CC BY 3.0.</i>	12
2.6	Stained pyramidal neuron in the hippocampus of an epileptic patient. <i>Source: Pyramidal hippocampal neuron 40x.jpg licensed under CC BY-SA 2.5.</i>	13
2.7	Blood supply to the brain from the heart. <i>Source: 2122 Common Carotid Artery.jpg licensed under CC BY 3.0.</i>	15
2.8	Circle of Willis. <i>Source: Circle of Willis en.svg, public domain.</i>	16
2.9	Arterial occlusion caused by atheroma and thrombus. <i>Source: Blausen 0089 BloodClot Motion.png licensed under CC BY 3.0.</i>	18
2.10	Sensory homunculus. <i>Source: 1421 Sensory Homunculus.jpg licensed under CC BY 3.0.</i>	24
3.1	Example EEG cap. <i>Source: EEG Recording Cap.jpg licensed under CC BY 2.0.</i>	32
3.2	International 10-20 system for EEG electrode placement. <i>Source: 21 electrodes of International 10-20 system for EEG.svg, public domain.</i>	32

LIST OF FIGURES

3.3	Exaggerated haemodynamic response. Neuronal activation begins at $t = t_0$ and stops at $t = t_1$. (i) Initial increase in HbR. (ii) Elevation of HbO and reduction of HbR during activation followed by post-activation response. (iii) Overshoot and return to baseline.	37
3.4	Extinction spectrum of pure water.	42
3.5	Extinction spectra of HbO and HbR.	42
3.6	BCI system overview.	45
3.7	Example of an fMRI scanner. <i>Source: Varian4T, public domain.</i>	53
3.8	Example of a PET scanner. <i>Source: PET scan licensed under CC BY 2.0.</i> 54	54
3.9	Example PET image.	55
3.10	Example of a MEG system. <i>Source: NIMH MEG, public domain.</i>	56
4.1	Design of the dual fNIRS/EEG recording module. S1-S3: fNIRS sources. D1-D3: fNIRS detectors. E1-E7: EEG sensors	64
4.2	Dual fNIRS/EEG module positioned over Subject A’s motor cortex. . .	66
4.3	2D EEG feature space for Channel 2 of Subject A, recording 1. Crosses represent Rest instruction features while circles represent movement instruction features.	68
4.4	2D EEG feature space for Channel 2 of Subject A, recording 1. Crosses represent Rest instruction features while circles represent movement instruction features.	69
4.5	Scatter plots of hybrid fNIRS/EEG BCI classification accuracies. (a) fNIRS results compared to EEG results (b) fNIRS results compared to Dual results (c) EEG results compared to Dual results (d) 3D scatter plot of fNIRS, EEG and Dual results. Dashed red lines in (a), (b) and (c) are linear regressions of the data.	70
4.6	HbO signals following fNIRS processing. Red lines indicate image sample times at 3.5, 7.5 and 11.5 seconds for GP model interpolation and HomER. 78	78
4.7	Spatial locations of sample data fNIRS light source (A), light detectors (open circles 1-4) and midpoints of each fNIRS channel (small circles). .	79
4.8	fNIRS optical imaging output from HomER and GP model interpolation. 80	80
4.9	Signals at each stage of production of transmitted light intensity from ideal haemodynamic response.	87

LIST OF FIGURES

4.10 Piecewise-linear model of a single cardiac pulse component.	88
4.11 Section of cardiac component of intensity signal interference.	88
4.12 Section of Mayer wave component of intensity signal interference.	89
4.13 Entire real and synthetic fNIRS signals, highlighting signal offsets.	91
4.14 20 second time-course of real and synthetic transmitted light intensity signals.	92
4.15 Spectral content of real and synthetic transmitted light intensity signals.	93
4.16 Synthetic fNIRS individual and average haemodynamic responses during rest and activity.	93
5.1 Illustration of a brain network showing nodes and edges. <i>Source: Brain network.png licensed under CC BY-SA 3.0.</i>	102
5.2 Kapandji thumb apposition scores.	107
5.3 Experimental protocol instruction timing	109
5.4 Simplified BSS process.	111
6.1 Block diagram of the offline BCI model.	122
6.2 Experimental protocol with indicated “CSP window” - the portion of a trial used for CSP	124
6.3 Marginal Relevance Selected frequency ranges.	141
6.4 Plots of healthy subject data CSP.	147
6.5 Plots of stroke-affected subject data CSP.	148
7.1 Frequency-dependent phase difference.	153
7.2 PSI score significant differences in Healthy v Stroke data. Blue indicates higher PSI score for Healthy, red indicates higher PSI score for Stroke. . .	159
7.3 PSI score significant differences in Stroke Early v Stroke Late data. Blue indicates higher PSI score for Stroke Early, red indicates higher PSI score for Stroke Late.	160
7.4 Healthy subject data: Same-subject, same-event PSI score significant differences for common average reference results. Blue/Red is not im- portant as dataset order is arbitrary.	163

LIST OF FIGURES

7.5	Stroke-affected subject data: Same-subject, same-event PSI score significant differences for common average reference results. Blue/Red is not important as dataset order is arbitrary.	164
7.6	Healthy subject data: Same-subject, cross-event PSI score significant differences for common average reference results. Blue indicates higher PSI score for Rest, red indicates higher PSI score for Active.	165
7.7	Stroke-affected subject data: Same-subject, cross-event PSI score significant differences for common average reference results. Blue indicates higher PSI score for Rest, red indicates higher PSI score for Active.	166
7.8	Hand in pneumatic glove when fully deflated.	169
7.9	Hand in pneumatic glove when fully inflated.	170
7.10	Pneumatic control system.	171
7.11	Full rehabilitation BCI system overview.	172
7.12	Time-course of classifier output with indicated event timings and illustrated glove air pressure.	174

List of Tables

3.1	EEG rhythms and physiological relationships.	36
4.1	Neuro-haemodynamic channels with associated EEG electrode, fNIRS source and fNIRS detector.	64
4.2	Subject demographics	65
4.3	LDA classification results for fNIRS features only, EEG features only and combined fNIRS/EEG features.	72
4.4	Summary of classification results.	73
4.5	Pearson's r correlation coefficients of hybrid BCI classification accuracies.	73
4.6	Statistics (rounded) of real and synthetic 690 nm and 830 nm signals.	94
5.1	Significant changes in stroke subject rCBF during finger movement compared to rest, as determined by Chollet et. al.	98
5.2	Healthy subject demographics	106
5.3	Stroke subject demographics	106
5.4	Stroke subject clinical information	108
5.5	Power v frequency plots of each EEG channel during motor execution of healthy subjects with power contour plots at 6, 10 and 22 Hz	113
5.6	Power v frequency plots of each EEG channel during motor execution of stroke patients with power contour plots at 6, 10 and 22 Hz	114
5.7	Topographies of 4 healthy subject ICA components during motor execution	115
5.8	Topographies of 4 stroke patient ICA components during motor execution	116
6.1	Sample feature for Marginal Relevance calculation.	129
6.2	Additional columns for calculating Marginal Relevance.	130

LIST OF TABLES

6.3	Single dataset 10-fold cross-validation classification accuracy %	134
6.4	Cross-dataset classification accuracy %	135
6.5	Grouped healthy classification accuracy %	136
6.6	Leave-one-out cross-validation of healthy data classification accuracy %	137
6.7	Longitudinal classification accuracy %	138
6.8	Comparison of BCI training methods for stroke classification	139
6.9	Frequency ranges (Hz) of selected CSP features for each dataset	140
7.1	EEG sensor groups	157
7.2	Rehabilitation BCI classification accuracy results.	174

GLOSSARY

ACA	Anterior Cerebral Artery
ADL	Activities of Daily Living
AP	Assistive Product
ATP	Adenosine Triphosphate
BCI	Brain Computer Interface
BMI	Brain-Machine Interface
BOLD	Blood Oxygenation Level Dependent
BSS	Blind Source Separation
CAR	Common Average Referencing
CBF	Cerebral Blood Flow
cFMA	Combined Fugl-Meyer Assessment
CIMT	Constraint-Induced Movement Therapy
CMS	Common Mode Sense
CNS	Central Nervous System
CSP	Common Spatial Patterns
DOI	Diffuse Optical Imaging
DPF	Differential Pathlength Factor
DRL	Driver Right Leg
ECoG	Electrocorticography
EEG	Electroencephalography
EMG	Electromyography
EPSP	Excitatory Post Synaptic Potential
ERD	Event-Related Desynchronisation
EROS	Event-Related Optical Signal
ERS	Event-Related Synchronisation
FBCSP	Finger Bank Common Spatial Patterns
FDG	Fluorodeoxyglucose
FES	Functional Electrical Stimulation
FLAIR	Fluid-Attenuated Inversion Recovery
FMMA	Fugl-Meyer Motor Assessment
fMRI	Functional Magnetic Resonance Imaging
fNIRS	Functional Near-Infrared Spectroscopy
fPCG	Fetal Phonocardiography
GP	Gaussian Process
GPC	Gaussian Process Classification
GPML	Gaussian Processes for Machine Learning
HbO	Oxygenated Haemoglobin
HbR	Deoxygenated Haemoglobin
HK	Haptic Knob

GLOSSARY

IADL	Instrumental Activities of Daily Living
ICA	Independent Component Analysis
ICP	Intracranial Pressure
IPSP	Inhibitory Post Synaptic Potential
LDA	Linear Discriminant Analysis
LED	Light Emitting Diode
LOOCV	Leave-One-Out Cross-Validation
LTD	Long-Term Depression
LTP	Long-Term Potentiation
MCA	Middle Cerebral Artery
mCIMT	Modified Constraint-Induced Movement Therapy
MEG	Magnetoencephalography
MI	Motor Imagery
MMSE	Mini Mental State Exam
MRelv	Marginal Relevance
MVAR	Multivariate Autoregressive
NIRS	Near-Infrared Spectroscopy
OD	Optical Density
PCA	Posterior Cerebral Artery
PET	Positron Emission Tomography
PMI	Photon Migration Imaging
PNS	Peripheral Nervous System
PPG	Photoplethsmography
PSI	Phase Slope Index
PSP	Post Synaptic Potential
QCI	Quasi-Causal Information
rCBF	Regional Cerebral Blood Flow
rTMS	Repetitive Transcranial Magnetic Stimulation
RVM	Relevance Vector Machines
S-FLEX	Sparse Basis Field Expressions
SCI	Spinal Cord Injury
SIS	Stroke Impact Scale
SMR	Sensorimotor Rhythms
SSVEP	Steady-State Visual Evoked Potential
SVM	Support Vector Machines
tDCS	Transcranial Direct Current Stimulation
TIA	Transient Ischaemic Attack
VR	Virtual Reality

Chapter 1

Introduction

1.1 Preface

Those who are fortunate enough to survive a stroke of the brain have traditionally been left to live a lower quality of life. In some cases of stroke, the impact on the life of the survivor may be minimal, such as weakness in a hand or an arm, but in other cases the impact may be devastating, such as loss of the ability to speak or to understand speech, severe behavioural or memory problems, or complete paralysis of one or more limbs. A stroke is damage to the brain caused by a lack of blood supply, due to either arterial blockage or haemorrhage, resulting in loss of brain function. Each year in Ireland, approximately 10,000 people are admitted to hospital following a stroke, while approximately 30,000 stroke survivors in Ireland live with the lasting effects [1]. Recent advances in biomedical technology, however, give hope that those lasting effects following a stroke may soon be eradicated. While those lasting effects of stroke are varied, one of them - weakness and paralysis of the hand/arm - has a potential remedy in the use of Brain-Computer Interface (BCI) systems. These BCI systems and the exploration, development and improvement of their application as a tool for post-stroke rehabilitation are the subject of this thesis.

A BCI is a system which measures and analyses brain activity and then translates that activity into control of another system. Biosignal acquisition systems for the brain such as electroencephalography (EEG) and functional Near-Infrared Spectroscopy (fNIRS) record data signals which may be processed by a BCI in real-time to deter-

mine control over a computer or machine. BCIs have been used to allow tetraplegics to control a computer [2] and to control a robotic arm [3], have allowed both healthy subjects and a subject with myopathy to control a motorised wheelchair [4] and BCIs have also recently been used in direct brain-to-brain communication between two healthy subjects where the thoughts of one person in India caused a person in France to see colours in their vision [5]. BCIs have also shown promise as a tool for stroke rehabilitation by encouraging the brain to form and strengthen neural pathways which take the place of those damaged by the stroke and ultimately restore lost motor ability to the stroke survivor [6, 7, 8]. Motor Imagery is a known method for recovering lost function after a stroke [9]. A BCI can be used in conjunction with this and similar methods to guide functional recovery by recording, analysing a feeding back information on subject engagement with rehabilitation therapies.

Until recently, no established post-stroke rehabilitation method made use of modern technologies. The established technique of Constraint-Induced Movement Therapy (CIMT) has been shown to be quite successful in returning motor ability to an affected limb, provided that some residual motor ability remains. By forcing the subject to use their weakened limb, perhaps combined with Motor Imagery (MI) therapy, a stroke patient may recover a range of motor abilities. In recent years, however, various technologies have been tested for post-stroke rehabilitation efficacy - rehabilitation robotics offers a motorised system to assist movement or to provide resistance training, virtual reality provides an immersive, interactive environment in which a subject's precise movements and activity may be recorded, and systems such as transcranial Direct Current Stimulation (tDCS) and repetitive Transcranial Magnetic Stimulation (rTMS) non-invasively stimulate the brain to modulate neuronal activity. As a stroke affects the brain, BCI was proposed as a potential tool for stroke rehabilitation because of the ability to measure brain activity and interact with the subject's body and mind networks and so more effectively recover motor ability. A review of modern stroke rehabilitation technologies has been conducted by Laffront et. al. [10].

BCI for this purpose of stroke rehabilitation is not yet a fully developed tool. The application of BCIs for this purpose is a very modern problem which is constantly seeing new improvements in system design and understanding of the underlying physiological effects. Researchers in the fields of engineering, mathematics, physics, psychology and medicine around the world are currently tackling this challenge in order to improve the

state of stroke rehabilitation technology. In order for BCI to reach the point where it is consistently successful as a stroke rehabilitation tool, both system design and physiological understanding must be progressed. This thesis is a contribution to that progression, in the hope that future stroke survivors will no longer have to accept a lower quality of life.

1.2 Objective

The objective of this thesis is to improve the current state of stroke rehabilitation tools which utilise electroencephalography (EEG) and functional Near-Infrared Spectroscopy (fNIRS) to record brain activity. This objective is approached from two perspectives. Firstly, novel improvements to specific aspects of EEG and fNIRS BCI research tools are explored and evaluated. Secondly, novel EEG-based tools for clinical evaluation of post-stroke functional recovery are explored and evaluated.

1.3 Contributions

The aim of this thesis is to improve rehabilitation BCI and to uncover new knowledge of the effects of stroke on BCI operation. The following is a comprehensive list of all contributions arising from the work described in this thesis:

- An investigation into the novel use of interpolation methods for fNIRS data imaging.
- The design of a novel hybrid fNIRS and EEG measurement system for BCI, using minimal channels and requiring minimal set-up time.
- A system for generating synthetic fNIRS data in software, allowing for unlimited fNIRS dataset generation and testing of fNIRS signal processing algorithms on those datasets.
- The design of a simple bio-feedback EEG rehabilitation BCI system using adaptations of commercially-available BCI hardware and software and a unique haptic feedback glove.

- The design of a full-head fNIRS/EEG sensor for use by the BCI Research Group, Institute for Infocomm Research (I2R), A*STAR, Singapore.
- The investigation of the effect of stroke on machine learned BCI parameters and the feasibility of their use as a measure of post-stroke neuroplastic changes.
- The exploration of the effect of stroke on EEG sensor-space connectivity measures.

1.4 Publications

1. D. Leamy, T. Ward and J. Kocijan, “Using Gaussian process models for near-infrared spectroscopy data interpolation,” in *Proceedings of the 7th IASTED International Conference Biomedical Engineering (BioMED 2010)*, Innsbrück, 2010. [11]
2. D. J. Leamy and T. E. Ward, “A novel co-locational and concurrent fNIRS/EEG measurement system: Design and initial results,” in *Engineering in Medicine and Biology Society (EMBC), 2010 Annual International Conference of the IEEE*, Buenos Aires, 2011, pp. 4230–4233. [12]
3. K. T. Sweeney, D. J. Leamy, T. E. Ward and S. McLoone, “Intelligent artifact classification for ambulatory physiological signals,” in *Engineering in Medicine and Biology Society (EMBC), 2010 Annual International Conference of the IEEE*, Buenos Aires, 2011, pp. 6349–6352. [13]
4. D. J. Leamy, T. E. Ward and K. T. Sweeney, “Functional Near Infrared Spectroscopy (fNIRS) synthetic data generation,” in *Engineering in Medicine and Biology Society, EMBC, 2011 Annual International Conference of the IEEE*, Boston, 2011, 6589–6592. [14]
5. D. J. Leamy, R. Collins and T. E. Ward, “Combining fNIRS and EEG to improve motor cortex activity classification during an imagined movement-based task,” in *Foundations of Augmented Cognition. Directing the Future of Adaptive Systems*, Orlando, 2011. [15]

6. J. Yu, Y. Pan, K. K. Ang, C. Guan and D. J. Leamy, “Prefrontal cortical activation during arithmetic processing differentiated by cultures: a preliminary fNIRS study,” in *Engineering in Medicine and Biology Society (EMBC), 2012 Annual International Conference of the IEEE*, San Diego, 2012. [16]
7. D. J. Leamy, J. Kocijan, K. Domijan, J. Duffin, R. A.P. Roche, S. Commins, R. Collins and T. E. Ward, “An exploration of EEG features during recovery following stroke - implications for BCI-mediated neurorehabilitation therapy”, *J Neuroeng Rehabil.*, vol. 11, no. 1, pp. 9, Jan., 2014. [17]
8. A. L. Coffey, D. J. Leamy and T. E. Ward, “A novel BCI-controlled pneumatic glove system for home-based neurorehabilitation,” in *Engineering in Medicine and Biology Society (EMBC), 2014 36th Annual International Conference of the IEEE*, Chicago, 2014. [18]

1.5 Outline

This thesis is composed of eight chapters in total, including this introductory chapter. Chapter 2 introduces the reader to the physiological systems and functions of interest, from the nervous system, to neuronal activity, to the effects of stroke and neural adaptation. Chapter 3 introduces the technology which is used to record and investigate brain function and the effects of stroke on that brain function. Chapter 4 is composed primarily of three conference-published papers which describe multiple efforts to improve differing aspects of BCI tools, including fNIRS imaging, hybrid EEG and fNIRS sensor design and synthetic fNIRS data generation. Chapter 5 discusses current knowledge about the effects of stroke on brain activity and describes an experimental recording of rest and movement-related EEG activity in healthy and stroke-affected subjects to be used for further investigation. Chapter 6 describes an analysis of that recorded EEG from an offline BCI perspective in an attempt to explore the effects of stroke on BCI operation and to investigate the potential utility of an implicit EEG BCI-based biomarker for neurorehabilitation. Chapter 7 describes efforts to conduct connectivity analysis on that same dataset and investigate an explicit biomarker of neurorehabilitation, followed by a description of the development and test of a low-cost

biofeedback BCI. Chapter 8 concludes the thesis with a summary, a discussion of future works arising from this thesis and concluding remarks.

Chapter 2

The Stroke-Affected Brain

2.1 Introduction

The human brain is the most complex system known to man. Hundreds of billions of neurons, each with thousands of connections to other neurons and each connection with differing strength, are responsible for the thoughts, hopes, dreams, perceptions and emotions of every person. The human brain is capable of producing wondrous art and exhilarating symphonies, capable of designing machines to take it to other planets and has recently (in the time frame of the brain's existence) begun to get a grasp on understanding itself. This near-infinitely complex structure is subject, unfortunately, to damage and malfunction. Damage to the brain is more personal than, say, a broken leg, because the brain is where we are, where our mind exists. Due to the complexity of the brain, such damage is not easy to fix and we do not yet understand how to remedy every malfunction. Huge milestones of medicine do not appear suddenly but are the summation of hours, years or lives of work. This thesis is as a stepping stone towards eventually being able to fix the damage caused by stroke.

Prior to discussing how modern technology may treat stroke and improve the lives of stroke survivors, the physiology of the brain and the mechanics of stroke must be introduced. The physiology and function of the human brain is introduced in this chapter along with the consequences of a lack of nutrient supply and the brain's natural mechanism for adaptation and learning. The causes, resulting effects and the traditional

treatment of stroke are also explained here as a starting point for understanding the impact of new knowledge and new technologies described in following chapters.

2.2 Anatomy and Function of the Healthy Human Brain

2.2.1 The Nervous System

The nervous system is the organised network of neurons and glia tasked with control of muscle movement, sense, perception, memory, operation of internal organs and more. The nervous system is comprised of two parts: the *central nervous system* (CNS), consisting of the brain and spinal cord, and the *peripheral nervous system* (PNS), consisting of neurons connecting every other part of the body to the spinal cord. These neurons provide two-directional signal pathways around the body for functions such as the sense of touch, heart beat control, gastrointestinal control and muscle control.

The *brainstem*, *cerebellum* and *cerebrum* are the three major parts of the brain, as shown in Figure 2.1. The brainstem connects the spinal cord to the remainder of the brain and some upper parts of it are involved in motor reflexes, regulation of the sleep cycle and respiration and cardiac function. The cerebellum is primarily involved in coordination and fine control of voluntary motor action. The cerebrum controls all other functions of the body, such as motor movement, sense, thought, emotion and perception.

The cerebrum is composed of three layers: the *basal ganglia*, the *limbic system* and the *cerebral cortex*. The basal ganglia resides at the centre of the brain mass and is associated with control of voluntary motor actions, routine behaviours, eye movements, procedural learning, cognition [19] and emotion [20, p. 120]. The limbic system is situated around the basal ganglia and is not a separate system but rather a collection of other brain regions not part of cerebral cortex such as the hippocampus, olfactory bulbs, amygdala, fornix, cingulate cortex and parahippocampal gyrus. The limbic system is associated with many functions, including adrenaline flow, emotion, behaviour, motivation, temperature control, long-term memory and olfaction [21, p. 731].

The outer layer of the cerebrum is the cerebral cortex. This 2–4 mm thick layer [22, p. 468] has a folded outer surface, featuring ridges (*gyri*) and grooves (*sulci*), which results in a much greater outer surface area than that afforded by the inside of

2.2 Anatomy and Function of the Healthy Human Brain

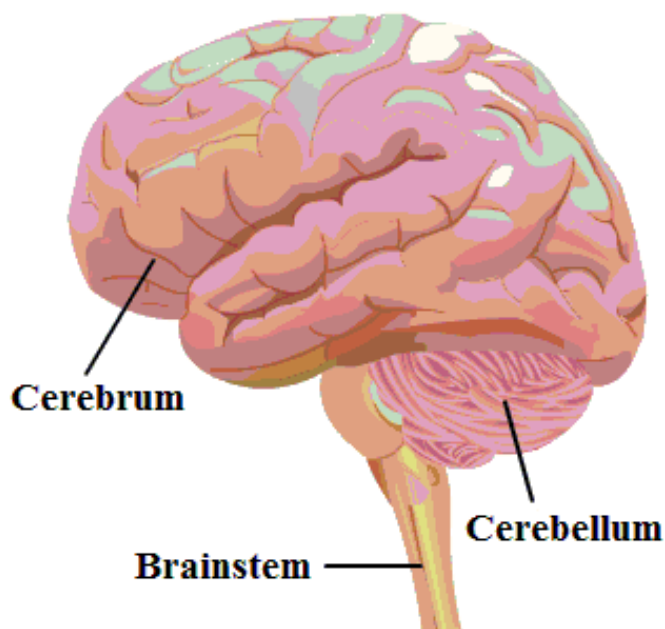


Figure 2.1: Main parts of the human brain. *Source: Brain parts (cropped and edited) licensed under CC BY-NC 2.0.*

a skull. The cerebral cortex is a paired structure, with the left and right hemispheres separated by the medial longitudinal fissure, where each hemisphere primarily relates to the opposite side of the body. Each hemisphere is subdivided into four lobes: the *frontal lobe*, *parietal lobe*, *temporal lobe* and *occipital lobe* [22, p. 469], as shown in Figure 2.2.

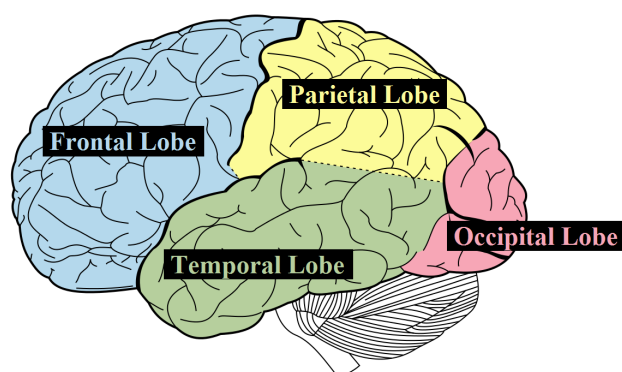


Figure 2.2: Lobes of the cerebral cortex. *Source: Public domain*

2.2 Anatomy and Function of the Healthy Human Brain

The cerebral cortex is organised into separate functional regions. Neuronal activity in each region has been found to be related to particular tasks or responses. These areas can be separated into three types: *motor areas*, for planning and processing of all motor signals, *sensory areas*, for receiving and processing sensation signals, and *association areas*, for secondary signal processing of signals from all primary motor and sensory areas.

Of particular interest to this thesis is the primary motor area of cortex (“motor cortex”), highlighted in Figure 2.3. This region of the brain is the primary area for the planning and initiation of volitional movement [22, p. 474]. Different regions along the vertical axis of the motor cortex are responsible for muscles in different parts of the body. The size of each region of motor cortex representing particular muscles increases with the complexity of the muscle movement controlled. Therefore, the mouth and hand regions are comparatively large, due to the typical complex muscle movements required of these areas, while the areas where the arm and neck are represented are relatively small.

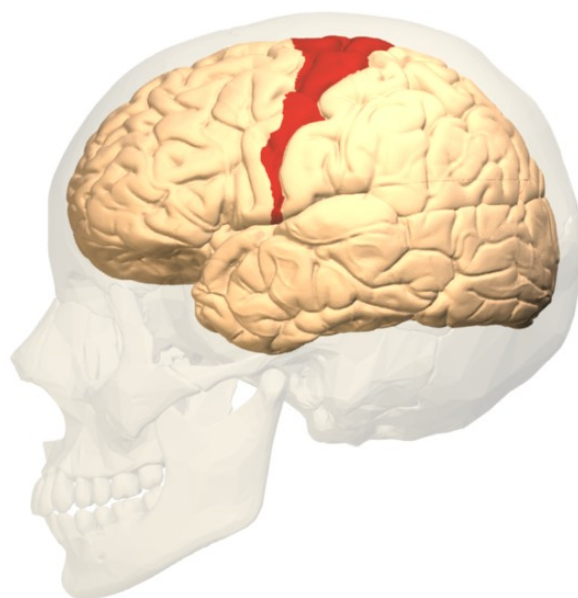


Figure 2.3: Motor cortex highlighted in red. *Source: Brodmann area 4 lateral.jpg licensed under CC BY-SA 2.1 JP.*

2.2.2 The Neuron

A neuron is a type of electrically excitable cell which is used in both the PNS and CNS. 10% of brain mass is made up of neurons while the remaining mass is glial cells - cells which serve support functions for the brain. There are between 100 and 150 billion neurons in the brain, with each neuron connecting to approximately 1,000–10,000 other neurons. All neurons in the brain have broadly the same structure, as illustrated in Figure 2.4. A *cell assembly* is a group of cells which are capable of briefly acting as a single structure. Neurons behave in this manner such that all neurons in an assembly exhibit the same electrical patterns at the same rate of activation [23, p. 6].

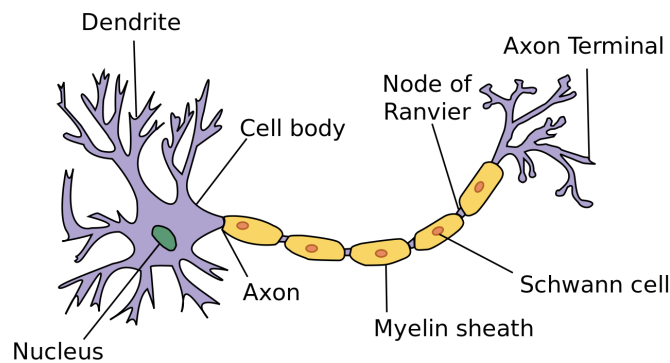


Figure 2.4: Structure of a myelinated neuron. *Source: Neuron.svg licensed under CC BY 3.0.*

The wall of a neuron cell exhibits an ionic transmembrane potential. At resting state, the interior of the cell is -70 mV compared to the exterior primarily due to concentrations of sodium ions (Na^+) and potassium ions (K^+), with a relatively small contribution from chloride ions (Cl^-). These concentrations are maintained through combined forces of diffusion gradients, electric field gradients, availability of pores in the membrane and active transportation of Na^+ and K^+ ions against the established gradients through *sodium-potassium pumps* in the cell membrane.

2.2.2.1 The Action Potential

Importantly, the permeability of the membrane to sodium and potassium ions is voltage- and time-dependant. Should a section of the membrane depolarise to a threshold of approximately -55 mV, the permeability of the membrane to Na^+ ions increases such

2.2 Anatomy and Function of the Healthy Human Brain

that Na^+ rushes into the cell, depolarising the membrane further and again increasing Na^+ permeability. The voltage-dependant membrane permeability to K^+ response is slower than Na^+ so after the membrane has hyperpolarised, permeability to K^+ increases and K^+ rushes out of the cell, depolarising the membrane again. This voltage pattern, shown in Figure 2.5, is known as an *action potential* and occurs at any point in a neuron membrane when the transmembrane potential reaches the depolarisation threshold from some stimulus. The appearance of an action potential is also referred to as a neuron activation or neuronal “firing”.

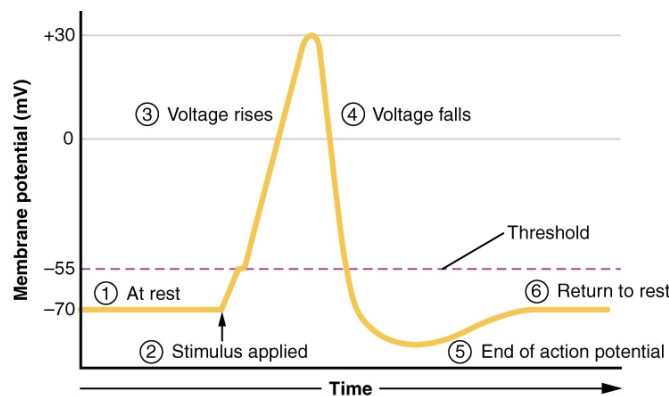


Figure 2.5: Evolution of the action potential. *Source: 1222 Action Potential Labels.jpg licensed under CC BY 3.0.*

The occurrence of the action potential in one part of the membrane causes depolarisation to the threshold in the neighbouring areas of the membrane and the same response. Therefore, the action potential propagates along a neuron cell away from the point of initial stimulation. Following an action potential, there is a recovery period during which it is impossible to cause another action potential. The smallest amount of time possible between action potentials is approximately 0.001 s, so a neuron may fire up to a maximum of 1000 times per second.

As seen in Figure 2.4, the axon is coated with sheaths of Myelin, a fatty substance. These Myelin sheaths prevent transmembrane ionic flow along the axon except at the gaps between the sheaths (*Nodes of Ranvier*) meaning that the action potential “jumps” along the axon at these points. Propagation of the action potential is faster in this way than with unmyelinated neurons, which are found in other parts of the nervous system.

2.2 Anatomy and Function of the Healthy Human Brain

Transmission time for action potentials along cortical axons range is typically 1–10 ms but this may increase up to 30 ms for the longest axons [23, p. 8].

In order for a neuron to become active, it must first experience some stimulus which initially depolarises the transmembrane voltage to the activation threshold. This occurs naturally due to stimulus at the cell dendrites (explained below in subsection 2.2.2.2), resulting in the action potential propagating along the neuron to the ends of the axons. In the brain, dendrites and axons are the points of communication with other neurons. Information and stimulus from another neuron is received via the dendrite while information and stimulus is sent via the axon to the dendrite of another neuron. Essentially, the dendrites are the cell *input* while the axons are the cell *output*. The number of dendrites per cell depends on the location of the neuron in the brain but there is only one axon, which may divide into several branches. Neurons in mammalian brains are usually referred to as *pyramidal neurons* for their triangular shape, as seen in Figure 2.6.

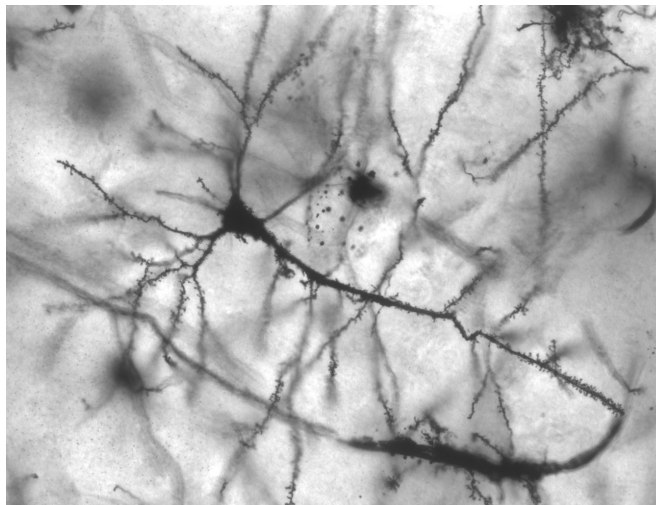


Figure 2.6: Stained pyramidal neuron in the hippocampus of an epileptic patient. *Source: Pyramidal hippocampal neuron 40x.jpg licensed under CC BY-SA 2.5.*

2.2.2.2 The Synapse

A *synapse* is the functional connection between axons and dendrites of two neurons. Two general types of synapse exist, electrical and chemical, which describes the mech-

2.2 Anatomy and Function of the Healthy Human Brain

anism for signal transmission. Electrical synapses transmit by allowing direct current flow between neurons whereas chemical synapses operate through the release and absorption of substances called *neurotransmitters*. At a synapse, the neurons are referred to as *presynaptic* and *postsynaptic*, due to the direction of stimulus. While the same neuron is always presynaptic or postsynaptic at a chemical synapse, current flow may be bi-directional at an electrical synapse. The gap between neurons at an electrical synapse is about 2–3 nm, while at a chemical synapse the gap is about 20 nm. Due to direct current flow transmission, electrical synapses are also faster than chemical synapses. Electrical synapses, however, are in the minority in the brain as their usual function is to synchronise electrical activity among neurons rather than to facilitate inter-neuronal communication [24, p. 79].

The majority of synapses in the brain are chemical. Signal transmission with these types of synapses broadly follows these steps [24, p. 80]:

1. An action potential arrives at the presynaptic membrane.
2. Depolarisation increases membrane permeability to Ca^{++} .
3. Due to high transmembrane concentration gradient, Ca^{++} rushes into the neuron.
4. Ca^{++} causes neurotransmitter release into the synaptic cleft.
5. Neurotransmitter binds to receptors in the postsynaptic membrane, which induces a *post synaptic potential* (PSP) in the cell which may be either excitatory (EPSP) or inhibitory (IPSP).

A single neuron has thousands of dendrites, each of which may have differing levels of excitatory and inhibitory potentials induced in them at their synapses. PSP amplitude is typically in the order of millivolts and so it is very unlikely that a single synapse transmission will be strong enough (approximately +20 mV) to induce an action potential in the postsynaptic neuron. However, all PSPs are effectively integrated in a neuron such that if the summation of all PSPs at an instant depolarises the membrane to the activation threshold, then the neuron will produce an activation potential [24, p. 103]. In this way, neuronal firing is dependant on numerous factors, such as the number of dendritic synapses, the magnitude of EPSPs and IPSPs produced at those synapses and the distance between synapses and soma.

2.2.3 The Vascular System of the Brain

The supply of blood to the brain to provide nutrients and to allow cell metabolism is referred to as *cerebral blood flow* (CBF). Normal cerebral blood flow to a healthy adult brain is 750 to 900 ml per minute, which accounts for 15% of cardiac output [21, p. 761]. This supply of blood must remain highly regulated for the brain to function normally. The brain performs this regulation quite well, keeping cerebral blood flow at a normal level even in persons with high blood pressure [21, p. 762].

Blood is supplied to the brain via four arteries - the left and right vertebral arteries and the left and right internal carotid arteries, as shown in Figure 2.7. These arteries connect at the base of the brain to form a structure called the *Circle of Willis*, shown in Figure 2.8. This structure provides adequate perfusion for the brain in the case of any of the four arteries becoming obstructed.

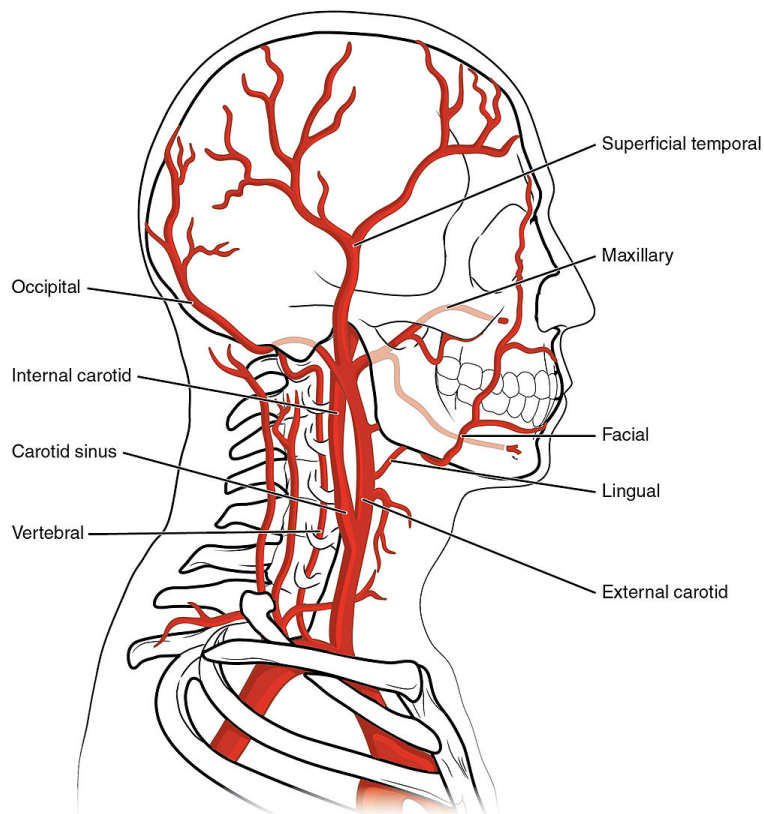


Figure 2.7: Blood supply to the brain from the heart. *Source: 2122 Common Carotid Artery.jpg licensed under CC BY 3.0.*

2.2 Anatomy and Function of the Healthy Human Brain

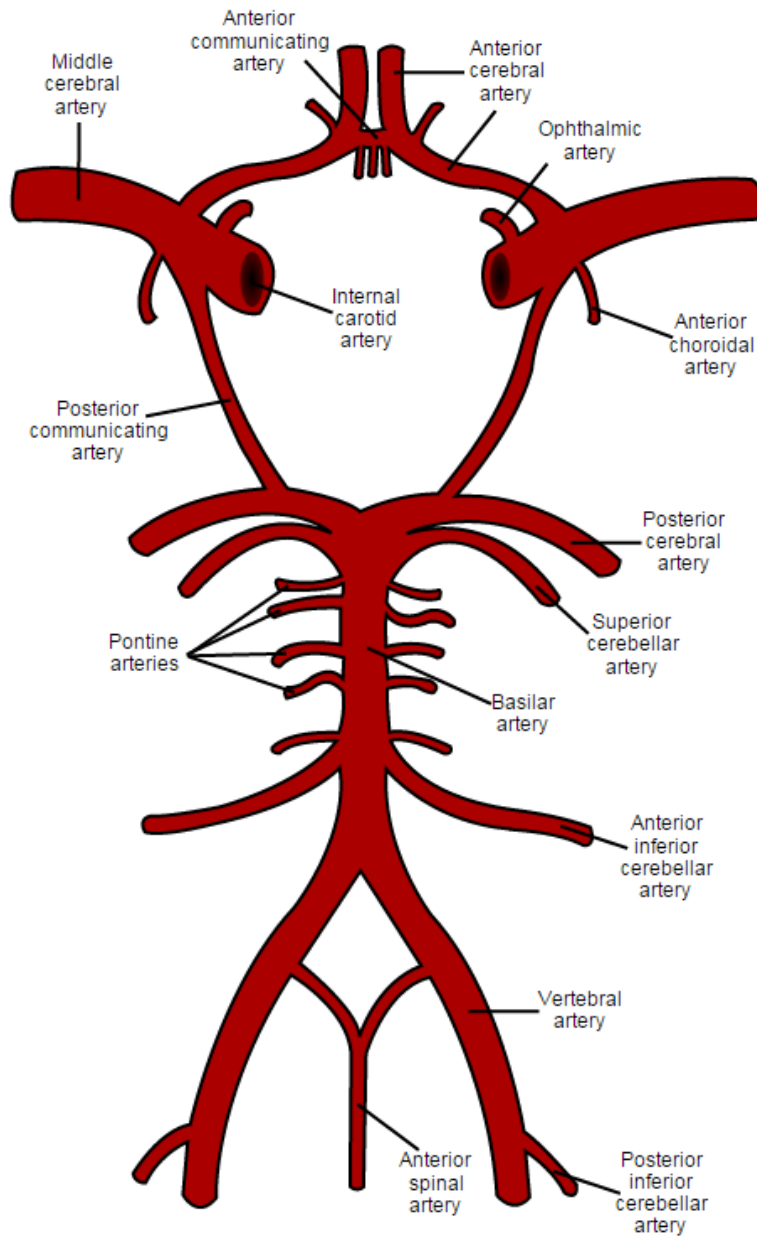


Figure 2.8: Circle of Willis. *Source: Circle of Willis en.svg, public domain.*

The smaller arteries leading away from the Circle of Willis supply blood to more localised regions of the brain. The *middle cerebral artery* (MCA) supplies blood to most of the lateral surface of the cerebrum, the *anterior cerebral artery* (ACA) supplies blood to the medial surface of the cerebrum and deeper layers within the cerebrum and the *posterior cerebral artery* (PCA) supplies blood to the infero-lateral surface of the

2.3 Pathophysiology, Effects and Treatment of Stroke

temporal lobe, the lateral and median surfaces of the occipital lobe and deeper layers within the cerebrum [22, p. 724].

Regulation of cerebral blood flow is of critical importance to the brain as any significant deviation from the ideal can result in abnormal effects and potentially serious damage. In the case of a complete cut-off of blood supply to the brain, a person becomes unconscious in as soon as 5 to 10 seconds. At the cellular level, a brief loss of blood supply can cause cellular damage and if the blood supply is not resumed quickly, *infarction* (“cell death”) is possible. Should blood supply be stopped for an extended time, tissue death is a certainty. [24, The Blood Supply of the Brain and Spinal Cord].

2.3 Pathophysiology, Effects and Treatment of Stroke

A *stroke* is a brain infarction resulting from cessation of blood supply. Following a stroke event, the area surrounding the infarction becomes inflamed and brain function here ceases immediately. The brain tissue liquefies, ultimately leaving a cavity in the brain. There are two mechanisms by which blood supply is lost to an area of the brain: by *arterial haemorrhage* (also known as a *haemorrhagic stroke*) or by *arterial occlusion* (also known as an *ischaemic stroke*) [25, p. 546].

2.3.1 Haemorrhagic Stroke

Haemorrhagic stroke is an arterial bursting and subsequent bleeding in the brain resulting in cell damage and death. Cell damage is caused by hypoxia due to loss of blood supply, an irritant effect of the blood on brain mass, and increased intracranial pressure (ICP). ICP damages the brain by physically pressuring cells and by restricting CBF. This type of stroke is more dangerous than ischaemic strokes but only accounts for 10–15% of stroke events [26].

2.3.2 Ischaemic Stroke

Ischaemic stroke is an arterial blockage resulting in brain cell damage and death. There are four types of ischaemic stroke: *thrombotic stroke* (blood clot at the site of blockage), *embolic stroke* (blood clot or other floating mass from elsewhere in the blood stream causing the blockage, see Figure 2.9), *systemic hypoperfusion* (general decrease in blood

2.3 Pathophysiology, Effects and Treatment of Stroke

supply) and *venous thrombosis* (blood clot in the *dural venous sinuses*, which drain blood from the brain). Severity of cell damage depends on proximity to the blockage site where the nearest cells (*core*) experience immediate cell death while cells further away (*penumbra*) may still receive some blood supply from neighbouring areas and may only be partially damaged [26].

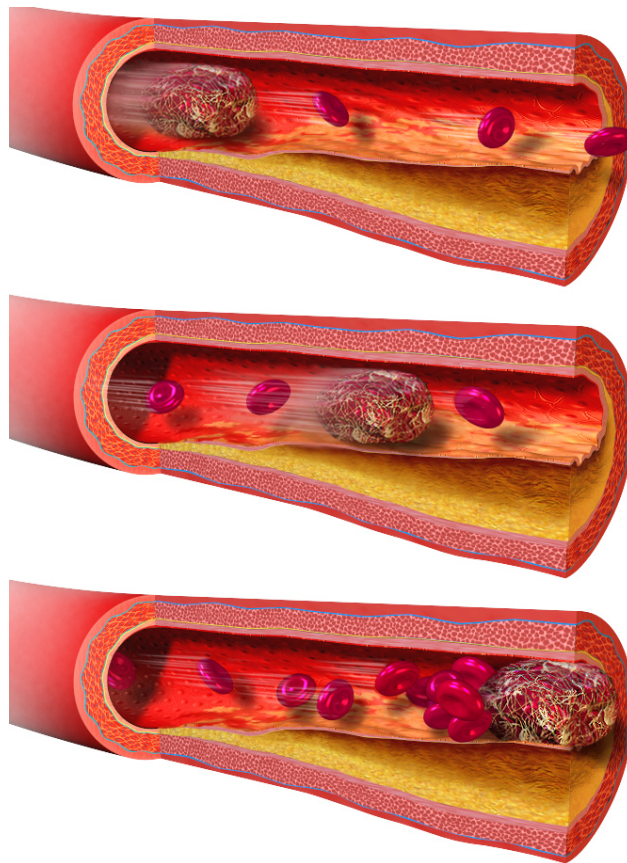


Figure 2.9: Arterial occlusion caused by atheroma and thrombus. *Source: Blausen 0089 BloodClot Motion.png licensed under CC BY 3.0.*

The process of ischaemic cell death is called the *ischaemic cascade* [26, 27, 28], which is summarised here as:

1. Lack of oxygen from the blood supply causes inhibition of oxidative phosphorylation in the cell membrane, which produces the cellular fuel adenosine triphosphate (ATP) [29].

2.3 Pathophysiology, Effects and Treatment of Stroke

2. The cell begins anaerobic metabolism, which produces harmful by-products like lactic acid and hydrogen ions.
3. As ATP is required for the membrane sodium-potassium pump to function, there is a resulting increase of intracellular Na^+ and decrease of intracellular K^+ and thus abject cell depolarisation.
4. Cell depolarisation results in the inflow of calcium ions, Ca^{++} , and water.
5. Intracellular water results in neuronal and glial swelling.
6. Intracellular Ca^{++} causes the release of the neurotransmitters *glutamate* and *aspartate*.
7. Release of glutamate cause more Ca^{++} to flow into the cell.
8. Excess calcium causes the production of harmful enzymes and metabolic products, such as oxygen free radicals, which damages cell membranes, damages genetic material and damages structural proteins of the neuron.
9. Following cell death, toxins and apoptotic molecules are released, causing further cell damage.
10. Inflammation occurs in the damaged area.

2.3.3 Transient Ischaemic Attack

A *transient ischaemic attack* (TIA) is similar to an ischaemic stroke but the blockage is temporary and doesn't result in acute infarction [30]. While recovery from a TIA is relatively quick, there is an increased likelihood that the patient will suffer a full stroke in the months following a TIA [31, 32, 33]. TIAs are therefore important indicators that a person may soon suffer a stroke but do not have severe lasting effects.

2.3.4 Effects of a Stroke

The lasting effects of a stroke depend on the area of the brain which has been damaged. In the case of stroke caused by arterial occlusion, infarction occurs in the area supplied by the blocked artery. Therefore, if the blocked artery is large, supplying blood to a

2.3 Pathophysiology, Effects and Treatment of Stroke

large area of the brain, then the damage will be more wide-spread and the effect will likely be greater than if the blocked artery was small and supplied blood to a small region of the brain.

For example, a haemorrhage or occlusion of a large artery, such as the internal carotid artery or MCA, may result in immediate coma, loss of consciousness or death. As MCA supplies blood to the areas of the brain related to speech comprehension, word formation, motor areas and sensory areas, occlusion of this artery may also result in loss of speech control, loss of motor control and loss of sensation [21, p. 763]. A blockage of the PCA may result in loss of vision as it supplies blood to the occipital lobe. A blockage of the ACA may result in confusion, loss of problem-solving skills or personality changes [25, p. 548].

Worldwide, stroke is the third highest cause of years of life lost [34, p. 46]. Previous studies have found that the fatality rates of all types of first-ever stroke are about 12% at 7 days, 20% at 30 days, 30% at 1 year 60% at 5 years and 80% at 10 years [35, 36]. In Ireland, approximately 10,000 people are admitted to hospital following a stroke each year. Over 30,000 people in Ireland are survivors of stroke, likely suffering from at least one lasting disability as a result, such as hemiparesis (48%), inability to walk (22%), need for assistance with activities of daily living (ADL) (24-53%), clinical depression (32%) and cognitive impairment (33%) [1]. Other studies found that at 12 months after first-ever stroke, one-third of patients had died, 40-50% live independent lives and 20-30% require assistance with activities of daily living [37, 38]. Additionally, stroke sufferers are prone to fatigue [39, 40, 41, 42], which has implications for experimental data recording which will be addressed in this thesis.

Numerous tools are available to clinicians to evaluate the effects of a stroke on a patient. Iterations of the Stroke Impact Scale (SIS) [43, 44, 45] are examples of such tools for assessing a range of stroke outcomes, including strength, hand motor control, activities of daily living/instrumental activities of daily living (ADL/IADL), mobility, memory, thinking, emotion and communication. Another tool, specifically for assessing cognitive effects of a stroke is the Mini-Mental State examination [46]. Many more tools have been developed, often for assessing specific facets of living with and recovering from a stroke. A list of some such tools is available online¹.

¹<http://www.strokecenter.org/professionals/stroke-diagnosis/stroke-assessment-scales/>

2.3.5 Treatment and Therapy

Survival and recovery rates following stroke are best when a patient is admitted to a hospital stroke unit rather than a general medical ward [47]. A stroke unit is an area in a hospital where patients with acute stroke are admitted to be diagnosed, treated and rehabilitated for as long as is required. A “stroke team” made up of one or more doctors, nurses, physiotherapists, occupational therapists, speech and language therapists, social workers and dieticians work in this treatment of a patient in a stroke unit. There may also be a pharmacist, clinical neuropsychologist and orthotics/prosthetics specialist available [48, p. 208].

The traditional objective of stroke rehabilitation is to teach the patient to adapt to their new disabilities in order to minimise the impact that the stroke has on the patient’s life. A stroke patient would be taught how to perform activities of daily living, such as buttoning a shirt or tying shoe laces, without the use of their paralysed hand. The brain naturally heals somewhat following a stroke and this recovery is helped by active participation in therapy by the patient. Finally, with respect to stroke treatment, all rehabilitation efforts should start as soon as possible as evidence shows that the sooner rehabilitation begins, the better the recovery outcome [49].

2.4 Neuroplasticity

The brain should be thought of as a mould-able, changeable, plastic structure which constantly uses experiences and the current environment to form its precise organisation. If the brain was not plastic in this way, it would not be able to form memories, learn new facts or learn new skills. Each of these capabilities of the brain are only possible through the adaptable connections between the neurons that comprise it. If those connections between neurons could not change then normal life would be impossible. From birth, pre-existing neuronal connections begin to adapt to our experiences and over our lives neuronal connections strengthen and weaken (*cortical plasticity*) while some connections die entirely or new connections are formed (*neurogenesis*). This ability of the brain to adapt to the current environment, to sensory stimuli and to experience is referred to as *neuroplasticity*.

2.4.1 Cortical Plasticity

The core mechanism of plasticity in the brain is cortical plasticity - that is, the strength of connections between neurons is not fixed but actually changeable. As discussed in subsection 2.2.2, neurons interact through transmission of action potentials along neuronal pathways which utilise a synapse. At each synapse, an activation potential at the presynaptic axon induces an EPSP or IPSP in the postsynaptic dendrite, which is then integrated by the postsynaptic neuron with all other instantaneous PSPs and may result in an activation potential. Thus, the greater the magnitude of the EPSP at a particular synapse, the greater the strength of that synapse and the greater the influence that presynaptic neuron has on postsynaptic activation. That strength of a synapse, which may also be seen as the strength of a neuronal pathway, is dependent on the quantity of neurotransmitters released by the pre-synaptic neuron and received by the post-synaptic neuron. Due to the dependence of cortical plasticity on synaptic strength, it may also be referred to as *synaptic plasticity*.

2.4.1.1 Short-Term Synaptic Plasticity

Short-term synaptic plasticity refers to alterations in synaptic strength which last up to a few minutes. *Synaptic facilitation* is a sudden increase in synaptic strength which occurs when two axonal action potentials reach the synapse within a few milliseconds of each other. The quick succession of action potentials results in elevated levels of Ca^{++} inside the axon. The elevated Ca^{++} level results in higher amounts of subsequent neurotransmitter release and thus higher magnitude PSP in the postsynaptic neuron. *Synaptic depression* is a sudden decrease in neurotransmitter release levels caused by lowered availability of neurotransmitter following higher-than-normal release rates. Synaptic strength is lowered until the reserves of presynaptic neurotransmitter are replenished. *Synaptic potentiation* and *augmentation* refer to increasing ability of incoming Ca^{++} to release neurotransmitters. Augmentation lasts for a few seconds while potentiation last for tens of seconds up to a few minutes [24, p. 164–165].

2.4.1.2 Long-Term Synaptic Plasticity

Other activity can permanently increase synaptic strength (*long-term potentiation (LTP)*) or permanently decrease synaptic strength (*long-term depression (LTD)*). In 1949, Don-

Hebb published his theory on one such type of neuronal activity for permanently altered synaptic strength [50]. Hebb postulates that if the axon of a pre-synaptic neuron A consistently releases neurotransmitters as the post-synaptic neuron B is activated, a metabolic change occurs in one or both neurons such that the strength of the synapse between A and B increases. This central tenet can be summarised as “Cells that fire together, wire together”, although, technically, the pre-synaptic cell must fire immediately before the post-synaptic cell [51]. This neuroplastic effect caused by coordinated neuronal firing is also known as *Hebbian learning*, *Hebbian plasticity* or *associative plasticity*.

In order for a postsynaptic neuron to undergo LTP, it must possess some *coincidence detector* such that LTP occurs when both neurons at a synapse exhibit an activation potential. This is possible due to the postsynaptic receptor for the neurotransmitter NMDA permitting sudden influx of Ca^{++} in the presence of glutamate during depolarisation [52]. LTD is a natural requirement for all synaptic transmission as, without it, synaptic strength could only increase. LTD appears to occur when postsynaptic Ca^{++} levels increase slowly, which triggers an internalisation in postsynaptic receptors for the neurotransmitter AMPA, thus decreasing sensitivity [24, p. 179].

Spike-timing dependent plasticity refers to the susceptance of neurons to LTP and LTD, dependant on the specific timings of activation potentials on both sides of a chemical synapse. Both LTP and LTD appear dependant on postsynaptic Ca^{++} , where LTP occurs with a sudden, large influx of Ca^{++} and LTD occurs with a slow, steady influx of Ca^{++} .

2.4.1.3 Representational Plasticity

As mentioned in subsection 2.2.1, the cortex can be segmented into areas in which cortical activity is related to various actions and functions of the body and mind. In effect, the surface of the cortex can be seen as a *cortical map*. Take, for example, the *somatosensory cortex*, the region of the brain that processes physical touch signals from around the body located along the postcentral gyrus posterior to the primary motor cortex. As with the primary motor cortex, different regions along the length of the somatosensory cortex are related approximately to activity in specific regions of the body, as shown in the homunculus (“little person”) representation of Figure 2.10.

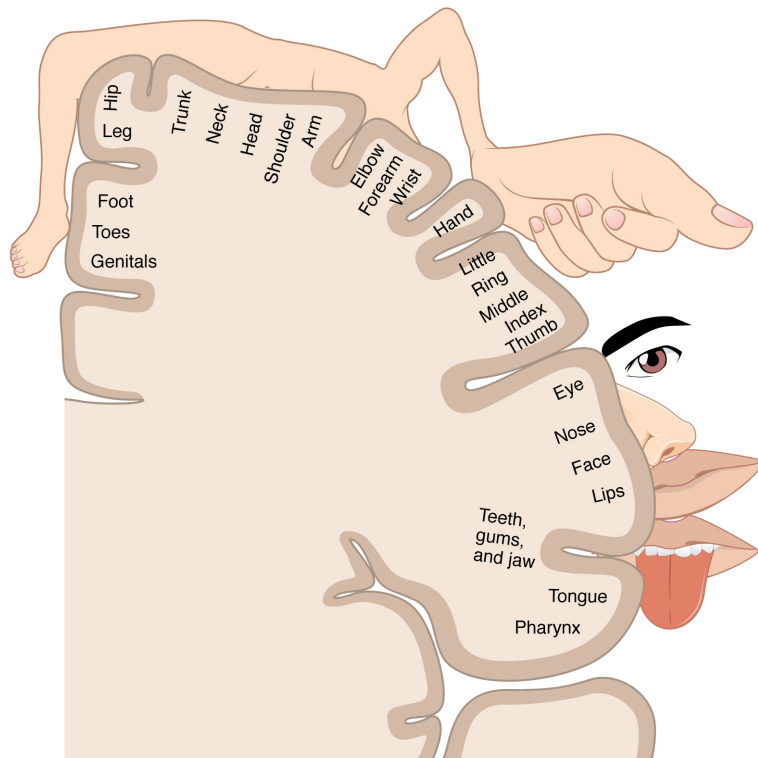


Figure 2.10: Sensory homunculus. *Source: 1421 Sensory Homunculus.jpg licensed under CC BY 3.0.*

The representation areas may be modified (“*cortical remapping*”) by experience, sensory input, injury and learning [52, 53]. An early study conducted by Merzenich et. al [54] investigated cortical remapping by transecting and ligating a median nerve of owls and monkeys, such that the somatosensory cortex for that limb received no information. They then investigated the median nerve representation some months later and found that it had disappeared. The area in which it previously existed was taken over by neighbouring representations. Similar investigations with monkeys reported the same result - with no sensory input, a representation area disappears and neighbouring representations fill the available space i.e. neurons in that region now processed sensory information of neighbouring neurons [55, 56]. Similarly for humans, one study demonstrated that long-time right-handed string musicians (violinists, violoncellists and a guitarist) had enhanced cortical representation for their left hand in their contralateral somatosensory cortex compared to non-musician control subjects

[57]. This enhanced representation is due to the heightened sense of precise touch in the musician's left hands which must press the instrument's strings in a precise manner. Another study demonstrated that reading Braille is associated with an expanded cortical representation for the Braille-reading finger [58, 59]. These, and similar studies, demonstrate the plastic nature of the brain. As experience and sensory input changes, the brain adapts.

2.4.2 Neurogenesis

Neurogenesis simply refers to the growth of new neurons from undifferentiated stem cells. Prior to 1992, the prevailing belief was that a person was born with all of their neurons and, over time, they would lose them but never grow any new neurons. Research in the mid-90's began to challenge that belief until work published in 1998 demonstrated neurogenesis in the hippocampus of the adult brain for the first time [60]. Neurogenesis is a process that occurs primarily during childhood but slows down as a person ages. However, when a stroke or other injury to the brain occurs, the process begins again in order to repair damaged neuronal connections and contribute to the overall neuroplastic process of the brain [61, 62]. Like cortical plasticity, neurogenesis is influenced by external factors and experience. Together, these two functions of the brain may therefore be influenced positively by rehabilitation therapy. From this point, cortical plasticity, representational plasticity and neurogenesis will be addressed together as neuroplasticity.

2.4.3 Stroke Rehabilitation Through Neuroplasticity

The neuroplastic process is constantly affected by a person's experience which results in sensory information and neuronal activity in the brain. Regular activations of synapses keeps the synapse strong while a lack of activation results in a weakened neuronal connection. As one synapse weakens through non-use, other synaptic inputs may begin to exert a greater influence over neuronal activation. Thus, a neuron with the correct connections to other neurons may switch roles as synaptic strengths fluctuate with use. For example, amblyopia, also known as "Lazy Eye", is a disorder where visual acuity in one eye is decreased [63]. As the visual centre of the brain receives weaker or otherwise interfering signals from the affected eye, the brain may begin to favour only vision in

the healthy eye or may lose the ability to process binocular vision. This adaptation to effectively ignore sensory information is a phenomenon referred to as *learned non-use* [64]. Treatment of amblyopia initially involves a treatment of the underlying condition such that vision signals arriving at the brain are now normal. Although the brain has adapted to incorrectly process vision signals, despite the corrected underlying condition, it may be possible to force the brain to re-learn correct processing of the vision signals [63]. This may, in certain cases, involve covering the good eye with a patch, forcing the brain to process vision signals which it had learned to ignore. This forced learning is an externally-controlled neuroplastic adaptation to fix a neurological disorder.

A stroke is an injury which the brain adapts to very quickly. While the neuroplastic process begins initially in response to the stroke event, it continues to function in the months following a stroke as the brain adapts. Without any intervention, the brain may spontaneously repair some of the stroke damage and recover some lost function, particularly in the first 30 days after stroke, continuing up to 90 days after stroke [65, 66]. However, the neuroplastic processes may be influenced by the activities and experiences of the stroke survivor. An objective of stroke rehabilitation intervention is to provide these experiences to the patient such that the neuroplastic process results in increased recovery of lost function.

As discussed earlier, stroke usually results in some loss of function due to neuronal cell death. The destroyed neurons evidently were involved in the lost function but may not have been the source of the function - possibly merely a secondary or tertiary processing region for that function. In that case, neurons at the source of the function may still be intact and operating as normal soon after the stroke event. It is possible, however, to exploit the neuroplastic process of the brain to strengthen previously-unused neural pathways, which are unaffected by the stroke, so that they provide the lost function [67]. Such stroke rehabilitation therapies are based on the idea that the brain is malleable and can be encouraged to form new pathways. Rather than merely teaching the patient to adapt their lives to their disability, these therapies try to adapt the brain to the damage to reduce or eliminate the lasting effect of the stroke [68].

Three phases are involved in post-stroke functional recovery [69]. Firstly, reversal of immediate biological reactions to the stroke event (tissue hypometabolism, neurovascular uncoupling, aberrant neurotransmission [70, 71]) and initiation of cell repair. Secondly, functional cell plasticity to change synaptic strength of existing neuronal

connections. Thirdly, neurogenesis for formation of new neuronal connections for up to 4 months after stroke [72].

Standard motor rehabilitation therapy following hemiparetic stroke (stroke resulting in paralysis of one limb) involves a mix of neurofacilitation techniques, task-specific training and task-oriented training. Neurofacilitation techniques involve attempts to retain motor control as much as possible in the patient through promoting normal movement and inhibiting abnormal movement (see subsection 2.4.4). Task-specific training attempts to improve ability to perform certain tasks. Task-oriented training focusses on retaining functional tasks which involve coordination between various systems (cognitive, neural, musculoskeletal etc.). Time spent performing therapy tasks is subject-specific but approximately 30–60 minutes of therapy each day is typical, beginning in the days following the stroke event. Motor recovery under these conditions proceeds quickly in the first month of therapy, slows down in the months following, and finally plateaus at around 6 months post-stroke [73].

2.4.4 Constraint-Induced Movement Therapy

Constraint-Induced Movement Therapy (CIMT) is a stroke rehabilitation therapy which attempts to reduce the effect of a stroke on motor control of a patient’s limbs [74, 75]. It is based on the theory of “learned non-use”, where a patient with weakened strength in their stroke-affected limb will compensate for their disability by increasingly relying on their corresponding non-affected limb. Repeated reliance on the healthy limb means that the neural pathways involved in movement of the stroke-affected limb become weak through non-use, hindering any recovery of strength that would otherwise be possible. CIMT is therefore very similar to the treatment for amblyopia. The non-affected limb is physically constrained such that the patient is unable to use it for 90% of their waking time while at the same time participating in physical therapy which forces them to use their stroke-affected limb. Though the subject may not perform the therapy tasks well initially, through repeated engagement, new neural pathways strengthen to eventually increase strength and motor control in the stroke-affected limb.

Wolf et. al. conducted a study [76] into the effectiveness of CIMT for stroke rehabilitation. 222 stroke patients who had suffered their first-ever stroke between 3 and 9 months beforehand participated in the study. 116 patients took part in normal

therapy while 106 patients participated in CIMT. Patients who participated in CIMT scored statistically significantly higher on outcome measures than the control group. Recent adaptations of CIMT, such as combining modified-CIMT (mCIMT) and mental practice [77], continue to improve on this therapy. Unfortunately, CIMT relies on the patient having enough motor strength to be able to execute a motor task with their healthy limb constrained. Therefore, a stroke patient without any motor control cannot participate in CIMT in this form.

2.4.5 Other Stroke Rehabilitation Therapies

Numerous stroke rehabilitation therapies exist with varying levels of technological involvement. Some therapies, such as CIMT, Repetitive Task Training [78] or Bilateral Training [79], are “low-tech”, involving little more than a specific action to be followed. Some other therapies involve the use of some technology, such as Moving Platform Training [80, 81] or Treadmill Training [82] (both for lower limb motor recovery). Rehabilitation therapies may also utilise some advanced technologies, such as Robotics [83] or Electrostimulation [84]. A review of these rehabilitation therapies and others is available elsewhere [85].

Following stroke, much of the brain networks involved in motor control remain active. As will be discussed in later chapters, post-stroke patterns of brain activation can be observed with neuroimaging techniques, allowing us to observe the effects of stroke on brain activation (section 5.2). For now, it’s important to highlight the fact that much of the brain is still active when a stroke patient attempts to operate a stroke-affected limb. Even in the case of complete paralysis, brain networks associated with motor control are seen to be active [86]. An opportunity therefore exists to utilise Hebbian learning: use recordings of brain activity to determine if a patient is attempting to execute a motor task and provide biofeedback at the appropriate time, thus encouraging the strength of new neural pathways. This high-tech rehabilitation therapy is discussed in the following chapter.

2.5 Summary

Stroke is a complicated disorder, which can be studied and analysed from numerous perspectives. Other fields of research may tackle stroke as a problem to be studied,

2.5 Summary

to be predicted or to be prevented. The perspective taken here in this chapter and in the remainder of this thesis is that stroke is a problem to be fixed, the effects of which are to be eradicated through healing and returning the sufferer to their pre-stroke lives as well as possible. As such, the causes and mechanisms of stroke are not of utmost importance here, only the lasting physical damage and opportunities for treatment and for new knowledge. The next chapter describes modern methods which may provide the best answer the brain has to healing itself.

Chapter 3

Brain-Computer Interfacing for Stroke Rehabilitation

3.1 Introduction

Traditional methods for stroke rehabilitation are still dominant. Despite the recent leaps and bounds in rehabilitation technology advancement, these methods are shunned in favour of the tried-and-tested low-tech methods or simple adjustment to the injury. High-tech solutions, however, are not entirely absent from clinical settings; medical professionals simply tend to be overly wary of new technology. One modern high-tech method for stroke rehabilitation involves the use of Brain-Computer Interfacing (BCI), where a stroke subject's brain activity is measured and analysed in real-time to provide appropriate feedback to encourage rehabilitation through Hebbian learning effects.

Rehabilitation BCI is complicated and can involve the use of multiple computers and multiple signal measurement systems. It requires at least some operational knowledge and possibly, in the case of more complicated systems, a dedicated operating technician. Rehabilitation BCI has been the subject of significant research recently and may yet prove to be a successful rehabilitation tool. While BCIs have advanced significantly in recent times, rehabilitation BCI places extra restrictions on operation, particularly with respect to ease of set up, financial cost and comfort of the subject during use. In order for rehabilitation BCI to be accepted as the primary tool for stroke rehabilitation,

it must not only perform well under research and therapy conditions, but must also not discourage the stroke patient from engaging with it.

This chapter introduces the brain measurement systems in use for this thesis, electroencephalography (EEG) and functional near-infrared spectroscopy (fNIRS), and their application for rehabilitation BCI. This chapter also briefly discusses other brain imaging methods and discusses current challenges facing rehabilitation BCI.

3.2 Electroencephalography

An electroencephalogram (EEG) is a recording of the electrical activity of the brain [87]. Electrodes are placed at various points on the scalp of a person to measure oscillatory differential voltages. These scalp-recorded oscillations are the result of electric field disturbances produced during neuronal activation. EEG was first recorded in 1924 by German psychiatrist Hans Berger [88], who was interested initially in discovering a physiological basis for psychic phenomena but, following disappointing results, turned his research attention to the electrical activity of the brain and coined the term *electroencephalogram* [89].

3.2.1 Recording

EEG is usually recorded using small silver/silver chloride (Ag/AgCl) electrodes (0.5–1.0 cm in diameter) placed almost in direct contact with the scalp. In order to electrically couple the electrode to the scalp underneath, a conducting electrolyte gel is usually placed between the electrode and scalp. EEG electrodes are commonly held in place with the use of a flexible *EEG cap* (as shown in Figure 3.1) although other methods of fixing electrode to scalp, such as straps, caps and adhesion, are also adequate provided that the electrode does not move during recording. In standard EEG recording, electrode placement follows the *International 10-20 System* for 21 electrodes [90] (as shown in Figure 3.2), the *modified* version, also known as the *10-10 System*, for 75 electrodes [91, 92] and the *10-5 System*, or *five percent system*, for placement of up to 128 electrodes [93]. This standardised nomenclature allows for easier communication of electrode placement in literature.



Figure 3.1: Example EEG cap. *Source: EEG Recording Cap.jpg licensed under CC BY 2.0.*

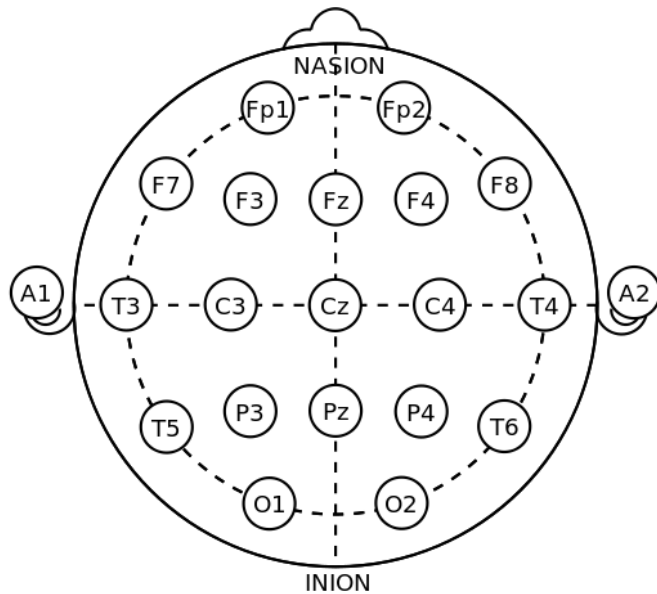


Figure 3.2: International 10-20 system for EEG electrode placement. *Source: 21 electrodes of International 10-20 system for EEG.svg, public domain.*

Various traditional EEG measurement systems use electrodes for different purposes but each require a *ground electrode* to be attached to the scalp. This electrode is required to serve as a common reference point for all voltages of the EEG system and can be placed almost anywhere on the subject's head. The desired number of *Record-*

ing electrode or *active electrodes* are placed on the scalp. For a *referential recording*, one or two reference electrodes are placed on the subject's head, typically on one or both mastoids or ear lobes. Each recorded EEG channel is then the voltage difference between a recording electrode and the reference. For a *bipolar recording*, a dedicated reference electrode is not used and each EEG channel is the voltage difference between two adjacent recording electrodes.

Alternative reference-free EEG measurement methods are *Common average referencing* (CAR) and *Laplacian referencing* [94]. In CAR, the average of all *other* EEG channels is used as the reference voltage for a given EEG channel. A *small Laplacian* reference is the average of only the closest neighbouring EEG channels while a *large Laplacian* is the weighted average of further nearby EEG channels. These referencing methods, along with bipolar recordings, effectively spatially filter the recorded EEG as only EEG sources which are very local to the recording electrodes will result in a differential voltage. Configurations of reference and recording electrode placement are also referred to as *electrode montages*.

Some modern EEG measurement systems are capable of measuring *reference-free* EEG data. For example, the BioSemi Active Two (BioSemi Inc., The Netherlands) replaces the ground electrode with a *Common Mode Sense (CMS)* electrode and a *Driven Right Leg (DRL)* electrode. These electrodes create a feedback loop which drives the EEG subject's common-mode voltage to the reference voltage of the EEG measurement system, reducing interference. As reference-free EEG is recorded with this system, the user may subsequently choose reference electrodes in software, rather than being tied to a reference method during recording¹.

3.2.2 Source

In subsection 2.2.2, neuronal activation was described in terms of time-varying voltages but this activation also produces time-varying ionic currents. Transmembrane potential is maintained by concentrations of ions (mainly Na^+ , K^+ and Cl^-) and any change to the transmembrane potential is due to the transfer of ions across the cell membrane. As described previously, the two main causes of deviation to the transmembrane potential are the action potentials and PSPs. The action potential produces a large flow of ionic

¹<http://www.biosemi.com/faq/cms&drl.htm>

current while PSPs produce relatively low amplitude current. In general, EPSPs (post-synaptic depolarisation) are caused by inflow of positive ions while IPSPs (postsynaptic polarisation) are caused by inflow of negative ions or outflow of positive ions [95].

For both action potentials and PSPs, differing transmembrane voltages along the length of a neuron generates local active current sinks and sources in the extracellular medium. For an action potential, the generated current sinks and sources are transmitted along the neuron. At the “front” of the action potential positive ions (mainly Na^+) flow into the cell while at the “tail” positive ions (mainly K^+) flow out. For PSPs, generated current sinks and sources are strongest at the synapse. EPSPs produce local membrane current sinks at the synapse with distributed passive current sources along the neuron while IPSPs produce local current sources and distributed passive current sinks [23, p. 6]. The distributed passive sinks and sources are necessary as there is no accumulation of charge in the medium [95].

The brain, surrounding meninges, skull and various layers of the skin are effectively a non-homogeneous volume-conductor. Current sinks and sources generated along a neuron produce a time-varying electric field within the volume of the head - each neuron may be treated as a *current dipole* [95]. As with any current flow within a conducting medium, the resulting electric field is measurable at all points in the medium. The electric field produced by a single cortical neuron is too small to be measured on the surface of the head but as neurons in cell assemblies act together as one and all pyramidal cortical neurons are oriented perpendicular to the surface, the summed electric field of all neurons of a cell assembly is strong enough to be measured on the scalp. Individual neurons, or small cell assemblies, throughout the brain constantly produce their own electric fields. However, since these neurons are not oriented in the same direction and do not act together, a measurement of their summed electric field appears as random background noise in all EEG recordings.

3.2.3 EEG Signals

A recorded EEG signal is oscillatory by nature and can be treated as a mixture of sine wave components. Each of these components can be parametrised by their amplitude (A_{nm}), frequency (f_{nm}), and phase (ϕ_{nm}), where n indicates frequency component and

m indicates electrode pair. As a waveform may be expressed as a Fourier series i.e. by the sum of its components, an EEG channel voltage $V_m(t)$ can be expressed as

$$V_m(t) = \sum_{n=1}^N A_{nm} \sin(2\pi f_{nm}t - \phi_{nm}) \quad (3.1)$$

EEG oscillations, also referred to as *rhythms*, are grouped into named categories, as indicated in Table 3.1. The most important of these is the alpha rhythm, which appears as a strong component of EEG in awake, alert people with eyes closed, particularly when measured towards the posterior of the head. EEG activity of this and all other rhythms has been related to various brain functions [87], as also indicated in Table 3.1. EEG rhythm analysis is commonly used for diagnosis in a clinical setting but also has use elsewhere. Particularly for this thesis, analysis of varying EEG rhythms is used to decode the mental state of a subject and subsequently control an external system (section 3.4).

3.2.4 Movement-Related EEG

Upper-band alpha rhythm (10–12 Hz) and lower-band beta rhythm (13–18 Hz) EEG is desynchronised (blocked) during voluntary movement, localised over sensorimotor areas. EEG rhythm blocking which occurs in relation to an action is referred to as *Event-Related Desynchronisation (ERD)*. Contralateral mu rhythm ERD begins approximately 2 seconds prior to movement onset and is interpreted to be related to priming or presetting of neurons in the primary sensorimotor area [87, p.958–960]. *Event-Related Synchronisation (ERS)* describes an increase in rhythmic EEG activity in relation to an action. After movement, beta rhythm ERS (or *post-movement beta synchronisation, PMBS*) is found in the contralateral sensorimotor areas, peaking approximately 600 ms after movement offset [96]. These patterns also occur during imagined and attempted movement (3.4.2).

3.3 Functional Near-Infrared Spectroscopy

Frequency Range	Name	Notes
1–4 Hz	Delta	Usually unseen in healthy brain. Prominent during deep sleep. Otherwise, used for clinical diagnosis.
4–8 Hz	Theta	Stronger in young children than adults. Related to emotional processes.
8–13 Hz	Alpha (α)	Detectable at all points on the scalp but weakest in frontal regions. Attenuated by mental activity, open eyes and other stimuli.
8–13 Hz	Mu (μ)	Found over motor areas. Strongly related to all motor function, including active, passive and reactive movement. Not detectable in every subject.
13–30 Hz	Beta (β)	Related to the onset of movement.
Above 30 Hz	Gamma	Related to active information processing.

Table 3.1: EEG rhythms and physiological relationships.

3.3 Functional Near-Infrared Spectroscopy

Functional near-infrared spectroscopy (fNIRS) is an optical measurement method used to record localised changing concentrations of oxygenated haemoglobin (HbO) and deoxygenated haemoglobin (HbR) in cortical tissue [97, 98]. Light of a particular wavelength is projected into the scalp of a subject. Due to the scattering effects of tissue, photons diffuse into the subject’s head. Each photon then either is “absorbed” at the atomic level or “bounces” around the head, undergoing multiple scattering events as the photon collides with molecules until the photon exits the head again. By emitting two wavelengths of light and measuring the intensity of light of each wavelength exiting the scalp at a known location relative to the point of entry, changing concentrations of HbO and HbR along the photon path can be deduced. This is explained in more detail below.

3.3.1 Cortical Haemodynamic Response

In subsection 2.2.3, the blood supply to the brain was introduced. This blood supply, however, is not fixed and changes in response to neuronal activation. The relationship between neuronal activation and the local haemodynamic response is referred to as *cerebrovascular coupling*. A neuron requires oxygen for metabolism in order to repeatedly activate, which is supplied by the vascular system via haemoglobin. When a neuron consumes the oxygen supplied by oxygenated haemoglobin, the haemoglobin becomes deoxygenated. As neurons in the same region usually activate together, they all can affect blood oxygenation levels when active. While a cortical region is at rest, HbO is supplied and consumed at a steady rate. During neuronal cell assembly activity, however, concentrations of both HbO and HbR follow a typical response pattern, as seen in Figure 3.3.

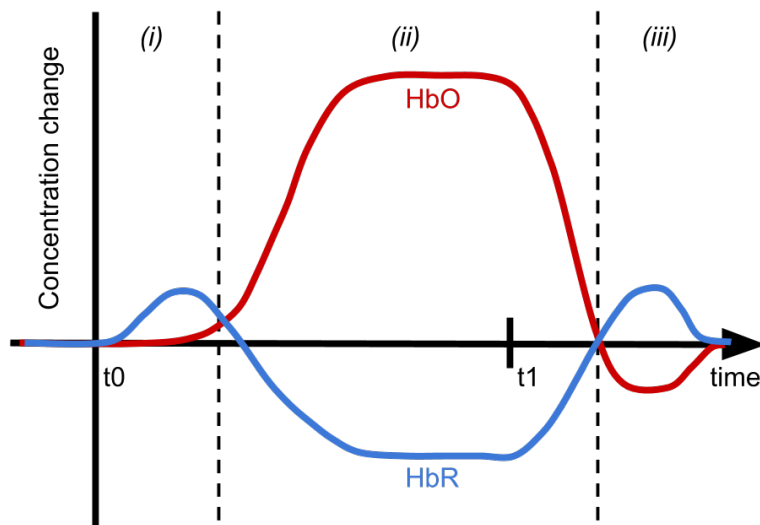


Figure 3.3: Exaggerated haemodynamic response. Neuronal activation begins at $t = t_0$ and stops at $t = t_1$. (i) Initial increase in HbR. (ii) Elevation of HbO and reduction of HbR during activation followed by post-activation response. (iii) Overshoot and return to baseline.

Upon activation, the first response is an increase in HbR concentration, referred to as the “initial dip”, due to the immediate consumption of oxygen. Following this, oxygen-rich blood is rushed to the active region of cortex and surrounding regions. Due to this massive inflow of HbO to the active region, concentration of HbO increases

3.3 Functional Near-Infrared Spectroscopy

while concentration of HbR decreases. Following cessation of activation and a return to neuronal rest, flow of HbO to the region is returned to baseline, resulting in an overshoot of both HbO and HbR concentration signals.

3.3.2 fNIRS measurement

An fNIRS system consists of multiple light sources, multiple light detectors, fibre-optic cables, a method for fixing the fibre-optic cable to the subject's head and a computer to control light sources and record electronic signals from the light detectors.

Various types of fNIRS light sources are available, such as light emitting diode (LED), or laser light. Laser light supplies a very narrow bandwidth of light and so is more favourable than LED but is also more expensive. If using laser light sources, an fNIRS system will use fibre-optic cables to transport the source light to the scalp of the subject. In the case of LED light sources, the LED may be placed close to the subject's scalp without requiring fibre-optics. However, as the LEDs heat up during use, care must be taken to not hurt the subject with heat.

Laser light detectors are too cumbersome to attach to the subject's scalp and so fibre-optics must be used to transport light from the subject's scalp and to the light measurement device. Various types of photodetectors may be used, such as silicon photodiodes, avalanche photodiodes, photomultiplier tubes and charge-coupled devices [99].

The points at which light enters and exits the scalp, usually via fibre-optic cables, are usually referred to as the *source* and *detector* positions (despite the actual light sources and detectors being situated far away from the head). Together, a source and detector are usually referred to as an *optode*. There is no standardised method for affixing the sources and detectors to the subject's scalp. Each fNIRS system manufacturer usually designs their own method for use with their system.

3.3.3 Propagation of light in tissue

As mentioned above, a photon of light entering a transmission medium which is capable of absorbing the photon will either pass through the material unaffected, be absorbed by the material or be "scattered" through deflection at the molecular level. When

3.3 Functional Near-Infrared Spectroscopy

transmitting numerous photons from a light source of a known intensity into the material, the intensity of the light exiting the material at a certain point can be measured with a photon detector. Due to the scattering and absorption effects of the material, the intensity of the detected light leaving the head will be lower than the source light entering the head. The relationship between *incident* light intensity entering the material and *transmitted* light intensity exiting the material in a purely absorbing material (no scattering effects) is given by the Lambert-Bouger law:

$$I = I_0 e^{-\mu_a d} \quad (3.2)$$

where I = transmitted intensity, I_0 = incident intensity, μ_a = absorption coefficient of the material and d = distance between entry and exit points.

The absorbance, A , of a material (also called the *optical density (OD)*) may then be expressed as:

$$A = \ln(I_0/I) = \mu_a d \quad (3.3)$$

The Beer-Lambert law expresses this equation in terms of molecular concentration of the absorbing material in a solution:

$$A = \ln(I_0/I) = \epsilon c d \quad (3.4)$$

where ϵ = the specific absorption coefficient for unit absorber concentration (units: $\text{mol}^{-1}\text{m}^{-1}$, indicates the probability of a photon being absorbed by the material) and c = concentration of the absorbing material (units: mol). The Beer-Lambert law can also be expressed with a base 10 logarithm instead of the natural logarithm:

$$A = \log_{10}(I_0/I) = \alpha c d \quad (3.5)$$

where α = the specific extinction coefficient for unit absorber concentration (units: $\text{mol}^{-1}\text{m}^{-1}$). This expression relating optical density to absorber type, absorber concentration and distance only accounts for one absorbing material in the transmission

3.3 Functional Near-Infrared Spectroscopy

medium. When multiple absorbing materials with unique concentrations exist in the transmission medium, the contribution of each material to the overall optical density of the transmission medium must be accounted for:

$$A = \log_{10}(I_0/I) = \sum_{i=1}^n \alpha_i c_i d \quad (3.6)$$

The optical density of the transmission medium is not only affected by absorption. As mentioned earlier, photons may undergo scattering effects. Scattering deflects the direction of movement of the photon in a random direction and is a result of different materials with different refractive indices. Similar to Equation 3.3 above, the absorbance of a transmission medium due purely to scattering effects can be expressed as:

$$A = \ln(I_0/I) = \mu_s d \quad (3.7)$$

where μ_s = the scattering coefficient of the medium.

The Beer-Lambert law of Equation 3.5 can be modified to account for both absorption and scattering effects of a transmission medium. The absorption coefficient and absorber concentration terms are unaffected by scattering effects but the distance term is. Depending on the positions of light source and light detector on the transmission medium, the length of the average path taken by photons which arrive at the detector will be larger than the distance between the two points. In the adult human head, the average path taken by transmitted light is roughly banana-shaped with a length of approximately six times the source-detector separation [100, 101, 102]. Due to the increased pathlength caused by scattering, more absorption events occur as photons spend more time in the absorbing medium. The Modified Beer-Lambert law accounts for these effects:

$$A = \log_{10}(I_0/I) = \alpha c L B + G \quad (3.8)$$

where L = the distance between source and detector, B = differential pathlength factor (DPF) and G = a geometric factor to account for scattering losses. This expression accounts for both the absorbing and scattering effects of a photon transmission medium, such as the head.

3.3.4 Transmission Medium Optical Properties

Clearly, the absorption and scattering qualities of the head are critically important to fNIRS in order to calculate values for HbO and HbR concentration. Light for fNIRS recording must penetrate multiple layers of tissue, including skin, skull bone, cerebrospinal fluid and cortex. Each of these layers, and numerous smaller extra-cerebral layers, introduce their own scattering and absorption properties to the transmission medium. The scattering and absorption coefficients of these layers can be found elsewhere [102, 103]. The main effect of the scattering property of biological tissue is the shape of the photon path between source and detector but of more importance to fNIRS is the absorption property.

A substance which can absorb a photon is referred to as a *chromophore*. A chromophore has an extinction coefficient for each wavelength of photon, meaning that the choice of fNIRS wavelengths is very important in order to maximise signal quality. For fNIRS recording, the most common chromophores affecting recording are water, lipids, melanin, haemoglobin and cytochrome-c-oxidase (a respiratory enzyme).

Water is abundantly present in living cells and constitutes 80% of brain tissue [104]. The extinction coefficient of water is very low between 600 and 900 nm, as seen in Figure 3.4 [105]. Above 900 nm, the large extinction coefficient of water results in too much photon absorption for reliable fNIRS recordings. Lipids have low extinction coefficients in the wavelength range allowed by water. Melanin, the colouring pigment of the skin, has an unavoidable effect on fNIRS, where darker skin results in more photon absorption and even photon reflection on the scalp. Cytochrome-c-oxidase has a relatively high extinction coefficient spectrum but significantly lower concentration than haemoglobin, so can be ignored.

The last chromophore is the substance of interest to fNIRS - haemoglobin. The two forms of haemoglobin (oxygenated and deoxygenated) have unique extinction coefficient spectra, as shown in Figure 3.5 [106]. In order to measure HbO and HbR, two unique wavelengths of light must be transmitted together but, importantly, neither wavelength may be near the isobestic point where both substances have the same extinction coefficient (around 800 nm).

3.3 Functional Near-Infrared Spectroscopy

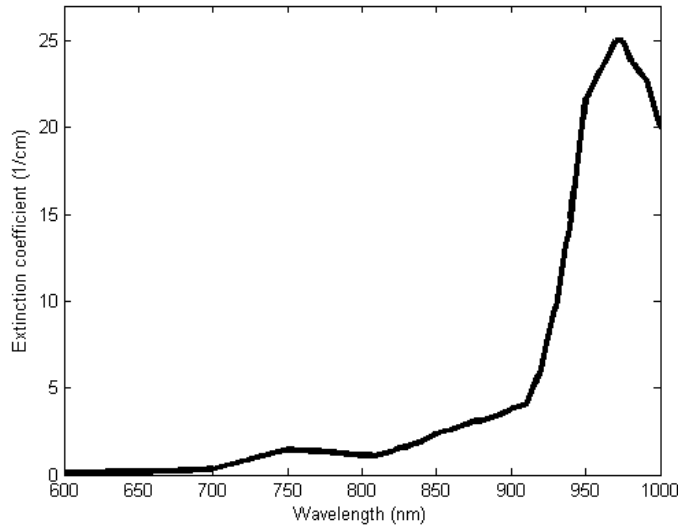


Figure 3.4: Extinction spectrum of pure water.

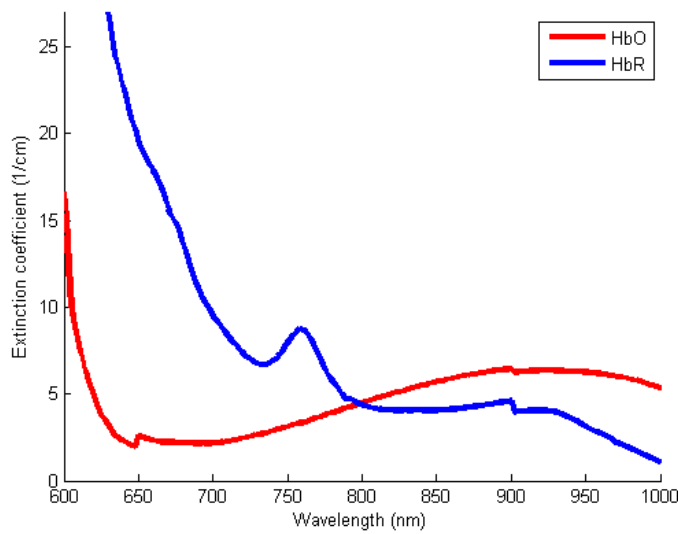


Figure 3.5: Extinction spectra of HbO and HbR.

3.3.5 Derivation of Haemodynamic Activity

Using the Modified Beer-Lambert law of Equation 3.8, the objective is to obtain c_{HbO} and c_{HbR} - concentration values of the chromophores HbO and HbR:

3.3 Functional Near-Infrared Spectroscopy

$$A = (\alpha_{HbO}c_{HbO} + \alpha_{HbR}c_{HbR})LB + G \quad (3.9)$$

Where α_{HbO} = the specific extinction coefficient of HbO and α_{HbR} = the specific extinction coefficient of HbR, c_{HbO} = concentration of HbO and c_{HbR} = concentration of HbR, L = source-detector separation, B = differential pathlength factor and G = geometric term to account for scattering losses. As G can be assumed to remain constant for small time intervals then following differentiation, Equation 3.9 becomes:

$$\Delta A/(B \cdot L) = (\alpha_{HbO}\Delta c_{HbO} + \alpha_{HbR}\Delta c_{HbR}) \quad (3.10)$$

ΔA can be measured for each fNIRS wavelength in use, L can be easily measured and a value for B can be decided upon. In order to determine values for c_{HbO} and c_{HbR} , at least two wavelengths of light (λ_1 and λ_2) must be used during fNIRS recording. Following such a recording, Equation 3.10 becomes:

$$\Delta A_{\lambda_1}/(B \cdot L) = (\alpha_{HbO,\lambda_1}\Delta c_{HbO} + \alpha_{HbR,\lambda_1}\Delta c_{HbR}) \quad (3.11)$$

$$\Delta A_{\lambda_2}/(B \cdot L) = (\alpha_{HbO,\lambda_2}\Delta c_{HbO} + \alpha_{HbR,\lambda_2}\Delta c_{HbR}) \quad (3.12)$$

These simultaneous equations can be represented in matrix form as:

$$\begin{bmatrix} \Delta A_{\lambda_1} \\ \Delta A_{\lambda_2} \end{bmatrix} / (B \cdot L) = \begin{bmatrix} \alpha_{HbO,\lambda_1} & \alpha_{HbR,\lambda_1} \\ \alpha_{HbO,\lambda_2} & \alpha_{HbR,\lambda_2} \end{bmatrix} \begin{bmatrix} \Delta c_{HbO} & \Delta c_{HbR} \end{bmatrix} \quad (3.13)$$

And so to obtain delta concentration signals, the following equation is applied at every data sample time:

$$\begin{bmatrix} \Delta c_{HbO} & \Delta c_{HbR} \end{bmatrix} = \begin{bmatrix} \alpha_{HbO,\lambda_1} & \alpha_{HbR,\lambda_1} \\ \alpha_{HbO,\lambda_2} & \alpha_{HbR,\lambda_2} \end{bmatrix}^{-1} \begin{bmatrix} \Delta A_{\lambda_1} \\ \Delta A_{\lambda_2} \end{bmatrix} / (B \cdot L) \quad (3.14)$$

3.3.6 fNIRS Signal Components

The purpose of fNIRS is to measure changing concentrations of HbO and HbR in the cortex of the subject. However, while cortical haemoglobin is the signal of interest and the largest contributor to a fNIRS signal, haemoglobin in the skin also contributes. As fNIRS light must pass through the skin twice, any HbO or HbR in the skin will have an effect on the fNIRS signal. There are two main interference signals: the cardiac pulse and the Mayer wave [107, 108].

The cardiac pulse component is very similar to a photoplethsmograph (PPG) signal [109] and is usually clear on a fNIRS signal recording. The frequency content of the cardiac signal is higher than the cortical response and so band-pass filtering is usually adequate to remove this interference. The Mayer wave is a very low-frequency (~ 0.1 Hz) vascular pressure wave. This component may be visible when viewing a long time-course of a fNIRS signal. Again, the frequency content of the Mayer wave is so low that it may either be ignored or filtered out.

Other sources of fNIRS interference are noisy light detector electronics, other light sources (such as sunlight from an open window) and movement artefact, which may alter source-detector separation or increase blood-flow to one region [110].

3.4 Brain-Computer Interfacing

A *Brain-Computer Interface* (BCI) is a system for translating brain activity into control signals for a device [111, 112]. Through measurement and analysis of brain signals, the BCI user's mental efforts may be decoded and control signals for another system (e.g. computer or machine) may be generated. There are four main applications of BCIs, as identified by Millán [112]: *Communication and Control*, *Motor Substitution*, *Entertainment* and *Motor Recovery*. The differences between these types of BCI are subtle and mainly lie in the type of output and the intended overall function.

3.4.1 Components of a BCI

The three main physical components of all BCIs are: the subject whose brain activity is being recorded, a measurement device to record the subject's brain activity, and a computer to process the recorded brain activity signals and generate an output. The

measurement device performs signal acquisition of the subject's brain activity and signal digitisation for the computer. The computer then performs numerous signal processing operations, the most important of which are feature extraction and classification. This is the stage at which the BCI decodes the subject's mental efforts and decides on the appropriate output. The BCI output may then produce control signals for some internal function of the same computer or may generate output signals to control an external device. An overview of a BCI system with these components is shown in Figure 3.6. If the computer control signals produced by a BCI ultimately controls an external machine, the entire system may sometimes be referred to as a *Brain-Machine Interface* (BMI).

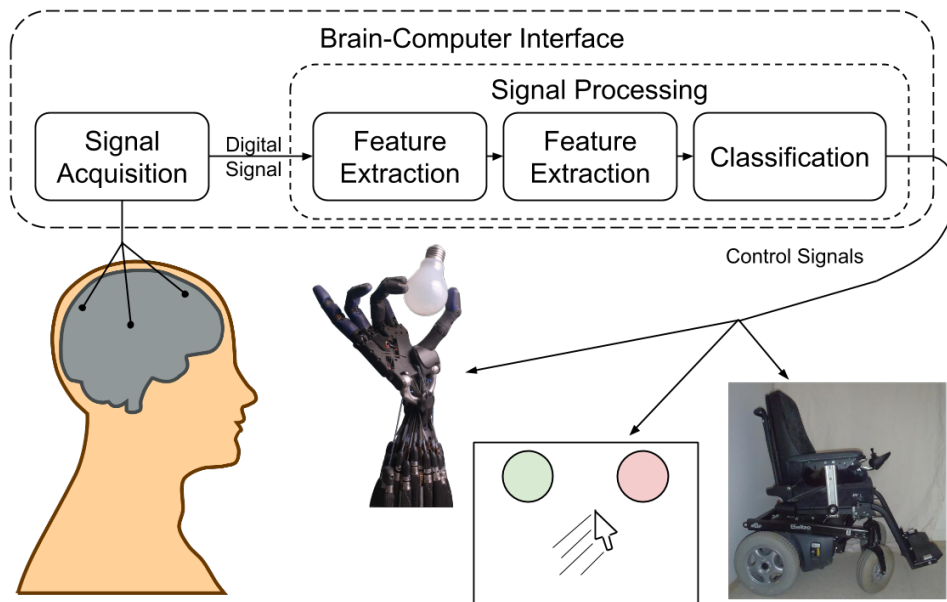


Figure 3.6: BCI system overview.

3.4.2 Mental Efforts for BCI Operation

There are different mental strategies that a subject may employ to operate a BCI. *Motor imagery* (MI) is the mental rehearsal of motor action without any movement [113]. This type of mental action involves much of the same brain activity as overt movement, such as movement planning and processing, and so may be as easily detectable. *Passive*

movement involves moving the subject's body (typically the hand or arm) and measuring the resulting brain activity. This activity is not used to then control a system but does activate similar regions to overt movement and is useful for analysis (e.g. [114]). Finally, *overt movement* may be used in BCI operation, where the subject performs a motor action. This action is useful with assistive devices where the subject may not be able to perform the motor action fully but a BCI and device may help the subject perform the task.

3.4.3 Signal Acquisition

Signal Acquisition is simply the recording and digitisation of the subject's brain activity. The exact nature of the acquired signal(s) depends on the recording modality used. EEG and fNIRS are both popular BCI signal acquisition methods but other measurement modalities, such as magnetoencephalography (MEG) or electrocorticography (ECoG), may also be used. Naturally, different signal acquisition methods have different requirements for recording set-up. For example, EEG systems require that the electrodes be placed on the subject's head in the correct position and that electrode gel be applied. fNIRS measurement requires attachment of large optical fibres to the subject's head and often requires that the subject wear laser safety goggles. Both of these modalities, however, allow the subject to be standing, sitting or lying down. Other modalities, such as MEG, functional magnetic resonance imaging (fMRI) and positron emission tomography (PET), require that the subject remain very still inside or under a large machine (see section 3.5). Despite the requirement that the subject remain still, methods for measuring, reducing and eliminating movement artefact from EEG and fNIRS signals have been developed recently [13, 110, 115, 115, 116].

3.4.4 Signal Processing

Following signal acquisition, the BCI computer next digitally processes the raw signal input in order to determine the appropriate output. Signal processing may occur in one or two stages, depending on BCI design. A *naïve BCI* is one in which no prior data about the current subject is used to determine signal processing and so there is only one stage - BCI operation. Alternatively, a recording of a subject's brain activity

may be used to calibrate the BCI before operation in order to determine BCI signal processing parameters - *trained BCI*.

3.4.4.1 Preprocessing

The purpose of the preprocessing stage is to prepare the signals/data for further analysis. Acquired data usually undergoes some relatively simple operations such as temporal filtering, resampling, normalisation, scaling or splitting. The preprocessing steps used depend on the signal type and signal condition. Further preprocessing may involve artefact removal techniques. For example, Independent Component Analysis (ICA) is commonly used to isolate and remove artefact components of EEG signals. As the acquired fNIRS signals are optical intensity measurements, the signals must be converted to ΔHbO and ΔHbR , by implementing the steps described above in subsection 3.3.5.

If the data is then to be used to train the BCI signal processing steps, the analysis takes place off-line following data recording. Once the analysis is complete and the real-time signal processing steps have been determined, the following feature extraction and feature classification operate only on real-time recorded data.

3.4.4.2 Feature Extraction

Feature extraction is the process of translating an amount of measured data into some number of values which represent a characteristic of that data. For example, some simple derived features of a set of numbers might be the mean, variance and maximum value. For BCI, feature extraction may be significantly more complicated, involving significant signal processing. In this work, a “feature” is a multi-dimensional number which represents some aspect or quality of brain activity for a given amount of time. A feature of brain activity can be defined in many ways but the intention of the BCI designer is that these features, which represent separate brain activation states, are unique enough that they can be easily identified as belonging to their actual state. The features represent the values either to train a classifier or to be classified by a classifier.

Following preprocessing, the acquired brain data can be further processed to extract numbers which quantify some quality or aspect of the data. For example, a feature may be a measure of the power of a range of frequencies in EEG data, or a measure of

the change in amplitude of HbO signals in fNIRS. Further values may be combined to obtain a multi-dimensional feature for classification.

3.4.4.3 Classification

In general, classification is the process of determining which category an observation is a member of. For BCI, classification is the challenge of determining which type of brain activation state a feature belongs to. A classifier usually applies decision rules to a feature to conclude which brain activation state a feature represents. The complexity of the decision boundary used by a classifier ranges from very simple Linear Discriminant Analysis (LDA) up to very complex artificial neural networks. A BCI classifier should accurately determine brain activation state while also not requiring too much computer processing power. It is up to the BCI designer to decide on appropriate classification methods. A more detailed introduction to EEG BCI classification methods is available elsewhere [117].

3.4.5 Output

Following classification, the BCI responds to the classifier output. Depending on the classifier result, the BCI may generate a control signal. The nature of the control signal is dependent on the ultimate purpose of the BCI. For example, a BCI may be used to control an on-screen computer pointer. Alternatively, a BCI output may be used to control the movement of an external device, such as a motorised wheelchair. The control signal generated simply depends on the result of signal processing.

3.4.6 Communication and Control BCI

Communication and Control BCI attempts to impart the most control of an external device on the user. For healthy subjects, this type of BCI is merely interesting as it offers mind-control of devices which could be controlled by motor actions which the subject is already capable of. For subjects who have suffered some severe disability, such as tetraplegia, where motor ability is lost but brain function is normal, communication and control BCIs impart control over external devices which would otherwise be impossible. For example, BCI-controlled virtual keyboards [118, 119] and BCI-controlled

web browsers [120, 121] allow a disabled person to use a computer without the use of any motor function.

3.4.7 Motor Substitution BCI

Motor Substitution BCI is similar to Communication and Control BCI but the device being controlled takes the place of a motor action. For example, BCI-controlled wheelchairs have been developed to limited success [122, 123]. Through the correct mental efforts, a BCI wheelchair user may direct wheelchair movement with differing levels of control such that, rather than expecting the subject to precisely control every movement of the wheelchair, some autonomy is used to keep the wheelchair moving in the user-intended direction. In cases where a subject has suffered injury to their motor nerves resulting in motor paralysis (as is the case with Spinal Cord Injury (SCI) [124], for example), BCI-controlled functional electrical stimulation (FES) [125, 126] restores some lost function. The paralysed muscles are electrically stimulated into contraction when the BCI detects the correct brain activity of the subject.

3.4.8 Entertainment BCI

Entertainment BCI is again similar to Communication and Control BCI but the intention is to entertain the user. For example, BCIs have been used to control games (e.g. pinball [127] and strategy [128]; see Marshall et. al. [129] for a full review), experience movement in a virtual reality (VR) environment [130, 131] and compose and perform music [132]. According to Wolpaw [111]: “Successful BCI operation requires that the user develop and maintain a new skill, a skill that consists not of proper muscle control but rather of proper control of specific electrophysical signals”. As such, BCI training and practice is required to improve accurate BCI use. BCI-based entertainment allows for a more encouraging and enjoyable BCI training experience, which is of importance for those users who require BCI for important activities.

3.4.9 Rehabilitation BCI

Motor Recovery BCI, or *Rehabilitation BCI*, is the fourth application of BCI and also the most unique. Whereas the previous applications all intend to impart the greatest level of control over the output device as possible to the BCI user, a rehabilitation BCI

aims to encourage recovery of lost function caused by damage to the brain. In this way, a rehabilitation BCI should be viewed as a therapeutic device with particular use for post-stroke motor rehabilitation [133, 134, 135]. Importantly, rehabilitation BCI is not required for patients who still retain some motor function after stroke. In those cases, other rehabilitation therapies which use that residual motor function, such as CIMT (subsection 2.4.4), are more reliable. For the many stroke patients who lost all motor function and cannot participate in motor activation therapy, their brain signals alone must be used to drive rehabilitation BCI therapy. In one study, 30 out of 56 (54%) of stroke patients screened for CIMT eligibility (who did not display aphasia) had no motor function and so could not participate [75] while other estimates say 20–25% of stroke patients are ineligible for CIMT [74, 136].

The objective of all rehabilitation therapy is to improve the quality of life of the patient. With respect to stroke rehabilitation BCI, there are two main approaches to this. Firstly, the stroke patient’s quality of life can be substantially improved by training them to independently use a communication and control BCI, motor substitution BCI or entertainment BCI. As mentioned above, BCI use is a skill. For subjects who have suffered significant damage to the brain and have lost motor ability and brain function which is usually used for BCI operation, learning this skill is significantly more difficult. Secondly, BCI operation with haptic feedback might be able to restore lost motor function [133]. This is discussed further in subsection 3.4.9.2.

3.4.9.1 Motor Imagery in Place of Motor Execution

Post-stroke functional recovery relies on the neuroplastic processes (described in section 2.4) for reorganisation. Through representational plasticity, the brain recruits new areas of the brain to take over from the stroke-damaged areas or to otherwise adapt the brain to recover the lost function [137]. Previous studies have shown that active movement therapy, such as CIMT, result in improved motor function as the representation area for the stroke-affected limb expands into neighbouring areas [138]. For those patients who are unable to participate in stroke rehabilitation therapies which require motor execution, alternative strategies are required. One such strategy is the use of motor imagery to access and utilise motor function-related regions of the brain which would otherwise remain idle [9, 139].

Page et. al. [140] reported on the effectiveness of motor imagery for arm motor rehabilitation. 32 chronic stroke patients with residual arm motor ability were separated into two groups. The first group participated in physical practice therapy only, while the second group participated in physical practice *and* mental imagery. The group who performed mental imagery attained significantly higher measures of motor ability after 6 weeks of therapy. While this result demonstrates the effectiveness of motor imagery for encouraging motor rehabilitation, it's important to note that there was no assurance that the stroke patients fully complied with the motor imagery task, potentially affecting the study outcomes. Motor imagery compliance is important for effective rehabilitation therapy yet it is difficult to determine whether the subject is truly engaging with the task. Some tools for assessing motor imagery compliance exist, such as the Chaotic Motor Imagery Assessment Battery [141]. However, BCI may be used to measure, quantify and feedback on stroke patient engagement with motor imagery [142, 143], thus ensuring better rehabilitation outcomes.

3.4.9.2 Closing the Sensorimotor Loop: Biofeedback BCI

As a complement to traditional stroke rehabilitation therapy, the neuroplastic process may be induced through BCI operation by providing the subject with real-time feedback on their current brain activity. Such real-time feedback provides the subject with an experience that is directly related to their brain activity and may support representational plasticity for functional recovery [144]. Core to the concept of neuroplasticity through BCI is Hebbian learning, as discussed in subsection 2.4.1.2. Assuming that motor function has been lost due to a severed connection between the sensorimotor cortex (combined sensory and motor areas) and the paretic muscles following stroke, concurrent activation of both the motor and sensory area may help strengthen existing connections [144]. Using a BCI, excitation of the sensory areas may be provided by orthosis as the subject correctly activates the relevant motor areas.

There are a number of challenges and considerations facing such rehabilitation BCI, as identified by Grosse-Wentrup et. al. [144]: (1) It is unclear yet which neural states are optimal for biofeedback BCI rehabilitation, along with measurement modality and measurement location. (2) Accuracy of feedback is naturally critically important for Hebbian learning as even healthy subjects perform worse when given inaccurate

feedback [145]. (3) The delay between motor area activation and sensory area excitation is also important and neurons must fire almost simultaneously to induce LTP. (4) Feedback modality is a concern as it's not yet clear whether visual, haptic or direct stimulation feedback is most effective. A comprehensive, reliable rehabilitation BCI must take each of these concerns into consideration.

The concept of a biofeedback BCI to facilitate motor function recovery through induction of neuroplastic processes has not yet been extensively studied but some recent studies have shown promise. A recent rehabilitation BCI study by Ramos-Murguilday et. al. [146] demonstrated improved motor ability in stroke patients with movement-related biofeedback. The study consisted of thirty-two chronic stroke patients without the ability to extend their fingers, separated into a control group and an experimental group. The subjects were instructed to desynchronise EEG-measured sensorimotor rhythms (SMR) of the ipsilesional motor cortex by attempting to move their impaired hand with a reaching and grabbing action. Upon determination of the correct SMR activity in the experimental group, the subject's hand was moved by an orthosis attached to the subject's hand. For the control group, orthosis movement was random. Following this therapy, the experimental group showed significantly improved hand motor control as measured by combined Fugl-Meyer assessment (cFMA).

Another recent study by Ang et. al. [147] further suggests that biofeedback BCI may be useful as a rehabilitation tool. This study investigated the effectiveness of BCI-controlled Haptic Knob (HK) orthosis biofeedback (BCI-HK group) compared to HK use without BCI (HK group) and Standard Arm Therapy (SAT group). During therapy sessions, patients in the BCI-HK group performed motor imagery of their impaired hand opening and closing. If the BCI determined that the subject was performing the task correctly, the HK opened and closed their hand. For patients in the HK group, their hand was moved by the orthosis without BCI control while the SAT group underwent repetitive task training therapy. By the end of the study, motor abilities of the BCI-HK group, as assessed by Fugl-Meyer motor assessment (FMMA), were shown to be significantly higher than that of the SAT group. This result, along with the above Ramos-Murguilday et.al. study result, suggests that BCI-mediated biofeedback therapy may be a viable tool for stroke rehabilitation.

3.5 Other Imaging Methods

3.5.1 fMRI

The brain imaging method Functional Magnetic Resonance Imaging (fMRI) is based on atomic magnetic properties of various substances in the brain. In fMRI, a subject lies inside a large magnetic device. When functional, a very strong static magnetic field is formed to align nuclei in regions of the brain of interest before another magnetic field is used to elevate the nuclei to a higher magnetisation level. When this second magnetic field is removed, the nuclei return to their original magnetic states while also releasing some energy. Measurements of this energy can locate its source in three dimensional space in the subject's head.

Oxygenated and deoxygenated haemoglobin present different magnetic output under the same magnetic field activity. Therefore, fMRI can infer brain activation by measurement of blood oxygenation, similar to fNIRS [148]. Such a measurement is known as Blood Oxygenation Level Dependent (BOLD) contrast fMRI [149]. fMRI systems are very large and expensive and are usually only found in hospitals as a diagnostic tool. An example of a fMRI system is shown in Figure 3.7.

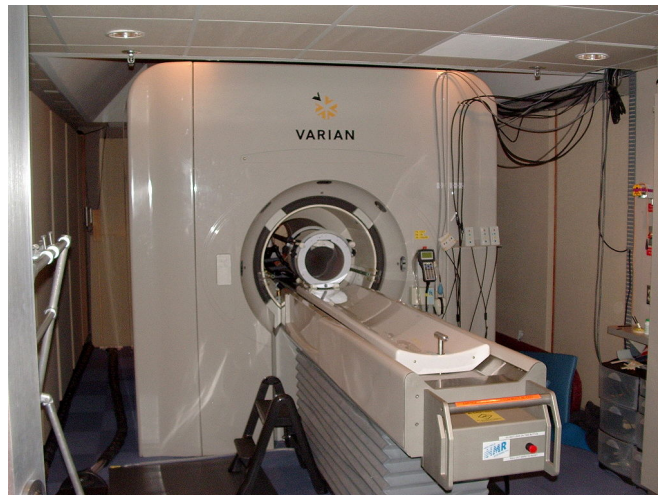


Figure 3.7: Example of an fMRI scanner. *Source: Varian4T, public domain.*

3.5.2 PET

Positron emission tomography (PET) is an imaging method which can produce accurate three-dimensional images of physiological function of the body [150]. To prepare for a PET recording, a radioactive isotope (typically *fluorine-18* (*F-18*)) is tagged (“molecularly attached”) to a molecule (typically, the sugar *fluorodeoxyglucose* (*FDG*)) and a solution with this molecule is introduced to the patient’s blood circulation. As the molecule is transported around the circulatory system, the tagged molecules may collect at certain points as the molecule is consumed. As the isotope tagged to the molecule radioactively decays, it emits pairs of gamma rays. By placing the patient in the PET machine, such as that seen in Figure 3.8, these gamma ray emissions can be detected and used to reconstruct a three dimensional image of their source. Areas in which the molecule has collected are easily visible in the resulting images, as seen in Figure 3.9.



Figure 3.8: Example of a PET scanner. *Source: PET scan licensed under CC BY 2.0.*

3.5.3 MEG

Magnetoencephalography (MEG) is a brain imaging technique based on measurements of the magnetic field produced during neuronal activity. As explained previously, neuronal activation causes a potential difference to exist along the length of a neuron, which causes a current to flow around the neuron and an electric field effect, which is

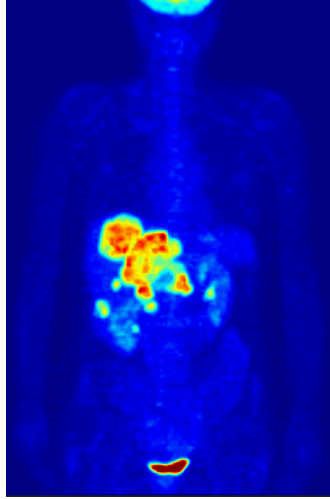


Figure 3.9: Example PET image.

ultimately measurable on the scalp of the subject with an EEG system. Additional to the electric field, a very weak magnetic field is produced by each neuron activation. Closely-spaced synchronised neuronal activations together produce a measurable magnetic field. Although this magnetic field is very weak compared to background activity, specialised MEG systems are capable of measuring cortical activity in this way [151]. MEG recordings have higher temporal resolution than fMRI and high spatial resolution than EEG. Similar to fMRI and PET systems, MEG systems are large and very expensive. An example MEG system is shown in Figure 3.10.

3.6 Current Challenges Facing Rehabilitation BCI



Figure 3.10: Example of a MEG system. *Source: NIMH MEG, public domain.*

3.6 Current Challenges Facing Rehabilitation BCI

Challenges and considerations highlighted by Grosse-Wentrup et. al. [144] are not the only concerns for rehabilitation BCI. Numerous publications have called for additional development of rehabilitation BCI in other respects. Some of these challenges and opportunities are highlighted here.

3.6.1 Patient Experience

Wolpaw et. al. [111] stress that the subject satisfaction with BCI use rests not only on the speed and accuracy of BCI operation but also on the ease of use of the system. The various physical requirements for operation of a BCI depend on the measurement modality employed for signal acquisition. At one extreme, fMRI and PET require that the subject lie still within an enclosed space of a large machine. In a study of the *experience* of an fMRI procedure, Szameitat et. al. [152] reported that 87% of healthy subjects and 77% of stroke patients rated the experience as *acceptable to comfortable*. 15 out of 70 healthy subjects (21.4%) and 6 out of 21 stroke patients (28.6%) reported

3.6 Current Challenges Facing Rehabilitation BCI

something strange about their experience, such as tiredness, dizziness, disorientation or in one case, claustrophobia. In a similar study, Hadidi et. al. [153] recently reported on 9 stroke patients who underwent two 1.5 hour-long fMRI procedures without any feeling of claustrophobia. While all of the subjects in the Szameitat et. al. study reported that they would participate again, 28.6% of stroke patients experiencing some level of discomfort is discouraging for repeated use. EEG and fNIRS, however, offer a more comfortable experience as the subject may sit upright in a chair during preparation and during measurement. Despite movement artefact affecting both modalities, they are more robust to movement than fMRI and so place fewer physical restrictions on the subject. The experience of the subject when participating in BCI operation is critically important as a negative experience deters the subject from participating in therapy.

Wolpaw et. al. [111] also highlight the importance of *cosmesis* - the aesthetic appeal of the BCI system to look at and the cosmetic appeal when the subject uses it. While this is quite a subjective concern, any rehabilitation system needs to encourage the patient to use it, or at least not discourage them. According to Wolpaw et. al., “the primary emphasis should be on identifying and providing those BCI applications most desired by the user”. While aesthetic appeal is thus important for rehabilitation BCI adoption, Daly and Wolpaw [133] highlight other considerations for long-term BCI use including convenience, technical requirements, safety and reliability.

The convenience of a BCI is intrinsically related to its portability. At-home rehabilitation therapy means that a patient does not have to travel to a clinic or hospital so for rehabilitation BCI, which requires a portable system, can be transported to the patient. In this respect, rehabilitation BCI based on fMRI, PET or MEG *cannot* be portable due to the size of such systems. Both EEG and fNIRS, however, are portable enough to find use in at-home rehabilitation BCI system. Buch et. al. [154] reported that while their MEG-based BCI for chronic stroke is not practical for long-term or portable use, they suggest that EEG would perform to a similar level. Ang et. al. [147] also highlighted the need for additional research and larger studies to enhance the portability and usability of BCIs. The portability and usability of rehabilitation BCI is addressed in section 7.5.

3.6.2 Financial Cost of Research

The availability of BCI technology is naturally related to financial cost of the system. fMRI, MEG and PET systems may easily cost upwards of €1,000,000 in hardware, operational costs and maintenance costs (see Keppler [155] for a cost analysis of PET). Due to high financial costs, such systems are primarily found in hospital settings. This affects BCI research in two ways. First, a lack of access to measurement systems means that interested research groups are unable to perform experiments with that measurement system, thus stifling development. Secondly, higher costs and lower access preclude adoption of rehabilitation BCI based on that technology. While fMRI, MEG and PET are prohibitively expensive or otherwise inaccessible for *most* academic research groups, it is still true that less expensive brain measurement systems, such as EEG and fNIRS, are prohibitively expensive for some research groups or for interested individual researchers. As long as a measurement modality is inaccessible to an interested researcher, development of systems based on that modality, such as rehabilitation BCI, is stifled.

Millán et. al. [112] highlighted an opportunity for a significant decrease in the financial cost of BCI hardware if BCI-based gaming ever becomes popular and reaches the mass market. Assuming that such mass-market BCIs are reliable enough to conduct research or to adapt for widespread rehabilitation BCI use, then a significant price drop can only facilitate BCI development. However, this is an unpredictable scenario which should not be depended on. Instead, other efforts should be made to lowering the financial cost of BCI research by lowering hardware costs so more researchers may conduct their own experiments or by increasing access to appropriate datasets for interested researchers. The financial cost of rehabilitation BCI is addressed in section 7.5 while easy access to datasets is addressed in section 4.5.

3.6.3 Signal Acquisition Alternatives

BCIs have been developed with a range of measurement modalities, including EEG [156, 157], fNIRS [158, 159], MEG [154, 160], fMRI [161, 162, 163] and ECoG [164, 165]. Millán et. al. [112] discuss the incorporation of any BCI technology into existing assistive products (APs; e.g. motorised wheelchair, prosthesis) as an additional channel. Such APs, operated by residual motor function, may be enhanced by BCI technology

3.6 Current Challenges Facing Rehabilitation BCI

to form a sort of *hybrid BCI*. These BCI modalities may also be combined with other biosignals, such as Steady-State Visual Evoked Potential (SSVEP), EEG BCI combined with heart rate variability [166], EEG BCI combined with forearm electromyography (EMG) [167], and EEG BCI combined with eye gaze tracking [168]. Finally, Millán et. al. suggest that hybrid BCIs could employ several measurement modalities simultaneously.

There is an opportunity for investigation and development of alternative measurement modalities, particularly with respect to hybrid brain measurement. In accordance with the above concerns of financial cost and portability for rehabilitation BCI applications, combining a low-cost and portable measurement modality with one that is cumbersome and expensive results in a slightly more expensive and slightly more inconvenient measurement system. Therefore, combining two (or more) low-cost, portable systems is of interest to rehabilitation BCI. Hybrid EEG and fNIRS measurement for BCI is addressed in section 4.3.

3.6.4 Non-Standardised fNIRS

Rehabilitation BCI development and widespread adoption may be impeded until operation of such BCI becomes standardised and simplified to the point where operators or users do not require significant training. Wolpaw et. al. [111] have stated that “BCI success will hinge also on the extent to which operation is standardized” and that “If BCIs are to function in homes or long-term care facilities, this dependence [on skilled personnel for operation] must be greatly reduced.” EEG is comparatively more standardised than fNIRS. For example, there is no consensus on optimal wavelengths for fNIRS operation. Each manufacturer determines their preferred wavelengths which are determined by hardware and so not adjustable by an operator. Similarly, there is no standardised method for affixing fNIRS optodes to the subject’s scalp. Each manufacturer again provides their own method. Some stages of fNIRS signal processing are also not standardised. Perhaps, given that fNIRS for BCI has been a relatively recent research interest, none of these points are surprising and it will only take more publications before researchers adopt some operational standards. The topic of non-standardised fNIRS image processing is addressed in section 4.4.

3.6.5 Effects of Stroke on BCI Parameters

Stroke-affected brains are physically and functionally different to healthy brains and so brain activity signals acquired from stroke patients are naturally significantly affected. During BCI training, recorded brain signals are analysed to produce signal processing parameters which attempt to optimise BCI accuracy. What has yet to be investigated, however, is the effect of stroke on those learned parameters. While, effectively, the parameter values appear to be inconsequential, providing that the BCI operates accurately, an investigation may reveal some useful information for rehabilitation BCI development. Such an investigation into the effects of stroke on learned BCI parameters is described in chapter 6.

3.7 Summary

This chapter describes current technology for measuring brain activation data and how such recordings can be used to control an external system via a BCI. There are numerous applications of BCI technology including post-stroke rehabilitation. Rehabilitation BCI works by either encouraging the stroke patient to engage motor areas, thus retaining and improving motor abilities, or by encouraging neural recovery through simultaneous activation of motor and sensory areas. Although described here is the operation of a BCI in real-time, such systems can also be implemented to operate off-line and analyse a set of pre-recorded data and produce classifier output. Using the technology described in this chapter and analysis methods based on BCI operation, the following chapters investigate improvements to EEG and fNIRS rehabilitation BCI systems.

Chapter 4

Progressing Rehabilitation BCI

4.1 Introduction

Previous chapters have introduced the physiological and technological basis for development of EEG and fNIRS rehabilitation BCI. As discussed in the previous chapter, there remain many opportunities for exploration and investigation into fNIRS and EEG rehabilitation BCI which have been identified by leading research groups. When approaching current challenges in a research topic, it is often best to begin with earlier, more established stages of development rather than the latest discoveries, particularly when investigating an inventive or exploratory concept. While incremental improvements on BCI performance are important contributors to BCI development, investigations which may significantly alter or advance the current state should be performed on an established base which is easily understood and not the focus of attention.

Whereas EEG BCI research has progressed rapidly, fNIRS BCI research is unfortunately lacking. A cursory search on biomedical publication database PubMed¹ returned 1155 publications which included the terms “BCI” and “EEG” in the past ten years. For that same time frame, the total number of publications with the terms “BCI” and “fNIRS” or “NIRS” returned was 64. Numerous reasons for a lack of fNIRS BCI interest may be speculated at, such as higher financial cost of NIRS hardware than EEG, or the lack of standardised fNIRS operating systems, or simply that EEG is already more popular and until fNIRS is shown to have a significant advantage over EEG it

¹<http://www.ncbi.nlm.nih.gov/pubmed/>

will remain a relatively niche research interest. Despite fNIRS being a very interesting measurement modality with BCI application, the relative lack of fNIRS development may be off-putting to the majority of researchers.

As fNIRS BCI is a relatively young field of research, early developments may provide a suitable launch pad for novel investigations. This chapter begins with early fNIRS BCI and approaches arising concerns with novel solutions.

4.2 Early fNIRS BCI

In 2007, Coyle et. al. [158] developed a simplified fNIRS BCI - one of the first of its kind. A single channel of fNIRS data was recorded, interrogating the subject's motor cortex contralateral to their dominant hand at 10-20 system locations C3 or C4. This early BCI used LEDs with wavelengths of 760 nm and 880 nm placed directly in contact with the subject's scalp with the aid of a mechanical mounting system. Three healthy subjects performed a motor imagery task to control a binary 'Mindswitch'. Subjects achieved an average classification accuracy of 80% with a range of 70-90%. The authors suggest that BCI performance could be enhanced by integrating other brain measurement modalities, such as EEG, noting that "optical signals are ideal for multi-modal studies, as the light signal does not interfere with electrical or magnetic fields". The authors note too that fNIRS is limited by the slow nature of the haemodynamic response, which limits the information transfer rate and they suggest that multiple fNIRS channels may help overcome this issue.

Three novel approaches to improving the current state of fNIRS BCI were taken: expanding fNIRS BCI with additional EEG measurement for hybrid BCI, novel imaging of fNIRS activity using a Gaussian Process interpolation technique and a synthetic fNIRS data generation algorithm for *in silico* testing. The first of these directly addresses the above author's suggested enhancement to fNIRS BCI while the other two address related concerns for fNIRS BCI development.

4.3 Additional fNIRS Channels with EEG Incorporation

Due to the fNIRS measurement set-up with source and detector not placed at the point of cortical interrogation, it is possible to position an EEG electrode at the midpoint

4.3 Additional fNIRS Channels with EEG Incorporation

of an fNIRS optode pair, thus sampling both haemodynamic and electrical activity from approximately the same cortical region at the same time. Such concurrent and co-locational fNIRS and EEG represents a sampling of neurovascular coupling - the interaction of electrical activity and haemodynamic response in active cortex. As discussed previously, this interaction is well understood but typically only one signal type is recorded from cortex for BCI operation. By recording both types of signal from the same location, a BCI is afforded richer information about cortical activity than one modality alone offers. This investigation involves using typical signal processing steps for fNIRS and EEG separately. Following feature extraction, feature sets are combined for classifier training and testing.

4.3.1 Novel Hybrid fNIRS/EEG Module Design

The custom-designed module to hold three fNIRS light sources, three fNIRS light detectors and seven EEG electrodes in the array is shown in Figure 4.1. There are seven fNIRS channels with the corresponding EEG electrodes located directly above the centre point of each fNIRS channel. This centre point of an fNIRS channel is the interrogated area of cortex, so electrical and haemodynamic activity is recorded from approximately the same area of cortex. Thus, this module design provides seven co-locational, dual-modality recording sites. Table 4.1 details the electrodes and optodes used for each neuro-haemodynamic channel. fNIRS data was recorded using a TechEn CW6 system (TechEn Inc., USA) with wavelengths of 690 nm and 830 nm and signals sampled at a sample rate of 25 samples per second. EEG data was recorded using a BioSemi Active-Two system (BioSemi Inc., The Netherlands) with DC-coupled data recorded at a sample rate of 2048 samples per second.

4.3.2 Experimental Tests

To test this BCI sensor, a simple experimental protocol was designed for an offline BCI test with two subjects. EEG and fNIRS data was processed according to the steps described in subsection 3.4.4, with features extracted from both measurement types separately. Classifier training and testing was carried out with the extracted features from both EEG and fNIRS and classifier accuracy was recorded for analysis.

4.3 Additional fNIRS Channels with EEG Incorporation

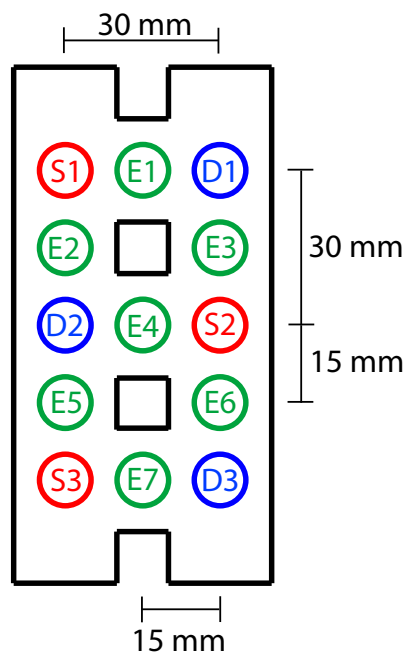


Figure 4.1: Design of the dual fNIRS/EEG recording module. S1-S3: fNIRS sources. D1-D3: fNIRS detectors. E1-E7: EEG sensors

Channel	EEG	fNIRS Source	fNIRS Detector
1	E1	S1	D1
2	E2	S1	D2
3	E3	S2	D1
4	E4	S2	D2
5	E5	S3	D2
6	E6	S2	D3
7	E7	S3	D3

Table 4.1: Neuro-haemodynamic channels with associated EEG electrode, fNIRS source and fNIRS detector.

4.3 Additional fNIRS Channels with EEG Incorporation

4.3.2.1 Subjects

Two subjects participated in two recording sessions each. Subject demographics are shown in Table 4.2. Handedness of both subjects was self-reported. During recording, the subject was seated in a comfortable chair facing a computer screen which presented instructions.

Subject	Gender	Age	Handedness
A	Male	37	Left
B	Male	26	Right

Table 4.2: Subject demographics

4.3.2.2 Experimental Protocol

Subjects were instructed to perform either self-paced finger-tapping or rest, according to on-screen instructions which read either ‘Tap’ for an active trial or ‘Relax’ for a rest trial. 20 alternating trials (10 of each class) were carried out per session. Each trial lasted 20 seconds, resulting in total experimental recording time of 400 seconds. Subjects performed 2 recording sessions, with a short break between sessions.

The central electrode, ‘E4’, of the fNIRS/EEG module was positioned directly over the subject’s motor cortex contralateral to hand activity - at EEG position C4 for left-handed Subject A and C3 for right-handed Subject B. Module position on Subject A’s head is shown in Figure 4.2.

4.3.2.3 Signal Processing

fNIRS raw intensity measurement signals were processed according to the steps described in subsection 3.4.4 with a differential pathlength factor of 6 to produce HbO and HbR delta concentration signals. Feature extraction of HbO and HbR signals for a single trial involved offsetting the trial data so the first sample value is zero, then averaging all data samples for the trial, giving an average change in signal amplitude over the full trial time.

ERD/ERS analysis was performed on the EEG, in accordance with the literature [169]. EEG data was first analysed for spectral content to identify the frequencies at

4.3 Additional fNIRS Channels with EEG Incorporation



Figure 4.2: Dual fNIRS/EEG module positioned over Subject A's motor cortex.

which ERS and ERD occurred in the μ and β frequency ranges respective to onset of a movement instruction and a rest instruction. Raw EEG data was then bandpass filtered with a 6th order Butterworth filter to the identified ERS/ERD ranges, squared to obtain a power signal and then smoothed using a lowpass 6th order Butterworth filter at 5 Hz.

The ERD/ERS reference window was chosen to be between 4.5 and 3.5 seconds before instruction onset. For a movement instruction, the activity window was chosen to be from 0 to 1 seconds after instruction onset. For a rest instruction, the activity window was chosen to be from 0.5 to 1.5 seconds after instruction onset. These windows were chosen to capture the expected timing of pre-movement μ -rhythm desynchronisation and post-movement β -rhythm synchronisation. These windowed μ and β range power signals were used for classification of EEG activity.

Therefore, for each instruction onset event, four features are extracted: change in μ -range power, change in β -range power, average change in HbO amplitude (ΔHbO) and average change in HbR amplitude (ΔHbR).

4.3.2.4 Classification

Each of the seven electro-haemodynamic channels have EEG and fNIRS features extracted. As such, each event for each channel can be defined by a four-dimensional feature (hybrid fNIRS/EEG) or by two two-dimensional features (EEG and fNIRS separately). To investigate classification accuracy of fNIRS and EEG acting in isolation, classification of each channel with only EEG or fNIRS features is carried out first. Following that, classification of the four-dimensional hybrid fNIRS/EEG features is carried out.

Linear Discriminant Analysis (LDA) is used for classifier training and testing with Leave-one-out-cross-validation (LOOCV). Specifically, for N trials, $N-1$ trials are used for classifier training and the remaining trial is used for classifier testing. This is repeated N times with each trial used for testing once. Overall classification accuracy is calculated as the number of correct classifications divided by N .

Example EEG and fNIRS feature spaces for Channel 2 from the first recording of Subject A are shown in Figure 4.3 and Figure 4.4. Crosses indicate feature locations for rest instructions while circles indicate feature locations for movement instructions.

4.3.2.5 Results

A table of classification results is presented in Table 4.3. Shown is the classification accuracy for each channel when operating on fNIRS features alone, EEG features alone and combined fNIRS/EEG features. A summary of average results is presented in Table 4.4. Subject A demonstrated average pre-movement μ -rhythm ERD in the 9–11 Hz range and average post-movement β -rhythm ERS in the 19–22 Hz range over all EEG channels. Subject B demonstrated average pre-movement μ -rhythm ERD in the 9–12 Hz range and average post-movement β -rhythm ERS in the 19–21 Hz range over all EEG channels.

Presented in Figure 4.5 are scatter plots of the classification accuracy results of all subjects, trials and channels from Table 4.3. Figure 4.5 (a) compares fNIRS results to EEG results, Figure 4.5 (b) compares fNIRS results to Dual results, Figure 4.5 (c) compares EEG results to Dual results. These plots also feature a linear regression to the data. Figure 4.5 (d) is a 3-dimensional stem plot of fNIRS, EEG and Dual results.

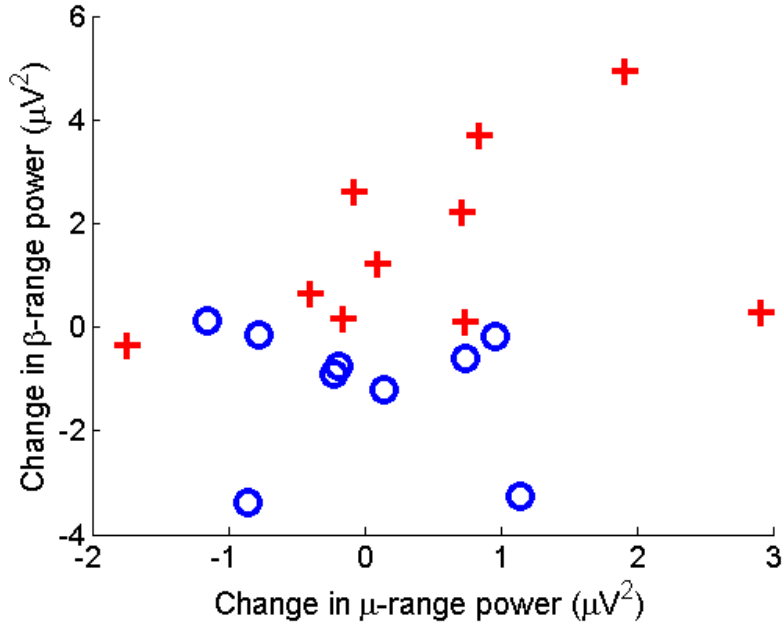


Figure 4.3: 2D EEG feature space for Channel 2 of Subject A, recording 1. Crosses represent Rest instruction features while circles represent movement instruction features.

A table of Pearson’s r correlation coefficients for classification accuracies is presented in Table 4.5.

4.3.3 Discussion

While only a low number of subjects and trials was used in this investigation, these classification results suggest that by utilising both fNIRS and EEG features for classification, an average increase in classification accuracy can be attained. Some analysis of these results, however, shows slightly different outcomes for each subject. For Subject A, classification with both modalities yielded better results than either fNIRS or EEG individually. For Subject B, however, classification with EEG features alone performed better than either fNIRS alone or combined fNIRS/EEG.

One possible explanation for this outcome for Subject B lies in the increased dimensionality of the feature space. While the 2-dimensional EEG features may have been easily separated by LDA, the 2-dimensional fNIRS features may not have been as easy to classify, as indicated by relatively poor classification results for fNIRS. Increasing the

4.3 Additional fNIRS Channels with EEG Incorporation

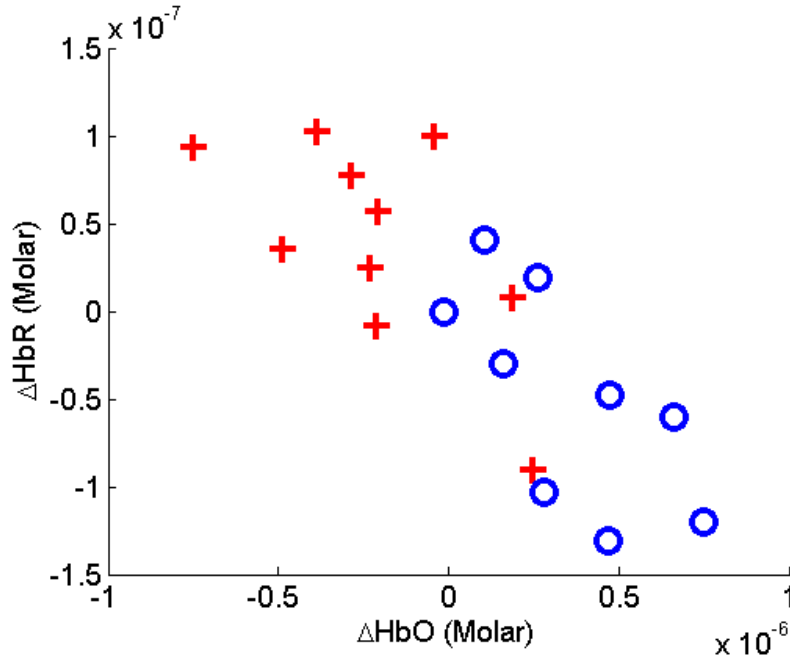


Figure 4.4: 2D EEG feature space for Channel 2 of Subject A, recording 1. Crosses represent Rest instruction features while circles represent movement instruction features.

dimensionality of each EEG feature to include fNIRS, where the new dimension features are not easily separated, appears to have negatively affected classifier performance.

Further analysis of these classification results reveals an interesting pattern. When classification of one modality performs well but classification of the other modality performs poorly, classification of both combined tends to perform about as well as the better-performing modality. For example Subject B, Trial 1, Channel 1, fNIRS classification is 47%, EEG classification is 79% and combined classification is 63%. In most situations like this, classification of the combined modalities performs much better than the worse performing modality. When classification of each modality performs well, classification of the combined features tends to be more successful than either. For example, Subject A, Trial 1, Channel 1, fNIRS classification is 84%, EEG classification is 79% and combined classification is 90%. Lastly, when classification of both separate modalities performs poorly, combined classification tends to also perform poorly. For example, Subject B, Trial 1, Channel 5, fNIRS classification is 47%, EEG classification is 68% and combined classification is 47%. This is the expected outcome for this

4.3 Additional fNIRS Channels with EEG Incorporation

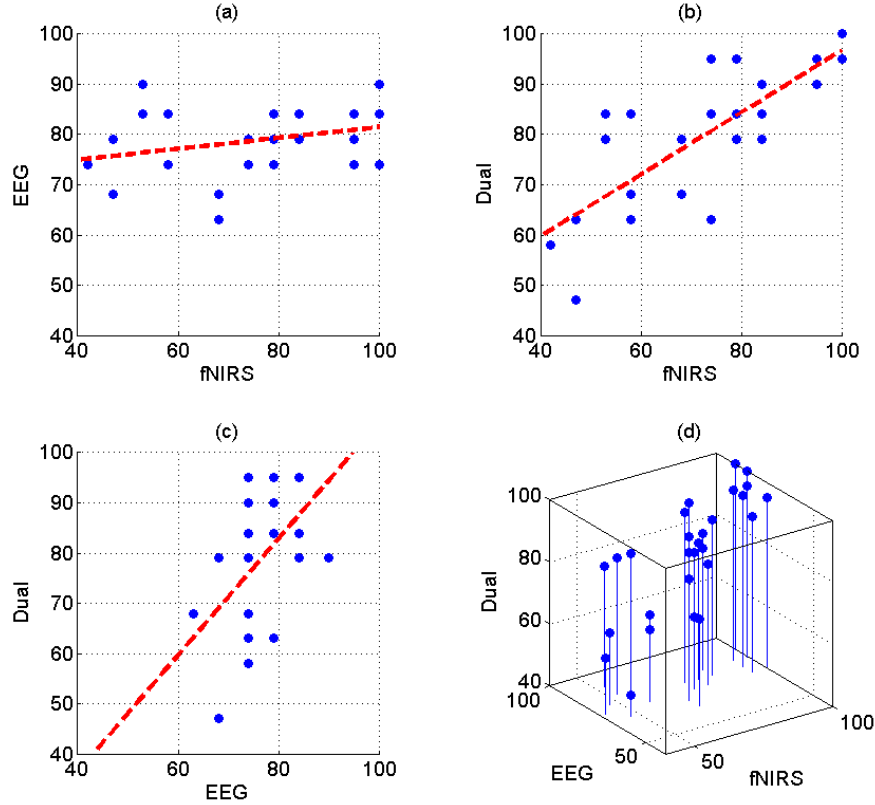


Figure 4.5: Scatter plots of hybrid fNIRS/EEG BCI classification accuracies. (a) fNIRS results compared to EEG results (b) fNIRS results compared to Dual results (c) EEG results compared to Dual results (d) 3D scatter plot of fNIRS, EEG and Dual results. Dashed red lines in (a), (b) and (c) are linear regressions of the data.

scenario.

The linear regressions of the 2-dimensional scatter plots of classification accuracies presented in Figure 4.5 (a)-(c) and the correlation coefficient results presented in Table 4.5 appear to support these observations that BCI classification accuracy based on either modality alone is improved by the inclusion of the other, particularly in the case of fNIRS. The low correlation coefficient between fNIRS and EEG results suggests that high fNIRS-based BCI performance does not predict high EEG-based BCI performance.

The implication of these results and analysis is that it appears that a hybrid fNIRS/EEG BCI may perform better than either an EEG or fNIRS BCI with similar channel density. Due to the low number of participants in this investigation, however,

4.3 Additional fNIRS Channels with EEG Incorporation

no conclusions may be drawn and this may motivate further investigation. Should the result hold following a more thorough investigation, it would appear that it's not *necessary* to include additional EEG or fNIRS sensors to a BCI system, and thus increase set-up time and likelihood of subject fatigue, to improve BCI performance. It may be possible that BCI performance is increased by either complementing an EEG BCI with fNIRS or by complementing an fNIRS BCI with EEG. This novel sensor design combines the advantages of EEG and fNIRS into one system to potentially improve BCI use experience for a stroke rehabilitation patient.

However, due to the compact cortical area interrogated by this hybrid module and the relatively low number of EEG channels, classification of stroke EEG may be difficult. EEG classification was based here on ERD/ERS features but EEG rehabilitation BCI typically uses a variation of the Common Spatial Patterns (CSP) algorithm (described in detail in subsection 6.3.3) which requires sampling of a wide areas of the head. The compact fNIRS sampling area also requires that the areas being interrogated will reliably respond haemodynamically. For stroke patients, the haemodynamic response may be significantly affected, rendering this compact fNIRS/EEG device unreliable. Recent hybrid fNIRS/EEG BCI studies by Yu et. al. [170], Liu et. al. [171] and Putze et. al. [172] have all employed full-head EEG and fNIRS measurement. While the current investigation into compact hybrid fNIRS/EEG certainly suggests that BCI performance can be improved, it may not be suitable for stroke rehabilitation BCI without further investigation.

4.3 Additional fNIRS Channels with EEG Incorporation

Channel	Subject A						Subject B					
	Trial 1			Trial 2			Trial 1			Trial 2		
	fNIRS	EEG	Comb.	fNIRS	EEG	Comb.	fNIRS	EEG	Comb.	fNIRS	EEG	Comb.
1	84%	79%	90%	100%	84%	95%	79%	84%	95%	79%	84%	84%
2	79%	79%	84%	95%	79%	95%	47%	79%	63%	53%	84%	84%
3	100%	74%	95%	100%	84%	100%	79%	74%	79%	84%	84%	84%
4	95%	84%	95%	84%	84%	79%	74%	74%	63%	53%	90%	79%
5	74%	74%	84%	42%	74%	58%	47%	68%	47%	74%	79%	95%
6	100%	90%	100%	95%	74%	90%	58%	74%	68%	79%	84%	79%
7	58%	84%	84%	68%	68%	79%	68%	63%	68%	58%	74%	63%
Average	84%	80%	90%	83%	78%	85%	65%	74%	69%	68%	83%	81%

Table 4.3: LDA classification results for fNIRS features only, EEG features only and combined fNIRS/EEG features.

4.3 Additional fNIRS Channels with EEG Incorporation

Subject	fNIRS	EEG	Dual
A	83.5%	79%	87.5%
B	66.5%	78.5%	75%
Average	75%	79%	81%

Table 4.4: Summary of classification results.

	fNIRS	EEG	Dual
fNIRS	1	0.293	0.800
EEG	0.293	1	0.559
Dual	0.800	0.559	1

Table 4.5: Pearson's r correlation coefficients of hybrid BCI classification accuracies.

4.4 Novel Spatial Imaging for Multichannel fNIRS

Coyle et. al.'s original fNIRS BCI employed a single fNIRS channel and thus a single spatial sampling point [158]. Increasing the number of fNIRS channels increases the number of spatial sampling points, which may be mapped on a two-dimensional plane. To make visual sense of spatially-sampled data, activity at non-sampled spatial locations may be approximated using any of a number of techniques. Previous attempts to construct a two-dimensional image of fNIRS activity have included linear interpolation [173] and a combination of nearest-neighbour and linear interpolation [174]. In contrast with these mathematically simple interpolation methods, the gold standard for fNIRS imaging uses a linear approximation to the photon diffusion equation [175], which is mathematically far more complex. Between these two extremes of spatial interpolation lie potentially useful techniques which if otherwise left unexplored may hinder future fNIRS BCI development.

One such unexplored interpolation method for fNIRS data is based on the Gaussian process (GP) model - a probabilistic, non-parametric black-box model. It differs from most other black-box modelling approaches in that it does not try to approximate the modelled system by fitting the parameters of selected basis functions but rather by searching for the statistical relationship among measured data. GP models are closely related to other machine learning approaches such as Support Vector Machines (SVM) and Relevance Vector Machines (RVM) and have been explored for various applications as a method for classification or regression and various interesting applications (e.g. medicine [176] and bioengineering [177]). In the field of geostatistics, GP regression models are used for probabilistic analysis of data and are more commonly known as 'Kriging'. Kriging has previously been used to interpolate MRI data [178] for 3D imaging of CT scans [179].

Here, a novel fNIRS imaging method based on GP model interpolation is investigated and compared to fNIRS imaging obtained through the photon diffusion equation method.

4.4.1 The Gaussian Process Model

The Gaussian process (GP) model is an example of the use of a flexible, probabilistic, non-parametric model with uncertainty predictions [180]. It fits naturally in the

4.4 Novel Spatial Imaging for Multichannel fNIRS

Bayesian modelling framework in which, instead of parameterising a mapping function $f(\mathbf{x})$, a prior is placed directly on the space of possible functions $f(\mathbf{x})$ which could represent the nonlinear mapping from input \mathbf{x} to output y . This prior represents the modeller's beliefs about the mapping, usually involving smoothness assumptions. This prior is combined with the likelihood of the identification (training) set of N observed input-output data pairs, $\{\mathbf{x}^i, y^i\}_{i=1}^N$, to provide the posterior distribution for model predictions, where $\mathbf{x}^i \in \mathbb{R}^D$ (such that \mathbf{X} is the $N \times D$ matrix of inputs) and $y^i \in \mathbb{R}$. The simplest type of prior over functions is the Gaussian one.

A Gaussian process is a Gaussian random function, fully characterized by its mean and covariance function. It can be viewed as a collection of random variables which have a joint multivariate Gaussian distribution where, for simplicity, it is assumed to be a zero-mean process $f(\mathbf{x}^1), \dots, f(\mathbf{x}^n) \sim \mathcal{N}(0, \mathbf{\Sigma})$, where $\Sigma_{pq} = C(\mathbf{x}^p, \mathbf{x}^q)$ is a function of the corresponding \mathbf{x}^p and \mathbf{x}^q which gives the covariance between $f(\mathbf{x}^p)$ and $f(\mathbf{x}^q)$. The covariance function, $C(., .)$, can be of any kind, provided that it generates a positive definite covariance matrix $\mathbf{\Sigma}$. Assuming a stationary process, where the covariance between two points depends only on the distance between them and is invariant to translation in the input space, a common choice of covariance function is

$$C(\mathbf{x}^p, \mathbf{x}^q) = v_1 \exp \left[-\frac{1}{2} \sum_{d=1}^D w_d (x_d^p - x_d^q)^2 \right] \quad (4.1)$$

where D is the input dimension and v_1, w_1, \dots, w_D are free parameters. Typically, covariance functions such as Equation 4.1 are chosen so that points closer together in the input space are more correlated than points farther apart (a smoothness assumption). The parameter v_1 controls the vertical scale of variation and the w_i 's are inversely proportional to the horizontal length-scale in dimension i ($\lambda_i = 1/\sqrt{w_i}$). Other forms of covariance functions not employed here are discussed elsewhere [180].

Let the input (target) relationship be $y = f(\mathbf{x}) + \epsilon$. Assuming an additive white noise with variance v_0 , $\epsilon \sim \mathcal{N}(0, v_0)$, a GP prior is put on $f(\cdot)$ with covariance function given by Equation 4.1 with unknown free parameters. Within this probabilistic framework, we have $y^1, \dots, y^n \sim \mathcal{N}(0, \mathbf{K}_{N+1})$ with $K_{N+1,pq} = \Sigma_{pq} + v_0 \delta_{pq}$, where $\delta_{pq} = 1$ if $p = q$, 0 otherwise.

Based on a set of N training data pairs, $\{\mathbf{x}^i, y^i\}_{i=1}^N$, the objective is to find the predictive distribution of y^* corresponding to a new given input \mathbf{x}^* . It is necessary to

4.4 Novel Spatial Imaging for Multichannel fNIRS

estimate the unknown parameters of the covariance function, v_1, w_1, \dots, w_D , as well as the noise variance v_0 . This is done via maximization of the log-likelihood

$$\log(p(\mathbf{y}|\mathbf{X})) = -\frac{1}{2} \log(|\mathbf{K}|) - \frac{1}{2} \mathbf{y}^T \mathbf{K}^{-1} \mathbf{y} - \frac{N}{2} \log(2\pi) \quad (4.2)$$

where Θ is the vector of parameters, $\Theta = [w_1 \dots w_D v_0 v_1]^T$ and \mathbf{K} is the $N \times N$ training covariance matrix.

The predictive distribution of y^* is $p(y^*|\mathbf{y}, \mathbf{X}, \mathbf{x}^*) = \frac{p(\mathbf{y}, y^*)}{p(\mathbf{y}|\mathbf{X})}$. It can be shown that this predictive distribution is Gaussian with mean and variance

$$\mu(\mathbf{x}^*) = \mathbf{k}(\mathbf{x}^*)^T \mathbf{K}^{-1} \mathbf{y} \quad (4.3)$$

$$\sigma^2(\mathbf{x}^*) = k(\mathbf{x}^*) - \mathbf{k}(\mathbf{x}^*)^T \mathbf{K}^{-1} \mathbf{k}(\mathbf{x}^*) \quad (4.4)$$

where $\mathbf{k}(\mathbf{x}^*) = [C(\mathbf{x}^1, \mathbf{x}^*), \dots, C(\mathbf{x}^N, \mathbf{x}^*)]^T$ is the $N \times 1$ vector of covariances between the test and training cases and $k(\mathbf{x}^*) = C(\mathbf{x}^*, \mathbf{x}^*)$ is the covariance between the test input and itself.

The vector $\mathbf{k}(\mathbf{x}^*)^T \mathbf{K}^{-1}$ can be interpreted as a vector of smoothing terms which weigh training outputs, \mathbf{y} , to make a prediction at the test point, \mathbf{x}^* . This is the reason why GP model predictions can be used for interpolation of missing data of the function of interest.

If the new input is far away from the data points, the term $\mathbf{k}(\mathbf{x}^*)^T \mathbf{K}^{-1} \mathbf{k}(\mathbf{x}^*)$ will be small and so $\sigma^2(\mathbf{x}^*)$ will be large. This indirectly also means that GP models are more suitable for interpolation of data than for extrapolation. Areas of the input space where there is little data, where the data has high complexity or where the data is noisy are highlighted through a high variance value at that interpolation point. This variance measure is not available through simpler interpolation methods and may prove useful in fNIRS spatial imaging.

4.4.2 GP Model fNIRS Imaging

The GP model described above was implemented in Matlab to process multichannel fNIRS data using Ramussen and Williams' Gaussian Processes for Machine Learning (GPML) code [181] and custom code. For a desired sample time of fNIRS data and for

4.4 Novel Spatial Imaging for Multichannel fNIRS

a desired field of interpolation points, the GP model calculates a two-dimensional array of Gaussian distributions with an estimated mean magnitude and estimated variance at each interpolation point. These two-dimensional arrays were then plotted to produce fNIRS spatial activity images.

GP interpolation requires that each fNIRS signal is assigned a precise spatial sample point. Although fNIRS signals are, in reality, affected by photon absorption along the full photon path between optode locations, the sample point is set at the midpoint between source and detector locations as this is where the photon path interrogates cortical tissue according to models [101]. The interpolation field is set to be a grid of size 20×20 .

4.4.3 HomER fNIRS Imaging

HomER (Hemodynamic Evoked Response) [182] is software for analysis and imaging of fNIRS signals, developed by The Center for Functional Neuroimaging Technologies [183] and the Martinos Center's Photon Migration Imaging Lab. The software, written in Matlab, is freely available online [184]. HomER utilises the Photon Migration Imaging (PMI) toolbox [185] to solve Diffuse Optical Imaging (DOI) forward and inverse problems, which can be used to produce images of spatially resolved hemodynamic responses. HomER is widely used in fNIRS research and is trusted to provide the highest available standard of fNIRS imaging.

For comparison of HomER imaging results to those obtained through GP model interpolation, the HomER interpolation field was also set to 20 points.

4.4.4 fNIRS Data Source

A sample 4-channel fNIRS data set included with HomER software was processed by both methods. This dataset was used because it features a large change in signal levels for Channel 1, little change for Channel 4 and a medium amount of change for Channel 2 and Channel 3. The time-course of HbO of each channel is shown in Figure 4.6. This explicit difference in responses of separate fNIRS channels facilitates easy comparison of resulting images between both fNIRS imaging methods.

The simulated source-detector layout for the data is shown in Figure 4.7. The layout consists of a single fNIRS light source at location A and four detectors at locations 1–4.

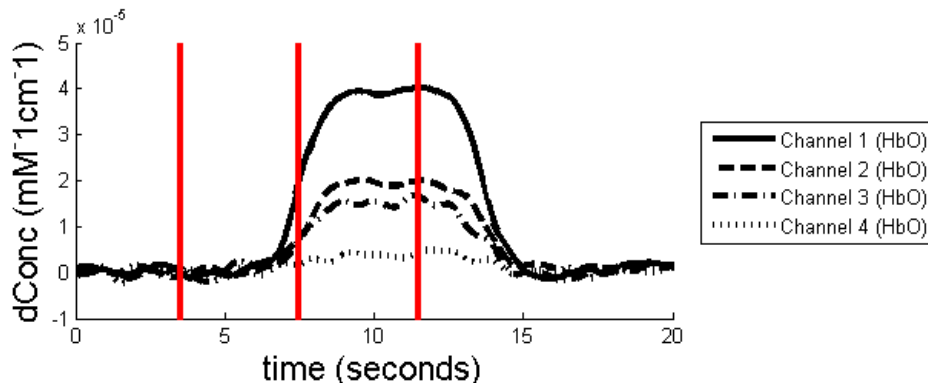


Figure 4.6: HbO signals following fNIRS processing. Red lines indicate image sample times at 3.5, 7.5 and 11.5 seconds for GP model interpolation and HomER.

The midpoint of each channel, which was also the spatial location of each channel, is indicated by a small red dot. The fNIRS light transmitted was at wavelengths of 690 nm and 830 nm. There are four paths of light for each detector and there are two wavelengths of light each, so the data set consists of eight signals. fNIRS signal processing steps described previously are applied to the raw 690 nm and 830 nm intensity signals to produce HbO and HbR delta concentration signals.

4.4.5 Analysis

Of the two available fNIRS signals from the sample 4-channel dataset, HbO was chosen over HbR for comparison between imaging methods as these signals exhibited greater amplitude changes. Both HomER and GP model-based interpolation were applied to the HbO data for comparison of fNIRS imaging output. GP model interpolation is unique in that it not only produces an interpolated magnitude map but also produces a variance map. The levels of variance at each interpolation point give an indication of how *reliable* the estimated magnitude value is at that point. This is a novel approach to fNIRS optical imaging and a novel application of GP models.

Three time samples, $t = 3.5s, 7.5s, 11.5s$ (indicated in Figure 4.6), were selected to compare imaging methods. GP model interpolation's two images (one for magnitude, one for variance) are used in conjunction to evaluate fNIRS activity and are compared to HomER's single image, for a given time sample. These time samples were selected

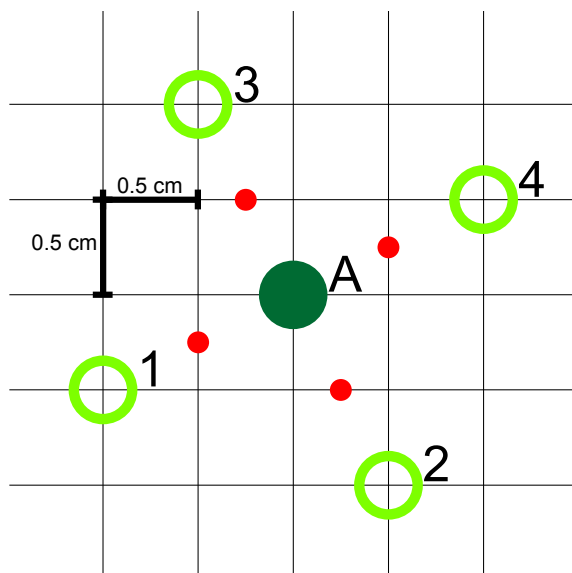


Figure 4.7: Spatial locations of sample data fNIRS light source (A), light detectors (open circles 1-4) and midpoints of each fNIRS channel (small circles).

because they contain three different levels of fNIRS activity.

4.4.6 Results

Output images of both methods are presented in Figure 4.8. (a)–(c) displays images produced by HomER at the three sample times, (d)–(f) displays images of GP model interpolation’s estimated magnitude values and (g)–(i) displays images of GP model interpolation’s estimated variance values. The red line of Figure 4.8 (h) and (i) is a contour of constant variance of 0.2×10^{-12} . All variances below this arbitrarily selected variance are shaded white, while variances above are shaded gradually from light grey to black.

From Figure 4.6 it is known that there is low HbO activity in all four channels at $t = 3.5s$. Accordingly, the HomER image (Figure 4.8 (a)) displays near-zero levels of activity. The corresponding GP model interpolation magnitude (“GP: Magnitude”) plot (Figure 4.8 (d)) similarly shows near-zero activity. The GP model interpolation variance (“GP: Variance”) plot (Figure 4.8 (g)) shows very low variance values for the entire image.

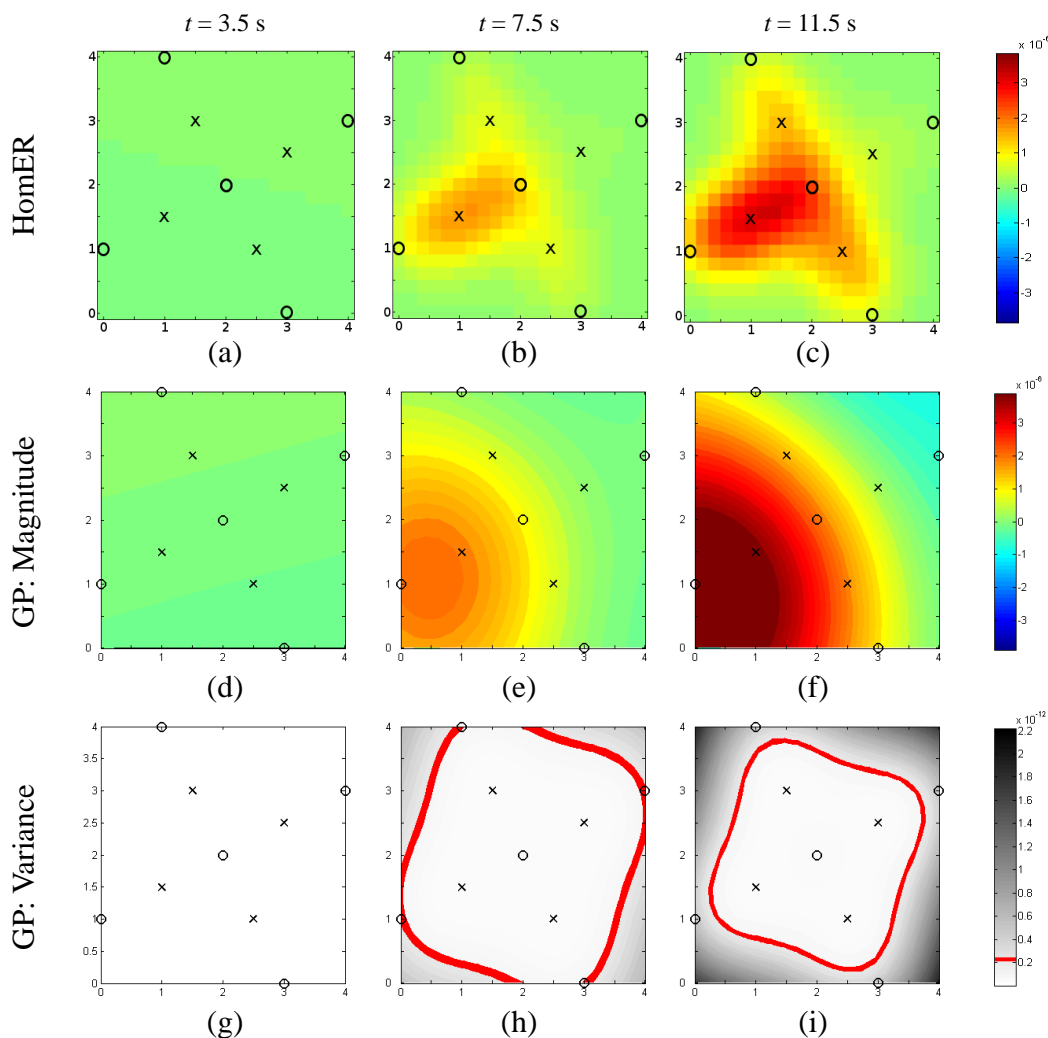


Figure 4.8: fNIRS optical imaging output from HomER and GP model interpolation.

At $t = 7.5$ s, there is increasing HbO signal activity, with highest signal level in Channel 1, slight increase in signal level in Channel 4 and the some increased signal level in Channel 2 and Channel 3. HomER's imaging of these signals (Figure 4.8 (b)) accordingly shows increased HbO activity along each channel path. GP: Magnitude (Figure 4.8 (e)) shows increased HbO signal levels in the region of Channel 1's sample point. GP: Variance (Figure 4.8 (h)) now shows increased variance values along some of the outer edge of the image.

4.4 Novel Spatial Imaging for Multichannel fNIRS

At $t = 11.5s$, HbO signals have reached their maximum value. HomER's imaging of the four channels of fNIRS activity (Figure 4.8 (c)) clearly depicts the highest signal value from Channel 1, the medium amplitudes for Channel 2 and Channel 3 and the small amplitude of Channel 4. The GP: Magnitude image (Figure 4.8 (f)) similarly depicts greatest signal amplitude in the direction of Channel 1, medium and similar amplitudes of Channel 2 and Channel 3, and the small amplitude of Channel 4. The GP: Variance image (Figure 4.8 (i)) indicates higher variance values than before around the outer edges of the image

4.4.7 Discussion

The viability of this novel GP model interpolation method for fNIRS imaging is evaluated by qualitative comparison to the current gold standard of fNIRS imaging, HomER. At $t = 3.5s$, there is little difference between HomER and GP images since all channels had near-zero amplitudes compared to the full magnitude scale. The little difference in signal magnitudes results in low GP variance values - indicating that GP model interpolation is very confident of the interpolated magnitude values obtained.

At $t = 7.5s$ and $11.5s$, differences in the images of both methods become more apparent. HomER's images depict fNIRS activity along the photon path of the channel, in accordance with models of photon migration which HomER uses. This results in an elongated shape of fNIRS activity with HomER fNIRS imaging. Of course, HomER, or any other fNIRS signal processing software, does not know exactly where HbO was concentrated along the photon path - it can only estimate according to the photon migration models. HomER fNIRS imaging makes an assumption that HbO concentration is equal along the photon path.

Similarly, HomER's images suggest reduced HbO activity at locations which do not lie along a photon path. For example, in Figure 4.8 (c), at the upper-left of the image, HomER suggests that there is no HbO activity in that region. HomER's fNIRS imaging suggests that there is no HbO response in that area with as much confidence as it suggests that there is a high level of HbO activity at the midpoint of Channel 1.

In contrast, since GP model interpolation does not use any photon path information, just like any other method that is based on interpolation and not photon migration models, it does not assume a lack of activity outside of the photon path. Instead, this

4.5 Accommodating fNIRS Research and Development

method assumes that activity in such regions is related to activity at the sample points. Although this is true for any interpolation method, GP model interpolation has the added advantage of the variance measure.

The GP variance images used in conjunction with the GP magnitude images present the “full picture” of GP model-estimated fNIRS activity. As Gaussian distribution variance increases, the images can inform the user of their reduced reliability, allowing the user to evaluate the images with more accuracy. HomER does not inform the user that areas outside of the photon path may be unreliable but GP model interpolation does. By only considering areas of GP: Magnitude that correspond with areas of GP: Variance with low variance, or within the red contour, GP model interpolation fNIRS imaging is qualitatively comparable to HomER.

The variance map is shown to be important for GP model interpolation. When there is little difference between fNIRS channel data, variances of interpolated Gaussian distributions are low and the variance map suggests that the user can trust the interpolated magnitude values. When the difference in magnitude between data sources increases, the variance of the mean magnitudes also increases. In the case of extrapolation, the variances can be very large. HomER remains the superior fNIRS imaging method, as it is based on knowledge of the physics of fNIRS operation - the photon migration model. By comparison, the mathematical models upon which GP-based interpolation is built do not describe the physical operation of fNIRS measurement. While GP-based imaging features the variance map which is not typical for an interpolation method, HomER is still a more physically accurate method for fNIRS imaging. Future work on GP-based fNIRS imaging may involve combining the variance map with the magnitude map and a more comprehensive comparison to existing fNIRS imaging methods. It has been shown here to be potentially useful and worth of further exploration.

4.5 Accommodating fNIRS Research and Development

In the introduction to their seminal fNIRS BCI paper, Coyle et. al. [158] noted that “At present the measurement of electrical activity from the brain, using electroencephalography (EEG) or electrocorticography (ECoG), is the favoured method for harnessing such [cognitive and motor] tasks for BCI development”. In the years since, this situation has not changed, as evidenced by the aforementioned publication counts of fNIRS

4.5 Accommodating fNIRS Research and Development

and EEG BCI research papers. The lack of access for researchers to fNIRS acquisition systems or to fNIRS data sets is likely a contributing factor to this relatively lower level of fNIRS research activity. EEG is an established brain signal acquisition method which can be low-cost and existing hardware can often be found in research settings and in clinical settings. Therefore, EEG is a very accessible signal acquisition method. fNIRS, however, is a relatively recent brain signal acquisition method. fNIRS hardware is relatively rare in research and clinical setting and is also relatively more expensive than EEG hardware, although far less expensive than fMRI or MEG.

Access to fNIRS data is therefore a concern for future fNIRS BCI development as potential researchers are prevented from developing fNIRS signal processing techniques and ultimately improving fNIRS BCI. One solution to this problem of lack of access to biomedical data is to simply make biomedical signal datasets freely available for anyone to access. The website PhysioNet [186] provides such a service, offering datasets of a wide range measurement modalities for free download, such as EEG, ECG, EMG, respiration, electrodermal activity (previously known as galvanic skin response) and many others. Currently, however, there is only one fNIRS dataset available, which comes with EEG data recorded by Dr. Kevin Sweeney for an investigation into artefact removal techniques [116, 187]. Therefore, fNIRS signal datasets are generally not accessible without a direct request to a fNIRS researcher for their recorded data or access to fNIRS hardware.

A secondary solution to the lack of access to biomedical datasets lies in synthetic data - signals produced in software to replicate real signals. Synthetic biosignal generation has been investigated for modalities such as foetal phonocardiographic (fPCG) recordings [188], EMG [189], ECG [190] and magnetoencephalography (MEG) [191]. This section describes the development of the first fNIRS synthetic signal generation algorithm. The success of this fNIRS synthetic signal generation process is evaluated by comparing synthetic fNIRS to real fNIRS.

4.5.1 Real fNIRS Data

Development of synthetic fNIRS data was based in part on real fNIRS data. This real data, representative of typical fNIRS signals, guided model design for generating synthetic data. This fNIRS data was recorded using a TechEn CW6 system (TechEn

4.5 Accommodating fNIRS Research and Development

Inc., USA), which used 690 nm and 830 nm wavelength light and sampled data at a sample rate of 25 Hz.

During fNIRS data recording, the subject was seated in a comfortable chair in front of a computer monitor and followed instructions on a screen in front of them to engage in a finger-tapping experimental protocol. 7 channels of fNIRS data were recorded from the subject's motor cortex contralateral to hand activity. The fNIRS channel that was most easily classifiable following fNIRS signal processing, feature extraction and classification was selected to guide the design of synthetic fNIRS signal generation. Specifically, this selected fNIRS channel sampled location C3 of the 10-20 system.

Additionally, a "shallow" fNIRS channel was recorded, with source-detector separation of 1.5 cm. Due to this lower source-detector separation, the photon path of this fNIRS channel passed only through the skin and did not interrogate the cortex. Therefore, raw light intensity of this channel was modulated only by haemoglobin in the superficial layers. This signal contains undesired interference which affects normal fNIRS recordings and is used to model this interference.

4.5.2 Synthetic Data Process

A hybrid model of the fNIRS signal process, consisting of a physiological model of the vascular response together with a spectrophotometric model relating haemodynamics to optical properties, was developed to generate synthetic data. A typical fNIRS optical intensity measurement contains the cortical haemodynamic response signal of interest buried in the much stronger natural interference and noise components. The data generated by this algorithm is controlled by hand-tuned parameters, which control various amplitudes and frequencies of the fNIRS signal components. While these parameters are currently hand-tuned, a future version may produce parameters based on analysis of a real fNIRS dataset, possibly optimising the parameters to closely match the real data. The algorithm discussed here, however, simply used parameters set by the user.

Light emitted into the scalp passes through the superficial layers before and after passing through the cortex [101]. These superficial layers contain blood vessels, which affect the intensity of the transmitted light. The largest components of the superficial signal are due to the cardiac cycle and low-frequency oscillations known as *Mayer*

4.5 Accommodating fNIRS Research and Development

waves [107, 108]. fNIRS measurement also contains broadband noise arising from environmental optical background and instrumental noise. fNIRS light intensity measurements have an associated offset due to non-varying aspects of the recording channel such as skull thickness, skin thickness, hair and source-detector separation. Synthetic raw intensity signals are therefore modelled as a sum of these separate components:

$$\Phi_s^\lambda(t) = \Phi_b^\lambda(t) + \Phi_c^\lambda(t) + \Phi_m^\lambda(t) + \Phi_n^\lambda(t) + \Phi_o^\lambda \quad (4.5)$$

where $\Phi_s^\lambda(t)$ is the synthetic intensity signal for a given wavelength λ , $\Phi_b^\lambda(t)$ is the raw intensity component as a result of the physiological response of interest, $\Phi_c^\lambda(t)$ is the cardiac pulse component, $\Phi_m^\lambda(t)$ is the Mayer wave component, $\Phi_n^\lambda(t)$ is the broadband noise component and Φ_o^λ is the offset.

4.5.2.1 Balloon Model Simulation

The haemodynamic response to activation is the primary component of the fNIRS model. The Balloon model [192, 193] is a biomechanical model of haemodynamic activity at the neuronal level in the cortex during activation. This is a well-known neurophysiological dynamics model linking mental state of haemodynamics and is defined by a differential equation [194] as

$$E(t) = 1 - (1 - E_0)^{\frac{1}{f_{in}(t)}} \quad (4.6)$$

$$\dot{q}(t) = \frac{f_{in}(t)}{\tau_0} \left[\frac{E(t)}{E_0} - \frac{q(t)}{v(t)} \right] + \frac{1}{\tau_v} [f_{in}(t) - v^{\frac{1}{\alpha}}] \frac{q(t)}{v(t)} \quad (4.7)$$

$$\dot{v}(t) = \frac{1}{\tau_v} [f_{in}(t) - v^{\frac{1}{\alpha}}] \quad (4.8)$$

$$\dot{p}(t) = \frac{1}{\tau_v} [f_{in}(t) - v^{\frac{1}{\alpha}}] \frac{p(t)}{v(t)} \quad (4.9)$$

where E , q , v and p denote oxygen extraction factor, normalised deoxygenated haemoglobin concentration ($\Delta c_{HbR}(t)$), normalised blood volume and normalised total haemoglobin concentration respectively. Normalised oxygenated haemoglobin concentration ($\Delta c_{HbO}(t)$) is obtained by subtracting q from p . The $f_{in}(t)$ waveform (blood flow into the ‘‘balloon’’) is specified by the user and normally reflects the stimulation sequence.

4.5 Accommodating fNIRS Research and Development

Other parameter values of the Balloon model are: $E_0 = 0.4$, $\tau_0 = 2$, $\tau_v = 30$ and $\alpha = 0.4$, similar to [194]. Non-normalised values of concentration can't be found without knowledge of initial concentrations or sample volume. The signals ($\Delta c_{HbR}(t)$) and ($\Delta c_{HbO}(t)$) are therefore scaled to an amplitude similar to real data before further processing.

4.5.2.2 Conversion to Raw Intensity Signals

Following generation of modelled ideal HbO and HbR concentration signals ($\Delta c_{HbO}(t)$ and $\Delta c_{HbR}(t)$), typical fNIRS signal processing steps are then carried out *in reverse order* to obtain corresponding ideal raw intensity signals. The first step of this reverse process is to utilise the Modified Beer-Lambert law to obtain modelled Optical Density signals:

$$\Delta A_b^\lambda(t) = (\varepsilon_{HbR}^\lambda \Delta c_{HbR}(t) + \varepsilon_{HbO}^\lambda \Delta c_{HbO}(t))BL \quad (4.10)$$

where $\Delta A_b^\lambda(t)$ is Optical Density signal of a wavelength (Absorbance Units (AU)), $\varepsilon_{HbR}^\lambda$ and $\varepsilon_{HbO}^\lambda$ are the molar extinction coefficients of HbR and HbO for a particular wavelength ($cm^{-1} mol^{-1} l$), $\Delta c_{HbR}(t)$ and $\Delta c_{HbO}(t)$ are the changes in concentration of HbR and HbO ($mol l^{-1}$), B is the differential pathlength factor (unitless) and L is source-detector separation (cm). Values for ε have been tabulated for a wide range of wavelengths [195].

Obtaining an approximation of the raw intensity signal ($\Phi_b^\lambda(t)$) requires an exponential function (described in [182]):

$$\Phi_b^\lambda(t) = exp(-\Delta A_b^\lambda(t)) \quad (4.11)$$

Simulation of Equation 4.9 to Equation 4.11 produces an ideal raw intensity measurement during activation. Interference, noise and offset are then added to this signal to replicate real-world fNIRS raw intensity measurements. Figure 4.9 shows the signal types from the Balloon model of haemodynamic response, to the scaled response, to optical density signals, to raw light intensity signals.

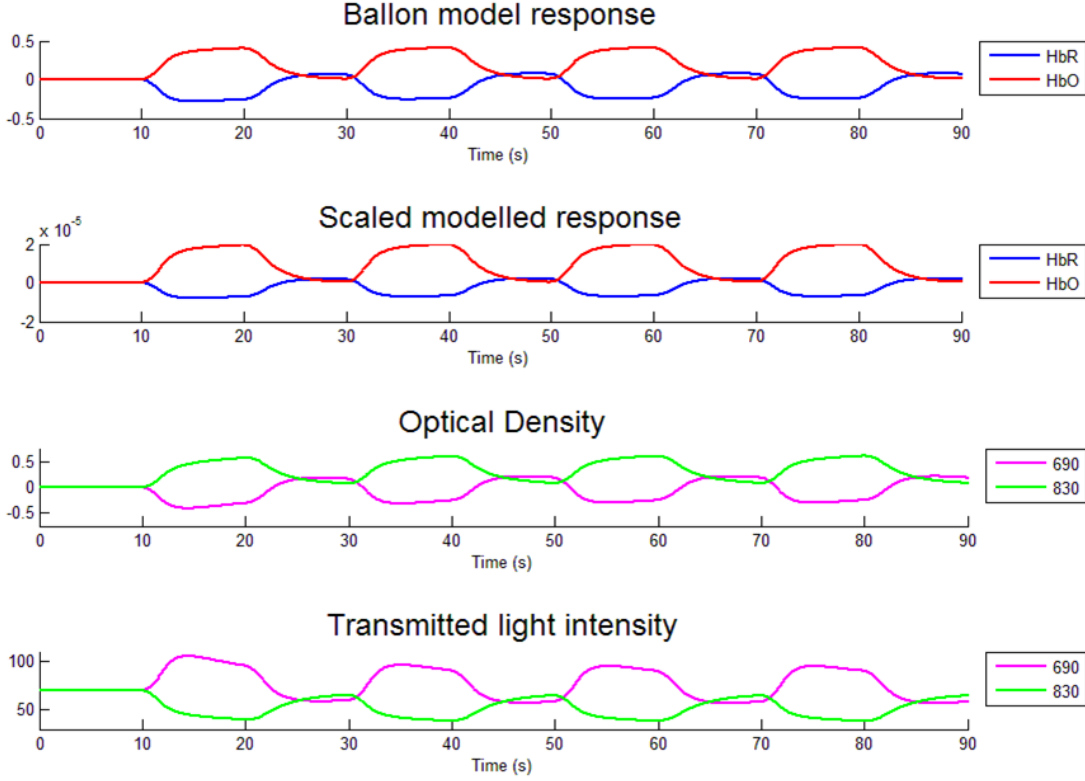


Figure 4.9: Signals at each stage of production of transmitted light intensity from ideal haemodynamic response.

4.5.2.3 Cardiac Interference

Cardiac cycle interference is modelled as a function approximating the observed cardiac signal component of the “shallow” fNIRS intensity signals as

$$\Phi_c^\lambda(t) = K_c^\lambda f(k(t), R(t)) \quad (4.12)$$

where Φ_c^λ is the cardiac pulse interference for a given wavelength, K_c^λ is the amplitude of the cardiac interference, $k(t)$ is a piecewise linear model of a single cardiac pulse and $R(t)$ is a time-varying heart rate signal. $f(\cdot)$ is the low-pass filtered, non-linear, unity-amplitude, cardiac interference signal which is identical for all wavelengths. Figure 4.11 displays a section of this cardiac component of intensity signal interference for both wavelengths.

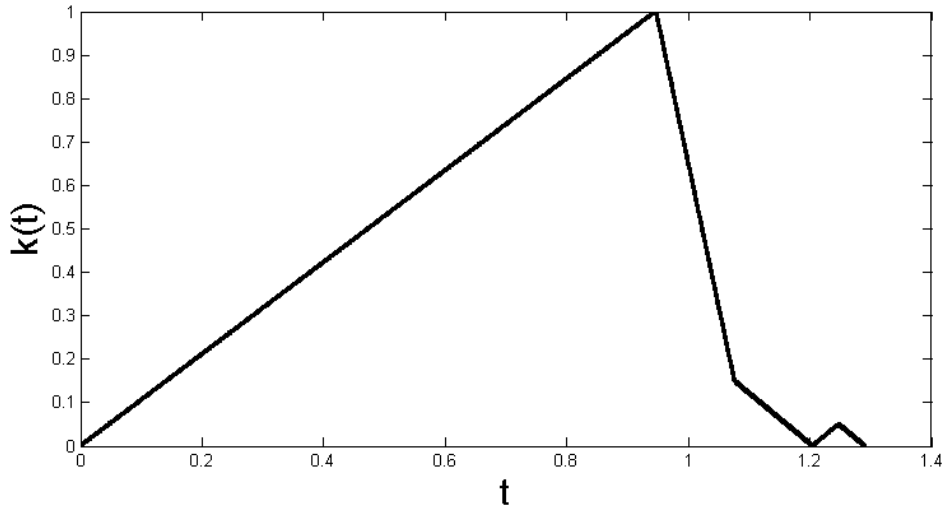


Figure 4.10: Piecewise-linear model of a single cardiac pulse component.

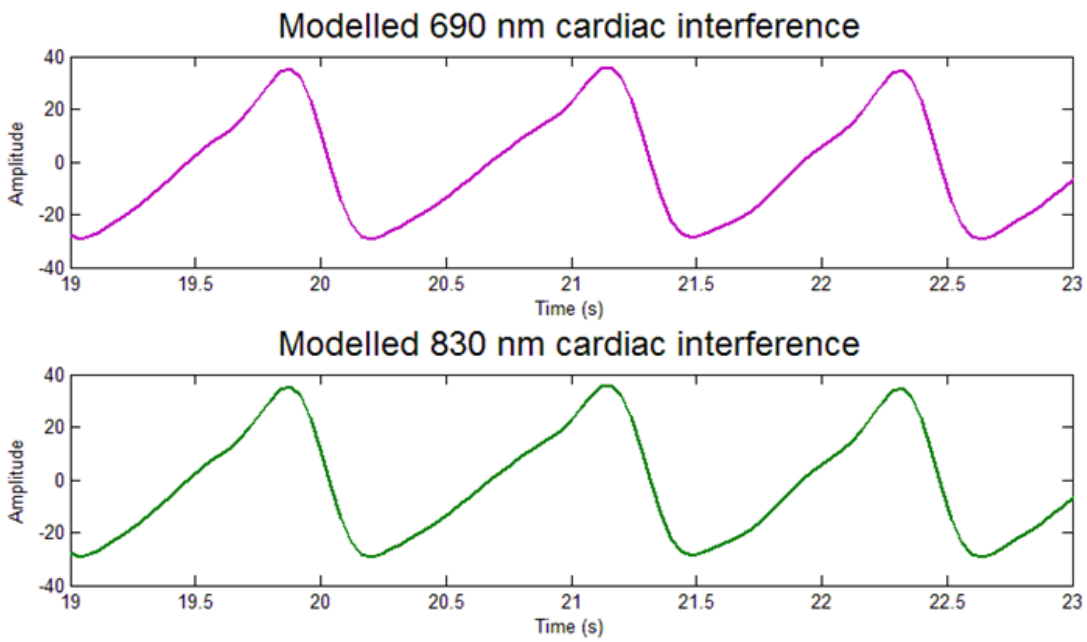


Figure 4.11: Section of cardiac component of intensity signal interference.

4.5.2.4 Mayer Wave Interference

Mayer waves are spontaneous changes in arterial blood pressure, oscillating at a frequency near 0.1 Hz in most subjects [108]. Mayer wave interference impacts fNIRS

4.5 Accommodating fNIRS Research and Development

measurements similarly to cardiac interference. The Mayer wave is modelled as a low-frequency sinusoidal oscillation with time-varying frequency, similar to Coyle et. al.[196], as

$$\Phi_m^\lambda(t) = K_m^\lambda \sin(2\pi f_m t + \theta_m) \quad (4.13)$$

where $\Phi_m^\lambda(t)$ is the Mayer wave interference for a specific wavelength, K_m^λ is the amplitude of the interference, f_m is the time-varying frequency of the Mayer wave and θ_m is random phase shift. Figure 4.12 shows a section of Mayer wave interference signal for both wavelengths.

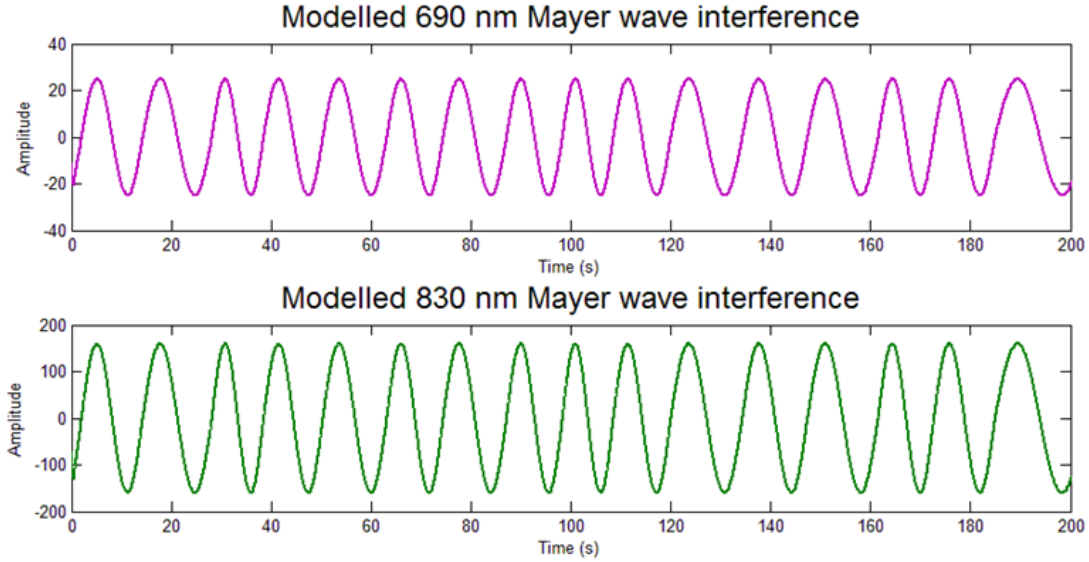


Figure 4.12: Section of Mayer wave component of intensity signal interference.

4.5.2.5 Noise Interference

An fNIRS system records broadband noise due to environmental optical background noise and instrumental noise. Based on observations of real fNIRS data, this interference is modelled as a normally distributed random noise signal as

$$\Phi_n^\lambda(t) = N(0, (\sigma_n^\lambda)^2)$$

4.5 Accommodating fNIRS Research and Development

where Φ_n^λ is the noise signal for a wavelength and σ_n^λ is the standard deviation of the normal distribution, which is manually set before processing.

4.5.2.6 Offset

Raw light intensity measurements have an associated offset due to non-time-varying aspects of the transmission medium of an fNIRS recording channel such as skin thickness, skull thickness, hair follicles and source-detector separation. Values of offset (Φ_o^λ) are wavelength-dependant and are manually set before processing.

4.5.3 Generating Synthetic Data

The fNIRS signal model was implemented in Matlab to generate synthetic fNIRS data. Multiple parameters of the model, such as offset or noise amplitude, are set before generating any data. These parameter values may be manually set to replicate a wide range of signals. To test the effectiveness of this model, parameter values were chosen based on the real fNIRS signals and then fine tuned to attempt to match that real data. The synthetic data is compared visually to the real data.

The Balloon model produces individual ideal HbO and HbR activation responses. For this, blood in-flow, $f_{in}(t)$, is modelled as a trapezoid with a rise time of 5 seconds, plateau time of 5 seconds, fall time of 5 seconds, rest time of 5 seconds and a plateau height of 1.7 for a 10 second active period followed by a 10 second rest period. This is then repeated to match the number of active and rest periods of the real fNIRS data and thus produce ideal HbO and HbR signals.

The HbO signal is scaled to an amplitude of $2e^{-5}$ and HbR is scaled to an amplitude of $0.8e^{-5}$. The real fNIRS signals use light of wavelengths 690 nm and 830 nm so the corresponding ideal Optical Density signals for these wavelengths is obtained using the modified Beer-Lambert law. For this, the differential path-length factor (DPF), B , is set to 5.93 in accordance with [195] and source-detector separation, L , is set to 3 cm, as this is the source-detector separation of the real fNIRS signals. The ideal raw intensity signals, $\Phi_b^{690}(t)$ and $\Phi_b^{830}(t)$ are then calculated from the ideal Optical Density signals.

To generate the cardiac interference intensity signals, $\Phi_c^{690}(t)$ and $\Phi_c^{830}(t)$, cardiac signal amplitudes, K_c^{690} and K_c^{830} , are set to 70 and 700 respectively and the normally-distributed heart rate parameter is set as $R(t) = N(52, 5)$. To generate the Mayer

4.5 Accommodating fNIRS Research and Development

wave interference intensity signals, $\Phi_m^{690}(t)$ and $\Phi_m^{830}(t)$, Mayer wave amplitudes, A_m^{690} and A_m^{830} , are set to 25 and 160 respectively and the normally-distributed oscillation frequency is set as $f_m = N(0.08, 0.01)\text{Hz}$. Noise signals, $\Phi_n^{690}(t)$ and $\Phi_n^{830}(t)$, have standard deviations σ_n^{690} and σ_n^{830} , set to 199.5. Finally, offset of the raw intensity signals is set to match the average amplitude of the real data, so $\Phi_o^{690} = 8053$ and $\Phi_o^{830} = 33124$.

Synthetic raw intensity signals which attempt to replicate a set of real fNIRS signals are then generated by summing together each of these components, as in Equation 4.5. At this point, the synthetic data can be compared visually to the real data. The haemodynamic response of interest, however, is not easily seen in the raw intensity signals. To observe this component, the synthetic signals undergo the same fNIRS signal processing steps as a real fNIRS recording and individual responses are averaged.

4.5.4 Results

Following generation of synthetic fNIRS raw intensity signals, comparison to real fNIRS raw intensity signals is first carried out by visual comparison of the temporal and spectral signal content. The full time-course of both real and synthetic transmitted light intensity signals is presented in Figure 4.13.

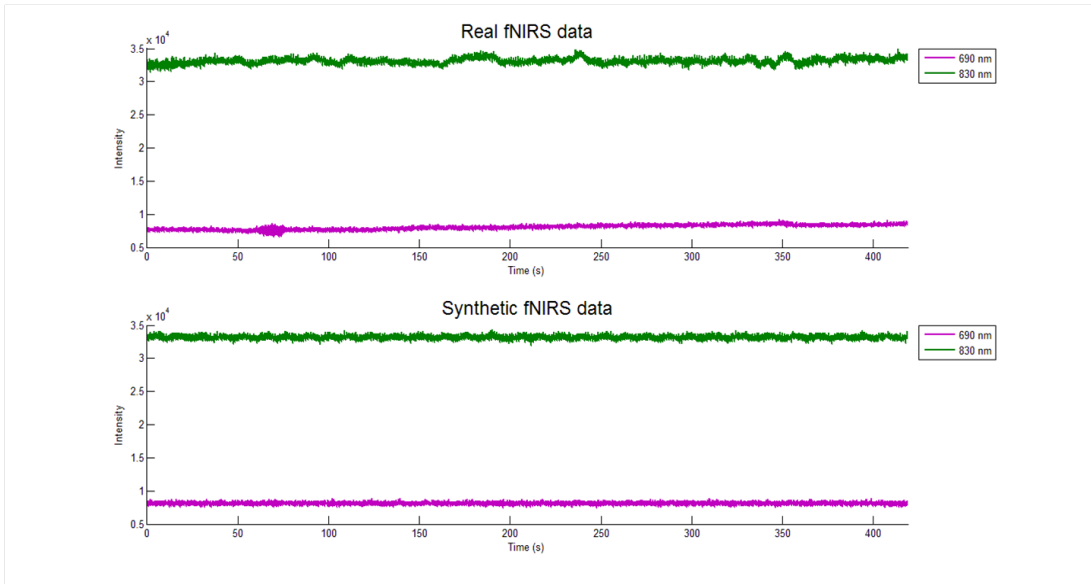


Figure 4.13: Entire real and synthetic fNIRS signals, highlighting signal offsets.

4.5 Accommodating fNIRS Research and Development

Presented in Figure 4.14 is a comparison of a 20-second section of the real and synthetic 690 nm and 830 nm intensity temporal signals. Presented in Figure 4.15 is a comparison of the spectral content of the real and synthetic 690 nm and 830 nm intensity signals with offset removed for clarity. Presented in Figure 4.16 are the processed modelled HbO and HbR responses for active and rest events along with average responses.

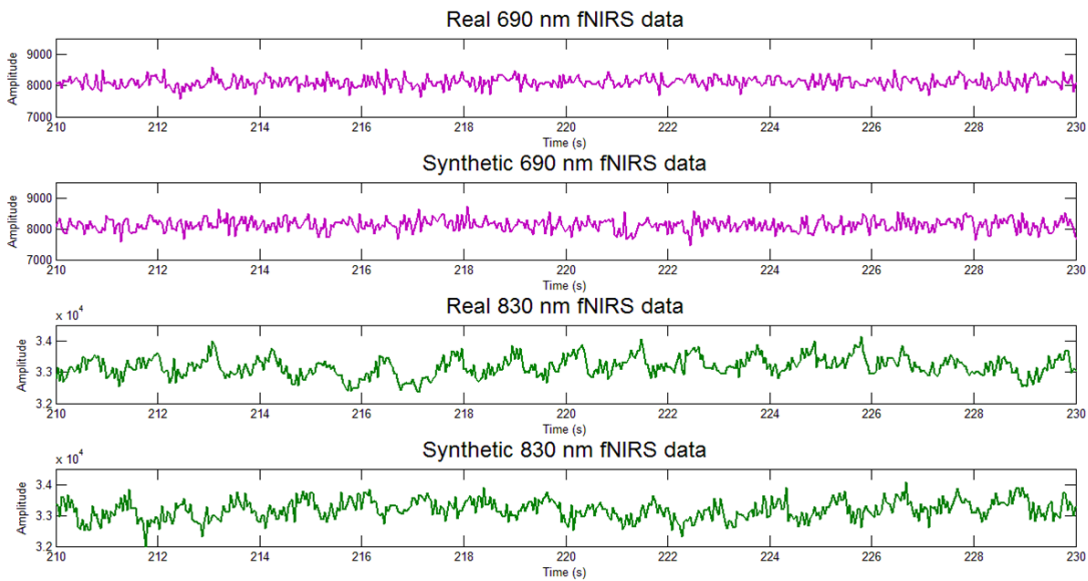


Figure 4.14: 20 second time-course of real and synthetic transmitted light intensity signals.

The real and synthetic 690 nm and 830 nm signals may also be compared quantitatively with statistics, as presented in Table 4.6. The values of this table have been rounded for clarity.

4.5.5 Discussion

A visual comparison of the synthetic and real fNIRS raw intensity temporal signals in Figure 4.14 shows that the synthetically generated signals are temporally similar to the real signals. The synthetic 830 nm signal is more obviously similar to the real signal, as the cardiac and noise components are clearly evident. The low-frequency Mayer wave component is also evident, although this component of the real and synthetic signals are out of phase. For the 690 nm signals, a visual comparison is more difficult as the

4.5 Accommodating fNIRS Research and Development

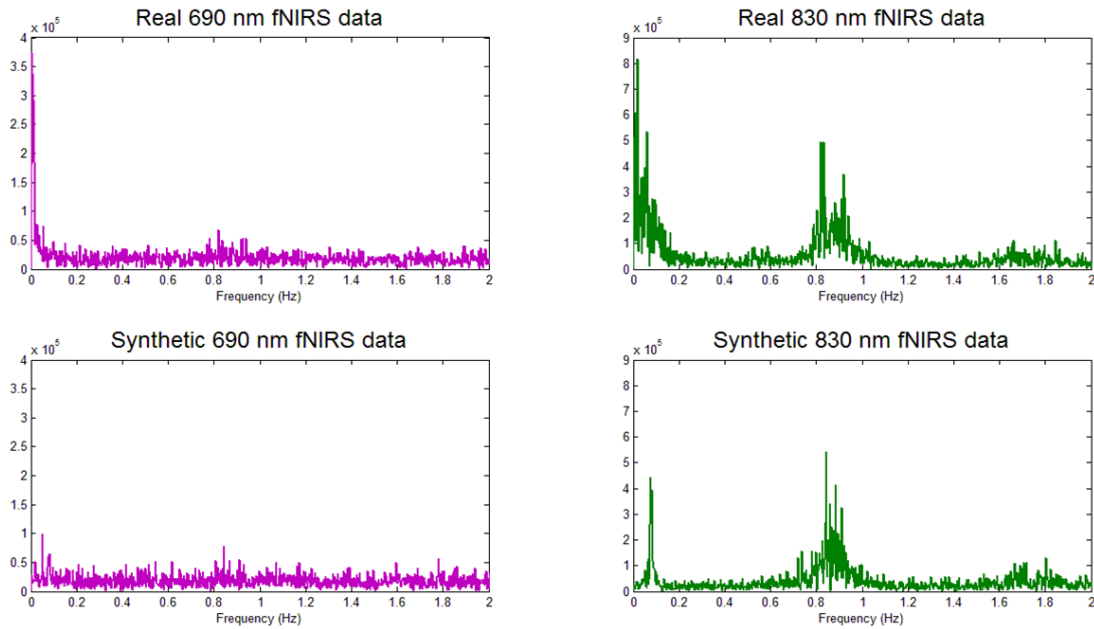


Figure 4.15: Spectral content of real and synthetic transmitted light intensity signals.

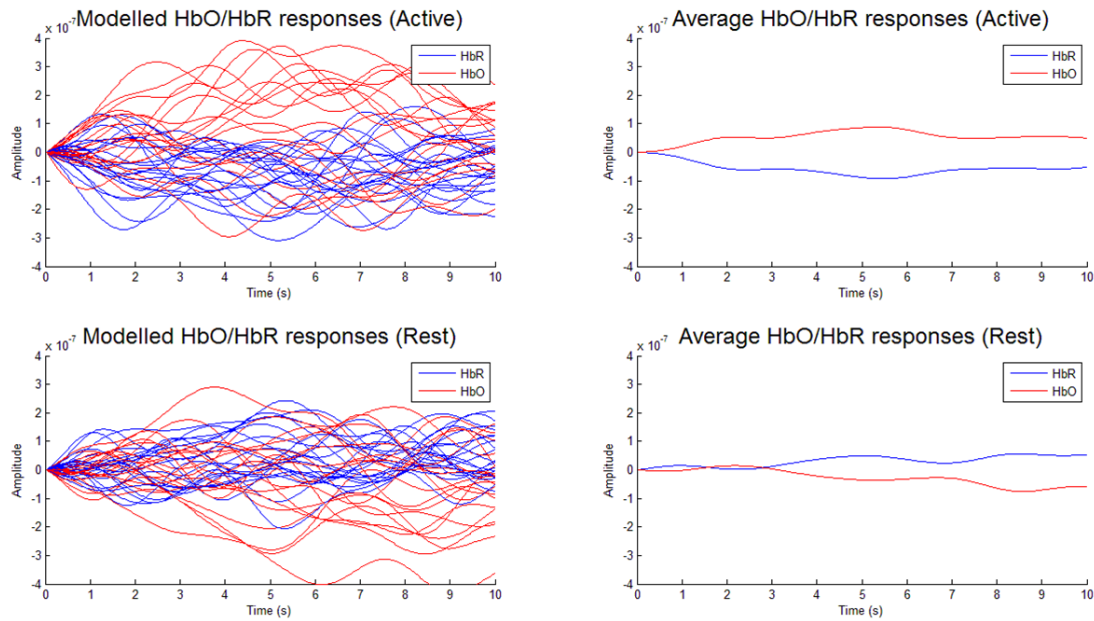


Figure 4.16: Synthetic fNIRS individual and average haemodynamic responses during rest and activity.

4.5 Accommodating fNIRS Research and Development

	nm	Real	Synthetic
Mean	690	8053	8128
	830	33124	33177
Standard Deviation	690	385	200
	830	476	307
Covariance(690 nm, 830 nm)		$\begin{bmatrix} 148520 & 42240 \\ 42240 & 226325 \end{bmatrix}$	$\begin{bmatrix} 40129 & 5559 \\ 5559 & 94486 \end{bmatrix}$

Table 4.6: Statistics (rounded) of real and synthetic 690 nm and 830 nm signals.

dominating component of the real signal is the noise component. The synthetic 690 nm signal also does not clearly show a cardiac or Mayer wave component and so is only temporally similar in this lack of evident signal component.

A visual comparison of the spectral components of real and synthetic fNIRS raw intensity signals in Figure 4.15 reveals similar similarities. The real 690 nm signal is again dominated by noise with the Mayer and cardiac components relatively miniscule. The synthetic 830 nm signal displays components that are evident in the real signal - particularly the cardiac component between 0.7 and 1.1 Hz. The haemodynamic response of interest has a spectral response between 0.5 - 0.6 Hz but is almost indiscernible from noise in the real 830 nm signal.

The largest difference between the real and synthetic 830 nm signals is at the low-frequency end of the spectrum - below 0.2 Hz. The variable low-frequency Mayer-wave component of the synthetic signal is evident around 0.1 Hz however the Mayer wave component of the real signal is obscured by other low-frequency and near-DC components. These low-frequency and near-DC component of the real signal are from no known physiological source and so are not included in the model.

An interesting aspect of synthetic fNIRS data generation is the flexibility when constructing the data - each parameter of the model can be fine-tuned to replicate a real fNIRS signal. Similarly, any component of the model can be generated in isolation or excluded entirely from the final signal. The statistical comparison of the real and synthetic raw intensity signals in Table 4.6 is useful in guiding the design of a synthetic fNIRS dataset. It should be noted that different real fNIRS signals may have very

different statistics and so the comparison in this table should only be seen as a point of interest rather than as a measure of the success of the synthetic data generation algorithm. One possible future expansion of this algorithm may be to use summary statistics, such as those in Table 4.6 to optimise parameters of the algorithm, to attempt to generate a synthetic dataset which matches a sample real dataset as closely as possible.

A possible expansion for this model is to randomly produce model parameters, producing any number of fNIRS datasets with unknown model parameters - potentially useful for investigating and testing fNIRS signal processing techniques. Additionally, other components such as the cardiac pulse component model of the Balloon model could be replaced as desired. Certain model parameters which are assumed to remain constant could be variable. For example, movement artefact could be modelled through adjustment of the DPF or source-detector separation parameters.

This synthetic fNIRS algorithm allows interested researchers to generate limitless realistic synthetic fNIRS data without access to real fNIRS data or an fNIRS measurement system. Synthetic fNIRS data could be useful for development of signal processing techniques or potentially as a learning tool. In any case, this algorithm allows for future fNIRS research and may ultimately lead to significant progress in fNIRS BCI design.

4.6 Summary

This chapter highlighted a number of issues with rehabilitation BCI systems and provided solutions to those problems. The single fNIRS channel ‘Mindswitch’ BCI was improved upon with the addition of more fNIRS channels and incorporation of EEG to form a hybrid BCI. This hybrid BCI measured spatial haemodynamic activity and so a novel fNIRS imaging method based on GP-model interpolation was presented. As researchers who may be interested in fNIRS measurement may not have access to fNIRS hardware or to fNIRS datasets, a synthetic fNIRS data generation algorithm was developed to aid research but also exists as an educational tool.

These solutions together represent improvements to rehabilitation BCI as a whole. However, each of these solutions were explored using exclusively healthy subjects. To investigate more meaningful and critical rehabilitation BCI improvements, brain activity of stroke patients must be recorded and analysed.

Chapter 5

Healthy and Stroke-Affected Brain Activity

5.1 Introduction

Previous chapters have demonstrated how a biofeedback BCI for stroke rehabilitation can be developed for use by healthy subjects who exhibit normal, healthy brain activity. While development of BCIs for healthy brain activity is acceptable for communication and control BCI, it is not appropriate for stroke rehabilitation BCI due to the effects that the stroke has on brain activity patterns. As a stroke causes physical damage to the brain, patterns of brain activity and patterns of interaction are adversely affected, resulting in abnormal brain activity and abnormal signals recorded through EEG, fNIRS or any other measurement modality.

Previous fMRI and PET studies have revealed the effect of stroke on patterns of brain activity related to motor execution. Further fMRI and EEG studies have investigated the effect of stroke on brain networks. If a rehabilitation BCI is based on a measurement modality which is affected by the subject's stroke, then the manifestation of these effects in the recorded signals must be explored and understood in order to design more effective rehabilitation BCIs. As such an exploration requires analysis of both healthy and stroke-affected brain activity data, experimental recordings must be performed.

This chapter discusses the known effects of stroke on brain activity, as revealed through fMRI, PET and EEG studies. While fMRI and PET are inappropriate measurement modalities for portable rehabilitation BCI, they produce highly accurate three-dimensional measurement data of brain activity and so are important for learning about the effects of stroke. Information from such studies may then be used to guide rehabilitation BCI design with other measurement modalities. Following this is a description of experimental recording sessions conducted with both healthy subjects and stroke patients. EEG was recorded while the subjects performed a finger-tapping task. Qualitative comparisons between healthy and stroke-affected EEG are made to attempt to reveal unique aspects of stroke-affected EEG which may inform future rehabilitation BCI design.

5.2 Effects of Stroke on Brain Activity

The effects of stroke on the functional operation of the brain have been investigated previously with various high-accuracy measurement modalities. Chollet et. al. [197] conducted a study using Positron Emission Tomography (PET) to measure regional cerebral blood flow (rCBF) in six first-time hemiplegic stroke patients. As a result of stroke, subjects had experienced unilateral upper-limb paralysis for at least two days before recovery of motor function. For each subject, six PET scans in total were conducted with two scans per each of three different conditions: subject at rest, finger movement of the previously-paralysed hand and finger movement of the unaffected hand.

Compared to rest, finger movement of the unaffected hand resulted in significantly increased rCBF in the contralateral sensorimotor cortex (+24.4%), ipsilateral cerebellar hemisphere (+14.0%), contralateral premotor cortex (+18.4%), contralateral supplementary motor area (+9.2%) and ipsilateral supplementary motor area (+7.1%). Compared to rest, finger movement of the previously-paralysed hand resulted in significantly increased rCBF in the contralateral sensorimotor cortex (+23.0%), ipsilateral sensorimotor cortex (+10.1%), contralateral cerebellar hemisphere (+10.0%), ipsilateral cerebellar hemisphere (+14.8%), contralateral premotor cortex (+12.6%), ipsilateral premotor cortex (+9.5%), contralateral supplementary motor area (+9.8%) and ipsilateral supplementary motor area (+7.9%). Significantly increased rCBF was also

5.2 Effects of Stroke on Brain Activity

observed bilaterally in the insular cortex and inferior parietal cortex during finger movement of the previously-paralysed hand, which was not observed during movement of the unaffected hand. A summary of these rCBF results is presented in Table 5.1.

Location	Stroke-affected hand	Unaffected hand
Contralateral Sensorimotor Cortex	+23.0%	+24.4%
Ipsilateral Sensorimotor Cortex	+10.1%	
Contralateral Cerebellar Hemisphere	+10.0%	
Ipsilateral Cerebellar Hemisphere	+14.8%	+14.0%
Contralateral Premotor Cortex	+12.6%	+18.4%
Ipsilateral Premotor Cortex	+9.5%	
Contralateral Supplementary Motor Area	+9.8%	+9.2%
Ipsilateral Supplementary Motor Area	+7.9%	+7.1%

Table 5.1: Significant changes in stroke subject rCBF during finger movement compared to rest, as determined by Chollet et. al.

Of these results, increased ipsilateral sensorimotor cortex rCBF during stroke-affected hand movement is most interesting as it demonstrates that the stroke subjects had recovered motor function through recruitment of that area for motor recovery, as suggested by the authors. The authors also conclude that various regions of the brain involved in motor action, such as the inferior parietal cortex, premotor cortex, primary motor cortex and insula, may represent a route for activation of the ipsilateral motor cortex. The authors summarise that cerebral motor regions behave primarily unilaterally but can respond bilaterally to compensate for damage.

Similar results were found by Weiller et al. [198] who used PET to measure rCBF in 10 healthy control subjects and 10 stroke patients during the same three conditions. Stroke-affected hand movement produced similar significantly higher rCBF in contralateral motor areas and ipsilateral cerebellum as hand movement of control subjects. Compared to control subjects, stroke-affected hand movement also produced significantly higher rCBF in ipsilateral premotor cortex, contralateral cerebellar hemisphere and bilateral insular cortex, as found by Chollet et. al. [197]. Additionally,

5.2 Effects of Stroke on Brain Activity

significantly increased rCBF was found during stroke-affected hand movement in the inferior parietal cortex, prefrontal and anterior cingulate cortices and basal ganglia.

In a cross-sectional study, Ward et. al. [86] recorded fMRI with blood oxygenation level dependant (BOLD) contrast from twenty-six healthy control subjects and twenty stroke patients who had suffered their first ischaemic stroke at least 3 months previously, resulting in at least two days of hand, wrist and finger weakness. Subjects took part in a hand-grip task during scanning. Control subjects performed the task with both dominant and non-dominant hands while stroke patients performed the task with their stroke-affected hand. All subjects were right-handed.

For healthy control subjects, similar activity was found as in the above PET studies [197, 198]. Specifically, activity was found in contralateral sensorimotor cortex, ipsilateral superior cerebellum and then bilateral activity in dorsolateral premotor cortex, ventrolateral premotor cortex, supplementary motor area, pre-supplementary motor area, cingulate motor areas, inferior parietal cortex intraparietal sulcus, insula cortex, cerebellar vermis and both inferior and superior cerebellar hemispheres.

In a similar investigation, Ward et. al. [199] carried out a longitudinal study for neural correlates with motor recovery after stroke. fMRI with BOLD contrast was recorded from four healthy control subjects and eight stroke patients who had suffered their first stroke 10-14 days before first recording. Multiple scans of all subjects took place over 12 months. During scanning, subjects performed a hand-grip task. Stroke patients performed the task with their stroke-affected hand, two control subjects performed the task with their dominant hand while the remaining two healthy control subjects performed the task with their non-dominant hand.

A negative correlation between task-related regional activity and motor recovery was found in all stroke patients, particularly in motor-related regions. Motor regions presenting this negative correlation for various stroke patients were ipsilesional M1 (five patients), contralesional M1 (four patients), dorsal premotor cortex (seven patients), ventral premotor cortex (five patients), supplementary motor area (six patients), cingulate motor regions (four patients) and cerebellum (seven patients).

In a group analysis, a negative correlation was found between task-related regional activity and motor recovery in ipsilesional M1, inferior contralesional M1, bilateral anterior and posterior dorsolateral premotor cortex, contralesional ventrolateral premotor cortex, ipsilesional supplementary motor area, pre-supplementary motor area,

prefrontal cortex, and caudal cingulate sulcus. Additionally, similar negative correlations were found in parietal, temporal and occipital lobes, as well as thalamus and globus pallidus.

A review of PET and fMRI investigations into motor recovery after stroke conducted by Calautti et. al. [200] revealed that stroke-affected brain activity patterns during motor activity were quite consistent. Fully recovered patients who had suffered striatocapsular stroke consistently displayed enhanced bilateral motor pathway activity, recruitment of sensory and secondary motor areas not normally related to movement and extension of the SM1 area towards the face area. Patients with cortical stroke consistently displayed over-activation of bilateral non-infarcted motor and non-motor areas, strong peri-infarct activity and ipsilesional premotor cortex activity.

These PET and fMRI studies reveal how such strokes affect activity of various regions of the brain and informs us of where to expect to observe increased brain activity when recording from stroke patients during a hand motor task. While these studies reveal brain activity, they unfortunately reveal nothing about how the stroke affects neural pathways and how separate brain regions interact during attempted movement. To investigate the effect of stroke on interaction between brain regions, a different type of analysis is required.

5.3 Brain Networks and Connectivity

The brain may be modelled as temporally- and spatially-interacting elements of a highly complex and organised system referred to as a *brain network* [201, 202, 203, 204, 205, 206]. This conceptual paradigm, based on graph theory, for analysing brain function has proven to be useful for framing interactions between functional areas of the brain. Brain imaging methods, such as fMRI, are capable of mapping anatomical regions of the brain and their interconnections, resulting in a network map which describes the structural connectivity of the brain, known as the human *connectome* [207]. The connectome comprises a complete map of the brain's structural connections, which shape large-scale neuronal dynamics [208].

Brain networks derived from anatomical observations result in a *structural* network describing physical connections between regions while physiological measurements result in a *functional* network describing interactions between regions. Connectivity

5.3 Brain Networks and Connectivity

between brain regions can be described in three ways. *Structural connectivity* describes anatomical connections between cortical and subcortical regions. Structural connectivity is considered to be stable over time frames up to a few minutes but can alter over longer time frames due to brain plasticity. *Functional connectivity* [209, 210, 211] describes patterns of statistical dependence (e.g. correlation, coherence, mutual information) between neuronal population elements of the brain network. Functional connectivity is highly time-dependent as functional connections between brain regions continually react to current experience. Importantly, functional connectivity is strictly a statistical relationship and does not imply or represent a causal relationship between brain regions. *Effective connectivity* [209, 210, 211] attempts to represent causal relationships between neural population elements of a brain network and, as such, is the most important type of connectivity for analysing brain networks. Causal relationships between neuronal element populations, however, are difficult to accurately discern. Most effective connectivity measures attempt to only estimate such connectivity with varying success [212].

In graph theory, a network is comprised of a series of nodes, with edges connecting the nodes. For a brain network, nodes represent neural element populations while edges represent one of the above forms of connectivity, as shown in Figure 5.1. The steps for brain network analysis are [203]: (1) Define the network nodes. Some possible options are using EEG electrode locations, performing EEG source localisation, using anatomical regions or derivation from fMRI imaging. (2) Estimate a continuous measure of association between nodes. This defines the edges of the network and can be derived through a range of coupling metrics for functional and effective connectivity. (3) Generate an association matrix to represent the strength of association between nodes. (4) Calculate network parameters of interest, such as node degree (number of connections), path length, connection cost or centrality (See Bullmore and Sporns [203] for a review of brain networks with graph theoretical analysis). A review of functional and effective connectivity measures for electrophysiological brain activity is available from Greenblatt et. al. [213].

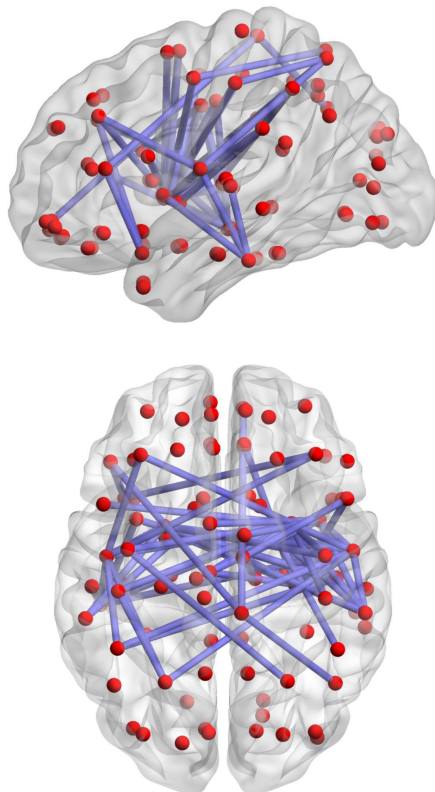


Figure 5.1: Illustration of a brain network showing nodes and edges. *Source: Brain network.png licensed under CC BY-SA 3.0.*

5.4 Effects of Stroke on Brain Connectivity

Grefkes et. al. [214] conducted an investigation into the effect of stroke on effective connectivity in the brain. fMRI fluid-attenuated inversion recovery (FLAIR) images were acquired from twelve healthy controls and twelve stroke patients as they performed a hand-clench task with left, right or both hands. Stroke patients had suffered their first subcortical stroke up to 5 weeks before recording resulting in unilateral upper limb weakness. Effective connectivity analysis found that during movement of the stroke-affected hand, stroke patients displayed increased effective connectivity between primary motor areas, with contralesional M1 inhibiting activity in ipsilesional M1. This was the only significant difference in effective connectivity between regions of interest compared to healthy controls during movement of the stroke-affected hand.

De Vico Fallani et. al. [215] investigated the effects of stroke on brain functional

5.4 Effects of Stroke on Brain Connectivity

organisation with full-head 128-channel EEG recorded from eight healthy subjects and one stroke subject during a finger-tapping task. This study used a theoretical graph approach to characterise task-related spectral coherence between EEG signals during preparation and execution of the motor task. Results suggested that subcortical stroke reduced the brain's capacity to integrate the communication between distant brain regions and lowered the modularity of brain networks. The overall connectivity of the stroke patient's brain network was found to be ruled by a lower number of brain regions than healthy subjects.

A similar EEG-based investigation by Gerloff et. al. [216] with eleven well-recovered chronic stroke patients found reduced EEG activity in the central region of the stroke-affected hemisphere and a relative shift of EEG patterns from the ipsilesional hemisphere to the contralesional hemisphere. EEG coherence analysis was used to assess inter-regional cortical connectivity and found a shift in connectivity towards the contralesional hemisphere. The authors concluded that the contralesional hemisphere is functionally integrated in the reorganised cortical network for stroke-recovered hand movement.

A review of investigations into the effects of stroke on cerebral networks [217] collates the findings of five studies [214, 218, 219, 220, 221] and provides a summary of the results. Stroke is found to affect a relatively large number of ipsilesional and contralesional interactions. Effective connectivity in all ipsilesional regions relating to stroke-affected hand movement may be affected. Inter-hemispheric interactions, particularly relating to ipsilesional primary motor cortex, are affected by stroke. Interaction between ipsilesional and contralesional primary motor cortex is found to be the most affected by stroke.

Without specific knowledge of the effect a subject's stroke has on their brain network, any significant differences discovered between brain activity data of healthy subjects and that subject is likely a result of the stroke. BCIs use such recordings without any prior knowledge of the subject's potentially abnormal brain network. For rehabilitation BCI, the effect that a stroke has on BCI performance is not clear yet may be important for future BCI development. Therefore, in order to explore what effects a stroke has on BCI performance, new experimental data must be collected.

5.5 Recording of Healthy and Stroke-affected EEG

While the studies in the previous section reveal some of the functional effects of stroke on brain activity during hand movement, their results are not directly relatable to the operation of EEG or fNIRS rehabilitation BCI nor do they attempt to inform rehabilitation BCI design. The signals utilised by stroke rehabilitation BCI are likely affected by the stroke in a similar way to the data studied above but it is not yet clear exactly how. In order to reveal exactly what effect the stroke has on those signals, an analysis based on BCI operation must be carried out. Such an analysis would not only reveal the effects of stroke on BCI operation but may also provide a unique method for quantifying the effects of stroke following stroke onset and during recovery. Such quantification of the effects of stroke on brain networks may be possible through machine-learning parameters derived during BCI training. A comparison of the parameters derived from stroke-affected data to those derived from healthy data may be useful in observing the change in brain networks of a stroke patient and further changes during recovery.

While fMRI and PET provide very high spatial resolution of brain activity, allowing for precise identification of activated brain regions, these modalities are unsuitably inconvenient for many typical stroke patients. fMRI and PET both require that the subject lie down inside a large machine and remain very still - an undesirable requirement for many stroke patients. Additionally, fMRI and PET systems are large, quite expensive and require a technical operator, further reducing their convenience as the measurement modality of a stroke rehabilitation system. By comparison, EEG may be a more suitable measurement modality for measuring and observing changing brain networks in stroke patients during recovery. EEG does not require a technical operator, is relatively simple to set up and the subject may be seated in a comfortable chair for the duration of the recording. EEG is more robust to movement of the subject than fMRI or PET although is not entirely unaffected.

In order for analyses of the effects of stroke on brain function to be carried out, a dataset must first be obtained. There are no appropriate datasets available and so an experimental recording session is required. For this recording from stroke patients, only EEG is used while fNIRS is omitted. Due to the additional experimental requirement of the wearing of laser safety goggles, the lower portability of fNIRS recording systems

5.5 Recording of Healthy and Stroke-affected EEG

(and, thus, lower suitability for potential at-home rehabilitation therapy) and the unnecessary extra experimental set up for hybrid fNIRS/EEG, fNIRS is not investigated for suitability in a stroke effect evaluation system. Described here is the longitudinal experimental recording of full-head EEG from healthy control subjects and stroke patients during a finger-tapping motor task.

5.5.1 Subjects

10 healthy subjects and 5 stroke patients took part in experimental recording sessions. Healthy subjects (8 men and 2 women, mean age 57.2 ± 17.6 years) each participated in one recording session. Stroke-affected subjects (3 men and 2 women, mean age 59.0 ± 9.4 years) each participated in two recording sessions. The first (“Early”) recording session for stroke subjects took place an average of 22.2 ± 12.9 days after their stroke event. The second (“Late”) recording session took place an average of 190.6 ± 26.1 days after the first recording session. This period of time between early and late sessions was chosen such that spontaneous recovery processes would have had time to run their course.

Healthy control subjects were recruited from Maynooth University. Demographic information of healthy subjects is presented in Table 5.2. Stroke patients were recruited from the Adelaide & Meath Hospital, Dublin. Inclusion criteria for the stroke patients are summarised as: Patients must (1) be cognitively high functioning, (2) be able to give informed consent and follow experimental instructions, (3) not suffer from a visual field defect or visual neglect, and (4) have upper limb motor paresis in either their dominant or non-dominant hand.

When possible, the Mini Mental State Exam (MMSE) [46] was used to ensure absence of serious cognitive impairment in the stroke patients. One subject was unable to conduct this test at the time of the first trial due to stroke-induced expressive dysphasia, severely affecting their ability to produce speech. This subject was included in the study following demonstration of cognitive requirements and consultation with the patient’s stroke physician.

The Kapandji finger apposition test [222] was used to determine motor ability in the stroke-affected hand. This test involves the subject attempting to touch the thumb on their stroke-affected hand to 10 points on the same hand in order from points 0 to 10, as shown in Figure 5.2. Four of the stroke subjects scored at least 6/10, meaning

5.5 Recording of Healthy and Stroke-affected EEG

ID	Sex	Dominant	
		hand	Age
H1	F	Right	75.8
H2	M	Left	43.5
H3	M	Right	61.2
H4	F	Left	67.4
H5	M	Right	40.7
H6	M	Right	71.0
H7	M	Right	50.7
H8	M	Right	21.2
H9	M	Right	71.9
H10	M	Right	68.6

Table 5.2: Healthy subject demographics

they were able to perform a finger-tapping action with all of their digits. One subject had minimal motor ability in their stroke-affected hand and obtained a Kapandji score of 0/10. Demographic information of stroke patients, including available MMSE and Kapandji scores at the times of both recordings is presented in Table 5.3.

				Early Session				Late Session			
				Time		Kapandji		MMSE		Time	
ID	Sex	Dominant hand	Tested hand	Age	from stroke	score	score	from Early	score	score	score
S1	M	Right	Right	58.8	6w 0d	6/10	28/30	25w 6d	6/10	28/30	28/30
S2	M	Right	Right	56.3	3w 2d	6/10	28/30	25w 2d	10/10	28/30	28/30
S3	M	Right	Left	75.0	2w 5d	0/10	29/30	25w 1d	3/10	30/30	30/30
S4	F	Right	Right	51.9	0w 6d	6/10	27/30	26w 0d	8/10	27/30	27/30
S5	F	Right	Right	53.0	3w 0d	9/10	N/A	33w 6d	9/10	28/30	28/30

Table 5.3: Stroke subject demographics

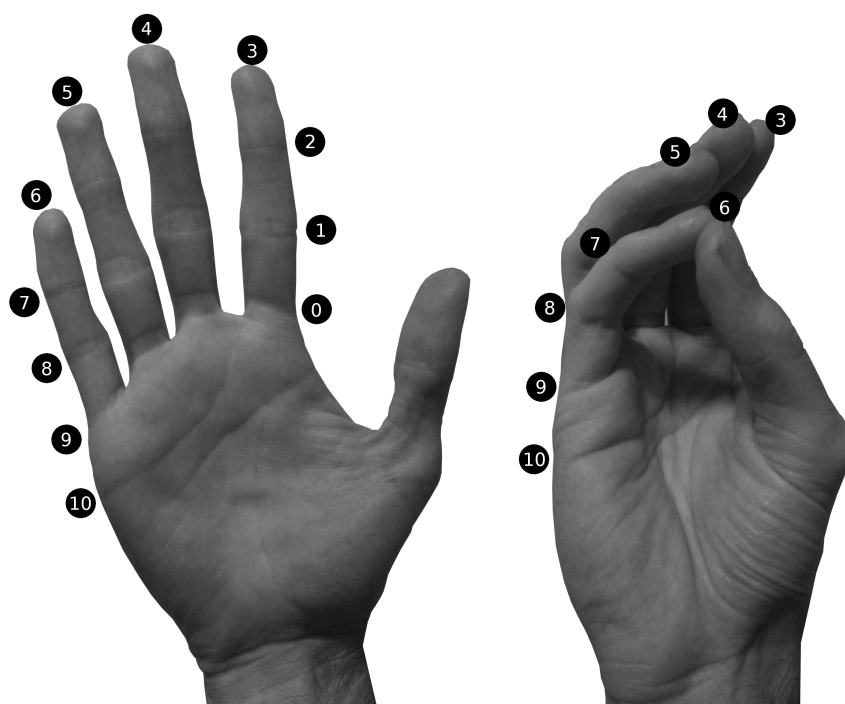


Figure 5.2: Kapandji thumb apposition scores.

For stroke subjects, the locations of brain tissue damage due to stroke were varied and included both cortical and subcortical bilateral tissues: the left and right posterior parietal cortex, left frontoparietal cortex, right temporo-parietal areas, right medial temporal lobe, left thalami and internal capsules, periventricular white matter lesions and centrum semiovale lesions. In all cases, the stroke was ischemic in nature. Subject-specific lesion information can be found in Table 5.4.

In accordance with ethical requirements, participants were provided with a verbal as well as a written description of the research and experimental protocol. Subjects provided written consent to the conduction of the experiment and the publication of their details. In the cases of two stroke patients who were unable to give written consent due to their stroke, verbal consent was accepted. Ethical approval for the experiments was granted by the SJH/AMNCH Research Ethics Committee of the Adelaide & Meath Hospital, Dublin and by the Ethics Committee of the Maynooth University. The recording sessions were conducted at the Adelaide & Meath Hospital, Dublin.

5.5 Recording of Healthy and Stroke-affected EEG

Stroke subject	Lesion information
S1	Left frontoparietal cortex acute ischemia (left middle carotid artery territory).
S2	Left parietal infarction, left thalami and internal capsule infarcts. Periventricular deep white matter change. Bilateral lacunar infarcts in the centrum semiovale and basal ganglia. 1.5 cm acute infarct in left centrum semiovale.
S3	Area of acute infarction adjacent to the body of the right lateral ventricle involving the right centre of semiovale.
S4	Right posterior parietal and temporo-parietal regions. Background periventricular ischemic changes involving left frontal parietal region.
S5	Medial right temporal lobe focal infarct. Periventricular deep white matter ischemic disease.

Table 5.4: Stroke subject clinical information

5.5.2 Experimental set-up and motor paradigm

During a recording session, the subject was seated in a comfortable chair in front of a laptop computer which presented experimental instructions. The subject was instructed to perform a finger-tapping task while the words “Move your fingers” were displayed on-screen and to entirely rest their hand while the word “Relax” was displayed on-screen. The finger-tapping task involved repeatedly touching the thumb to the tips of the 2nd to 5th digits on the same hand at a self-paced speed. At the beginning of the recording, the screen read “The experiment will begin shortly”. At the end of the recording, the screen read “Experiment now over. Please stay still”. Healthy subjects were instructed to perform the task with their dominant hand, while the stroke subjects were instructed to perform the task with their stroke-affected hand.

A recording session consisted of 20 movement instruction trials and 20 rest instruction trials, beginning with activation and alternating until all 40 trials had been

5.6 Qualitative differences between healthy and stroke-affected EEG

completed. Each trial lasted 10 seconds with no rest time between trials, as indicated in Figure 5.3.

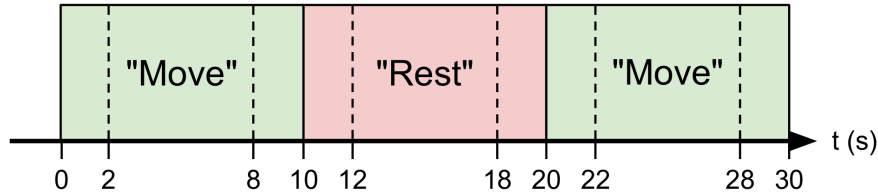


Figure 5.3: Experimental protocol instruction timing

Stroke subject S3 is the only stroke subject whose stroke affected their non-dominant hand and so was the only subject required to perform the task with their non-dominant hand. Subject S3 also attained a Kapandji score of 0/10 at the early session, meaning this subject couldn't physically perform the task. In this case, the subject *attempted* to perform the task. This subject fatigued during the first recording session and was only able to complete 32 trials.

5.5.3 EEG data acquisition

32-channel EEG data was acquired using a BioSemi ActiveTwo system (BioSemi B.V., Amsterdam, Netherlands) with Ag/AgCl electrodes positioned according to the 10/20 system. The system also recorded analogue event signals received from the instruction presentation laptop. Data was acquired at a sample rate of 1024 or 512 samples per second.

5.6 Qualitative differences between healthy and stroke-affected EEG

An initial qualitative analysis of the recorded datasets may reveal some similarities and dissimilarities between healthy and stroke-affected data. The purpose of recording the data is to investigate methods for observing the effects of stroke and so such an analysis may reveal aspects of the EEG to guide further analysis. This initial analysis is carried out in the EEGLAB [223] toolbox for MATLAB [224].

5.6 Qualitative differences between healthy and stroke-affected EEG

Initially, all datasets are downsampled from the acquisition sampling rate to 256 samples per second. This facilitates faster processing of the datasets and lowers memory requirements. As the EEG of interest is in the frequency range 2–30 Hz, the downsampling process has no effect on analysis results [225]. Analysis of the spectral content and of the independent components of the EEG signals then follows.

5.6.1 Spectral Components

The spectral content of the EEG signals is assessed using a simple FFT analysis. The spectral content of each EEG channel of each dataset during motor execution is obtained and presented in Table 5.5 and Table 5.6 (at the end of the chapter). Additionally presented for illustration are topographic maps of the power distributions at three frequencies: 6 Hz, 10 Hz and 22 Hz.

No differences between the spectral content of healthy and stroke-affected EEG are obvious from these images. Eight out of ten healthy datasets (H1, H2, H3, H5, H6, H8, H9 and H10), three out of five early session stroke datasets (S2E, S4E and S5E) and three out of five late session stroke datasets (S1L, S2L and S5L) display a spectral peak of power in the alpha range.

Topographically, 10 Hz power appears to be concentrated towards the posterior of the brain, at the occipital and parietal lobes, for all datasets. No consistent pattern is found for the topographical maps of 6 Hz and 22 Hz and so no more conclusions can be made other than to highlight the unpredictable distribution of EEG spectral power in both healthy and stroke-affected brain activity.

5.6.2 Independent Component Analysis

Blind source separation (BSS) is the separation of a set of *source signals* from a set of *mixed signals* with the use of zero (or very little) information about the source signals themselves [226]. The relationship between a set of recorded mixed signals and a set of sources can be represented in matrix form as:

5.6 Qualitative differences between healthy and stroke-affected EEG

$$\begin{bmatrix} \mathbf{x}_1 \\ \mathbf{x}_2 \\ \vdots \\ \mathbf{x}_P \end{bmatrix} = \begin{bmatrix} a_{11} & a_{12} & \cdots & a_{1(M+Q)} \\ a_{21} & a_{22} & \cdots & a_{2(M+Q)} \\ \vdots & \vdots & \ddots & \vdots \\ a_{P1} & a_{P2} & \cdots & a_{P(M+Q)} \end{bmatrix} \begin{bmatrix} \mathbf{s}_1 \\ \vdots \\ \mathbf{s}_M \\ \mathbf{v}_1 \\ \vdots \\ \mathbf{v}_Q \end{bmatrix} + \mathbf{N} \quad (5.1)$$

where $\mathbf{s}_i, \mathbf{v}_i, \mathbf{x}_i \in \mathbb{R}^{1 \times L}$ are the i^{th} row vectors of length L of the source signals, artefact signals and recorded signals, respectively. \mathbf{A} is the unknown mixing matrix and \mathbf{N} represents error and noise values. Equation 5.1 can be simplified and expressed algebraically as $\mathbf{X} = \mathbf{A}\mathbf{S}$. The objective then of a BSS algorithm is to find a un-mixing matrix \mathbf{W} such that $\hat{\mathbf{S}} = \mathbf{W}\mathbf{X}$, where $\hat{\mathbf{S}}$ is an estimation of the original sources and artefact, as depicted in Figure 5.4. It is important to note that \mathbf{W}^{-1} is an approximation to \mathbf{A} . BSS algorithms calculate \mathbf{W} almost exclusively on the matrix of recorded data \mathbf{X} .

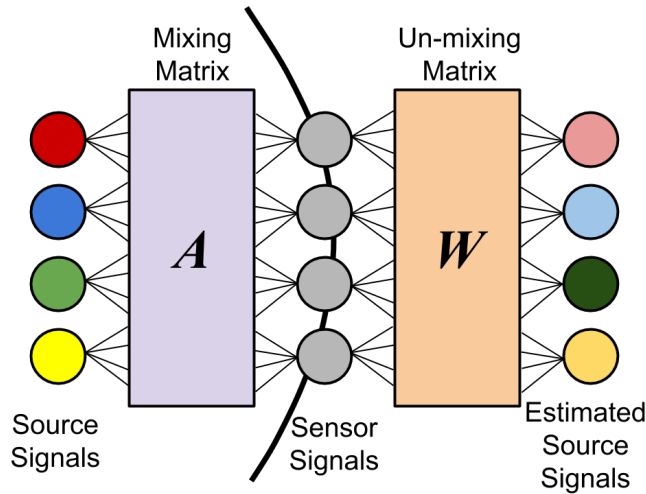


Figure 5.4: Simplified BSS process.

BSS methods are relevant to EEG data as each recorded EEG signal is a mix of all electrical sources in the brain due to the volume conductor effect of the head. While there may be millions of individual neurons firing at any given sample time, those neurons which are acting together in a cell assembly will be represented relatively strongly in multiple EEG channels. All other neuronal activity contributes to the noise

5.6 Qualitative differences between healthy and stroke-affected EEG

matrix. Neuronal cell assemblies may be considered as sources for BSS. The amplitude of each of these electrical sources in the recorded EEG signals may be represented by the mixing matrix \mathbf{A} .

One class of BSS algorithm for calculating an un-mixing matrix \mathbf{W} is Independent Component Analysis (ICA). ICA attempts to separate EEG signals into sources while adhering to a number of assumptions [226]: (1) Sources are mixed linearly and instantaneously. (2) Sources are perfectly noiseless - noise is introduced at the sensors. (3) The number of sources equals the number of recorded signals. (4) The mixing matrix does not change over time. (5) Sources are *independent* such that each source is generated by an unknown random process which is unique to that source. A detailed description of ICA is available elsewhere [226, 227].

Following application of the ICA algorithm ‘FastICA’ [228, 229] to the recorded EEG datasets, an un-mixing matrix \mathbf{W} was obtained for each dataset. The rows of \mathbf{W}^{-1} approximate the rows of \mathbf{A} , which describe the strength of each independent source in the corresponding sensor signal of \mathbf{X} . Accordingly, the columns of \mathbf{W}^{-1} describe the strength of each source in each sensor signal. As the location of each EEG sensor is known, topographic maps of the contribution of an independent source to each sensor signal may be plotted. Shown in Table 5.7 and Table 5.8 are such maps for four independent sources for each movement-related EEG dataset. ICA is a useful method for isolating an interference signal, such as EOG, or a noisy sensor, as such interfering sources are independent of brain sources. Of the available topographies, only four non-artefact maps are chosen for clarity.

No qualitative differences in ICA patterns are evident between groups of datasets, as expected. The main purpose of ICA is to remove sensor and movement artefact ICs from EEG. Topographic maps of remaining ICs, such as these, simply demonstrate distribution of independent EEG sources. A subject, or group of subjects, demonstrating a noticeable and strong pattern would suggest that there may have been a problem with EEG recording, pre-processing or any other issue with the recorded data. In this way, this qualitative ICA analysis is a useful “sanity check” of the recorded EEG data.

5.6 Qualitative differences between healthy and stroke-affected EEG

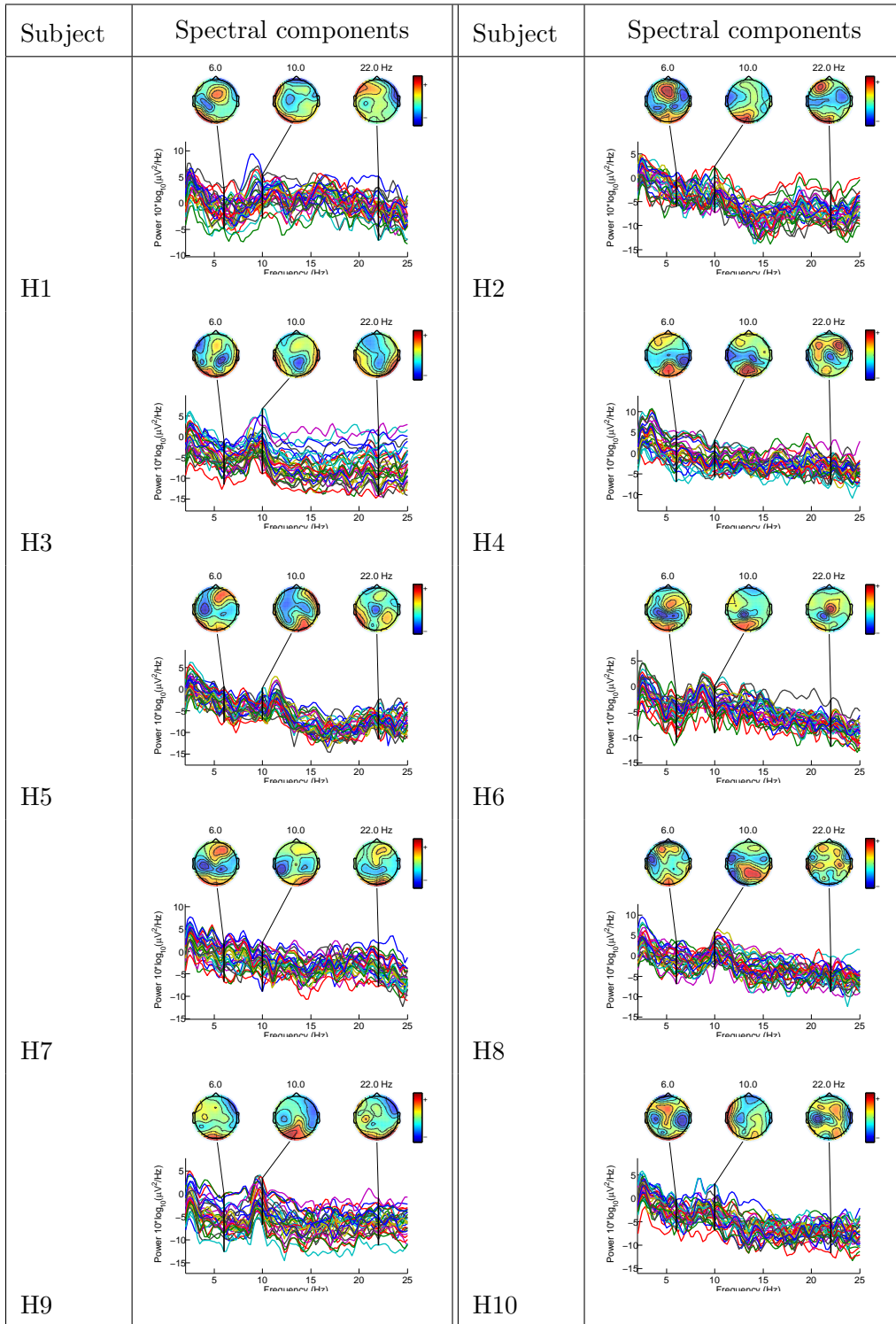


Table 5.5: Power v frequency plots of each EEG channel during motor execution of healthy subjects with power contour plots at 6, 10 and 22 Hz

5.6 Qualitative differences between healthy and stroke-affected EEG

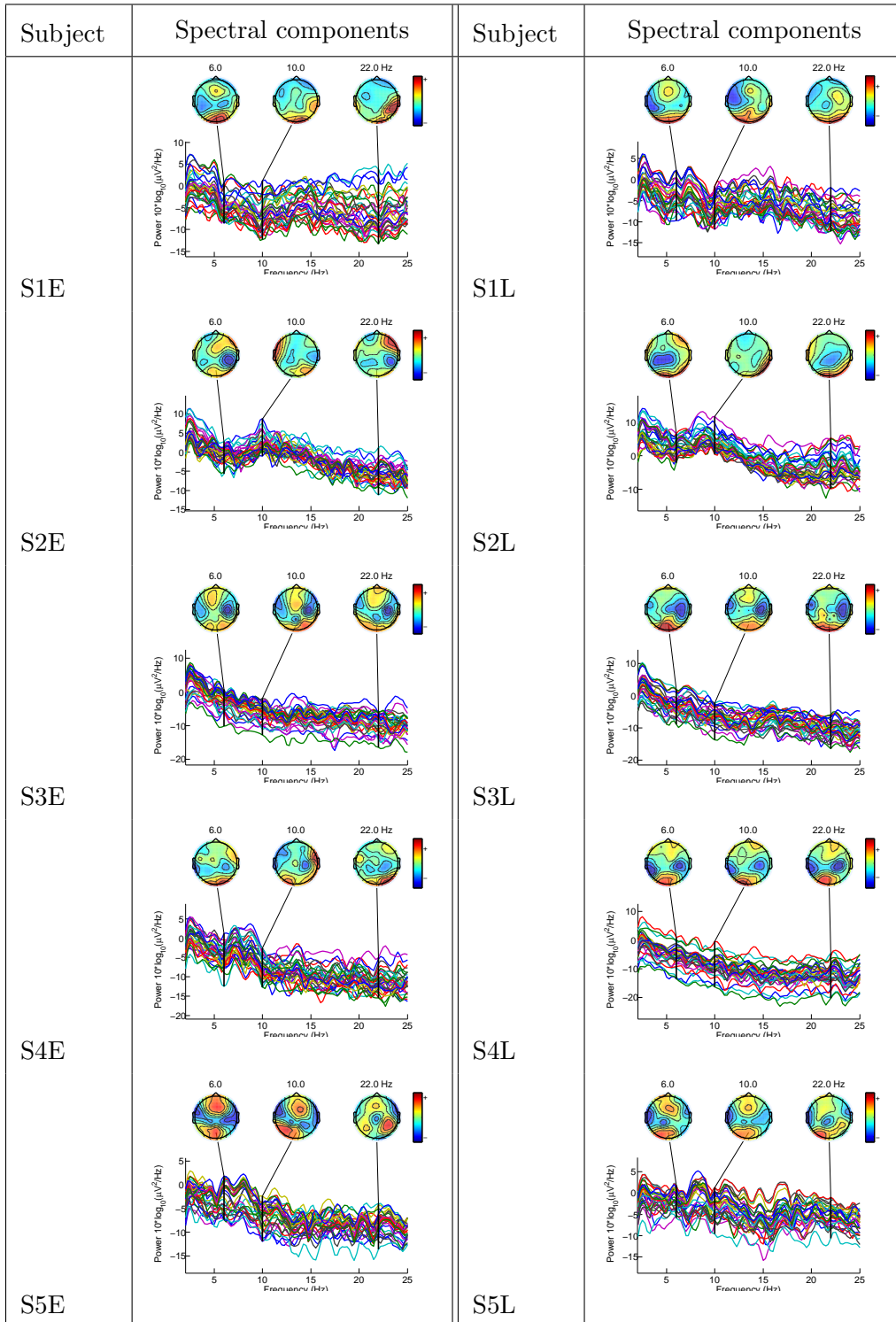


Table 5.6: Power v frequency plots of each EEG channel during motor execution of stroke patients with power contour plots at 6, 10 and 22 Hz

5.6 Qualitative differences between healthy and stroke-affected EEG

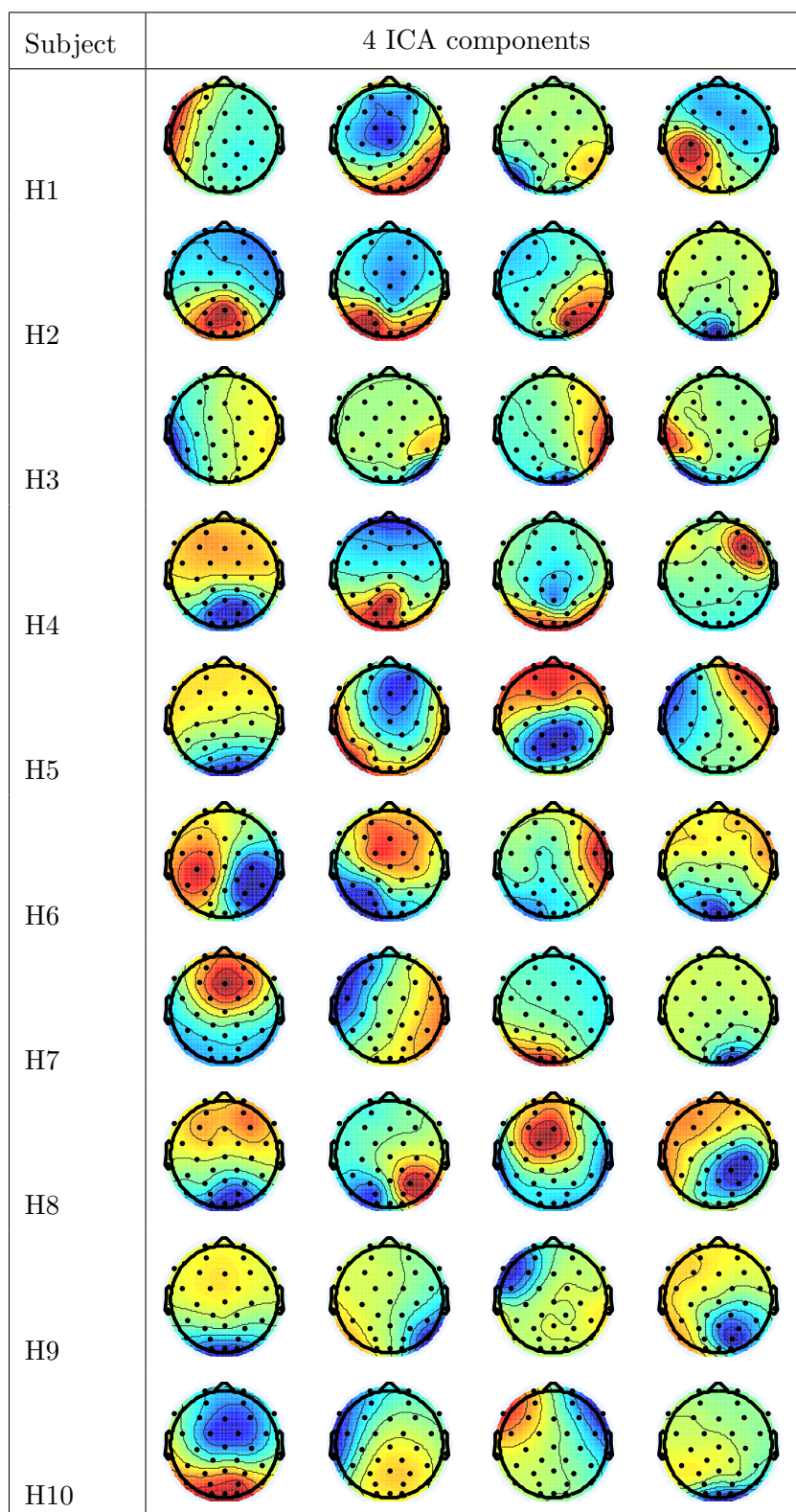


Table 5.7: Topographies of 4 healthy subject ICA components during motor execution

5.6 Qualitative differences between healthy and stroke-affected EEG

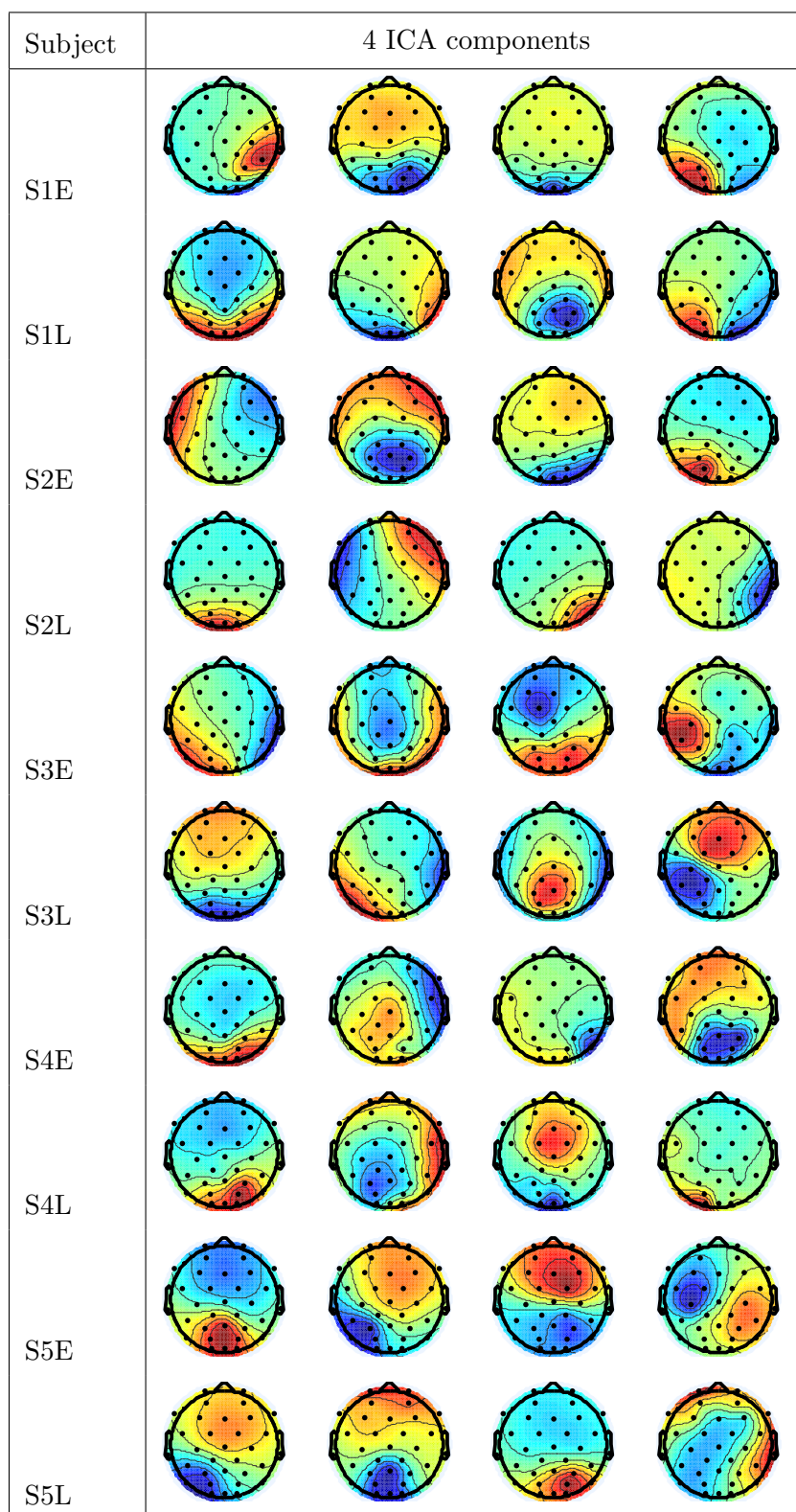


Table 5.8: Topographies of 4 stroke patient ICA components during motor execution

5.7 The Need for Further Analysis

Clearly, in order to investigate fully the effects of stroke on brain activity and brain networks and their manifestations in the operation of EEG-based rehabilitation BCI, further analysis is required. These initial quantitative analyses are not adequate to reveal the effects of stroke on the underlying brain networks but do at least indicate that whatever effect the stroke has is not detectable through simple analysis of spectral content or ICA.

In order to investigate fully the effect of stroke on rehabilitation BCI operation, the recorded EEG datasets must be analysed from a BCI perspective utilising typical BCI signal processing methods, including preprocessing, signal processing, feature extraction, classification and statistical analysis. The advantages of such an analysis are two-fold. Firstly, any unique aspects of stroke-affected EEG which may affect stroke rehabilitation BCI may be revealed, informing future rehabilitation BCI development and improving stroke rehabilitation therapy. Secondly, any differences found between healthy and stroke-affected EEG following BCI analysis may potentially represent a novel aspect for measuring the effects of stroke on underlying brain networks. As the dataset features longitudinal stroke EEG data, any changing aspect of BCI operation and analysis may be relatable to rehabilitation outcomes or changes in hand motor control of the stroke patients.

Additionally, there are new EEG-based tools for measuring effective connectivity which have not yet been applied to stroke-affected data. This dataset allows for further investigation into the applicability of new EEG connectivity analysis methods for quantification of the functional effects of stroke.

5.8 Summary

This chapter established that while the development of a biofeedback BCI is relatively straightforward for healthy EEG data, a stroke affects brain activity and brain networks in such a way that EEG produced by a stroke-affected brain is likely abnormal. A rehabilitation BCI based on the abnormal EEG of a stroke patient may not function in the expected way. In order to fully investigate the effects of stroke on EEG utilised

by stroke rehabilitation BCI, a dataset of healthy and stroke-affected EEG must be analysed from a BCI perspective.

As a suitable dataset for this analysis is not available, longitudinal EEG recordings with healthy and stroke-affected subjects were carried out while the subjects performed a finger-tapping task. Initial analysis of these datasets suggests that advanced analysis is required in order to reveal measurable effects of stroke on recorded EEG and underlying brain networks. This dataset may also be used, however, for further analysis of post-stroke functional connectivity. The following two chapters describe attempts to perform such analyses.

Chapter 6

Stroke Effects and Neuroplastic Change Observed Through Machine Learning

6.1 Introduction

As discussed in the previous chapters, stroke rehabilitation BCI cannot be progressed through analysis of healthy brain activity data alone. The previous chapter described experimental recordings to collect EEG data from healthy and stroke-affected subjects while they performed a finger-tapping task with their dominant or stroke-affected hand. Initial analysis of this EEG data revealed no obvious differences in EEG spectral components, spectral maps or ICA components between healthy and stroke-affected subjects. Therefore, a more in-depth analysis of this EEG data is required in order to investigate the effects of stroke on BCI operation. Any unique aspects of BCI operation with stroke-affected subjects may be useful in the future design and development of EEG-based stroke rehabilitation BCI.

This chapter broadly attempts to test the following three null hypotheses:

1. *“There is no difference in EEG BCI performance between healthy subjects and stroke-affected subjects 3 weeks post-stroke”.*

2. *“There is no difference in EEG BCI performance between healthy subjects and stroke-affected subjects 7 months post-stroke”.*
3. *“There is no difference in EEG BCI performance between stroke-affected subjects 3 weeks post-stroke and stroke-affected subjects 7 months post-stroke”.*

These hypotheses are tested for each possible BCI training configuration, as described below. Should any null hypothesis be rejected then further investigations into those differences are carried out.

This chapter describes an in-depth analysis into the effect of stroke on EEG BCI performance by implementing an offline BCI. The BCI is a novel design, comprised of Filter Bank Common Spatial Patterns (FBCSP), Marginal Relevance and Gaussian Process-based classification. The effect of stroke on BCI performance is observed through BCI classification accuracies with various BCI training and testing data and additionally through BCI parameters derived through machine learning. While the primary objective of this analysis is to discover the effect of stroke on EEG BCI performance, these results also contribute toward an investigation into the most suitable pre-recorded dataset for rehabilitation BCI training and also into the potential for utilising machine-learned BCI parameters as a biomarker for post-stroke neurorehabilitation.

6.2 Study Objectives

6.2.1 Choice of Rehabilitation BCI Training Data

Before a BCI can be operated in real-time, as is naturally required for rehabilitation BCI, various real-time signal processing parameters of the BCI must be set. Typically one (or more) pre-recorded datasets are analysed to determine the optimal BCI parameters for classification of that training dataset. Once these parameters are determined, they are then used for real-time BCI operation. There are various possibilities for training dataset, such as recording a training dataset for the subject immediately before real-time BCI operation, or using one or more datasets recorded previously by the subject, or using datasets recorded previously by other people. Part of the investigation described in this chapter is into the optimal choice of BCI training dataset for rehabilitation BCI.

This choice is particularly important for stroke rehabilitation BCI as stroke subject fatigue may be a concern. Having a subject participate in a recording session before every rehabilitation BCI therapy session will serve to reduce effective therapy time as the subject tires and cannot engage in therapy. Therefore, if another choice of BCI training data is acceptable, rehabilitation therapy will be improved.

6.2.2 Effect of Stroke on BCI Performance

The damage and disruption caused by a stroke to brain function may result in stroke-affected subjects simply losing capability to use a BCI as well as healthy subjects. If classification of stroke subject brain activity is less reliable than for healthy subjects, future design of rehabilitation BCI should take this into consideration. Other differences between healthy and stroke-affected EEG in the context of BCI operation are yet to be discovered. BCI parameters, determined through machine learning methods on the training dataset, may reveal differences between healthy and stroke-affected EEG.

6.2.3 A Biomarker for Post-Stroke Neurorehabilitation

The primary objective is to discover the differences between healthy and stroke-affected EEG which concern rehabilitation BCI operation. This naturally leads to another investigation: if such differences exist and are observable through BCI analysis, can they be related to the stroke subject's current state of neurorehabilitation? There exist very few measures of stroke recovery and so this investigation may have clinical application.

When training a BCI on healthy EEG, it may be possible to use classification accuracy of stroke-affected EEG as a measure of the effect of stroke on brain activity. Training and testing a BCI on the same data naturally results in perfect or near-perfect classification accuracy. As the BCI testing dataset then differs from the training dataset, classification accuracy may drop. Therefore, BCI classification accuracy may have use as a measure of the similarity of a stroke-affected brain to a healthy brain.

6.3 Offline BCI Analysis

The dataset described previously in Chapter 5 was used for this investigation and is repeated briefly here. 32-channel EEG was recorded from ten healthy subjects and five stroke subjects while they participated in an overt finger-tapping task. Stroke subjects participated in two recording sessions: an “early” recording session up to 3 weeks post-stroke and a “late” recording session approximately 7 months post-stroke.

Analysis of the EEG data involved implementation of an off-line BCI based on Filter Bank Common Spatial Patterns (FBCSP) [230, 231] and illustrated in Figure 6.1. All processing of EEG data and implementation of the BCI was carried out in Matlab 7 [224] using a combination of scripts from EEGLAB [232], Ramussen and Williams’ Gaussian Processes for Machine Learning (GPML) code [181] and custom scripts.

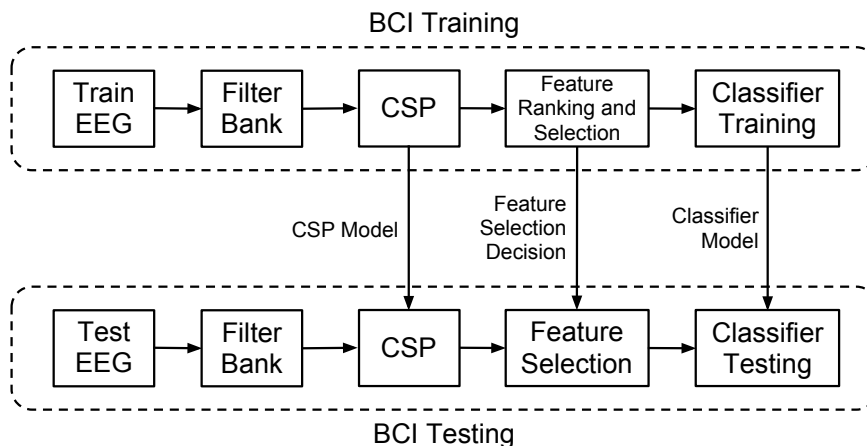


Figure 6.1: Block diagram of the offline BCI model.

FBCSP is an adaptation of the Common Spatial Patterns (CSP) algorithm [233] with the primary difference being a stage of temporal filtering of EEG through a multiple frequency range filter bank. The general steps of FBCSP are:

1. Filter the EEG into a number of frequency ranges.
2. Apply the CSP algorithm separately to each frequency range, decompose the EEG and perform feature extraction.
3. Rank and/or select features.
4. Train or test the classifier.

A simple temporal filter was used for the filtering stage before the CSP algorithm (described below) was applied to each filtered ‘Train EEG’ dataset. The CSP algorithm analyses the filtered EEG data and produces a CSP model, which is then used to process the filtered EEG. Feature extraction from the CSP output generates values which may be then used for training a classifier. The CSP model is stored for later use in the BCI Testing stage. Of those features extracted, only a subset are desired for classification. To choose which subset of features to use for classification, each feature is ranked by Marginal Relevance (MRelv) and the indices of those selected features (the “Feature Selection model”) are stored for BCI Testing. The final stage of BCI Training is to train a classifier model on the selected features. In this case, Gaussian Process Classification (GPC) was implemented and a classifier was trained. Details on CSP, MRelv and GPC are provided below.

Following BCI training, the BCI testing stage follows similar steps. First, the ‘Test EEG’ dataset is temporally filtered with the same filter bank parameters as before. Next, the CSP model from BCI Training is applied to the filtered EEG data. Feature extraction produces features that may be used for classification. However, only the features with the same indices as those selected in BCI Training are retained. Finally, those selected features are classified by the previously-trained classifier.

Analysis of the EEG datasets amounted to the choice of EEG for training and testing the BCI(‘Train EEG’/‘Test EEG’). A number of combinations of EEG data for training and testing were to be used. The simplest implementation involved using one single dataset to train the BCI, resulting in a CSP model, feature selection model and classifier model for that dataset and then use those models to process a different dataset and obtain a classification accuracy result. Another option was to use multiple datasets to train the BCI and then use other individual datasets for BCI testing. Finally, it was possible to use a subset of data from one dataset to train the BCI and another subset of that same dataset to test the BCI.

EEG datasets are identified primarily by Subject ID as seen in Table 5.2 and Table 5.3. Stroke subjects took part in an “early” (E) and a “late” (L) session and the datasets from these sessions are labelled accordingly. Therefore, healthy subject datasets are labelled H1–H10, early stroke datasets are labelled S1E–S5E and late stroke datasets are labelled S1L–S5L. EEG was inspected for artefact using EEGLAB’s

automatic epoch rejection algorithm, which did not reject any trials of data and so all data was retained for further processing.

6.3.1 Pre-processing

As some subjects performed the task with their right hand and some with their left, brain activation patterns cannot be compared across all subjects. Therefore, all left-handed EEG datasets were “mirrored” such that the EEG sensor locations of those datasets were laterally swapped. Following this, hemispheres were identified as either contralateral or ipsilateral to hand activity.

6.3.2 Temporal Filtering

EEG data was then temporally filtered with a filter bank made up of 9 frequency ranges. A zero-phase 4th-order Butterworth filter was used to filter the EEG signals into the frequency ranges 4–8, 8–12, 12–16, 16–20, 20–24, 24–28, 28–32, 32–36 and 36–40 Hz, producing an EEG dataset for each frequency range. The filtered EEG was then epoched into time segments for each trial of rest and activity. Segments began 2 seconds following trial onset and lasted 6 seconds, as shown in Figure 6.2.

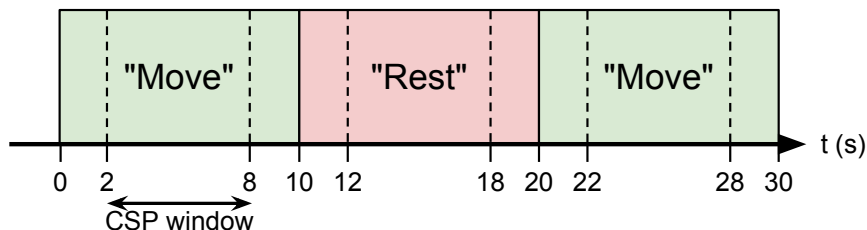


Figure 6.2: Experimental protocol with indicated “CSP window” - the portion of a trial used for CSP

6.3.3 Common Spatial Patterns

Common Spatial Patterns (CSP) [233, 234, 235, 236] is a method for analysing multi-channel EEG which has been recorded during two classes of activity e.g. ‘movement’ versus ‘rest’ or ‘left hand movement’ versus ‘right hand movement’. The CSP algorithm operates on a set of windowed sensor space EEG trials, E , to produce a data-driven

supervised set of spatial filters, W , which are used to project E to “CSP space” signals a.k.a. “CSP signals”, Z , as follows:

$$Z_i = W^\top E_i \quad (6.1)$$

where $E_i \in \mathbb{R}^{c_t \times t}$ is the i th trial of multi-channel EEG, $W \in \mathbb{R}^{c_t \times c_t}$ is a CSP projection matrix a.k.a. “CSP model”, $Z_i \in \mathbb{R}^{c_t \times t}$ is the i th trial of decomposed CSP signals, c_t is the total number of EEG channels, t is the number of time samples per trial and \top denotes the transpose operator.

Each *column* of W is a spatial filter and defines the proportion of each EEG signal in E_i to use when generating the new CSP signals of Z_i . The dimensions of Z_i are the same as E_i i.e. the number of channels of Z_i equals the number of channels of E_i , which also equals the number of spatial filters of W . Each *row* of W^{-1} is a *spatial pattern* and can be seen as a time-invariant EEG source distribution vector. Plotting this vector produces an image that illustrates this presumed source of EEG activity.

The objective of the CSP algorithm is to produce a set of spatial filters which, when used to decompose EEG signals, will produce a new set of signals whose *variances* are optimally distinct for two classes of activity. These variances may then be used for classifier training and classifier testing.

6.3.3.1 The CSP algorithm

The method by which the CSP algorithm produces these spatial filters is based on the simultaneous diagonalisation of two covariance matrices [234]. The normalised spatial covariance of EEG data of the i th trial, E_i , is obtained as:

$$C_i = \frac{E_i E_i^\top}{\text{trace}(E_i E_i^\top)} \quad (6.2)$$

where $\text{trace}(E_i E_i^\top)$ is the sum of the diagonal elements of E_i . For each of the two classes of activity to be separated, spatial covariance \bar{C} is calculated by averaging the normalised spatial covariances of trials belonging to each group (e.g. group 1 and group 2). The composite spatial covariance is then obtained as:

$$C_c = \bar{C}_1 + \bar{C}_2 \quad (6.3)$$

The matrix C_c can be factorised as $C_c = U_c \lambda_c U_c^\top$, where U_c is the matrix of eigenvectors and λ_c is the diagonal matrix of eigenvalues. Eigenvalues are assumed to be sorted in descending order.

The whitening transformation

$$P = \sqrt{\lambda_c^{-1}} U_c^\top \quad (6.4)$$

equals the variances in the space spanned by U_c , meaning all eigenvalues of PC_cP^\top are equal to one. By transforming the spatial covariances \bar{C}_1 and \bar{C}_2 as

$$\bar{S}_1 = P\bar{C}_1P^\top \quad (6.5)$$

$$\bar{S}_2 = P\bar{C}_2P^\top \quad (6.6)$$

then \bar{S}_1 and \bar{S}_2 share common eigenvectors i.e. if $\bar{S}_1 = B\lambda_1B^\top$ then $\bar{S}_2 = B\lambda_2B^\top$ and $\lambda_1 + \lambda_2 = I$ where I is the identity matrix.

Since the sum of two corresponding eigenvalues across λ_1 and λ_2 is 1, then the eigenvector with the largest eigenvalue for \bar{S}_1 *must* have the smallest eigenvalue for \bar{S}_2 , and vice-versa

Finally, the CSP projection matrix is composed as:

$$W = (B^\top P)^\top \quad (6.7)$$

6.3.3.2 Feature extraction

Following generation of the CSP model, W , the EEG signals E are decomposed into CSP signals Z with application of Equation 6.1. The variances of the CSP signals are extracted as features to create a feature set. A subset of these will be selected for classifier training and testing. Feature extraction proceeds as:

$$v_i = \log \left(\frac{\text{var}(Z_i)}{\sum_{i=1}^{i_t} \text{var}(Z_i)} \right) \quad (6.8)$$

$$V = \begin{bmatrix} v_1^\top \\ v_2^\top \\ \vdots \\ v_{i_t}^\top \end{bmatrix} \quad (6.9)$$

$$y = \begin{bmatrix} y_1 \\ y_2 \\ \vdots \\ y_{i_t} \end{bmatrix} \quad (6.10)$$

where $v_i \in \mathbb{R}^{c_t \times 1}$ is the set of features for the i th trial, $V \in \mathbb{R}^{i_t \times c_t}$ is the feature set for all trials, $y \in \mathbb{R}^{i_t \times 1}$ is the true class label vector, i_t is the total number of trials and c_t is the total number of channels.

The next stage of the BCI training involves ranking and selection of a subset of features from the full feature set to be used for classifier training. At this stage in BCI testing, the subset of features to select would be predetermined. However, this description of BCI operation and CSP in particular does not apply to FBCSP.

6.3.3.3 CSP with multiple frequency ranges

The crucial difference in FBCSP is that the CSP algorithm is not applied to only one set of EEG data. Since, in FBCSP, the EEG data has been temporally filtered into b frequency ranges, a CSP model must be obtained for EEG of each frequency range. The CSP algorithm operates on EEG data from the b th frequency range, E_b , producing a CSP model for that frequency range, W_b . As before, this CSP model is used to project the trials of EEG data onto CSP signal space to produce CSP signals for the b th frequency range, Z_b . The set of all CSP models for all frequency ranges is referred to as the FBCSP model.

Feature extraction using variances is similar to before, however, formation of the feature set is different. This new feature set uses features from each frequency range as follows:

$$v_{b,i} = \log \left(\frac{\text{var}(Z_{b,i})}{\sum_{i=1}^{i_t} \text{var}(Z_{b,i})} \right) \quad (6.11)$$

$$\bar{v}_i = [v_{1,i}^\top, v_{2,i}^\top, \dots, v_{b_t,i}^\top] \quad (6.12)$$

$$\bar{V} = \begin{bmatrix} \bar{v}_1 \\ \bar{v}_2 \\ \vdots \\ \bar{v}_{i_t} \end{bmatrix} \quad (6.13)$$

$$\bar{y} = \begin{bmatrix} \bar{y}_1 \\ \bar{y}_2 \\ \vdots \\ \bar{y}_{i_t} \end{bmatrix} \quad (6.14)$$

where $v_{b,i} \in \mathbb{R}^{c_t \times 1}$ is the set of features for each trial i and frequency range b , $\bar{v}_i \in \mathbb{R}^{1 \times (b_t \cdot c_t)}$ is the features for each frequency range ordered into a single feature vector for each trial, $\bar{V} \in \mathbb{R}^{i_t \times (b_t \cdot c_t)}$ is the full feature set for all trials, $\bar{y} \in \mathbb{R}^{i_t \times 1}$ is the true class label vector, i_t is the total number of trials, b_t is the total number of frequency ranges and c_t is the total number of channels.

The “feature set”, \bar{V} , is thus formed by calculating the variance of trials of CSP signals for all frequency ranges. Each row of \bar{V} is the features for a single trial of data while each column of \bar{V} is the values of a single feature for each trial. Each trial, or event, has $b_t \times c_t$ features that represent that event. Each feature is an additional dimension to the event, resulting in event having a large number of dimensions. This high dimensionality of the events is too large for effective classification. Some features of an event are more useful for defining class membership so only a subset need to be used for effective classification. By taking a subset of features, the dimensionality of the events is also reduced, improving classifier performance.

6.3.4 Marginal Relevance

To choose which subset of features (i.e. columns of \bar{V}) to retain for classifier training, the method of Marginal Relevance (MRelv) was used to rank each feature. Following feature ranking, feature selection took place based on MRelv scores. MRelv uses the true class label vector, \bar{y} , to identify the group (or class of activity) that each trial belongs to i.e. Active or Rest.

The MRelv score for each feature (each column of \bar{V}) is the ratio of their between-group to within-group sum of square differences. Features whose values for one class of activity differ greatly from the values for the other class are awarded higher MRelv scores. This idea underpins statistical methodologies such as ANOVA and is explained in more detail elsewhere [237], where it was used to screen out features when a large number of spurious features are present.

To see how Marginal Relevance is calculated, take the following example feature from a set (Table 6.1). In this example, there are four events with feature value and group/class label for that event. The objective is to calculate a simple score measuring how separated feature from each group are.

Event	Value	Group
1	3	0
2	0	1
3	4	0
4	2	1

Table 6.1: Sample feature for Marginal Relevance calculation.

The group 0 average value is 3.5 while the group 1 average value is 1. Using this information, the next step is to calculate the squared difference of each feature value to the average value of their own group (within-group) and to the other group (between-group), as seen below in Table 6.2.

For this feature, the within-group sum of square differences is $0.25+1+0.25+1 = 2.5$ while the between-group sum of square differences is $4 + 12.25 + 9 + 2.25 = 27.5$. The Marginal Relevance score for this feature then is the ratio of within-group sum of square

Event	Value	Group	Group		Within-group		Between-group
			Average	Within-group difference	difference squared	Between-group difference	difference squared
1	3	0	3.5	-0.5	0.25	+2	4
2	0	1	1.0	-1	1	-3.5	12.25
3	4	0	3.5	+0.5	0.25	+3	9
4	2	1	1.0	+1	1	-1.5	2.25

Table 6.2: Additional columns for calculating Marginal Relevance.

differences to between-group sum of square differences $27.5/2.5 = 11$. This process is carried out for each feature in a feature set to assign a MRelv score and rank features.

Due to the nature of CSP and the method by which the CSP model, W , is produced, CSP signals are taken in pairs for classification. Each CSP signal corresponds to another on the opposite side of the CSP signal matrix Z . For example, the 1st and last CSP signals (those produced by the first and last rows of the spatial filter W) should be taken together for classification. Similarly, the 3rd and 3rd-from-last should be used together for classification. Accordingly, following feature ranking, the top four ranked features and their corresponding features were retained for classifier training and testing [230]. The indices of the selected features were recorded for BCI testing and formed a feature selection model. During BCI testing there is no feature ranking and only the features predetermined by the feature selection model are used for classifier testing.

6.3.5 Gaussian Process classification

The Gaussian process model has been described earlier in this thesis in subsection 4.4.1 with application in regression. Beside regression, GP models can also be used for probabilistic classification [180, 238, 239]. In the case of classification, the output data, y , are no longer connected simply to the underlying function, f , as in the case of regression but are discrete. Since the classification is binary, variable y can have one value for one class and another for the other class, e.g. $y \in \{1, -1\}$. The classification of a new data point x^* involves two steps instead of one. In the first step, a latent function f , which models qualitatively with a GP model how the likelihood of one class versus the other changes over the x axis, is evaluated. In the second step, the output of the latent function f is squashed onto the range $\{0, 1\}$ using any sigmoidal function, e.g.

$\pi(f) = \text{prob}(y = 1|f)$. This means that the squashed output of GP model represents the *probability* of a data point belonging to one of two types.

The result then, after this Gaussian process classification (GPC) during the BCI testing stage, is that each feature to be classified is assigned a probability value in the range $\{0, 1\}$, where a score of 0 indicates complete confidence that the event belongs to one class and a score of 1 indicates complete confidence that the event belongs to the other class. In practice, the majority of events take intermediate values. As the probability score for each event lies on a range, a decision threshold must be applied to these scores to make the final decision on binary class membership. A decision threshold of 0.5 is used as it is the mean value of the range of possible GPC scores.

GPC is the chosen classification method because, in comparison to the more commonly used method of Naive Bayesian classification for BCI, GPC makes no assumptions about the underlying class boundary between regressors - including allowing for non-linear class boundaries. As this analysis is concerned with stroke-affected EEG, this is a more robust classification method to use when there are uncertainties of the class space. At the other extreme, neural networks would provide the most detailed class boundary but GPC requires optimization of relatively few parameters.

6.3.6 Analyses

The signal processing steps above describe how separate EEG datasets are processed for BCI training and BCI testing. BCI analysis then continues through the choice of data for training and testing. Numerous combinations of training and testing data are used for investigation, as described below.

6.3.6.1 Single dataset 10-fold cross validation

Trials of a single dataset at a time are split into ten subgroups, separated in temporal order. Nine of the subgroups are used as data for training the BCI (i.e. “Train EEG”), meaning they are used for: (1) training the FBCSP model, (2) selection of the top ranking features using MRelv and (3) training the GPC model. For the remaining subgroup, the previously trained FBCSP model is applied, the same MRelv-determined subset of features are retained and those features are then classified by the previously-trained GPC model. This process is then repeated with each of the ten subgroups

used to test the BCI and the other nine used to train the BCI. The purpose of this analysis is to establish the consistency of the EEG responses and the classification features derived during processing of a single dataset. Classification results of each subset are averaged together. A poor average classification result would indicate that the responses recorded in a dataset were inconsistent and thus possibly unsuitable for deriving a general response.

6.3.6.2 Individual healthy dataset models applied to all data

A single healthy dataset is used to train the BCI (“Train EEG”), producing the FBCSP model, feature selection model and GPC model. Each other dataset, stroke and healthy, is then used in turn to test the BCI (“Test EEG”). This resulted in a set of one-on-one BCIs where one subject’s EEG patterns were classified against each healthy subject’s EEG patterns. Classification accuracy here may represent a level of similarity of EEG patterns between individual subjects. Although this is an atypical BCI modality approach, it allows investigation of the variability of classification rates when comparing healthy and stroke subject EEG.

6.3.6.3 Grouped healthy dataset model applied to stroke data

A “general” BCI is trained on the 10 healthy subject datasets. Trials from all healthy datasets are collated into one dataset, E , producing a general FBCSP model, W , and CSP signals, Z . Following feature extraction, the feature set, \bar{V} , is much larger as it now contains events from all healthy datasets but the number of features per event is the same as before. After feature ranking and selection, the general GPC model is produced. Such a BCI modality is common in communication and control BCI as healthy subjects may use this trained BCI without having to record a training set themselves. Each stroke dataset is then used to test the BCI, resulting in classification accuracy scores that may be viewed as measures of the similarity of stroke EEG to healthy EEG.

6.3.6.4 Leave-one-out cross-validation of healthy datasets

As before, a general healthy BCI is trained on all healthy datasets but one. The remaining healthy dataset is then used to test the BCI and this process is repeated for

each healthy dataset. This approach produces classification results that are useful for comparison to the previous stroke classification results on general healthy BCI.

6.3.6.5 Early Stroke datasets used to classify corresponding Late Stroke datasets

Each stroke subject recorded an “Early” and “Late” dataset. For each stroke subject, their early dataset is used to train the BCI and their late dataset is used to test. Classification accuracy of the late dataset represents a measure of the similarity of the EEG patterns of each stroke subject between recording sessions. A high classification accuracy indicates little change while a relatively low classification accuracy indicates significant change in EEG patterns - presumably due to neuroplastic change during stroke recovery.

6.3.6.6 Frequency ranges of selected CSP features

Another result of interest is the frequency ranges of selected CSP features for each dataset. To investigate this, the frequency ranges of the selected CSP features is recorded. For each group of Healthy, Early Stroke and Late Stroke, a histogram of selected frequency ranges is generated to investigate which frequency ranges were favoured and to highlight any differences between groups.

6.4 Results

6.4.1 Single dataset 10-fold cross validation

Classification results following 10-fold cross-validation on each dataset are shown in Table 6.3. 8/10 healthy subject datasets scored 100% classification accuracy and the remaining 2/10 scored 97.5% while only 5/10 stroke datasets scored 100% and the remaining 5/10 scored between 85% and 97.5%. 2/5 early stroke datasets scored 100% while 3/5 late stroke datasets scored 100%. A range of k values for k-fold cross validation of k = 2, 4, 6... 16 were tested but no significant changes in these results compared to k = 10 were seen and so are not presented here.

Wilcoxon Rank Sum tests were used to test statistical differences between subject groups. There were no significant differences found between Healthy (Median = 100) and All Stroke (Median = 98.75) ($Z = 1.64$, $p < 0.05$, $r = 0.37$), between Healthy (Median = 100) and Early Stroke (Median = 97.5) ($p < 0.05$), between Healthy (Median = 100) and Late Stroke (Median = 100) ($p < 0.05$) or between Early Stroke (Median = 97.5) and Late Stroke (Median = 100) ($p < 0.05$).

Dataset	S1E	S1L	S2E	S2L	S3E	S3L	S4E	S4L	S5E	S5L
Accuracy	97.50	100.00	100.00	87.50	93.75	100.00	100.00	85.00	95.00	100.00
Dataset	H1	H2	H3	H4	H5	H6	H7	H8	H9	H10
Accuracy	100.00	100.00	97.50	97.50	100.00	100.00	100.00	100.00	100.00	100.00

Table 6.3: Single dataset 10-fold cross-validation classification accuracy %

6.4.2 Individual healthy dataset models applied to all data

A table of individual classification accuracies when training the models and classifier on each healthy dataset and then testing on all other datasets is presented in Table 6.4.

Wilcoxon Rank Sum tests were used to evaluate statistical differences between these classification results for the Healthy, All Stroke, Early Stroke and Late Stroke groups. There were significant differences found between Healthy (Median = 82.5) and All Stroke (Median = 70.0) ($Z = 5.55$, $p < 0.05$, $r = 0.40$), between Healthy (Median = 82.5) and Early Stroke (Median = 71.25) ($Z = -3.97$, $p < 0.05$, $r = 0.34$) and between Healthy (Median = 82.5) and Late Stroke (Median = 61.25) ($Z = -5.18$, $p < 0.05$, $r = 0.44$). There was no significant difference found between Early Stroke (Median = 71.25) and Late Stroke (Median = 61.25) ($Z = 1.75$, $p < 0.05$, $r = 0.17$).

6.4.3 Grouped healthy dataset model applied to stroke data

Classification accuracies of each stroke dataset when the BCI is trained on all of the healthy EEG datasets grouped together is presented in Table 6.5.

Wilcoxon Signed Rank tests were used to test for statistical significance in the change in classification accuracy when using grouped healthy datasets to train the BCI as compared to the average results when using individual healthy datasets to train BCIs. No significant change ($p < 0.05$) in classification accuracy was found for datasets

6.4 Results

		Train EEG dataset										Avg	SD
		H1	H2	H3	H4	H5	H6	H7	H8	H9	H10		
Test EEG dataset	S1E	62.5	75.0	97.5	85.0	72.5	47.5	87.5	90.0	87.5	72.5	77.8	14.9
	S1L	75.0	70.0	80.0	75.0	42.5	77.5	57.5	70.0	82.5	67.5	69.8	11.9
	S2E	70.0	62.5	60.0	77.5	50.0	62.5	70.0	50.0	87.5	65.0	65.5	11.5
	S2L	57.5	50.0	55.0	55.0	40.0	55.0	60.0	52.5	62.5	57.5	54.5	6.2
	S3E	75.0	53.1	81.3	75.0	62.5	78.1	84.4	78.1	81.3	75.0	74.4	9.5
	S3L	77.5	60.0	87.5	72.5	52.5	85.0	70.0	80.0	92.5	90.0	76.8	13.1
	S4E	70.0	57.5	40.0	65.0	60.0	65.0	67.5	52.5	62.5	72.5	61.3	9.5
	S4L	52.5	70.0	40.0	50.0	55.0	70.0	47.5	55.0	60.0	57.5	55.8	9.4
	S5E	90.0	55.0	65.0	90.0	75.0	80.0	55.0	72.5	65.0	72.5	72.0	12.5
	S5L	82.5	57.5	60.0	77.5	80.0	55.0	47.5	85.0	70.0	95.0	71.0	15.4
	H1		72.5	75.0	92.5	97.5	97.5	87.5	100.0	97.5	100.0	91.1	10.6
	H2	62.5		37.5	62.5	80.0	55.0	67.5	90.0	55.0	82.5	65.8	16.3
	H3	95.0	65.0		85.0	80.0	65.0	87.5	95.0	80.0	90.0	82.5	11.3
	H4	80.0	72.5	77.5		57.5	65.0	77.5	82.5	90.0	90.0	76.9	10.7
	H5	85.0	72.5	55.0	52.5		52.5	65.0	80.0	60.0	85.0	67.5	13.5
	H6	100.0	65.0	65.0	97.5	87.5		80.0	70.0	95.0	87.5	83.1	13.7
	H7	92.5	65.0	92.5	82.5	87.5	72.5		92.5	92.5	65.0	82.5	11.9
	H8	100.0	80.0	60.0	90.0	90.0	80.0	72.5		90.0	92.5	83.9	12.1
	H9	95.0	55.0	67.5	97.5	80.0	92.5	65.0	100.0		97.5	83.3	17.0
	H10	87.5	67.5	80.0	85.0	85.0	87.5	70.0	95.0	100.0		84.2	10.5
Healthy datasets											80.1	14.4	
All Stroke datasets											67.9	13.7	
Early Stroke datasets											70.2	12.8	
Late Stroke datasets											65.6	14.3	

Table 6.4: Cross-dataset classification accuracy %

S1E, S1L, S2L, S3E and S4E. A significant increase ($p < 0.05$) in classification accuracy for datasets S3L, S4L, S5E and S5L was found and a significant decrease ($p < 0.05$) for dataset S2E was found.

Test dataset	Accuracy
S1E	87.5
S1L	62.5
S2E	52.5
S2L	55.0
S3E	75.0
S3L	87.5
S4E	65.0
S4L	65.0
S5E	82.5
S5L	90.0
All average	72.3 ± 14.1
Early average	72.5 ± 14.0
Late average	72.0 ± 15.8

Table 6.5: Grouped healthy classification accuracy %

6.4.4 Leave-one-out cross-validation of healthy datasets

Classification accuracies of each healthy dataset when the BCI is trained on all other healthy datasets grouped together is presented in Table 6.6.

Wilcoxon Rank Sum tests were used to evaluate statistical differences between these classification results for the Healthy, All Stroke, Early Stroke and Late Stroke groups when grouped healthy datasets were used to train the BCI. There was a significant difference found between Healthy (Median = 94) and All Stroke (Median = 70) ($Z = 3.04$, $p < 0.05$, $r = 0.68$), between Healthy (Median = 94) and Early Stroke (Median = 75) ($p < 0.05$) and between Healthy results (Median = 94) and Late Stroke results (Median = 65) ($p < 0.05$). There was no significant difference found between Early Stroke results (Median = 75) and Late Stroke results (Median = 65) ($p < 0.05$). The Z and r statistics were not calculated when very few data points were available. These between-group significant difference results are the same as those obtained when using individual BCIs trained on healthy datasets.

Test dataset	Accuracy
H1	100.0
H2	90.0
H3	95.0
H4	80.0
H5	87.5
H6	97.5
H7	92.5
H8	95.0
H9	95.0
H10	85.0
Average	91.8 ± 6.1

Table 6.6: Leave-one-out cross-validation of healthy data classification accuracy %

6.4.5 Early Stroke datasets used to classify corresponding Late Stroke datasets

Classification results of each Late Stroke dataset when training the BCI with the corresponding Early Stroke dataset are shown in Table 6.7. Classification accuracy of the five Late Stroke datasets ranged from 62.5% to 95% with a median of 75.0%. We can compare these classification accuracy results to those obtained when training the BCI on individual healthy datasets and those obtained when training on grouped healthy datasets.

Wilcoxon Signed Rank tests were used to compare these longitudinal classification results to those obtained when using BCIs trained on individual Healthy datasets. A significant ($p < 0.05$) increase was seen for S1L, S2L and S3L while there was no significant change ($p < 0.05$) found for S4L and S5L.

Comparing the longitudinal classification accuracies to those obtained when training the BCI on grouped healthy datasets, we see that S1L improved from 62.5% to 82.5%, S2L improved from 55% to 72.5%, S3L improved from 87.5% to 95%, S4L reduced from 65% to 62.5% and S5L reduced from 90% to 75%.

Train EEG dataset	Test EEG dataset	Accuracy
S1E	S1L	82.5
S2E	S2L	72.5
S3E	S3L	95.0
S4E	S4L	62.5
S5E	S5L	75.0
Average		77.5 ± 12.1

Table 6.7: Longitudinal classification accuracy %

6.4.6 Comparison of all BCI training methods for stroke

A table of collated classification results of each BCI training method for each stroke dataset is presented in Table 6.8.

6.4.7 Frequency ranges of selected CSP features

Presented in Table 6.9 are the frequency ranges of the CSP features selected for classifier training for each full dataset. A corresponding histogram of this data grouped for Healthy, Stroke Early and Stroke Late datasets is presented in Figure 6.3. This histogram suggests that, for healthy EEG, the frequency ranges of the CSP features in the 16–20 Hz and 20–24 Hz are most frequently selected. Early stroke datasets display some of the healthy datasets' preference for selection of features in the 16–24 Hz range however there is also increased selection of features in the 8–16 Hz range. Late stroke datasets appear to shift towards further selection of CSP features in lower frequency ranges, with a noticeable increase in selection in the 4–16 Hz range and a relative decrease in selection from 16 Hz upwards.

Dataset	Individual Healthy		Grouped Healthy	Early Stroke
	Avg	StDev		
S1E	77.8	14.9	87.5	
S1L	69.8	11.9	62.5	82.5
S2E	65.5	11.5	52.5	
S2L	54.5	6.2	55.0	72.5
S3E	74.4	9.5	75.0	
S3L	76.8	13.1	87.5	95.0
S4E	61.3	9.5	65.0	
S4L	55.8	9.4	65.0	62.5
S5E	72.0	12.5	82.5	
S5L	71.0	15.4	90.0	75.0
All average	67.9 ± 8.3		72.3 ± 14.1	
Early average	70.2 ± 6.7		72.5 ± 14.0	
Late average	65.6 ± 9.9		72.0 ± 15.8	77.5 ± 12.1

Table 6.8: Comparison of BCI training methods for stroke classification

Dataset	Rank of selected features			
	1st	2nd	3rd	4th
S1E	16-20	12-16	8-12	16-20
S1L	8-12	4-8	8-12	4-8
S2E	8-12	8-12	12-16	20-24
S2L	36-40	32-36	32-36	12-16
S3E	12-16	8-12	16-20	20-24
S3L	12-16	12-16	16-20	12-16
S4E	24-28	8-12	16-20	20-24
S4L	24-28	12-16	20-24	16-20
S5E	16-20	12-16	24-28	16-20
S5L	4-8	4-8	8-12	4-8
H1	16-20	20-24	16-20	16-20
H2	24-28	36-40	20-24	24-28
H3	36-40	16-20	24-28	36-40
H4	16-20	16-20	20-24	16-20
H5	20-24	24-28	20-24	16-20
H6	12-16	8-12	12-16	12-16
H7	12-16	16-20	16-20	12-16
H8	20-24	16-20	20-24	24-28
H9	12-16	16-20	8-12	16-20
H10	20-24	16-20	20-24	16-20

Table 6.9: Frequency ranges (Hz) of selected CSP features for each dataset

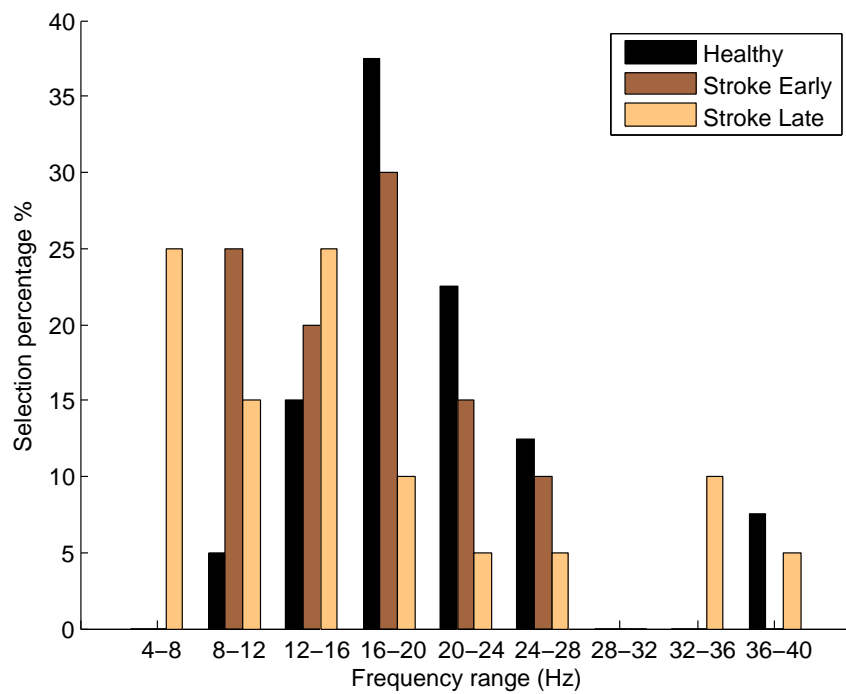


Figure 6.3: Marginal Relevance Selected frequency ranges.

6.5 Discussion

6.5.1 Effect of Stroke

The results of statistical analysis of single dataset 10-fold cross-validation classification accuracies suggest that stroke-affected EEG data is no more likely to contain misclassified trials than healthy EEG. Given that even with healthy subjects engaging successfully in a motor task, flawless classification is not always possible, then it would not be unreasonable to expect similar or even worse consistency in stroke-affected brains. This analysis suggests that there is no difference between the consistency of healthy and stroke-affected EEG patterns. It is important to note, however, the very low statistical power of this test due to the low number of data points available for comparison (5 for each of late and early stroke subject data, 10 for healthy subject data). Therefore, other factors, such as a lapse in concentration on the part of the subject, a restless hand movement, an involuntary leg twitch or possibly the effects of fatigue could reasonably cause a change in the event-related EEG, confounding the efforts of the classifier. A similar analysis with a larger cohort would be required before drawing a conclusion on this topic.

It is assumed that each subject performed the task correctly and to the best of their ability. Visual supervision of the subjects did not reveal any movement incidents and neither did artefact analysis of trial data. Subject S3 reported being fatigued during their early experimental session, resulting in only 36 out of the potential 40 trials being completed. Dataset S3E also scored the 2nd lowest 10-fold cross-validation classification rate of all datasets at 93.75%. This may suggest a link between fatigue and low k-fold cross-correlation results but that the lowest scoring dataset was S4L, where no fatigue was reported. This illustrates the difficulty of describing the processes which underlie the variable EEG features identified.

Classification accuracy results of cross-dataset BCI analysis with training the BCI on each healthy dataset and testing on each other dataset provided another perspective on the differences between healthy and stroke-affected EEG patterns. While this BCI method is not practical and would not be used for a real rehabilitation BCI, the differences between the classification scores attained by each type of dataset does bear some discussion. As seen in Table 6.4, the average classification accuracy for Healthy datasets is $80.1 \pm 14.4\%$, for Early Stroke datasets is $70.2 \pm 12.8\%$ and for Late Stroke

datasets is $65.6 \pm 14.3\%$. Statistical tests revealed significant differences between the Healthy and Stroke Datasets overall. Average stroke classification accuracy by individual healthy dataset-trained BCIs is significantly lower than healthy. This suggests that, although some individual classification results between datasets were quite variable and unexpected (training on H4 resulted in 90% accuracy for S5E but 52.5% for H5, for example) there appears to be, on average, a difference in EEG patterns between stroke data and healthy data. These cross-dataset EEG classifications are important because the reasons for such varying classification successes may be important for advancing rehabilitation BCI and our understanding of stroke-affected EEG, yet these are not results that we would see if we restricted ourselves to the more typical general BCI method.

Aggregating and analysing classification results in the previous manner is useful for exploring aspects of stroke-affected EEG for BCI but does not represent a typical zero-training BCI implementation. By training the BCI on all healthy datasets and testing on individual stroke datasets, stroke datasets are analysed in a more typical way for zero-training BCI. The results presented in Table 6.5 can be seen as a measure of the similarity of the EEG patterns of each stroke dataset to general healthy EEG patterns. By taking the leave-one-out cross-validation results of healthy datasets in Table 6.6 as a baseline for expected results with healthy EEG patterns, the stroke dataset classification results suggest, through the lower classification accuracy of 72.3% on average than 91.8% for healthy, that a difference in EEG patterns has been quantified and observed.

6.5.2 Rehabilitation BCI Training Data

Table 6.8 collates the BCI classification accuracies of each stroke dataset with each method described above. This table is useful when discussing which method is best for training a rehabilitation BCI with focus on the Late Stroke datasets - S1L, S2L, S3L, S4L and S5L. The ‘Individual Healthy’ column does not represent an actual rehabilitation BCI training option and so is not considered here. ‘Grouped Healthy’ represents a zero-training BCI while ‘Early Stroke’ represents a BCI which had been trained many months previously. Together, these results represent BCIs which, at the time of late recording session require no training session before BCI testing. For three out of the

five Late Stroke datasets, higher classification accuracy was obtained when training the BCI on the subject's own Early Stroke dataset. The remaining two datasets, S4L and S5L obtained higher classification accuracy when the BCI was trained on grouped Healthy data. Thus, there is no definitive conclusion on which of these two options is better.

The third option for training a rehabilitation BCI is for the subject to participate in a BCI training recording session immediately before real-time BCI use. While no such separate dataset had been recorded, as long as we can assume that a subject's EEG patterns do not change significantly between BCI training and immediate testing, then the 10-fold cross validation results of Table 6.3 indicate how successfully such a BCI could operate. In this case, each stroke subject attained higher classification accuracy than the zero-training or one-time-training options above. This suggests that performing a BCI training session immediately before BCI testing produces the most accurate results. This result, however, does not account for extra fatigue induced by extra time the subject spends participating in BCI operation.

Therefore, the decision to record a training session of EEG activity for each subject may depend on a trade-off between improved classification accuracy and any possible negative effects of subjecting a stroke patient to an EEG recording session. Possible negative effects include anxiety (as many stroke patients are elderly and may have apprehension about participating in an EEG recording session), loss of therapy time (as time spent training leads to a reduction in time spent using the BCI in a therapeutic mode) and fatigue (because a stroke patient may become fatigued as a result of training, leaving little energy for the therapeutic interaction). In these patients where the above factors are prevalent the BCI may have to be trained using healthy data. The disadvantage of this approach from a therapy perspective is that the inferior performance of the classifier may lead to frustration on the part of the patient and a potential rejection of the therapy.

6.5.3 CSP Plots

Presented in Figure 6.4 and Figure 6.5 are CSP plots of the highest ranked CSP features for both classes of activity for all datasets. There are too few datasets available for these

plots to provide any more than a qualitative analysis of the differences between stroke-affected and healthy CSP plots. These plots demonstrate more left/right asymmetry in the common spatial patterns of healthy datasets than stroke-affected datasets. As the differences between the two groups is not strong enough to draw any conclusions, these plots merely suggest that stroke-affected CSP plots are not dissimilar to healthy CSP plots.

6.5.4 Biomarker for Neurorehabilitation

Marginal Relevance rankings of CSP features presented in Table 6.9 and Figure 6.3 reveal that the particular BCI implemented here selected features of varying frequency ranges for each group of subject data. For healthy data, EEG activity in the frequency ranges of 6–20 Hz and 20–24 Hz was favoured. For early stroke data, lower frequency ranges, particularly 8–12 Hz, were selected more than healthy data. Finally, for late stroke data, the lowest frequency ranges were selected more than others. Therefore, this data and histogram demonstrates a shift in BCI parameters following stroke and stroke recovery.

BCI classification accuracy may be treated as a measure of the similarity of one EEG dataset to another. In this way, the BCI analyses described here may quantify the deviation of stroke-affected EEG patterns from typical healthy EEG patterns. Additionally, as data was recorded soon after the stroke subject suffered their stroke and again data was recorded months later, these classification results may be viewed as a measure of the change in EEG patterns over that time. The usefulness in these numbers may lay in their relation to the measures of each subject's motor control, the Kapandji score (Table 5.3). However, the classification accuracies and the change in classification accuracies of stroke datasets when the BCI is trained on grouped healthy data bare little relation to the subject's Kapandji score or change in Kapandji score. Additionally, there is no relation between each subject's Kapandji scores and their late dataset classification accuracy with a BCI trained on their early data. It would only be speculative to try to relate these terms. It is possible that a link may be found with a similar analysis and a much larger dataset. It is also likely that changing EEG patterns, effect of the stroke and rate of recovery are dependant on clinical factors, such

as lesion location, or on environmental factors, such as subject engagement with traditional rehabilitation therapy. Perhaps a link between these factors and BCI parameters may be uncovered in the future.

Given the changes in the EEG pattern in stroke compared to the stereotypical patterns for healthy subjects and their evolution over time it appears that there is scope for improved machine learning techniques which can work from short session data and continually adapt to the user. There is some recent work in this area for healthy subjects using passive movement approaches [240] and data space adaptation techniques [241]. However, it is incredibly important to note the tension between using machine learning to adapt the interface to the EEG patterns on one hand and forcing the patient to adapt to a classifier which is targeting the appropriate cortical networks for healthy movement on the other. To understand this somewhat subtle point, it is worth noting that natural recovery in stroke is often suboptimal (spasticity, abnormal muscle synergies, etc.) and these neurological symptoms can be related to pathophysiological motor and compensatory networks that have arisen from the reorganization process. It is these changes which are most likely reflected in the EEG measurements reported here. If a machine learning algorithm consistently adapts to the patient to optimize communication with the feedback interface the therapy may well lead to reinforcement of these maladaptive changes. It may be better that the patient adapts to a classifier which is set up to expect EEG features which are more typically associated with engagement of those areas of cortex more associated with healthy movement. The catch is that such a classifier may be far too frustrating to use and therefore some trade-off between encouraging engagement and directing recovery will have to be met for an effective BCI instrument in this use case scenario. This issue should be contrasted with the corresponding case for communication and control BCI which instead adapts to whatever aspects of a subject's EEG is under volitional control requiring less adaptation on the part of the user.

The classification accuracy and BCI parameters results here suggest that offline BCI analysis may potentially have utility as a clinical tool to produce a biomarker of neurorehabilitation. While this is currently a proof-of-concept, the analysis results here suggest that differences between healthy and stroke-affected brains are measurable in this way. Significant further development of this concept would be required before real application to assist in rehabilitation therapy efforts.

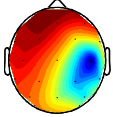
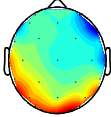
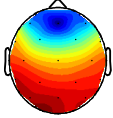
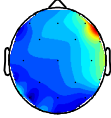
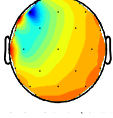
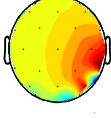
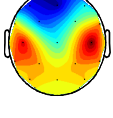
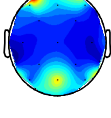
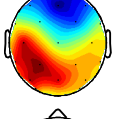
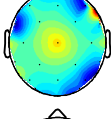
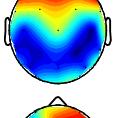
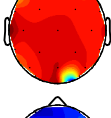
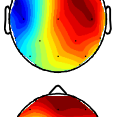
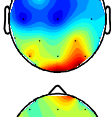
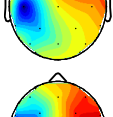
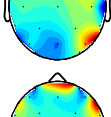
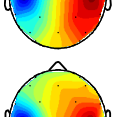
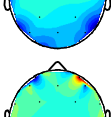
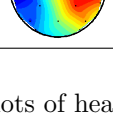
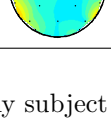
Dataset	Hand	CSP Plots		Frequency Range
		Active	Rest	
H1	L			16-20 Hz
H2	R			8-12 Hz
H3	R			8-12 Hz
H4	L			36-40 Hz
H5	R			12-16 Hz
H6	R			12-16 Hz
H7	R			24-28 Hz
H8	R			24-28 Hz
H9	R			16-20 Hz
H10	R			4- 8 Hz

Figure 6.4: Plots of healthy subject data CSP.

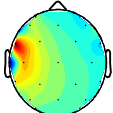
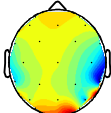
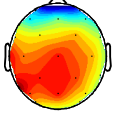
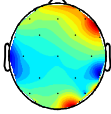
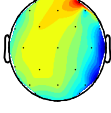
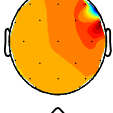
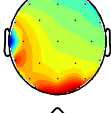
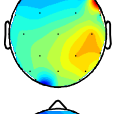
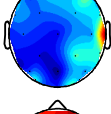
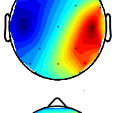
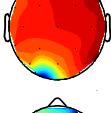
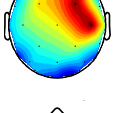
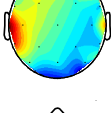
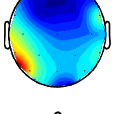
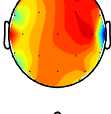
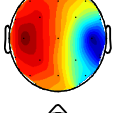
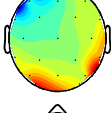
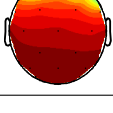
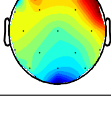
Dataset	Hand	CSP Plots		Frequency Range
		Active	Rest	
S1E	R			16-20 Hz
S1L	R			8-12 Hz
S2E	R			8-12 Hz
S2L	R			36-40 Hz
S3E	R			12-16 Hz
S3L	R			12-16 Hz
S4E	L			24-28 Hz
S4L	L			24-28 Hz
S5E	R			16-20 Hz
S5L	R			4- 8 Hz

Figure 6.5: Plots of stroke-affected subject data CSP.

6.6 Summary

This chapter investigated the effect of stroke on EEG BCI performance through an offline BCI analysis but also produced other interesting outcomes. BCI classification accuracies were investigated as a measure of the difference in brain activation patterns between the BCI training dataset and the BCI testing dataset. Classification of stroke subject EEG when the BCI was trained on either individual or grouped healthy EEG was lower than when healthy subject EEG was tested. These classification accuracies may have application as a biomarker of post-stroke neurorehabilitation following a larger-scale investigation. Additionally, machine-learned BCI parameters were investigated as a biomarker of neurorehabilitation with the frequency range of selected features showing a progressive change from healthy, to 3 weeks post-stroke, to 6-7 months post-stroke. It appears that BCI classification accuracy and machine-learned BCI parameters may have utility in a clinical setting for assessing post-stroke recovery. However, due to the relatively low number of subjects and recording sessions, these findings merely serve as a first look into this utility. A significantly larger amount of data and analysis is required for conclusive outcomes.

Rehabilitative BCIs must take these differences in EEG patterns between healthy subjects and stroke-affected subjects into account in order for the system to be effective and to aid in recovery. The ideal scenario of a zero-training rehabilitative BCI is possible using healthy EEG but the classification accuracy is lower than for healthy subjects which could be excessively frustrating for patients. Classification accuracy of stroke EEG is improved significantly through subject-specific BCI training sessions even 6 months prior however this comes with a cost in terms of loss of rehabilitation time and potentially over-adaptation to the user, which may be detrimental in terms of optimal recovery. It is clear that a rehabilitative BCI must have different technical requirements to those for a communication and control BCI and these differences must be considered when developing the appropriate machine learning scheme for this use case.

While BCI classification accuracies and BCI parameters may have utility as biomarker of neurorehabilitation, they are not direct representations of the stroke-affected brain network. For an explicit biomarker of neurorehabilitation, another analysis is required which attempts to directly measure the effect of stroke on a brain. Attempts to discover such a biomarker are the subject of the next chapter.

Chapter 7

Post-Stroke Connectivity Analysis and a Portable Stroke Rehabilitation BCI

7.1 Introduction

The previous chapter achieved two objectives: to explore the effect of stroke on EEG BCI parameters in order to inform future rehabilitation BCI design and to investigate a potential *implicit* biomarker of post-stroke neuroplastic change based on those parameters. The biomarker results are particularly interesting because they are directly affected by the stroke patient's brain network. However, while the effect is direct, the representation is not because the post-stroke brain network is represented in BCI parameters which have no direct relation to the subject's functional neurophysiological condition. Essentially, BCI parameters are poor representations of functional activity and are likely of little use in a clinical setting.

An *explicit* biomarker of neuroplastic change is far more desirable - one that directly represents that functional state of a stroke-affected brain, which is interpretable and relatable to a stroke survivor's functional neurophysiological condition. Such a biomarker is desirable because of potential utility in a clinical setting, where it may be used to inform and guide stroke rehabilitation therapy. Such a biomarker may be

attainable through connectivity analysis, as described in section 5.3.

In the previous chapter, analysis involved the automatic extraction of the best signal features for classification but these features did not explicitly represent brain activity - they are not easily interpretable by a human. This chapter expounds the use of an analysis method which is designed to uncover interactions between regions of the brain. Activity in a region of the brain produces an electrical signal which passes along a neural pathway and may contribute to the induction of activity in another region of the brain. If activity is induced, this electrical interaction can be seen as the movement of information from the “driver” region to the “recipient” region and is referred to as information flow [209, 211] - a term originating in Information Theory to describe the transfer of information between two variables in a process. Information flow refers to effective connectivity - *“the influence that one neuronal system exerts over another”* [242] - and the terms are used here interchangeably.

This chapter begins with a description of efforts to derive an explicit measure of neuroplastic change, based on connectivity analysis of the recorded healthy and stroke subject EEG dataset through application of a recent information flow estimation algorithm, followed by a discussion of future directions in this research space. This chapter then ends with a description of the design and development of a low-cost, portable biofeedback EEG BCI which may be used for rehabilitation BCI research and serves as a proof-of-concept for at-home stroke rehabilitation.

7.2 Connectivity Measurement

The simplest method for estimating functional connectivity between two zero-mean variables x and y appears to be covariance, the measure of how much two random variables change together, defined as $cov(x, y) = E(xy)$, $cov(x, y) \in \mathbb{R}$ or the normalised covariance $\rho(x, y) = E(xy)/(|E(x)||E(y)|)$, $\rho \in (-1, 1)$, where $E(\cdot)$ is the expected value operator and $|\cdot|$ is the absolute value operator. However, for scalp-recorded EEG time series, these are not appropriate due to the volume conductor effect of the head where brain sources are expressed in multiple EEG recordings and due to the fact that correlation is an instantaneous operation which cannot identify the direction of information flow. An obvious improvement to deal with the instantaneous nature of the correlation operation is to employ a time-lagged normalised correlation operation

$\rho(x, y, \tau) = E(x(t)y(t - \tau))/(|E(x(t))||E(y(t))|)$ for a range of time delays τ . These correlation methods have been employed previously in the analysis of EEG [243] data and data of another near-infrared measurement modality, Event-Related Optical Signal (EROS) [244]. As correlation is unable to determine the direction of information flow between two variables, or time series, other methods which are capable of measuring directional interactions are favoured for connectivity analysis.

7.2.1 Granger Causality

With respect to brain networks, Granger causality refers to the concept that interactions between two brain sources, or nodes of a brain network, can be identified and measured. In 1956, Weiner [245] proposed that a causal relationship exists between two time series is measurable if statistical information of one time series improves prediction accuracy of the other time series. In 1969, Granger [246] adapted this idea and those of other similar papers to provide a definition of causality which has come to be known as Granger causality. The central tenet of Granger causality is that time series \mathbf{X} *Granger-causes* time series \mathbf{Y} if past values of \mathbf{X} predict future values of \mathbf{Y} better than past values of \mathbf{Y} alone. This idea can then be expanded to include past values of multiple additional time series, to measure the causal relationship between all time series available.

Various tools have been developed to measure Granger causality between time series. The Multivariate autoregressive (MVAR) model method estimates the linear combination of past values of each time series which best predict the current values of each of those time series. Methods based on signal entropy and information, such as quasi-causal information (QCI) [247] and correntropy [248]. A full review on connectivity measures for EEG data can be found elsewhere [213].

7.2.2 Phase Slope Index

Brain network connectivity may also be estimated from non-Granger causality-based methods. As mentioned previously, the two main paradigms for studying brain activity are brain networks and brain rhythms. The rhythmic activity of the brain can be analysed to infer connectivity in the brain network using a suite of space-frequency and space-time-frequency methods applied to scalp EEG time series. Phase Slope

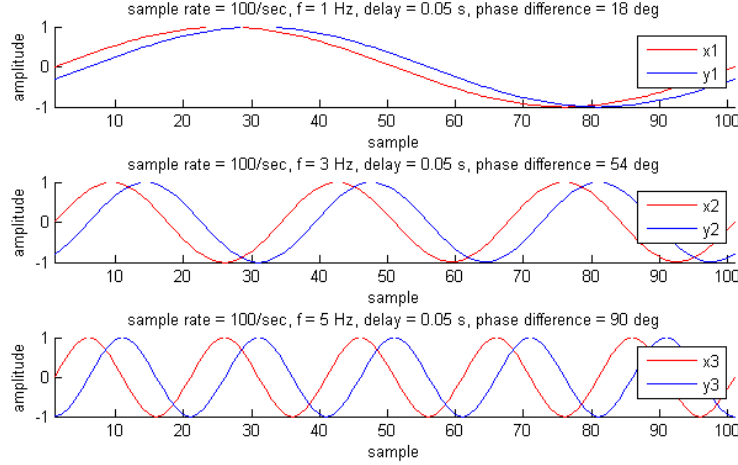


Figure 7.1: Frequency-dependent phase difference.

Index (PSI) was first investigated as one such method by Nolte et. al. in 2008 [249], who reported that this method performed much better than Granger causality-based methods. PSI performed better by only paying attention to the phase information and ignoring information affected by volume conduction. The central tenet of PSI is that if two sources of EEG are interacting as “cause-and-effect”, where activity in one region of the brain drives activity in another region, then some components of the recorded “cause” signal will appear delayed and attenuated in the recorded “effect” signal. Interactions between brain regions require time and if the propagation speed is always the same, then the phase difference between activity at interacting regions increases with frequency of oscillation. The concept of phase difference increasing with frequency is illustrated in Figure 7.1.

Coherence is a statistical measure of the relation between two time series $y_i(t)$ and $y_j(t)$, which may also be used to find the causality between EEG signals. Coherence between two time series is a complex number, defined as:

$$S_{ij}(f) = \langle y_i(f)y_j^*(f) \rangle \quad (7.1)$$

where $\langle \cdot \rangle$ denotes the expectation value. The phase spectrum $\Phi(f)$ between the two time series is linear and proportional to the time delay τ . The slope of $\Phi(f)$ can be

7.3 Connectivity Analysis of Acquired Dataset with PSI

estimated, where a positive slope indicates a causal direction from $y_i(t)$ to $y_j(t)$ and a negative slope indicates a causal relation in the reverse direction.

Using the above cross-spectral density operation, the coherence is defined as:

$$C_{ij}(f) = S_{ij}(f) / \sqrt{S_{ii}(f)S_{jj}(f)} \quad (7.2)$$

where $S_{ii}(f)$ and $S_{jj}(f)$ are the auto-spectral densities of $y_i(t)$ and $y_j(t)$, respectively. The “phase slope index” between the two time series is then defined as

$$\tilde{\Psi}_{ij} = \Im \left(\sum_{f \in F} C_{ij}^*(f) C_{ij}(f + \delta f) \right) \quad (7.3)$$

where δf is the frequency resolution, $\Im(\cdot)$ denotes taking the imaginary part and F is the set of frequencies over which the slope is summed. $\tilde{\Psi}$ vanishes if the imaginary part of coherence vanishes, so PSI is insensitive to mixtures of non-interacting sources [250, 251]. Therefore, unlike other methods for calculation of connectivity, PSI is robust to EEG’s natural volume conduction of mixed sources [212]. Finally, the “PSI scores”, $\tilde{\Psi}$, are normalised with their standard deviation, which is estimated using the Jackknife method:

$$\Psi = \tilde{\Psi} / \text{std}(\tilde{\Psi}) \quad (7.4)$$

The disadvantage of PSI is that it estimates net information flow rather than absolute. Should two sources transmit equal amounts of information to each other at the same time, then the average phase slope of the sources over the frequency range of interest will be zero. In this way, PSI is at a disadvantage to Granger causality-based methods for connectivity analysis. However, due to PSI’s reported robustness to volume conduction, there is no need to perform source localisation prior to analysis.

7.3 Connectivity Analysis of Acquired Dataset with PSI

The Healthy and Stroke-affected EEG data was analysed in Matlab [224] using a combination of EEGLAB [232], PSI code¹ and custom scripts to attempt to estimate connectivity in each subject’s brain networks during each class of activity. The resulting

¹<http://doc.ml.tu-berlin.de/causality/>

7.3 Connectivity Analysis of Acquired Dataset with PSI

normalised PSI scores would be analysed to determine if there are any statistically significant differences between PSI-estimated information flow of healthy and stroke-affected subjects.

7.3.1 PSI with Common Average Referencing

7.3.1.1 Processing Steps

In order to compare active hand EEG activity across all subjects, left-handed EEG data was “mirrored”. As a result, EEG signals are no longer referred to by their location on the 10-20 system but rather by “Contralateral” and “Ipsilateral”, to describe the side of the brain opposite to the side of hand movement and on the same side as hand movement, respectively. EEG data was then re-referenced using common average referencing before being epoched into 10 second-long trials of data beginning at instruction onset. Each trial of data was labelled appropriately as either “rest” or “active”.

Finally, signals were assessed for movement artefact. 40 datasets were created: “rest” and “active” for each of the ten healthy subject datasets, for the five early stroke datasets and for the five late stroke datasets. Stroke datasets are labelled SXE or SXL where X indicates subject number, E indicates “early” and L indicates “late”.

The PSI algorithm operates on a set of trials of epoched data, such as one of the 40 EEG datasets described above. For each trial of data in each dataset, the Ψ matrix of size 32×32 is produced, as there are 32 EEG channels and so a matrix of interactions between each of those channels is obtained. The diagonal of the PSI matrix is always undefined, as there is no information flow from a signal to itself. It is important to note that, as PSI estimates *net* information flow, the magnitude of PSI score between any two signals is always of the same but with opposite sign.

PSI is capable of estimating information flow for any frequency range - allowing for information of any frequency range to be estimated. Rather than limiting this initial investigation into the method to narrow frequency ranges, the frequency range 5 to 30 Hz was chosen. As the 40 datasets contained 20 trials of EEG data, 20 Ψ matrices were obtained for each dataset. Each of these matrices contained $32 \times 32 = 1,024$ elements. 32 of those matrix elements along the diagonal are null, leaving $1,024 - 32 = 992$ PSI scores for each trial of data, describing net information flow between each

7.3 Connectivity Analysis of Acquired Dataset with PSI

scalp-recorded EEG channel. As there were 20 trials per dataset, there were $992 \times 20 = 19,840$ PSI scores per dataset available for subsequent statistical analysis. Each EEG channel pair had 20 PSI values representing net information flow between them. These PSI scores will next be statistically analysed.

7.3.1.2 Statistical Analysis

Two-sided t-tests with a significance level of 5% were employed in order to determine significant differences between the PSI scores of different datasets. To determine if stroke had caused a statistically significant difference in information flow between two EEG sensor locations, the PSI scores for a particular source-destination sensor pair for all healthy subjects would be compared to the corresponding PSI scores for a stroke subject. The statistical test would indicate any significant increase or decrease in PSI scores.

Unfortunately, two immediate issues stand out. Firstly, there is no guarantee that the EEG sensors are in precisely the correct location for each recording. Should the EEG sensors have not been positioned in the exact same location across recording sessions and across subjects, statistically significant differences may be found with no relevance to brain networks, due to differing recording locations. Secondly, such an approach would produce results displaying the statistical analysis results of 992 source-destination pairs. As one of the stated goals of this investigation is to produce an analysis method that is relatively simple for clinicians to observe brain networks in patients, 992 separate statistical results are not simple to read.

In an attempt to reduce the sensitivity of this analysis to imprecise EEG sensor positioning and to reduce the complexity of the statistical results, EEG sensors were grouped into broad functional areas. The EEG sensor groups chosen were Contralateral Motor Area, Ipsilateral Motor Area, Anterior/Frontal, Occipital/Parietal, Fz and Cz. EEG sensors Fz and Cz are positioned over the Supplementary Motor Area, an area of cortex involved in the planning of motor movements [252]. A table of these EEG groupings, with the EEG locations in each group, is shown in Table 7.1.

As a result of this EEG sensor grouping, the PSI scores did not represent information flow between sensors but between groups. Although, within a group of PSI scores, there may be information flow in opposite directions between areas, a statistical analysis of

7.3 Connectivity Analysis of Acquired Dataset with PSI

EEG Group	EEG sensors in group
Anterior/Frontal (A/F)	Fp1, Fp2, AF3, AF4, F7, F8
Contralateral Motor Area (CoM)	F3, FC1, FC5, T7, C3, CP1, CP5, P7, P3
Ipsilateral Motor Area (IpM)	F4, FC2, FC6, T8, C4, CP2, CP6, P8, P4
Fz	Fz
Cz	Cz
Parietal/Occipital (P/O)	PO3, PO4, O1, O2, Oz

Table 7.1: EEG sensor groups

the PSI scores would reveal any significant differences in information flow between areas when comparing individual stroke subjects to healthy subjects. Any statistically significant differences can be compared to established knowledge about the effects of stroke, can be compared to the demographic details of a stroke subject and can be compared to the motor control recovery seen in a stroke subject between recording sessions.

The first statistical test involved comparing the PSI scores from all healthy subjects to individual stroke subject datasets. All PSI scores for a particular source-destination area pair for all healthy subjects were collected and statistically compared to the PSI scores of the same source-destination area pair for each stroke subject. The second statistical test involved comparing the PSI scores of a stroke subject's early recording session to their late recording session PSI scores. In both cases, the results indicated a significant increase, a significant decrease or no significant difference in PSI scores.

7.3.1.3 Results

Figure 7.2 displays significant differences in information flow between healthy and stroke datasets during motor activity. Figure 7.3 displays significant differences in information flow between stroke early session datasets and corresponding late session datasets, for both rest and active conditions. Each square on these grids represents a single source-destination group pair. The source EEG group ("EEG From") is found along the horizontal axis while the destination EEG group ("EEG To") is found on the vertical axis. As there are 6 EEG groups (Table 7.1) there are 36 small squares on each grid.

7.3 Connectivity Analysis of Acquired Dataset with PSI

Squares along the diagonal are ignored, as information flow from an area to itself is not considered.

For a particular grid position, a blue square indicates significantly higher PSI values for the former dataset while a red square indicates significantly higher PSI values for the latter dataset. A white square indicates no statistically significant difference in PSI scores of the two datasets. Due to the nature of PSI, a significantly higher PSI score in one direction is equal to a significantly lower PSI score in the reverse direction, so these images are diagonally symmetrical with opposite colours.

Information on the datasets being statistically compared is found in the title of each grid. For Figure 7.2, the average healthy data dataset is the “former” while each stroke dataset is the “latter”. For Figure 7.3, the early dataset is the “former” while the late dataset is the “latter”.

These result images indicate significant differences in PSI values between healthy and stroke-affected EEG during motor activity and significant differences in PSI values between same-subject stroke early and stroke late datasets during both rest and motor activity. Based on these images, it appears that stroke-affected differences in brain networks have been identified in the stroke subjects. For stroke subjects, there appears to be increased information flow out of Cz to all other locations, as indicated by the red squares in the Cz column of Figure 7.2. There also appears to be increased information flow into Fz, as indicated by the blue squares in the Fz column of Figure 7.2. Significant differences in PSI scores when comparing stroke early and stroke late datasets of Figure 7.3 could only be attributed to neuroplastic change and so these results suggest an explicit biomarker of plasticity has been uncovered, which is easy to implement with EEG equipment and is easy to read and comprehend for a clinician. Unfortunately, before coming to such conclusions, the results must be validated.

7.3.1.4 Validation

To ensure that these results are truly meaningful, they must be validated. Unfortunately, due to the limited amount of subject data, it’s not possible to average results across all stroke subjects and so results can only be considered in isolation. Without the ability to average across a substantial amount of similar subjects/conditions, the results can only serve as encouragement for further investigation. Also, the stroke early

7.3 Connectivity Analysis of Acquired Dataset with PSI

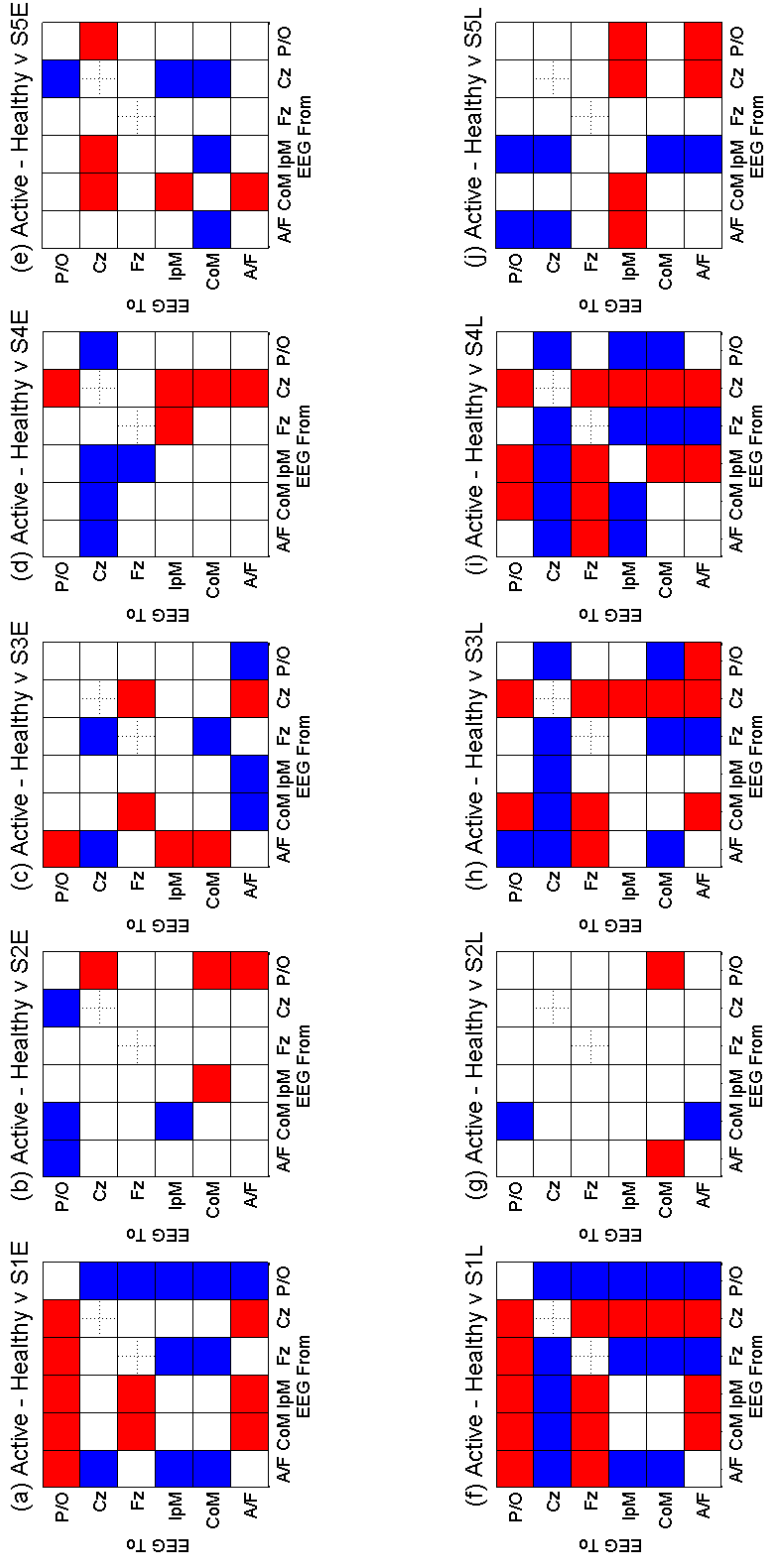


Figure 7.2: PSI score significant differences in Healthy v Stroke data. Blue indicates higher PSI score for Healthy, red indicates higher PSI score for Stroke.

7.3 Connectivity Analysis of Acquired Dataset with PSI

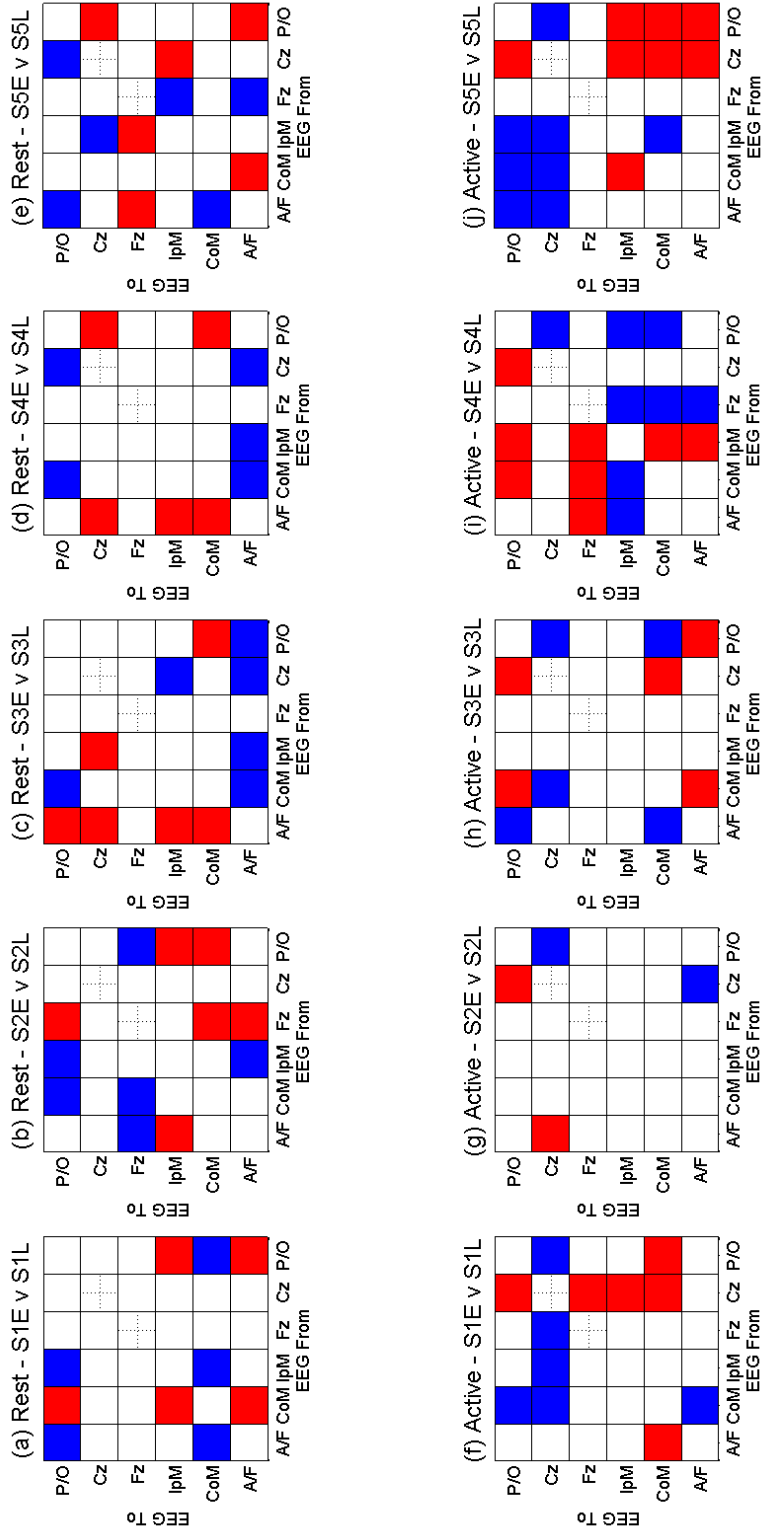


Figure 7.3: PSI score significant differences in Stroke Early v Stroke Late data. Blue indicates higher PSI score for Stroke Early, red indicates higher PSI score for Stroke Late.

7.3 Connectivity Analysis of Acquired Dataset with PSI

v stroke late results cannot be validated against healthy subjects as the healthy subjects only participated in a single recording session. Therefore, other steps must be taken to validate these results.

To validate these analysis results, statistical significance tests are applied to each individual dataset by splitting the trials of a dataset in two and testing against each other. Since the EEG sensors have not moved over the course of a single recording, then there is no need to group EEG sensors together. Additionally, trials are separated into odd- and even-numbered, so that any non-stationarities which manifest over the course of a recording have an influence. The expectation is that no significant difference is found between PSI scores of one half of a dataset against the other half.

Following processing of the datasets as before to obtain PSI scores, significant differences between halves of a dataset are shown in Figure 7.4 and Figure 7.5. EEG sensors have not been grouped here, so each plot is of a 32×32 grid, with each square representing the information flow from one EEG channel to another. For visual comparison, the results of non-grouped inter-dataset significant difference testing are shown in Figure 7.6 and Figure 7.7.

These results from Figure 7.4 and Figure 7.5 show that, within a single dataset for the same motor activity, statistically significant differences are found when, conceptually, there should be no difference and the plots should be clear. Ideally, at the same time as the validation results being clear, the cross-dataset plots should be populated. Although they are populated, they are still very similar to the validation plots.

Clearly, these test results invalidate the earlier healthy v stroke and stroke early v stroke late results. There should be no significant difference in PSI values between one half of a dataset and the other when the subject is performing the same action during the same recording session when the EEG sensors have not moved. Therefore, some aspect of the signal processing procedure is incorrect.

The reason for this outcome is that common average referencing can severely disrupt coherence calculations, which are used to calculate PSI values. Fein et. al. [253] concluded that “Phase relationships dramatically influence common reference data coherence” and that “coherence computed from common reference recordings must be interpreted very cautiously”. Guevara et. al. [254] demonstrated that the choice of EEG reference has a significant effect on synchronisation patterns and concluded that common average referencing provides no better results than using noisy reference-free

7.3 Connectivity Analysis of Acquired Dataset with PSI

EEG data, which itself performs poorly. The results obtained here with common average referencing corroborate these works.

As suggested in the 2012 review paper by Greenblatt et. al [213] of connectivity measures applied to electrophysiological data, the Laplacian operator may be of use as an alternative referencing method. A Laplacian reference for an EEG channel is a weighted sum of a number of nearest EEG channels [255]. To test whether Laplacian referencing results in valid PSI analysis outcomes, this referencing method is applied to the raw EEG data in place of common average referencing. For each EEG channel, a “Small Laplacian” reference is applied, using only up to four nearest EEG channels and weighted proportional to their distance [255]. Following referencing, the same processing steps as before were applied.

Unfortunately, the Laplacian referencing results were no better than common average referencing results. Again, significant differences were seen between trials of a single dataset. Therefore, despite recommendations from various works, Laplacian referencing resulted in invalid PSI results with sensor-space EEG.

7.3.2 Latest EEG Connectivity Analysis Knowledge

The reason for poor performance of PSI applied to sensor-space EEG recordings, despite Laplacian referencing, is revealed in a 2013 paper by Haufe et. al. [212] which assessed connectivity measures for EEG data. By simulating two interacting EEG sources inside a head model volume and the resulting scalp-recorded EEG signals, it was concluded that “even for measures robust to volume conduction the interpretation of EEG sensor-space connectivity is difficult”. The paper demonstrates that the choice of reference electrode is critical to the outcome of connectivity analysis. Wildly different results are found when utilising EEG locations TP9, TP10 and the nose for reference, for example. This paper also demonstrates that the EEG channel signal-to-noise ratio affects connectivity analysis outcomes and that the scalp Laplacian does not, in fact, solve the problems of volume conduction in EEG affecting connectivity analysis.

7.3 Connectivity Analysis of Acquired Dataset with PSI

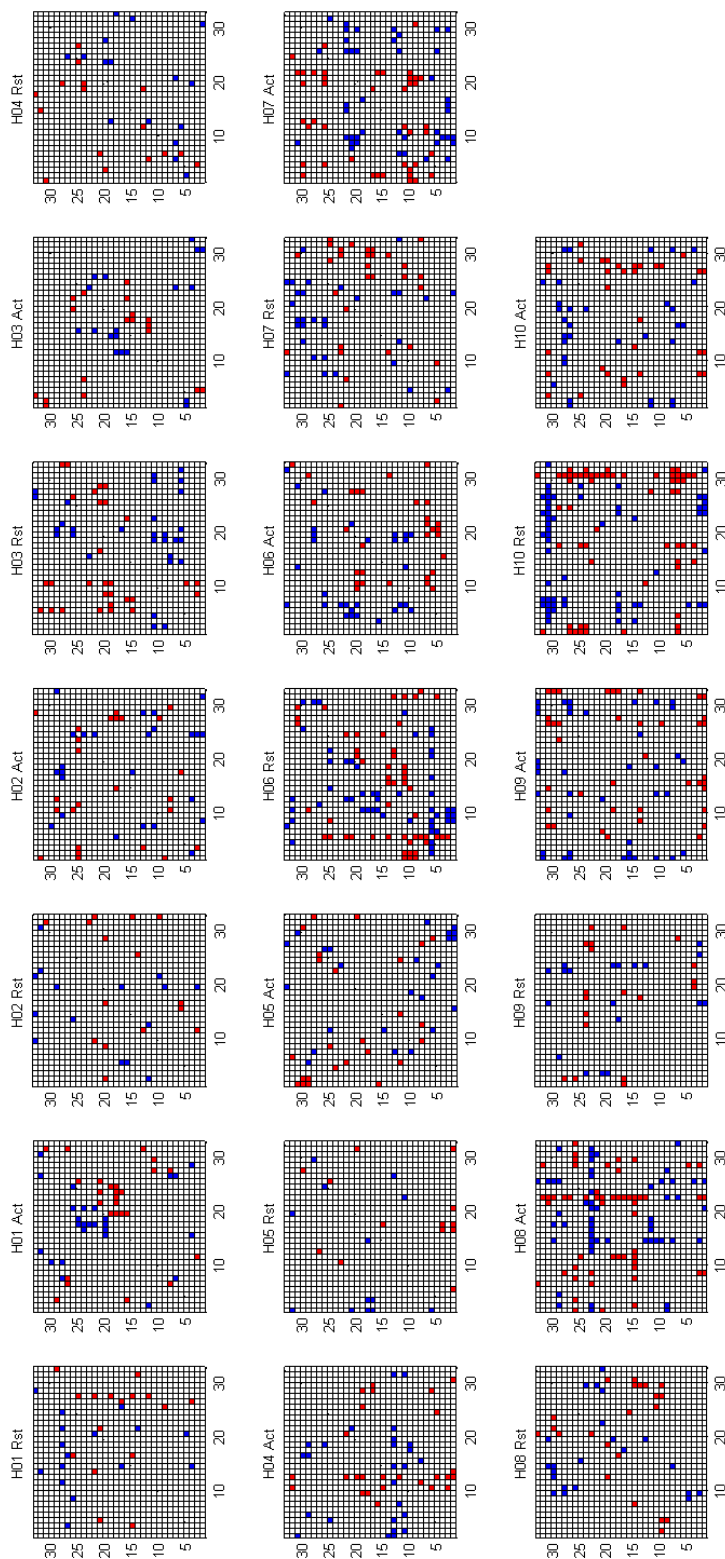


Figure 7.4: Healthy subject data: Same-subject, same-event PSI score significant differences for common average reference results. Blue/Red is not important as dataset order is arbitrary.

7.3 Connectivity Analysis of Acquired Dataset with PSI

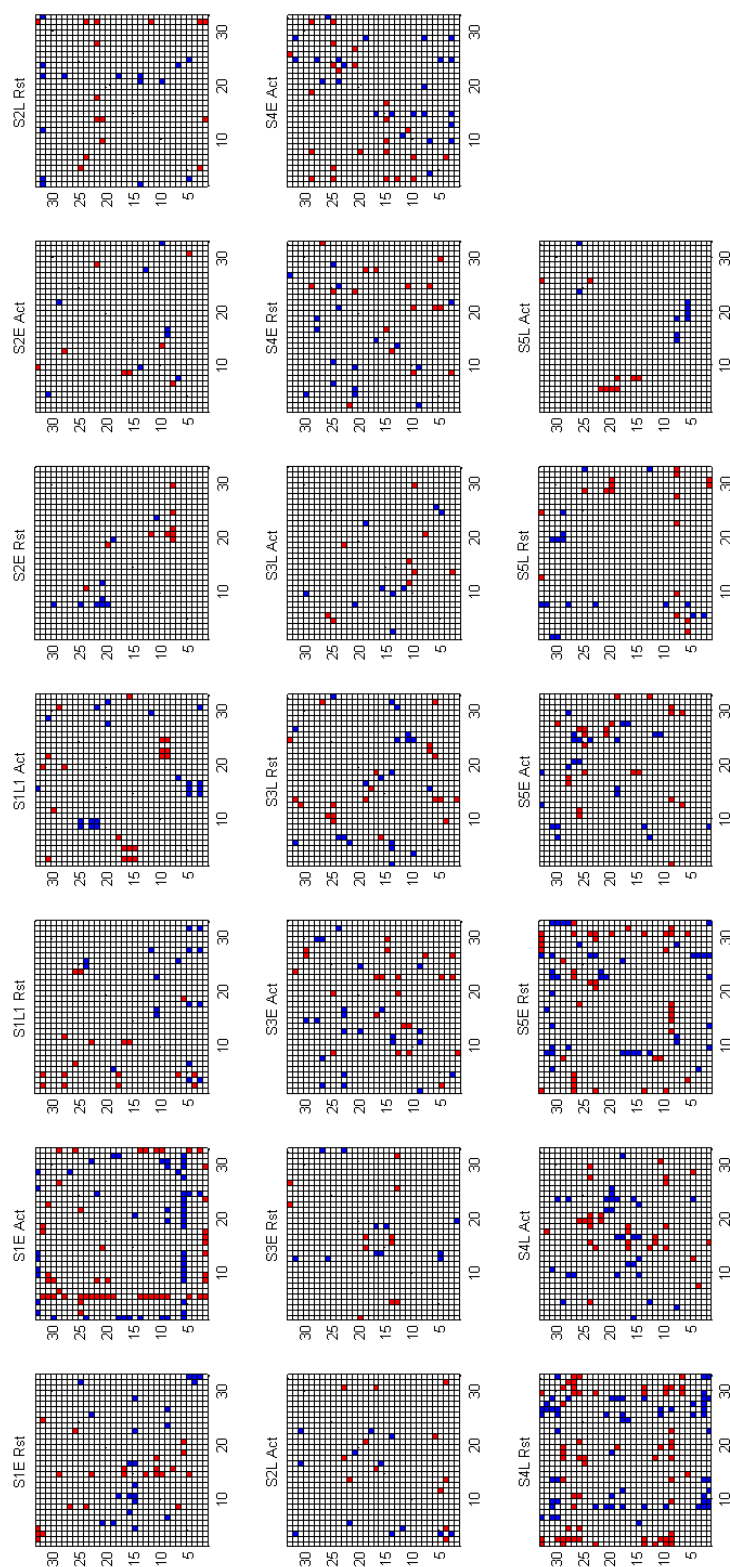


Figure 7.5: Stroke-affected subject data: Same-subject, same-event PSI score significant differences for common average reference results. Blue/Red is not important as dataset order is arbitrary.

7.3 Connectivity Analysis of Acquired Dataset with PSI

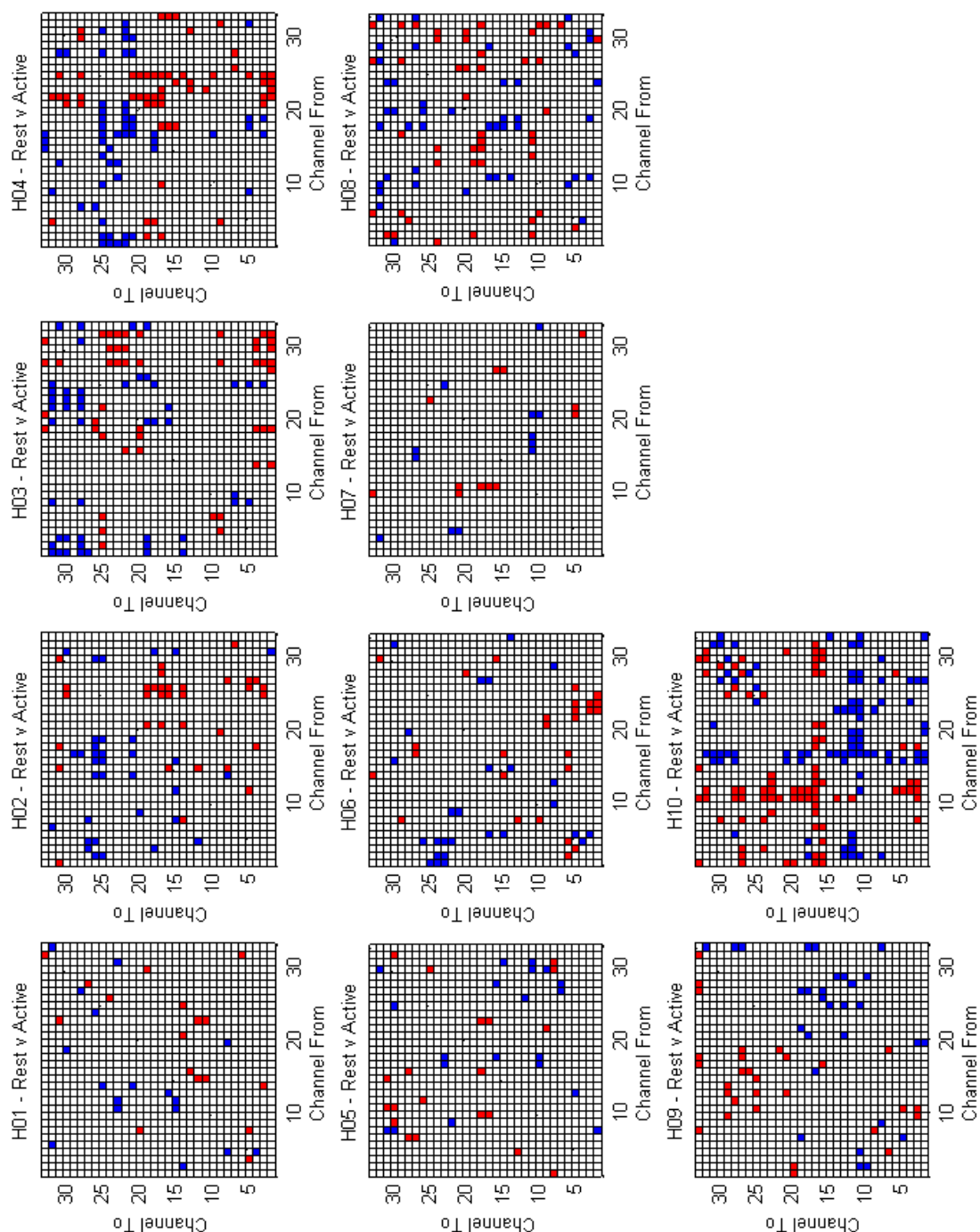


Figure 7.6: Healthy subject data: Same-subject, cross-event PSI score significant differences for common average reference results. Blue indicates higher PSI score for Rest, red indicates higher PSI score for Active.

7.3 Connectivity Analysis of Acquired Dataset with PSI

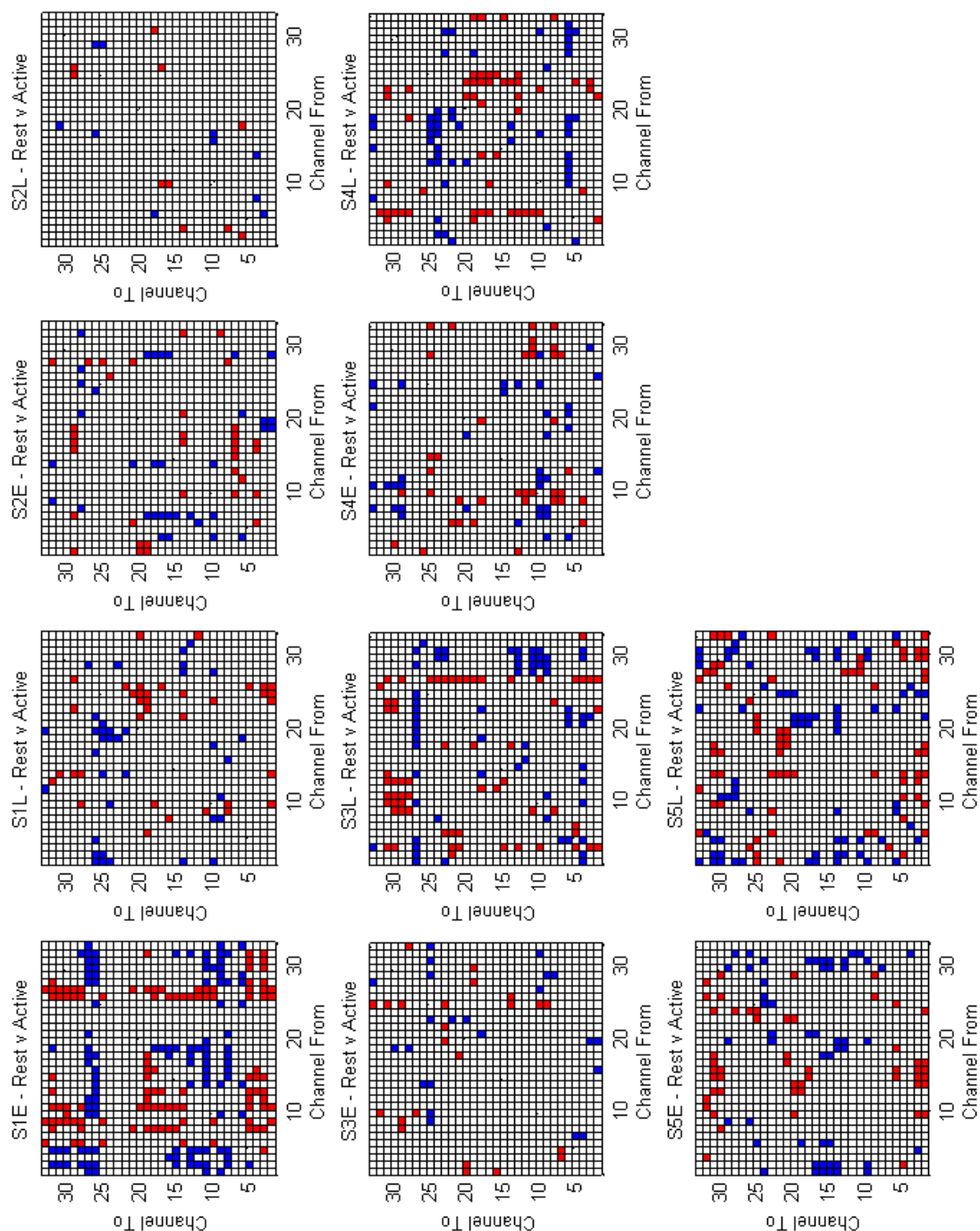


Figure 7.7: Stroke-affected subject data: Same-subject, cross-event PSI score significant differences for common average reference results. Blue indicates higher PSI score for Rest, red indicates higher PSI score for Active.

7.4 Future Stroke Connectivity Analysis

There is still potential for EEG-based connectivity analysis to become a useful, trusted clinical tool to assist in post-stroke rehabilitation. Unfortunately, as demonstrated here, it's not possible with PSI analysis of sensor-space EEG data. In their paper on EEG connectivity analysis, Haufe et. al. [212] also concluded that “In order to obtain better interpretable results, it is helpful to conduct connectivity analysis on source estimates” and that, following testing of three methods, the inverse source reconstruction method known as sparse basis field expressions (S-FLEX) [256] performed best. The authors finally concluded that “the assumptions made by a source estimation algorithm must match the properties of the sources to be constructed”. Other work has concluded that source localisation loses accuracy and reliability when fewer than 128 EEG sensors are used and that when 32 full-head EEG sensors are used, average source localisation error is 1.3 mm compared to 0.6 mm when using 128 or 192 full-head EEG sensors [257]. Despite this disadvantage compared to high-density EEG, source localisation with only 32 EEG channels is still possible and may yet prove useful for analysis of stroke EEG following an investigation with significantly more experimental subjects than used in this work.

The future of a clinical tool for producing a biomarker of neuroplastic recovery therefore rests on the reliability and accuracy of EEG source reconstruction algorithms. Assuming that such a reliable method is found then, as described above, the sources of brain activation may be estimated and their location and interactions may be analysed. The effects of stroke on brain activation patterns has been established through fMRI, PET and EEG studies, as described in section 5.2. The objective now is to investigate whether connectivity analysis of scalp-recorded EEG reveals clear differences in brain networks between healthy and stroke-affected brains.

Since activation patterns are known to change following stroke, it is safe to assume that, following source localisation, at least some estimated sources of stroke patients will differ from those of healthy subjects. For any estimated sources of stroke-affected brains which remain in similar locations to those of healthy brains, connectivity analysis will reveal any significant changes which will hopefully support current knowledge. Longitudinal studies may reveal shifting brain networks as the subject recovers. Ultimately, in this way, a clinical tool could possibly be developed to track post-stroke

neurorehabilitation which is more comfortable, less expensive and more portable than fMRI, PET or MEG.

7.5 Portable and Inexpensive Biofeedback BCI

Of fNIRS and EEG, it appears that the latter is currently superior brain measurement modality for rehabilitation BCI. EEG is significantly more developed than fNIRS while also being less expensive. In the author's experience, it is more difficult to set up an fNIRS recording than EEG while fNIRS performs less reliably, has a much slower response time and may introduce additional safety concerns to a subject's eyesight with the use of lasers. Until fNIRS is further developed, EEG is the more suitable choice for rehabilitation BCI.

As discussed in section 3.6, some concerns for rehabilitation BCI include the patient experience and the financial cost of research. Numerous factors may affect a stroke patient's engagement with therapy, such as the subject's mood, fear or other cognitive issues [258]. Another possibility is that the therapy itself is off-putting to the subject in some manner, perhaps by making the subject physically uncomfortable. Patient engagement with rehabilitation therapy is an important topic, which can be addressed in a variety of ways, including virtual reality [259] and video games [129, 260].

The problem of a stroke patient having to travel to therapy could be eliminated with at-home rehabilitation therapy. At-home stroke rehabilitation therapy has been shown to improve rehabilitation outcomes in terms of activities of daily living and also reduces risk of deterioration [261]. Advocates of home-based stroke rehabilitation suggest that there are several other advantages to moving towards home-based rehabilitation [262], such as freeing up hospital beds, reducing the risk of nosocomially-acquired illnesses and reducing the risk of distress from prolonged stay as an inpatient.

Currently, biofeedback BCI systems are too expensive and cumbersome for at-home deployment, particularly due to a robotic biofeedback component (e.g. [147, 263, 264, 265, 266, 267]). Widespread deployment of at-home rehabilitation BCI devices also depends on the financial cost of each system. As this cost lowers, such devices may be utilised more. Finally, the financial cost of biofeedback BCI systems is a deterrent to potential researchers interested in performing their own experiments and collecting their own data. This section describes a proof-of-concept design of a low-cost, portable EEG

rehabilitation BCI which uses a lightweight inflatable glove to supply haptic feedback to the subject.

7.5.1 Pneumatic Glove

The haptic feedback component of the system is a pneumatically-controlled hand therapy glove which provides finger and wrist extension to a limp or uncontrolled hand. The glove is lined with air bladders along the back of the glove and along each digit. The hand is attached to the glove by velcro straps at the wrist and at each digit while the glove is full deflated, as shown in Figure 7.8. As the air bladders fill with air, they become rigid and the hand is encouraged to conform to the shape of the glove, as shown in Figure 7.9. The glove utilised here is re-purposed and is no longer in production. However, a similar pneumatic glove, the *PneuGlove*, has been described elsewhere [268, 269] and would be a suitable low-cost replacement.



Figure 7.8: Hand in pneumatic glove when fully deflated.

A 12 V DC diaphragm vacuum pump supplies positive and negative air pressure to the system. Two electro-mechanic 3/2 solenoid valves control the supply of either positive or negative pressure to the glove from the air pump. An Arduino Uno (Arduino, Ivrea, Italy), which has been programmed to receive instruction over a serial communication link from a PC, controls the valves by controlling their power supply.



Figure 7.9: Hand in pneumatic glove when fully inflated.

Depending on the instruction received over serial link, the Arduino Uno will control the supply of positive or negative air pressure to the glove, thus inflating and deflating the glove. The pneumatic control system of air pump, valves, power supply, Arduino Uno and tubes is shown in Figure 7.10.

The time taken for the glove to move a subject's hand from minimal to maximal deflection is 12 seconds. The time taken to return from maximal to minimal deflection is 10 seconds. Therefore, the total time taken to move a subject's hand through the full range of possible movement is 22 seconds. More powerful air pumps could decrease this time, if desired.

7.5.2 EEG Brain-Computer Interface

A typical EEG BCI system was implemented using g.tec (g.tec Medical Engineering GMBH, Austria) EEG hardware and software. 27-channel EEG was recorded from positions FCz, FC1 - FC8, Cz, C1 - C8, CPz and CP1 - CP8 of the 10-20 system for electrode placement, covering the motor and central areas, with a g.USBamp amplifier sampling data at a rate of 256 samples per second. This g.tec system was used for this investigation because it is relatively easy to set up and works well almost out-of-the-box. Compared to BioSemi EEG systems, g.tec system hardware and software is easier

7.5 Portable and Inexpensive Biofeedback BCI

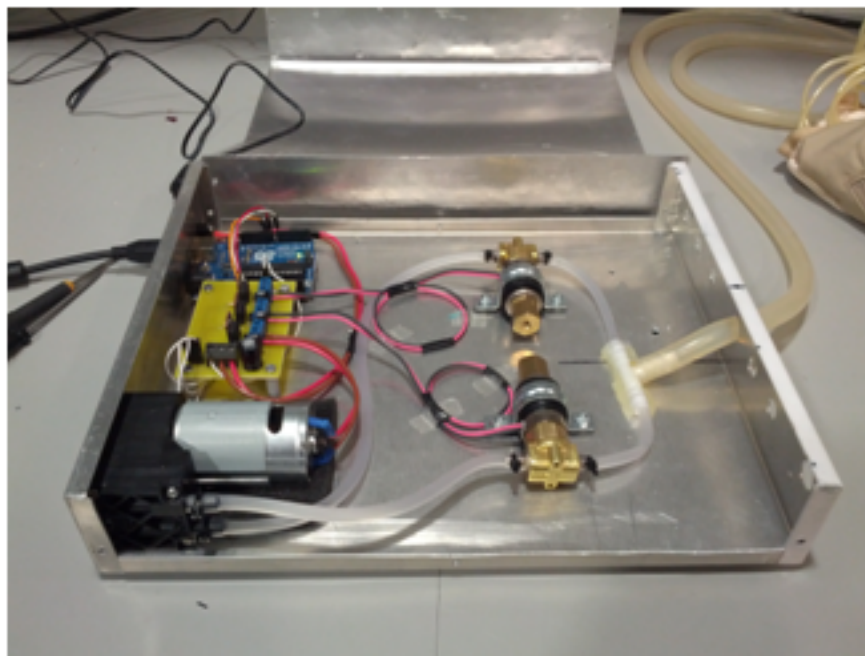


Figure 7.10: Pneumatic control system.

to use, which is important for portable rehabilitation systems potentially operated by therapists without expert EEG skills.

A modified version of g.tec BCI software was used to implement a real-time Common Spatial Patterns (CSP) BCI [270]. CSP is a typical BCI signal processing stage which involves deriving an optimal set of EEG spatial filters from a set of training data which, when applied to incoming real-time EEG, produces new signals whose variance can be used to discern between two classes of EEG activity. The operation of CSP is explained in more detail elsewhere [233, 236] and also in this thesis in subsection 6.3.3. An LDA classifier boundary is also trained from the set of training data for subsequent real-time classification.

All sampled EEG was band-pass filtered to the 0.5-30 Hz frequency range and had an additional 50 Hz notch filter applied. EEG was then filtered again to the 8-30 Hz range before CSP processing. The g.tec software [271] was used to exclude artifact-affected trials and noisy channels, to then perform CSP analysis and to finally train the LDA classifier on CSP signal variance for subsequent real-time testing.

During real-time operation, EEG was temporally filtered as before, spatially filtered

7.5 Portable and Inexpensive Biofeedback BCI

by the pre-trained CSP filters and then the variances of the top and bottom two CSP channels were classified to determine which class of activity the real-time EEG belonged to. The classifier produced a constant 1-dimensional output which was low-pass filtered with a moving-average filter of length 0.5 seconds to produce a smooth output. At a particular time after instruction onset, determined during BCI training, the classifier output was sampled. The value of this sampled classifier output determined which class of activity the subject was performing. Depending on which class of activity the subject was deemed to be performing, a control signal may have been sent to the Arduino to instruct that the glove be inflated then deflated. An overview of the full rehabilitation BCI system is presented in Figure 7.11.

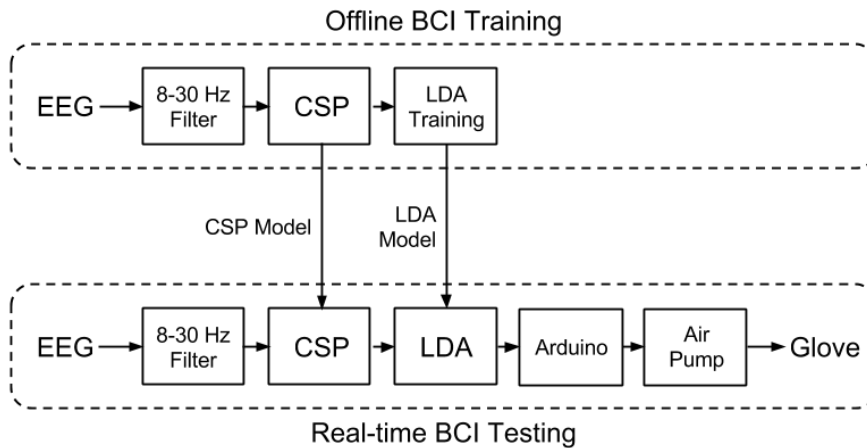


Figure 7.11: Full rehabilitation BCI system overview.

7.5.3 Subjects

Three subjects (all male, aged 24–28) participated in a system test. Subjects were all self-reported right handed and gave oral consent before participation. Subjects were recruited from Maynooth University.

7.5.4 Experimental Protocol

To demonstrate the operation and feasibility of this stroke rehabilitation BCI platform, subjects participated in the training and testing of an overt movement BCI. During

7.5 Portable and Inexpensive Biofeedback BCI

training and testing sessions, subjects were seated in a comfortable chair, had their hand affixed to the glove and followed instructions presented on a PC monitor in front of them at eye level. The subjects wore the pneumatic glove during both sessions. 20 rest trials and 20 active trials were presented in a randomized order in each session. During an active trial, the subject was instructed to perform self-paced dominant-hand digit contraction and extension, as this action resembles the movement induced by glove inflation and deflation.

For the training session, each trial lasted 8 seconds. At 0 s, the screen went blank. At 2 s, a fixation cross appeared on-screen. From 3 s to 4.5 s, an instruction arrow appeared, pointing right to indicate a movement instruction or pointing left for a rest instruction. From 4.5 s to 8 s, the fixation cross remained on-screen. The subjects were instructed to perform the action (rest or movement) as soon as the arrow appeared and to rest when the cross disappeared. For each subject, the recorded EEG was analysed to produce optimal CSP filters, to train the LDA classifier and to determine the optimal delay after instruction onset to sample the smoothed classifier output.

For the test session, each event lasted 30 seconds. Instruction presentation was the same as before except that the fixation-cross remained on-screen from 4.5 s to 30 s. During these 25.5 s, feedback of the classifier output was also presented on-screen in the form of a bar extending to the left or right of the centre of the screen. The sign of the sampled classifier output determines the decision to inflate then deflate the glove or to let it remain deflated. A positive sample value indicates movement classification while a negative sample value indicates rest classification. As inflation and deflation of the glove takes 22 seconds, there is sufficient time per trial for full range of hand movement induced by the glove.

7.5.5 Results

A table of classification accuracy results of the BCI test sessions is shown in Table 7.2. Presented in Figure 7.12 is a representative section of the time course of classifier output with timings for active and rest instruction onset, classifier sample times, classifier sample points and an illustration of the changing air pressure in the glove over time as it reacts to the classifier output.

7.5 Portable and Inexpensive Biofeedback BCI

Subject	Classification Accuracy
A	92.5%
B	90.0%
C	80.0%

Table 7.2: Rehabilitation BCI classification accuracy results.

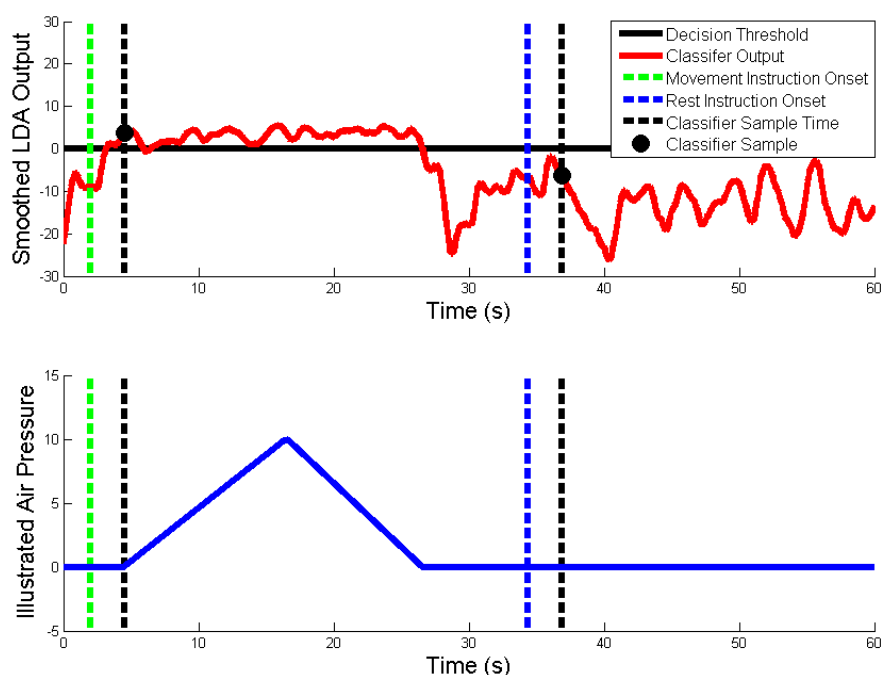


Figure 7.12: Time-course of classifier output with indicated event timings and illustrated glove air pressure.

7.5.6 Discussion

The focus of this work is not on the accuracy or performance of this BCI system. Instead, the focus here is on the viability of this portable, inexpensive BCI system as a real at-home solution for stroke rehabilitation therapy. The BCI software implemented here is relatively uncomplicated and, with some development or replacement, could easily perform much better. This BCI software demonstrably decoded the subject's actions with a good level of success and, though quite simple in hardware design, provided somatosensory feedback to the user, as is required to induce Hebbian learning

effects in a stroke patient.

By comparison to current state-of-the-art rehabilitation BCI systems, the custom pneumatic glove system here is considerably cheaper, considerably more portable and considerably easier to operate, particularly with respect to the haptic feedback device. The financial cost of rehabilitation robotics discourages and prevents some researchers from developing the field. This design proves that a biofeedback BCI system *is* accessible to more researchers and also provides a step towards at-home stroke rehabilitation systems.

The suitability of this system for at-home therapy use lies not only in the portability and usability of the system but also in the materials chosen. The pneumatic glove used is comfortable to wear and uses adjustable velcro straps, allowing it to fit different size hands. It is easy to don and doff therefore it is entirely possible for a family carer or even the user to use the system without technical assistance. The glove design inherently minimises movement restrictions placed on the user as there are no stiff mechanical parts. The pneumatic control system was designed with portability in mind, weighing less than 2 kg and is housed in a compact case. The system can be used with any PC, requiring only installation of the software.

This proof-of-concept work is based on a small number of trials with a small number of healthy test subjects. While a larger investigation, possibly with stroke-affected subjects, may provide more reliable BCI performance results, there is no reason to believe that the BCI will not perform well as the hardware and software are standard or minimally modified. It may be interesting to see how easily this system can be used by stroke patients. Further to this, it would be very interesting to see how well this system performs in a BCI-based stroke rehabilitation investigation.

7.6 Summary

This chapter describes concluding work on two applications of BCI for stroke: as a potentially useful clinical tool and as a portable at-home rehabilitation therapy device. The first part of this chapter describes attempts to perform connectivity analysis on sensor-space EEG which may reveal an explicit biomarker of post-stroke neuroplasticity. Such a biomarker, if adequately reliable, could be used in a clinical setting to assist in evaluation of post-stroke recovery. The advantage of such a tool is that it is based on

EEG measurement - a relatively cheap, comfortable and portable measurement modality. Connectivity analysis purported to be robust to the volume conduction effects of scalp EEG was investigated using standard EEG processing techniques. Following failure to obtain meaningful results, further investigation into EEG connectivity analysis literature revealed that connectivity analysis with sensor-space EEG is unreliable and that source localisation must be performed first. While an explicit biomarker of neurorehabilitation is not found here, this chapter serves as an example of how PSI-based connectivity analysis of sensor-space EEG is unsuitable and describes future direction of research on this topic. The description of the design and development of a low-cost, portable biofeedback BCI demonstrates a possible future for stroke rehabilitation in the community. Systems similar to the one described here may improve the lives of stroke survivors in the near future with more development.

Chapter 8

Conclusion

8.1 Summary and Discussion

The work described in this thesis has contributed toward the improvement of EEG and fNIRS-based methods for stroke rehabilitation. Two main approaches were taken towards this objective: improvement of current EEG and fNIRS rehabilitation BCI research tools, and investigation of novel tools for clinical evaluation of stroke rehabilitation. After introducing the physiological and technological basis for EEG and fNIRS rehabilitation BCI in chapter 2 and chapter 3, various challenges and opportunities for advancement of EEG and fNIRS rehabilitation BCI were identified and investigated in chapter 4. fNIRS BCI is a relatively young research topic and has not experienced the level of development of EEG. This is likely due to the popularity of EEG as a brain measurement modality and the relatively low financial cost of EEG hardware. While fNIRS is perfectly feasible as a brain measurement modality, hardware is more expensive, less commonly found in clinical or research setting and thus less accessible for research. fNIRS has some disadvantages compared to EEG in that skin tone, hair colour and hair thickness can make fNIRS measurement difficult. Additionally, due to the slow nature of the haemodynamic response, fNIRS has limited use as the sole measurement modality for rehabilitation BCI, which requires rapid action for feedback to the user. Despite this, fNIRS still has prospects in rehabilitation BCI.

By incorporating EEG and additional fNIRS channels to the simplified 1-channel fNIRS ‘Mindswitch’, both haemodynamic and electric brain activity was measured for

the motor cortex for BCI operation. The results of this test suggested that this hybrid fNIRS/EEG BCI approach results in improved BCI performance over either modality acting in isolation. The area covered by the designed fNIRS/EEG patch, however, was relatively small, precluding the use of some EEG processing techniques, such as CSP. Recent hybrid fNIRS/EEG work conducted by Fazli et. al. [272], Putze et. al [172] and by Yu et. al. [170] utilised either full-head or wide-area measurement. It may be more prudent to advance full-head hybrid fNIRS/EEG BCI and, once it is developed to a reliable state, begin to investigate a reduction in measurement channels to the advantage of the stroke patient's experience. On the topic of hybrid measurement, Pfurtscheller et. al. [273] suggest investigating the use of three measurement modalities. This would certainly be an exciting and interesting advancement of hybrid BCI.

GP-based spatial interpolation provided an interesting approach to fNIRS imaging. The spatial variance information was unfortunately not tested with any more than four fNIRS channels but results were encouraging enough to warrant further investigation with additional channels. As rehabilitation BCI is ideally portable, it may be necessary to employ image processing algorithms which are less intensive than the gold standards for accuracy. fNIRS imaging may be useful for tracking haemodynamics during cortical healing and GP-model interpolation may be useful in producing those images.

Synthetic fNIRS data generation has multiple uses. As a research tool, it may be useful for "sanity checking" a biosignal processing method or to produce a large amount of pseudo-random fNIRS data to compare signal processing methods. As an educational tool, observing the effect of each fNIRS component on signal processing output may be very valuable. There is significant room for development of this algorithm. For example, the effect of the subject's breathing pattern is not included, nor is a component for movement artefact. Further development of the algorithm may result in a tool for testing artefact removal techniques.

The biofeedback glove BCI is an example of how low the barrier of entry to rehabilitation BCI research currently is. This system was built using an inexpensive commercial EEG system, simple modifications to the included hardware and some inexpensive hardware. The system is very portable and will hopefully inspire researchers to construct a similar system of their own for research. It's important that a researcher who is interested in a particular topic be able to contribute. This system shows that conducting rehabilitation BCI research does not have to be a very expensive endeavour.

This system also serves as a basis for further improvements. For example, EEG signal processing could be upgraded to perform more accurately, more powerful air pumps could be used or the use of dry electrodes could be investigated. As rehabilitation BCI aims to improve the subject's experience, dry EEG electrodes reduce set-up time and so improve subject engagement.

The investigations which took place over chapter 5 and chapter 6 drew numerous conclusions. Firstly, despite stroke causing significant damage to the brain and altering its patterns of activation, EEG measured from healthy and stroke-affected brains is not noticeably different from spectral content or ICA investigations. As further investigation was warranted, the EEG was analysed from a BCI perspective in order to determine whether offline BCI analysis could determine differences between healthy and stroke-affected EEG, and, if such differences exist, determine the utility of those differences. Following the investigation with a BCI comprised of FBCSP, marginal relevance and GP classification, some conclusions were drawn. Firstly, classifying stroke-affected EEG with a BCI trained on healthy EEG may be useful as a biomarker of stroke recovery. Classification accuracies of healthy EEG were significantly higher than those of stroke EEG with a BCI trained on healthy data. Secondly, the effects of a stroke were observable through the frequency range of the selected features - another possible biomarker of stroke rehabilitation. As a subject suffered a stroke, the selected frequency range for classification decreased. What is yet to be determined, however, is whether the selected frequency ranges eventually return to those of healthy subjects, or whether selected frequency range is related to motor ability. Unfortunately, due to the small cohort size, these results do not provide conclusive proof of the utility of this biomarker. These results provide encouragement for a similar investigation with a larger number of stroke patients, conducted over a longer period of time, and with various BCI designs tested.

The stroke rehabilitation biomarker obtained through offline BCI is implicit by nature. BCI parameters and classification accuracies are not direct measures of neuronal activity but rather are only influenced by that activity. An explicit biomarker of stroke rehabilitation, one directly affected by neuronal activity, was the subject of attention in chapter 7. Investigations into the differences between healthy, early stroke and late stroke EEG were carried out through PSI connectivity analysis of the EEG sensor

data. Unfortunately, EEG sensor data was shown to be inappropriate for PSI connectivity analysis. However, there remains ample opportunity for a similar investigation with source localisation applied to the sensor data first. A clinical tool based on scalp recorded EEG, source localisation and PSI-estimated information flow is a possibility. Such a biomarker of stroke rehabilitation, presented in a clear manner, could be a useful tool to guide rehabilitation therapy in a clinical setting.

This thesis discusses rehabilitation BCI which utilises primarily haptic feedback. Each of the topics discussed here are equally as applicable to other stimulus methods, such as repetitive transcranial magnetic stimulation (rTMS) and transcranial direct current stimulation (tDCS) [274, 275, 276, 277] to improve rehabilitation outcomes. Additionally, the BCIs discussed here may be used in conjunction with functional electrical stimulation (FES) [278, 279] to further assist stroke patients. As a research topic, rehabilitation BCI exemplifies the best of biomedical engineering - using technology to improve the lives of those who need it most. This thesis contributes some solutions to problems faced by rehabilitation BCI and encourages further investigation.

8.2 Concluding Remarks

This thesis describes advances in knowledge of the effects of stroke on brain networks and in the design of stroke rehabilitation BCI systems. Novel investigations into the representation of stroke recovery in machine learned BCI parameters and connectivity measures were carried out and results of these investigations encourage potential use as a clinical tool to aid in stroke rehabilitation efforts. Other work improved stroke rehabilitation systems by exploring novel hybrid BCI designs and imaging methods. Finally, the barrier to EEG and fNIRS rehabilitation BCI was lowered through development of a software-based fNIRS dataset generator and design of a simple, low-cost biofeedback BCI system. The work described in this thesis has advanced the prospects EEG and fNIRS stroke rehabilitation brain-computer interfacing by improving system design, understanding of the effects of stroke and facilitating further rehabilitation BCI research. The author hopes that his work contributes to the alleviation of suffering in stroke survivors.

References

- [1] FRANCES HORGAN, ANNE HICKEY, HANNAH MCGEE, AND DESMOND O'NEILL. **Irish heart foundation national audit of stroke care**, 2008. 1, 20
- [2] LAURA KAUMANEN, PASI JYLÄNKI, JANNE LEHTONEN, PEKKA RANTANEN, HANNU ALARANTA, AND MIKKO SAMS. **EEG-based brain-computer interface for tetraplegics**. *Comput Intell Neurosci*, page 23864, 2007. 2
- [3] LEIGH R HOCHBERG, DANIEL BACHER, BEATA JAROSIEWICZ, NICOLAS Y MASSE, JOHN D SIMERAL, JOERN VOGEL, SAMI HADDADIN, JIE LIU, SYDNEY S CASH, PATRICK VAN DER SMAGT, ET AL. **Reach and grasp by people with tetraplegia using a neurally controlled robotic arm**. *Nature*, **485**(7398):372–375, 2012. 2
- [4] TOM CARLSON, ROBERT LEEB, GUILLAUME MONNARD, ABDUL AL-KHODAIRY, AND JOSÉ DEL R MILLÁN. **Driving a BCI Wheelchair: A Patient Case Study**. In *Proceedings of TOBI Workshop III: Bringing BCIs to End-Users: Facing the Challenge*, number EPFL-CONF-174373, pages 59–60, 2012. 2
- [5] CARLES GRAU, ROMUALD GINHOUX, ALEJANDRO RIERA, THANH LAM NGUYEN, HUBERT CHAUVAT, MICHEL BERG, JULIA L. AMENGUAL, ALVARO PASCUAL-LEONE, AND GIULIO RUFFINI. **Conscious brain-to-brain communication in humans using non-invasive technologies**. *PLoS One*, **9**(8):e105225, 2014. 2
- [6] STEFANO SILVONI, ANDER RAMOS-MURGUIALDAY, MARIANNA CAVINATO, CHIARA VOLPATO, GIULIA CISOTTO, ANDREA TUR-OLLA, FRANCESCO PICCIONE, AND NIELS BIRBAUMER. **Brain-computer interface in stroke: a review of progress**. *Clinical EEG and neuroscience official journal of the EEG and Clinical Neuroscience Society ENCS*, **42**(4):245–52, 2011. 2
- [7] SURJO R SOEKADAR, NIELS BIRBAUMER, AND LEONARDO G COHEN. **Brain-computer-interfaces in the rehabilitation of stroke and neurotrauma**. *Psychology*, **48**(6):1–19, 2011. 2
- [8] KAI KENG ANG AND CUNTAI GUAN. **Brain-Computer Interface in Stroke Rehabilitation**. *JCSE*, **7**(2):139–146, 2013. 2
- [9] NIKHIL SHARMA, VALERIE M POMEROY, AND JEAN-CLAUDE BARON. **Motor imagery: a backdoor to the motor system after stroke?** *Stroke*, **37**(7):1941–1952, Jul 2006. 2, 50
- [10] I LAFFONT, K BAKHTI, F COROIAN, L VAN DOKKUM, D MOT- TET, N SCHWEIGHOFER, AND J FROGER. **Innovative technologies applied to sensorimotor rehabilitation after stroke**. *Annals of physical and rehabilitation medicine*, **57**(8):543–551, 2014. 2
- [11] DARREN LEAMY, TOMAS WARD, AND JUŠ KOČLIJAN. **Using Gaussian process models for near-infrared spectroscopy data interpolation**. In A. HIERLEMANN, editor, *Proceedings of the 7th IASTED International Conference Biomedical Engineering (BioMED 2010)*, pages 257–262, Innsbruck, Austria, February 2010. IASTED, IASTED. 4
- [12] D.J. LEAMY AND T.E. WARD. **A novel co-locational and concurrent fNIRS/EEG measurement system: Design and initial results**. In *Engineering in Medicine and Biology Society (EMBC), 2010 Annual International Conference of the IEEE*, pages 4230–4233, 2010. 4
- [13] K.T. SWEENEY, D.J. LEAMY, T.E. WARD, AND S. MCLOONE. **Intelligent artifact classification for ambulatory physiological signals**. In *Engineering in Medicine and Biology Society (EMBC), 2010 Annual International Conference of the IEEE*, pages 6349–6352, 2010. 4, 46
- [14] D.J. LEAMY, T.E. WARD, AND K.T. SWEENEY. **Functional Near Infrared Spectroscopy (fNIRS) synthetic data generation**. In *Engineering in Medicine and Biology Society, EMBC, 2011 Annual International Conference of the IEEE*, pages 6589–6592, 2011. 4
- [15] DARREN J LEAMY, RÓNÁN COLLINS, AND TOMAS E WARD. **Combining fNIRS and EEG to improve motor cortex activity classification during an imagined movement-based task**. In *Foundations of Augmented Cognition. Directing the Future of Adaptive Systems*, pages 177–185. Springer, 2011. 4
- [16] JUANGHONG YU, YAOZHANG PAN, KAI KENG ANG, CUN- TAI GUAN, AND DARREN J LEAMY. **Prefrontal cortical activation during arithmetic processing differentiated by cultures: A preliminary fNIRS study**. In *Engineering in Medicine and Biology Society (EMBC), 2012 Annual International Conference of the IEEE*, pages 4716–4719. IEEE, 2012. 5

REFERENCES

- [17] DARREN J. LEAMY, JUŠ KOCIJAN, KATARINA DOMJIAN, JOSEPH DUFFIN, RICHARD AP ROCHE, SEAN COMMINS, RONAN COLLINS, AND TOMAS E. WARD. **An exploration of EEG features during recovery following stroke - implications for BCI-mediated neurorehabilitation therapy.** *J Neuroeng Rehabil*, **11**(1):9, 2014. 5
- [18] A.L. COFFEY, D.J. LEAMY, AND T.E. WARD. **A novel BCI-controlled pneumatic glove system for home-based neurorehabilitation.** In *Engineering in Medicine and Biology Society (EMBC), 2014 36th Annual International Conference of the IEEE*, pages 3622–3625, 2014. 5
- [19] ANDREA STOCOCCO, CHRISTIAN LEBIERE, AND JOHN R. ANDERSON. **Conditional routing of information to the cortex: a model of the basal ganglia’s role in cognitive coordination.** *Psychol Rev*, **117**(2):541–574, Apr 2010. 8
- [20] JAMES A WEYHENMEYER. **Rapid Review Neuroscience.** 2007. 8
- [21] GUYTON AND HALL. *Textbook of Medical Physiology.* Elsevier, 11th edition edition, 2005. 8, 15, 20
- [22] G. J. TORTORA AND S. R. GRABOWSKI. *Principles of Anatomy and Physiology.* Wiley, 10 edition, 2003. 8, 9, 10, 17
- [23] PAUL L NUNEZ AND RAMESH SRINIVASAN. *Electric fields of the brain: the neurophysics of EEG.* Oxford university press, 2nd edition edition, 2006. 11, 13, 34
- [24] FITZPATRICK D ET AL. PURVES D, AUGUSTINE GJ. *Neuroscience.* Sunderland (MA): Sinauer Associates, 5th edition edition, 2001. 14, 17, 22, 23
- [25] BARBARA E GOULD. *Pathophysiology for the health professions.* Elsevier, 3rd edition edition, 2006. 17, 20
- [26] PRABAL DEB, SUASH SHARMA, AND KM HASSAN. **Pathophysiological mechanisms of acute ischemic stroke: an overview with emphasis on therapeutic significance beyond thrombolysis.** *Pathophysiology*, **17**(3):197–218, 2010. 17, 18
- [27] COSTANTINO IADECOLA AND JOSEF ANRATHER. **The immunology of stroke: from mechanisms to translation.** *Nature medicine*, **17**(7):796–808, 2011. 18
- [28] CHANGHONG XING, KEN ARAI, ENG H LO, AND MARC HOMMEL. **Pathophysiologic cascades in ischemic stroke.** *International Journal of Stroke*, **7**(5):378–385, 2012. 18
- [29] PETER LIPTON. **Ischemic cell death in brain neurons.** *Physiological reviews*, **79**(4):1431–1568, 1999. 18
- [30] J DONALD EASTON, JEFFREY L SAVER, GREGORY W ALBERS, MARK J ALBERTS, SEEMANT CHATURVEDI, EDWARD FELDMANN, THOMAS S HATSUKAMI, RANDALL T HIGASHIDA, S CLAIBORNE JOHNSTON, CHELSEA S KIDWELL, ET AL. **Definition and Evaluation of Transient Ischemic Attack A Scientific Statement for Healthcare Professionals From the American Heart Association/American Stroke Association Stroke Council; Council on Cardiovascular Surgery and Anesthesia; Council on Cardiovascular Radiology and Intervention; Council on Cardiovascular Nursing; and the Interdisciplinary Council on Peripheral Vascular Disease: The American Academy of Neurology affirms the value of this statement as an educational tool for neurologists.** *Stroke*, **40**(6):2276–2293, 2009. 19
- [31] GRAEME J HANKEY, JAMES M SLATTERY, AND CHARLES P WARLOW. **Transient ischaemic attacks: which patients are at high (and low) risk of serious vascular events?** *Journal of Neurology, Neurosurgery & Psychiatry*, **55**(8):640–652, 1992. 19
- [32] LYNDA D LISABETH, JENNIFER K IRELAND, JAN MH RISSER, DEVIN L BROWN, MELINDA A SMITH, NELDA M GARCIA, AND LEWIS B MORGENSTERN. **Stroke risk after transient ischemic attack in a population-based setting.** *Stroke*, **35**(8):1842–1846, 2004. 19
- [33] DAWN KLEINDORFER, PETER PANAGOS, ARTHUR PANCIOLI, JANE KHOURY, BRETT KISSELA, DANIEL WOO, ALEXANDER SCHNEIDER, KATHLEEN ALWELL, EDWARD JAUCH, ROSIE MILLER, ET AL. **Incidence and short-term prognosis of transient ischemic attack in a population-based study.** *Stroke*, **36**(4):720–723, 2005. 19
- [34] WORLD HEALTH ORGANISATION. **World Health Statistics 2014.** 20
- [35] GRAEME J HANKEY, KONRAD JAMROZIK, ROBYN J BROADHURST, SUSANNE FORBES, PETER W BURVILL, CRAIG S ANDERSON, AND EDWARD G STEWART-WYNNNE. **Five-year survival after first-ever stroke and related prognostic factors in the Perth Community Stroke Study.** *Stroke*, **31**(9):2080–2086, 2000. 20
- [36] KATE HARDIE, GRAEME J HANKEY, KONRAD JAMROZIK, ROBYN J BROADHURST, AND CRAIG ANDERSON. **Ten-year survival after first-ever stroke in the Perth Community Stroke Study.** *Stroke*, **34**(8):1842–1846, 2003. 20
- [37] JM BAMFORD, PAG SANDERCOCK, MS DENNIS, JPS BURN, AND CP WARLOW. **A prospective study of acute cerebrovascular disease in the community: the Oxfordshire Community Stroke Project–1981–86. 2. Incidence, case fatality rates and overall outcome**

REFERENCES

- at one year of cerebral infarction, primary intracerebral and subarachnoid haemorrhage. *Journal of Neurology, Neurosurgery & Psychiatry*, **53**(1):16–22, 1990. 20
- [38] JEANNETTE W HOP, GABRIËL JE RINKEL, ALE ALGRA, AND JAN VAN GIJN. **Case-Fatality Rates and Functional Outcome After Subarachnoid Hemorrhage A Systematic Review.** *Stroke*, **28**(3):660–664, 1997. 20
- [39] VICTORIA LOUISE BARBOUR AND GILLIAN ELIZABETH MEAD. **Fatigue after Stroke: The Patient’s Perspective.** *Stroke research and treatment*, **2012**:863031, 2012. 20
- [40] KATHLEEN MICHAEL. **Fatigue and stroke.** *Rehabilitation nursing the official journal of the Association of Rehabilitation Nurses*, **27**(3):89–94, 103, 2002. 20
- [41] ANNERS LERDAL, LINDA N BAKKEN, SIREN E KOUWENHOVEN, GUNN PEDERSEN, MARIT KIRKEVOLD, ARNSTEIN FINSET, AND HESOOK S KIM. **Poststroke fatigue—a review.** *Journal of Pain and Symptom Management*, **38**(6):928–949, 2009. 20
- [42] FIONA DUNCAN, SIMIAO WU, AND GILLIAN E MEAD. **Frequency and natural history of fatigue after stroke: A systematic review of longitudinal studies.** *Journal of Psychosomatic Research*, **73**(1):18–27, 2012. 20
- [43] PAMELA W DUNCAN, DENNIS WALLACE, SUE MIN LAI, DALLAS JOHNSON, SUSAN EMBRETSON, AND LOUISE JACOBS LASTER. **The Stroke Impact Scale Version 2.0 evaluation of reliability, validity, and sensitivity to change.** *Stroke*, **30**(10):2131–2140, 1999. 20
- [44] PW DUNCAN, SM LAI, RK BODE, S PERERA, J DEROSA, ET AL. **Stroke Impact Scale-16 A brief assessment of physical function.** *Neurology*, **60**(2):291–296, 2003. 20
- [45] FRANCISCO JAVIER CAROD-ARTAL, LUCIANE FERREIRA CORAL, DANIELE STIEVEN TRIZOTTO, AND CLARISSA MENEZES MOREIRA. **The Stroke Impact Scale 3.0 Evaluation of Acceptability, Reliability, and Validity of the Brazilian Version.** *Stroke*, **39**(9):2477–2484, 2008. 20
- [46] M. F. FOLSTEIN, S. E. FOLSTEIN, AND P. R. MCHUGH. **“Minimal state”. A practical method for grading the cognitive state of patients for the clinician.** *J Psychiatr Res*, **12**(3):189–198, Nov 1975. 20, 105
- [47] STROKE UNIT TRIALISTS’ COLLABORATION. **Organised inpatient (stroke unit) care for stroke.** *Cochrane Database Syst Rev*, **4**(4), 2007. 21
- [48] GRAEME J HANKEY. *Stroke: Your questions answered.* Churchill Livingstone London, second edition edition, 2007. 21
- [49] B INDREDAVIK, F BAKKE, SA SLØRDAHL, R ROKSETH, AND LL HÅHEIM. **Treatment in a Combined Acute and Rehabilitation Stroke Unit Which Aspects Are Most Important?** *Stroke*, **30**(5):917–923, 1999. 21
- [50] DONALD OLDING HEBB. *The organization of behavior: A neuropsychological approach.* John Wiley & Sons, 1949. 23
- [51] NATALIA CAPORALE AND YANG DAN. **Spike timing-dependent plasticity: a Hebbian learning rule.** *Annu. Rev. Neurosci.*, **31**:25–46, 2008. 23
- [52] DEAN V BUONOMANO AND MICHAEL M MERZENICH. **Cortical plasticity: from synapses to maps.** *Annual review of neuroscience*, **21**(1):149–186, 1998. 23, 24
- [53] MICHAEL M MERZENICH AND RC DECHARMS. **Neural representations, experience, and change.** 1996. 24
- [54] M. M. MERZENICH, J. H. KAAS, J. WALL, R. J. NELSON, M. SUR, AND D. FELLEMAN. **Topographic reorganization of somatosensory cortical areas 3b and 1 in adult monkeys following restricted deafferentation.** *Neuroscience*, **8**(1):33–55, Jan 1983. 24
- [55] M. M. MERZENICH, R. J. NELSON, M. P. STRYKER, M. S. CYNADER, A. SCHOPPMANN, AND J. M. ZOOK. **Somatosensory cortical map changes following digit amputation in adult monkeys.** *J Comp Neurol*, **224**(4):591–605, Apr 1984. 24
- [56] T. P. PONS, P. E. GARRAGHTY, AND M. MISHKIN. **Lesion-induced plasticity in the second somatosensory cortex of adult macaques.** *Proc Natl Acad Sci U S A*, **85**(14):5279–5281, Jul 1988. 24
- [57] CHRISTO PANTEV, ALMUT ENGELIEN, VICTOR CANDIA, AND THOMAS ELBERT. **Representational cortex in musicians.** *Annals of the New York Academy of Sciences*, **930**(1):300–314, 2001. 25
- [58] A. PASCUAL-LEONE AND F. TORRES. **Plasticity of the sensorimotor cortex representation of the reading finger in Braille readers.** *Brain*, **116** (Pt 1):39–52, Feb 1993. 25
- [59] R. H. HAMILTON AND A. PASCUAL-LEONE. **Cortical plasticity associated with Braille learning.** *Trends Cogn Sci*, **2**(5):168–174, May 1998. 25
- [60] PETER S ERIKSSON, EKATERINA PERFILEVA, THOMAS BJÖRK-ERIKSSON, ANN-MARIE ALBORN, CLAES NORDBORG, DANIEL A PETERSON, AND FRED H GAGE. **Neurogenesis in the adult human hippocampus.** *Nature medicine*, **4**(11):1313–1317, 1998. 25

REFERENCES

- [61] STEVEN C CRAMER, RAJENDRA SHAH, JENIFER JURANEK, KIT R CRAFTON, AND VU LE. **Activity in the peri-infarct rim in relation to recovery from stroke.** *Stroke*, **37**(1):111–115, 2006. 25
- [62] M ANGELS FONT, ADRIÁ ARBOIX, AND JERZY KRUPINSKI. **Angiogenesis, neurogenesis and neuroplasticity in ischemic stroke.** *Current cardiology reviews*, **6**(3):238, 2010. 25
- [63] ANN L WEBBER AND JOANNE WOOD. **Amblyopia: prevalence, natural history, functional effects and treatment.** *Clinical and experimental optometry*, **88**(6):365–375, 2005. 25, 26
- [64] E. TAUB, G. USWATTE, V. W. MARK, AND D M M. MORRIS. **The learned nonuse phenomenon: implications for rehabilitation.** *Eura Medicophys*, **42**(3):241–256, Sep 2006. 26
- [65] P. W. DUNCAN, L. B. GOLDSTEIN, D. MATCHAR, G. W. DIVINE, AND J. FEUSSNER. **Measurement of motor recovery after stroke. Outcome assessment and sample size requirements.** *Stroke*, **23**(8):1084–1089, Aug 1992. 26
- [66] STEVEN C CRAMER. **Repairing the human brain after stroke: I. Mechanisms of spontaneous recovery.** *Annals of neurology*, **63**(3):272–287, 2008. 26
- [67] TIMOTHY H. MURPHY AND DALE CORBETT. **Plasticity during stroke recovery: from synapse to behaviour.** *Nat Rev Neurosci*, **10**(12):861–872, Dec 2009. 26
- [68] RALUCA MOUCHA AND MICHAEL P. KILGARD. % bf Cortical plasticity and rehabilitation. *Prog Brain Res*, **157**:111–122, 2006. 26
- [69] TADEUSZ WIELOCH AND KAROLY NIKOLICH. **Mechanisms of neural plasticity following brain injury.** *Current opinion in neurobiology*, **16**(3):258–264, 2006. 26
- [70] OTTO W WITTE, HANS-J BIDMON, KLAUS SCHIENE, CHRISTOPH REDECKER, AND GEORG HAGEMANN. **Functional differentiation of multiple perilesional zones after focal cerebral ischemia.** *Journal of Cerebral Blood Flow & Metabolism*, **20**(8):1149–1165, 2000. 26
- [71] YOUNG R KIM, IN J HUANG, SEONG-RYONG LEE, EMIRI TEJIMA, JOSEPH B MANDEVILLE, MAURITS PA VAN MEER, GEORGE DAI, YONG W CHOI, RICK M DIJKHUIZEN, ENG H LO, ET AL. **Measurements of BOLD/CBV ratio show altered fMRI hemodynamics during stroke recovery in rats.** *Journal of Cerebral Blood Flow & Metabolism*, **25**(7):820–829, 2005. 26
- [72] PÄR THORED, ANDREAS ARVIDSSON, EMANUELE CACCI, HENRIK AHLENIUS, THERESE KALLUR, VLADIMIR DARSALIA, CHRISTINE T EKDAHL, ZAAL KOKAIA, AND OLLE LINDVALL. **Persistent production of neurons from adult brain stem cells during recovery after stroke.** *Stem cells*, **24**(3):739–747, 2006. 27
- [73] JUDITH D SCHAECHTER, CHRISTOPHER I MOORE, BRENDAN D CONNELL, BRUCE R ROSEN, AND RICK M DIJKHUIZEN. **Structural and functional plasticity in the somatosensory cortex of chronic stroke patients.** *Brain*, **129**(10):2722–2733, 2006. 27
- [74] EDWARD TAUB, GITENDRA USWATTE, RAMA PIDIKITI, ET AL. **Constraint-induced movement therapy: a new family of techniques with broad application to physical rehabilitation—a clinical review.** *Journal of rehabilitation research and development*, **36**(3):237–251, 1999. 27, 50
- [75] JAMES C GROTTA, ELIZABETH A NOSER, TONY RO, CORWIN BOAKE, HARVEY LEVIN, JAREK ARONOWSKI, AND TIMOTHY SCHALLERT. **Constraint-induced movement therapy.** *Stroke*, **35**(11 suppl 1):2699–2701, 2004. 27, 50
- [76] STEVEN L WOLF, CAROLEE J WINSTEIN, J PHILIP MILLER, EDWARD TAUB, GITENDRA USWATTE, DAVID MORRIS, CAROL GIULIANI, KATHYE E LIGHT, DEBORAH NICHOLS-LARSEN, EXCITE INVESTIGATORS, ET AL. **Effect of constraint-induced movement therapy on upper extremity function 3 to 9 months after stroke: the EXCITE randomized clinical trial.** *Jama*, **296**(17):2095–2104, 2006. 27
- [77] STEPHEN J PAGE, PETER LEVINE, AND JANE C KHOURY. **Modified constraint-induced therapy combined with mental practice: thinking through better motor outcomes.** *Stroke*, **40**(2):551–554, Feb 2009. 28
- [78] B. FRENCH, L. H. THOMAS, M. J. LEATHLEY, C. J. SUTTON, J. McADAM, A. FORSTER, P. LANGHORNE, C I M. PRICE, A. WALKER, AND C. L. WATKINS. **Repetitive task training for improving functional ability after stroke.** *Cochrane Database Syst Rev*, (4):CD006073, 2007. 28
- [79] KIM C STEWART, JAMES H CAURAUUGH, AND JEFFERY J SUMMERS. % bf Bilateral movement training and stroke rehabilitation: a systematic review and meta-analysis. *Journal of the neurological sciences*, **244**(1):89–95, 2006. 28
- [80] SHRAGA HOCHERMAN, RUTH DICKSTEIN, AND TOMAS PILLAR. **Platform training and postural stability in hemiplegia.** *Archives of physical medicine and rehabilitation*, **65**(10):588–592, 1984. 28
- [81] RUTH DICKSTEIN, SHRAGA HOCHERMAN, ELISABETH DANNENBAUM, NAOR SHINA, AND THOMAS PILLAR. **Stance stability and EMG changes in the ankle musculature of**

REFERENCES

- hemiparetic patients trained on a moveable platform. *Neurorehabilitation and Neural Repair*, **5**(4):201–209, 1991. 28
- [82] ANNE M MOSELEY, ANGELA STARK, IAN D CAMERON, AND ALEX POLLOCK. **Treadmill training and body weight support for walking after stroke.** *Cochrane Database Syst Rev*, **4**, 2005. 28
- [83] JAN MEHRHOLZ, THOMAS PLATZ, JOACHIM KUGLER, AND MARCUS POHL. **Electromechanical and robot-assisted arm training for improving arm function and activities of daily living after stroke.** *Cochrane Database Syst Rev*, **4**(4), 2008. 28
- [84] VALERIE M POMEROY, L KING, ALEX POLLOCK, ALISON BAILY-HALLAM, AND PETER LANGHORNE. **Electrostimulation for promoting recovery of movement or functional ability after stroke.** *Cochrane Database Syst Rev*, **2**, 2006. 28
- [85] PETER LANGHORNE, FIONA COUPAR, AND ALEX POLLOCK. **Motor recovery after stroke: a systematic review.** *Lancet Neurol*, **8**(8):741–754, Aug 2009. 28
- [86] NS WARD, MM BROWN, AJ THOMPSON, AND RSJ FRACKOWIAK. **Neural correlates of outcome after stroke: a cross-sectional fMRI study.** *Brain*, **126**(6):1430–1448, 2003. 28, 99
- [87] ERNST NIEDERMEYER AND FH LOPES DA SILVA. *Electroencephalography: basic principles, clinical applications, and related fields.* Lippincott Williams & Wilkins, 2005. 31, 35
- [88] HANS BERGER. **Über das elektroencephalogramm des menschen.** *European Archives of Psychiatry and Clinical Neuroscience*, **87**(1):527–570, 1929. 31
- [89] LF HAAS. **Hans Berger (1873–1941), Richard Caton (1842–1926), and electroencephalography.** *Journal of Neurology, Neurosurgery & Psychiatry*, **74**(1):9–9, 2003. 31
- [90] HERBERT HENRI JASPER. **The ten twenty electrode system of the international federation.** *Electroencephalography and clinical neurophysiology*, **10**:371–375, 1958. 31
- [91] AMERICAN CLINICAL NEUROPHYSIOLOGY SOCIETY ET AL. **Guideline 5: Guidelines for standard electrode position nomenclature.** *American journal of electroneurodiagnostic technology*, **46**(3):222, 2006. 31
- [92] GEORGE H KLEM, HANS OTTO LÜDERS, HH JASPER, AND C ELGER. **The ten-twenty electrode system of the International Federation.** *Electroencephalogr Clin Neurophysiol*, **52**(suppl.):3, 1999. 31
- [93] ROBERT OOSTENVELD AND PETER PRAAMSTRA. **The five percent electrode system for high-resolution EEG and ERP measurements.** *Clinical neurophysiology*, **112**(4):713–719, 2001. 31
- [94] D. J. MCFARLAND, L. M. MCCANE, S. V. DAVID, AND J. R. WOLPAW. **% bf Spatial filter selection for EEG-based communication.** *Electroencephalogr Clin Neurophysiol*, **103**(3):386–394, Sep 1997. 33
- [95] FERNANDO LOPES DA SILVA. **EEG: Origin and measurement.** In *EEG-fMRI*, pages 19–38. Springer, 2010. 34
- [96] G. PFURTSCHELLER, A STANCÁK, JR, AND C. NEUPER. **Post-movement beta synchronization. A correlate of an idling motor area?** *Electroencephalogr Clin Neurophysiol*, **98**(4):281–293, Apr 1996. 35
- [97] FRANS F JOBSIS. **Noninvasive, infrared monitoring of cerebral and myocardial oxygen sufficiency and circulatory parameters.** *Science*, **198**(4323):1264–1267, 1977. 36
- [98] MARTIN WOLF, MARCO FERRARI, AND VALENTINA QUARESIMA. **Progress of near-infrared spectroscopy and topography for brain and muscle clinical applications.** *J Biomed Opt*, **12**(6):062104, 2007. 36
- [99] GARY STRANGMAN, DAVID A BOAS, AND JEFFREY P SUTTON. **% bf Non-invasive neuroimaging using near-infrared light.** *Biological psychiatry*, **52**(7):679–693, 2002. 38
- [100] A. DUNCAN, J. H. MEEK, M. CLEMENCE, C. E. ELWELL, L. TYSZCZUK, M. COPE, AND D. T. DELPY. **Optical path-length measurements on adult head, calf and forearm and the head of the newborn infant using phase resolved optical spectroscopy.** *Phys Med Biol*, **40**(2):295–304, Feb 1995. 40
- [101] E. OKADA, M. FIRBANK, M. SCHWEIGER, S. R. ARRIDGE, M. COPE, AND D. T. DELPY. **Theoretical and experimental investigation of near-infrared light propagation in a model of the adult head.** *Appl Opt*, **36**(1):21–31, Jan 1997. 40, 77, 84
- [102] YUICH FUKUI, YUSAKU AJICHI, AND EIJI OKADA. **Monte Carlo prediction of near-infrared light propagation in realistic adult and neonatal head models.** *Appl Opt*, **42**(16):2881–2887, Jun 2003. 40, 41
- [103] EIJI OKADA AND DAVID T DELPY. **Near-infrared light propagation in an adult head model. I. Modeling of low-level scattering in the cerebrospinal fluid layer.** *Applied optics*, **42**(16):2906–2914, 2003. 41
- [104] HQ WOODARD AND DR WHITE. **The composition of body tissues.** *The British journal of radiology*, **59**(708):1209–1218, 1986. 41

REFERENCES

- [105] GEORGE M HALE AND MARVIN R QUERRY. **Optical constants of water in the 200-nm to 200- μ m wavelength region.** *Applied optics*, **12**(3):555–563, 1973. 41
- [106] SCOTT PRAHL ET AL. **Optical absorption of hemoglobin**, 1999. 41
- [107] HELLMUTH OBRIG, MARKUS NEUFANG, RÜDIGER WENZEL, MATTHIAS KOHL, JENS STEINBRINK, KARL EINHÄUPL, AND ARNO VILLRINGER. **Spontaneous low frequency oscillations of cerebral hemodynamics and metabolism in human adults.** *Neuroimage*, **12**(6):623–639, 2000. 44, 85
- [108] CLAUDE JULIEN. **The enigma of Mayer waves: Facts and models.** *Cardiovasc Res*, **70**(1):12–21, Apr 2006. 44, 85, 88
- [109] JOHN ALLEN. **Photoplethysmography and its application in clinical physiological measurement.** *Physiological measurement*, **28**(3):R1, 2007. 44
- [110] K.T. SWEENEY, H. AYAZ, T.E. WARD, M. IZZETOGLU, S.F. MCLOONE, AND B. ONARAL. **A methodology for validating artifact removal techniques for fNIRS.** In *Engineering in Medicine and Biology Society, EMBC, 2011 Annual International Conference of the IEEE*, pages 4943–4946, 2011. 44, 46
- [111] JONATHAN R WOLPAW, NIELS BIRBAUMER, DENNIS J MCFARLAND, GERT PFURTSCHELLER, AND THERESA M VAUGHAN. % bf Brain–computer interfaces for communication and control. *Clinical neurophysiology*, **113**(6):767–791, 2002. 44, 49, 56, 57, 59
- [112] J D R MILLÁN, RÜDIGER RUPP, GERNOT R MÜLLER-PUTZ, RODERICK MURRAY-SMITH, CLAUDIO GIUGLIEMMA, MICHAEL TANGERMANN, CARMEN VIDAURRE, FEBO CINCOTTI, ANDREA KÜBLER, ROBERT LEEB, ET AL. **Combining brain–computer interfaces and assistive technologies: state-of-the-art and challenges.** *Frontiers in neuroscience*, **4**, 2010. 44, 58
- [113] G. PFURTSCHELLER AND C. NEUPER. **Motor imagery and direct brain–computer communication.** **89**(7):1123–1134, 2001. 45
- [114] ANDER RAMOS-MURGUALDAY, MARKUS SCHÜRHOLZ, VITTORIO CAGGIANO, MORITZ WILDGRUBER, ANDREA CARIA, EVA MARIA HAMMER, SEBASTIAN HALDER, AND NIELS BIRBAUMER. **Pro-prioceptive feedback and brain computer interface (BCI) based neuroprostheses.** *PLoS One*, **7**(10):e47048, 2012. 46
- [115] KEVIN T. SWEENEY, TOMÁS E. WARD, AND SEÁN F. MCLOONE. **Artifact removal in physiological signals—practices and possibilities.** *IEEE Trans Inf Technol Biomed*, **16**(3):488–500, May 2012. 46
- [116] KEVIN T. SWEENEY, SEÁN F. MCLOONE, AND TOMÁS E. WARD. **The use of ensemble empirical mode decomposition with canonical correlation analysis as a novel artifact removal technique.** *IEEE Trans Biomed Eng*, **60**(1):97–105, Jan 2013. 46, 83
- [117] FABIEEN LOTTE, MARCO CONGEDO, ANATOLE LÉCUYER, AND FABRICE LAMARCHE. **A review of classification algorithms for EEG-based brain–computer interfaces.** *Journal of neural engineering*, **4**, 2007. 48
- [118] B. OBERMAIER, G. R. MÜLLER, AND G. PFURTSCHELLER. **”Virtual keyboard” controlled by spontaneous EEG activity.** *IEEE Trans Neural Syst Rehabil Eng*, **11**(4):422–426, Dec 2003. 48
- [119] JOHN WILLIAMSON, RODERICK MURRAY-SMITH, BENJAMIN BLANKERTZ, MATTHIAS KRAULEDAT, AND K-R MÜLLER. % bf Designing for uncertain, asymmetric control: Interaction design for brain–computer interfaces. *International Journal of Human-Computer Studies*, **67**(10):827–841, 2009. 48
- [120] MICHAEL BENSCH, AHMED A KARIM, JÜRGEN MELLINGER, THILO HINTERBERGER, MICHAEL TANGERMANN, MARTIN BOGDAN, WOLFGANG ROSENSTIEL, AND NIELS BIRBAUMER. **Nessi: an EEG-controlled web browser for severely paralyzed patients.** *Computational intelligence and neuroscience*, **2007**, 2007. 49
- [121] EMILY MUGLERAB, MICHAEL BENSCH, SEBASTIAN HALDERA, WOLFGANG ROSENSTIEL, MARTIN BOGDAN, NIELS BIRBAUMERAE, AND ANDREA KÜBLERAF. **Control of an internet browser using the P300 event-related potential.** *IJBEM*, **10**:56–63, 2008. 49
- [122] JDR MILLÁN, FERRAN GALÁN, DIRK VANHOYDONCK, EILEEN LEW, JOHAN PHILIPS, AND MARNIX NUTTIN. **Asynchronous non-invasive brain-actuated control of an intelligent wheelchair.** In *Engineering in Medicine and Biology Society, 2009. EMBC 2009. Annual International Conference of the IEEE*, pages 3361–3364. IEEE, 2009. 49
- [123] IÑAKI ITURRATE, JAVIER ANTELIS, AND JAVIER MINGUEZ. **Synchronous EEG brain-actuated wheelchair with automated navigation.** In *Robotics and Automation, 2009. ICRA’09. IEEE International Conference on*, pages 2318–2325. IEEE, 2009. 49
- [124] KIM D ANDERSON. **Targeting recovery: priorities of the spinal cord-injured population.** *Journal of neurotrauma*, **21**(10):1371–1383, 2004. 49

REFERENCES

- [125] GERNOT R MÜLLER-PUTZ, REINHOLD SCHERER, GERT PFURTSCHELLER, AND RÜDIGER RUPP. **Brain-computer interfaces for control of neuroprostheses: from synchronous to asynchronous mode of operation/Brain-Computer Interfaces zur Steuerung von Neuroprothesen: von der synchronen zur asynchronen Funktionsweise.** *Biomedizinische Technik*, **51**(2):57–63, 2006. 49
- [126] GERT PFURTSCHELLER, GERNOT R MÜLLER, JÖRG PFURTSCHELLER, HANS JÜRGEN GERNER, AND RÜDIGER RUPP. **‘Thought’-control of functional electrical stimulation to restore hand grasp in a patient with tetraplegia.** *Neuroscience letters*, **351**(1):33–36, 2003. 49
- [127] MATTHIAS KRAULEDAT, KONRAD GRZESKA, MAX SAGEBAUM, BENJAMIN BLANKERTZ, CARMEN VIDAURRE, KLAUS-ROBERT MÜLLER, AND MICHAEL SCHRÖDER. **Playing Pinball with non-invasive BCI.** In *Advances in Neural Information Processing Systems*, pages 1641–1648, 2009. 49
- [128] ANDREA FINKE, ALEXANDER LENHARDT, AND HELGE RITTER. **The MindGame: a P300-based brain-computer interface game.** *Neural Networks*, **22**(9):1329–1333, 2009. 49
- [129] DAVID MARSHALL, DAMIEN COYLE, SHANE WILSON, AND MICHAEL CALLAGHAN. **Games, gameplay, and BCI: The state of the art.** *Computational Intelligence and AI in Games, IEEE Transactions on*, **5**(2):82–99, 2013. 49, 168
- [130] ROBERT LEEB, FELIX LEE, CLAUDIA KEINRATH, REINHOLD SCHERER, HORST BISCHOF, AND GERT PFURTSCHELLER. **Brain-computer communication: motivation, aim, and impact of exploring a virtual apartment.** *Neural Systems and Rehabilitation Engineering, IEEE Transactions on*, **15**(4):473–482, 2007. 49
- [131] RICARDO RON-ANGEVIN, ANTONIO DÍAZ-ESTRELLA, AND FRANCISCO VELASCO-ALVAREZ. **A two-class brain computer interface to freely navigate through virtual worlds/Ein Zwei-Klassen-Brain-Computer-Interface zur freien Navigation durch virtuelle Welten.** *Biomedizinische Technik/Biomedical Engineering*, **54**(3):126–133, 2009. 49
- [132] EDUARDO RECK MIRANDA. **Brain-computer music interface for composition and performance.** *International Journal on Disability and Human Development*, **5**(2):119–126, 2006. 49
- [133] JANIS J DALY AND JONATHAN R WOLPAW. **Brain-computer interfaces in neurological rehabilitation.** *The Lancet Neurology*, **7**(11):1032–1043, 2008. 50, 57
- [134] G PFURTSCHELLER, G R MULLER-PUTZ, R SCHERER, AND C NEUPER. **Rehabilitation with Brain-Computer Interface Systems**, 2008. 50
- [135] J N MAK AND J R WOLPAW. **Clinical Applications of Brain-Computer Interfaces: Current State and Future Prospects**, 2009. 50
- [136] STEVEN L WOLF AND STUART A BINDER-MACLEOD. **Electromyographic biofeedback applications to the hemiplegic patient changes in upper extremity neuromuscular and functional status.** *Physical therapy*, **63**(9):1393–1403, 1983. 50
- [137] NICK S WARD. **Plasticity and the functional reorganization of the human brain.** *International Journal of Psychophysiology*, **58**(2):158–161, 2005. 50
- [138] JOACHIM LIEPERT, HEIKE BAUDER, WOLFGANG HR MILTNER, EDWARD TAUB, AND CORNELIUS WEILLER. **Treatment-induced cortical reorganization after stroke in humans.** *Stroke*, **31**(6):1210–1216, 2000. 50
- [139] SJOERD DE VRIES AND THEO MULDER. **Motor imagery and stroke rehabilitation: a critical discussion.** *Journal of Rehabilitation Medicine*, **39**(1):5–13, 2007. 50
- [140] STEPHEN J PAGE, PETER LEVINE, AND ANTHONY LEONARD. **Mental practice in chronic stroke results of a randomized, placebo-controlled trial.** *Stroke*, **38**(4):1293–1297, 2007. 51
- [141] NIKHIL SHARMA, PETER S JONES, TA CARPENTER, AND JEAN-CLAUDE BARON. **Mapping the involvement of BA 4a and 4p during motor imagery.** *Neuroimage*, **41**(1):92–99, 2008. 51
- [142] GIRIJESH PRASAD, PAWEL HERMAN, DAMIEN COYLE, SUZANNE McDONOUGH, AND JACQUELINE CROSBIE. **Using motor imagery based brain-computer interface for post-stroke rehabilitation.** In *Neural Engineering, 2009. NER’09. 4th International IEEE/EMBS Conference on*, pages 258–262. IEEE, 2009. 51
- [143] GIRIJESH PRASAD, PAWEL HERMAN, DAMIEN COYLE, SUZANNE McDONOUGH, AND JACQUELINE CROSBIE. **Applying a brain-computer interface to support motor imagery practice in people with stroke for upper limb recovery: a feasibility study.** *J Neuroeng Rehabil*, **7**:60, 2010. 51
- [144] MORITZ GROSSE-WENTRUP, DONATELLA MATTIA, AND KARIM OWEISS. **Using brain-computer interfaces to induce neural plasticity and restore function.** *J Neural Eng*, **8**(2):025004, Apr 2011. 51, 56
- [145] ÁLVARO BARBERO AND MORITZ GROSSE-WENTRUP. **Biased feedback in brain-computer interfaces.** *Journal of neuroengineering and rehabilitation*, **7**(1):34, 2010. 52

REFERENCES

- [146] ANDER RAMOS-MURGUIALDAY, DORIS BROETZ, MASSIMILIANO REA, LEONHARD LÄER, OZGE YILMAZ, FABRICIO L. BRASIL, GIULIA LIBERATI, MARCO R. CURADO, ELIANA GARCIA-COSSIO, ALEXANDROS VYZIOTIS, WOOSANG CHO, MANUEL AGOSTINI, ERNESTO SOARES, SURJO SOEKADAR, ANDREA CARIA, LEONARDO G. COHEN, AND NIELS BIRBAUMER. **Brain-machine interface in chronic stroke rehabilitation: a controlled study.** *Ann Neurol*, **74**(1):100–108, Jul 2013. 52
- [147] KAI KENG ANG, CUNTAI GUAN, KOK SOON PHUA, CHUANCHU WANG, LONGJIANG ZHOU, KA YIN TANG, GOPAL J. EPHRAIM JOSEPH, CHRISTOPHER WEE KEONG KUAH, AND KAREN SUI GEOK CHUA. **Brain-computer interface-based robotic end effector system for wrist and hand rehabilitation: results of a three-armed randomized controlled trial for chronic stroke.** *Front Neuroeng*, **7**:30, 2014. 52, 57, 168
- [148] T. J. HUPPERT, R. D. HOGE, S. G. DIAMOND, M. A. FRANCESCHINI, AND D. A. BOAS. **A temporal comparison of BOLD, ASL, and NIRS hemodynamic responses to motor stimuli in adult humans.** *Neuroimage*, **29**(2):368–382, Jan 2006. 53
- [149] SELJI OGAWA, TM LEE, AR KAY, AND DW TANK. **Brain magnetic resonance imaging with contrast dependent on blood oxygenation.** *Proceedings of the National Academy of Sciences*, **87**(24):9868–9872, 1990. 53
- [150] GERD MUEHLEHNER AND JOEL S KARP. **Positron emission tomography.** *Physics in medicine and biology*, **51**(13):R117, 2006. 54
- [151] MATTI HÄMÄLÄINEN, RIHTA HARI, RISTO J ILMONIEMI, JUKKA KNUUTILA, AND OLLI V LOUNASMAA. **Magnetoencephalography-theory, instrumentation, and applications to noninvasive studies of the working human brain.** *Reviews of modern Physics*, **65**(2):413, 1993. 55
- [152] ANDRÉ J SZAMEITAT, SHAN SHEN, AND ANNETTE STERR. **The functional magnetic resonance imaging (fMRI) procedure as experienced by healthy participants and stroke patients—A pilot study.** *BMC medical imaging*, **9**(1):14, 2009. 56
- [153] NILOUFAR NIAKOSARI HADIDI, KATHRYN R. CULLEN, LEAH M J. HALL, RUTH LINDQUIST, KATHLEEN C. BUCKWALTER, AND EMILY MATHEWS. **Functional magnetic resonance imaging as experienced by stroke survivors.** *Res Gerontol Nurs*, **7**(5):200–205, 2014. 57
- [154] ETHAN BUCH, CORNELIA WEBER, LEONARDO G COHEN, CHRISTOPH BRAUN, MICHAEL A DIMYAN, TYLER ARD, JURGEN MELLINGER, ANDREA CARIA, SURJO SOEKADAR, ALISSA FOURKAS, ET AL. **Think to move: a neuromagnetic brain-computer interface (BCI) system for chronic stroke.** *Stroke*, **39**(3):910–917, 2008. 57, 58
- [155] JENNIFER S KEPPLER AND PETER S CONTI. **A cost analysis of positron emission tomography.** *American Journal of Roentgenology*, **177**(1):31–40, 2001. 58
- [156] GERWIN SCHALK, DENNIS J MCFARLAND, THILO HINTERBERGER, NIELS BIRBAUMER, AND JONATHAN R WOLPAW. **BCI2000: a general-purpose brain-computer interface (BCI) system.** *Biomedical Engineering, IEEE Transactions on*, **51**(6):1034–1043, 2004. 58
- [157] BENJAMIN BLANKERTZ, GUIDO DORNHEGE, MATTHIAS KRAULEDAT, K MULLER, VOLKER KUNZMANN, FLORIAN LOSCH, AND GABRIEL CURIO. **The Berlin Brain-Computer Interface: EEG-based communication without subject training.** *Neural Systems and Rehabilitation Engineering, IEEE Transactions on*, **14**(2):147–152, 2006. 58
- [158] SHIRLEY M COYLE, TOMAS E WARD, AND CHARLES M MARKHAM. **Brain-computer interface using a simplified functional near-infrared spectroscopy system.** *Journal of neural engineering*, **4**(3):219, 2007. 58, 62, 74, 82
- [159] RANGANATHA SITARAM, ANDREA CARIA, AND NIELS BIRBAUMER. **Hemodynamic brain-computer interfaces for communication and rehabilitation.** *Neural Networks*, **22**(9):1320–1328, 2009. 58
- [160] JÜRGEN MELLINGER, GERWIN SCHALK, CHRISTOPH BRAUN, HUBERT PREISSEL, WOLFGANG ROSENSTIEL, NIELS BIRBAUMER, AND ANDREA KÜBLER. **An MEG-based brain-computer interface (BCI).** *Neuroimage*, **36**(3):581–593, Jul 2007. 58
- [161] NIKOLAUS WEISKOPF, RALF VEIT, MICHAEL ERB, KLAUS MATHIAK, WOLFGANG GRODD, RAINER GOEBEL, AND NIELS BIRBAUMER. **Physiological self-regulation of regional brain activity using real-time functional magnetic resonance imaging (fMRI): methodology and exemplary data.** *Neuroimage*, **19**(3):577–586, Jul 2003. 58
- [162] NIKOLAUS WEISKOPF, KLAUS MATHIAK, SIMON W BOCK, FRANK SCHARNOWSKI, RALF VEIT, WOLFGANG GRODD, RAINER GOEBEL, AND NIELS BIRBAUMER. **Principles of a brain-computer interface (BCI) based on real-time functional magnetic resonance imaging (fMRI).** *Biomedical Engineering, IEEE Transactions on*, **51**(6):966–970, 2004. 58
- [163] RANGANATHA SITARAM, ANDREA CARIA, RALF VEIT, TILMAN GABER, GIUSEPPINA ROTA, ANDREA KUEBLER, AND NIELS BIRBAUMER. **fMRI brain-computer interface: a tool**

REFERENCES

- for neuroscientific research and treatment. *Comput Intell Neurosci*, page 25487, 2007. 58
- [164] MARISKA J. VANSTEENSEL, DORA HERMES, ERIK J. AARNOUTSE, MARTIN G. BLEICHNER, GERWIN SCHALK, PETER C. VAN RIJEN, FRANS S. S. LEIJTEN, AND NICK F. RAMSEY. **Brain-computer interfacing based on cognitive control.** *Ann Neurol*, **67**(6):809–816, Jun 2010. 58
- [165] GERWIN SCHALK AND ERIC C. LEUTHARDT. **Brain-computer interfaces using electrocorticographic signals.** *IEEE Rev Biomed Eng*, **4**:140–154, 2011. 58
- [166] R. SCHERER, G. R. MÜLLER-PUTZ, AND G. PFURTSCHELLER. **Self-initiation of EEG-based brain-computer communication using the heart rate response.** *J Neural Eng*, **4**(4):L23–L29, Dec 2007. 59
- [167] R. LEEB, H. SAGHA, R. CHAVARRIAGA, AND J. DEL R MILLAN. **Multimodal Fusion of Muscle and Brain Signals for a Hybrid-BCI.** In *Engineering in Medicine and Biology Society (EMBC), 2010 Annual International Conference of the IEEE*, pages 4343–4346, 2010. 59
- [168] ROMAN VILIMEK AND THORSTEN O ZANDER. **BC (eye): Combining eye-gaze input with brain-computer interaction.** In *Universal Access in Human-Computer Interaction. Intelligent and Ubiquitous Interaction Environments*, pages 593–602. Springer, 2009. 59
- [169] GERT PFURTSCHELLER AND FH LOPES DA SILVA. **Event-related EEG/MEG synchronization and desynchronization: basic principles.** *Clinical neurophysiology*, **110**(11):1842–1857, 1999. 65
- [170] JUANHONG YU, KAI KENG ANG, CUNTAI GUAN, AND CHUANCHU WANG. **A multimodal fNIRS and EEG-based BCI study on motor imagery and passive movement.** In *Neural Engineering (NER), 2013 6th International IEEE/EMBS Conference on*, pages 5–8, 2013. 71, 178
- [171] YICHUAN LIU, HASAN AYAZ, ADRIAN CURTIN, BANU ONARAL, AND PATRICIA A SHEWOKIS. **Towards a Hybrid P300-Based BCI Using Simultaneous fNIR and EEG.** In *Foundations of Augmented Cognition*, pages 335–344. Springer, 2013. 71
- [172] FELIX PUTZE, SEBASTIAN HESSLINGER, CHUN-YU TSE, YUN-YING HUANG, CHRISTIAN HERFF, CUNTAI GUAN, AND TANJA SCHULTZ. **Hybrid fNIRS-EEG based classification of auditory and visual perception processes.** *Frontiers in neuroscience*, **8**, 2014. 71, 178
- [173] A. MAKI, Y. YAMASHITA, Y. ITO, E. WATANABE, Y. MAYANAGI, AND H. KOIZUMI. **Spatial and temporal analysis of human motor activity using noninvasive NIR tomography.** *Med Phys*, **22**(12):1997–2005, Dec 1995. 74
- [174] M. A. FRANCESCHINI, V. TORONOV, M. FILIACI, E. GRATTON, AND S. FANTINI. **On-line optical imaging of the human brain with 160-ms temporal resolution.** *Opt Express*, **6**(3):49–57, Jan 2000. 74
- [175] S R ARRIDGE. **Optical tomography in medical imaging.** *Inverse Problems*, **15**(2):R41–R93, 1999. 74
- [176] STEPHEN FAUL, GREGOR GREGORCIC, GERALDINE BOYLAN, WILLIAM MARNANE, GORDON LIGHTBODY, AND SEAN CONNOLLY. **Gaussian process modeling of EEG for the detection of neonatal seizures.** *IEEE Trans Biomed Eng*, **54**(12):2151–2162, Dec 2007. 74
- [177] K. AZMAN AND J. KOCLJAN. **Application of Gaussian processes for black-box modelling of biosystems.** *ISA Trans*, **46**(4):443–457, Oct 2007. 74
- [178] S. M. MATECHIK AND M. R. STYTZ. **Using Kriging to interpolate MRI data.** In *Proc. 16th Annual International Conference of the IEEE Engineering Advances: New Opportunities for Biomedical Engineers Engineering in Medicine and Biology Society*, pages 576–577, 3–6 Nov. 1994. 74
- [179] M. R. STYTZ AND R. W. PARROTT. **Using kriging for 3D medical imaging.** *Comput Med Imaging Graph*, **17**(6):421–442, 1993. 74
- [180] C.E. RASMUSSEN AND C.K.I. WILLIAMS. *Gaussian processes for machine learning.* MIT Press, 2006. 74, 75, 130
- [181] C.E. RASMUSSEN AND C.K.I. WILLIAMS. **Gaussian Processes for Machine Learning.** <http://www.gaussianprocess.org/gpml/code/matlab/doc/index.html>. 76, 122
- [182] THEODORE J HUPPERT, SOLOMON G DIAMOND, MARIA A FRANCESCHINI, AND DAVID A BOAS. **HomER: a review of time-series analysis methods for near-infrared spectroscopy of the brain.** *Appl Opt*, **48**(10):D280–D298, Apr 2009. 77, 86
- [183] **The Center for Functional Neuroimaging Technologies.** <http://www.nmr.mgh.harvard.edu/CFNT/index>. 77
- [184] **HomER - Hemodynamic Evoked Response NIRS Data Analysis GUI.** <http://www.nmr.mgh.harvard.edu/CFNT/index>. 77
- [185] **Photon Migration Imaging Toolbox for Matlab.** <http://www.nmr.mgh.harvard.edu/PMI/toolbox/>. 77
- [186] **PhysioNet.** <http://www.physionet.org/>. 83
- [187] KEVIN T SWEENEY, HASAN AYAZ, TOMÁS E WARD, MELTEM IZZETOGLU, SEÁN F MCLOONE, AND BANU ONARAL. **% bf A methodology for validating artifact removal techniques for physiological signals.** *Information Technology*

REFERENCES

- in *Biomedicine, IEEE Transactions on*, **16**(5):918–926, 2012. 83
- [188] M. CESARELLI, M. RUFFO, M. ROMANO, AND P. BIFULCO. **Simulation of foetal phonocardiographic recordings for testing of FHR extraction algorithms.** *Comput Methods Programs Biomed*, **107**(3):513–523, Sep 2012. 83
- [189] D. FARINA, A. CROSETTI, AND R. MERLETTI. **A model for the generation of synthetic intramuscular EMG signals to test decomposition algorithms.** *IEEE Trans Biomed Eng*, **48**(1):66–77, Jan 2001. 83
- [190] P.E. MCSHARRY, G.D. CLIFFORD, L. TARASSENKO, AND L.A. SMITH. **A dynamical model for generating synthetic electrocardiogram signals.** **50**(3):289–294, 2003. 83
- [191] JEAN-MICHEL BADIÉ, DELPHINE COSANDIER-RIMÉLÉ, CHRISTIAN G. BÉNAR, DENIS SCHWARTZ, PATRICK CHAUVEL, AND FABRICE WENDLING. **Realistic synthetic background neuronal activity for the analysis of MEG probe configurations.** *Conf Proc IEEE Eng Med Biol Soc*, **2007**:2460–2463, 2007. 83
- [192] R. B. BUXTON, E. C. WONG, AND L. R. FRANK. **Dynamics of blood flow and oxygenation changes during brain activation: the balloon model.** *Magn Reson Med*, **39**(6):855–864, Jun 1998. 85
- [193] RICHARD B. BUXTON, KÁMIL ULUDA, DAVID J. DUBOWITZ, AND THOMAS T. LIU. **Modeling the hemodynamic response to brain activation.** *Neuroimage*, **23** Suppl 1:S220–S233, 2004. 85
- [194] XU CUI, SIGNE BRAY, AND ALLAN L REISS. **Functional near infrared spectroscopy (NIRS) signal improvement based on negative correlation between oxygenated and deoxygenated hemoglobin dynamics.** *Neuroimage*, **49**(4):3039–3046, Feb 2010. 85, 86
- [195] MARK COPE. *The application of near infrared spectroscopy to non invasive monitoring of cerebral oxygenation in the newborn infant.* PhD thesis, University College London, Department of Medical Physics and Bioengineering, University College London, April 1991. 86, 90
- [196] S. COYLE, T. WARD, AND C. MARKHAM. **Physiological noise in near-infrared spectroscopy: implications for optical brain computer interfacing.** *Conf Proc IEEE Eng Med Biol Soc*, **6**:4540–4543, 2004. 89
- [197] F CHOLLET, V DIPIERO, RJS WISE, DJ BROOKS, RJ DOLAN, AND RSJ FRACKOWIAK. **The functional anatomy of motor recovery after stroke in humans: a study with positron emission tomography.** *Annals of neurology*, **29**(1):63–71, 1991. 97, 98, 99
- [198] CORNELIUS WEILLER, FRANÇOIS CHOLLET, KARL J FRISTON, RICHARD JS WISE, AND RICHARD SJ FRACKOWIAK. **Functional reorganization of the brain in recovery from striatocapsular infarction in man.** *Annals of neurology*, **31**(5):463–472, 1992. 98, 99
- [199] N. S. WARD, M. M. BROWN, A. J. THOMPSON, AND R S J. FRACKOWIAK. **Neural correlates of motor recovery after stroke: a longitudinal fMRI study.** *Brain*, **126**(Pt 11):2476–2496, Nov 2003. 99
- [200] CINZIA CALAUTTI AND JEAN-CLAUDE BARON. **Functional neuroimaging studies of motor recovery after stroke in adults: a review.** *Stroke*, **34**(6):1553–1566, Jun 2003. 100
- [201] OLAF SPORNS, DANTE R CHIALVO, MARCUS KAISER, AND CLAUS C HILGETAG. **Organization, development and function of complex brain networks.** *Trends in cognitive sciences*, **8**(9):418–425, 2004. 100
- [202] P. A. ROBINSON, C. J. RENNIE, D. L. ROWE, S. C. O’CONNOR, AND E. GORDON. **Multiscale brain modelling.** *Philos Trans R Soc Lond B Biol Sci*, **360**(1457):1043–1050, May 2005. 100
- [203] ED BULLMORE AND OLAF SPORNS. **Complex brain networks: graph theoretical analysis of structural and functional systems.** *Nature Reviews Neuroscience*, **10**(3):186–198, 2009. 100, 101
- [204] QAWI K TELESFORD, SEAN L SIMPSON, JONATHAN H BURDETTE, SATORU HAYASAKA, AND PAUL J LAURIENTI. **The brain as a complex system: using network science as a tool for understanding the brain.** *Brain connectivity*, **1**(4):295–308, 2011. 100
- [205] OLAF SPORNS. **The human connectome: a complex network.** *Ann N Y Acad Sci*, **1224**:109–125, Apr 2011. 100
- [206] NATALIE M ZAHR. **Graphs of Brain Networks.** *Alcoholism: Clinical and Experimental Research*, **37**(11):1813–1815, 2013. 100
- [207] OLAF SPORNS, GIULIO TONONI, AND ROLF KÖTTER. **The human connectome: A structural description of the human brain.** *PLoS Comput Biol*, **1**(4):e42, Sep 2005. 100
- [208] OLAF SPORNS. **Structure and function of complex brain networks.** *Dialogues in clinical neuroscience*, **15**(3):247, 2013. 100
- [209] KARL J FRISTON. **Functional and effective connectivity in neuroimaging: a synthesis.** *Human brain mapping*, **2**(1-2):56–78, 1994. 101, 151

REFERENCES

- [210] K. J. FRISTON, C. BUECHEL, G. R. FINK, J. MORRIS, E. ROLLS, AND R. J. DOLAN. **Psychophysiological and modulatory interactions in neuroimaging.** *Neuroimage*, **6(3)**:218–229, Oct 1997. 101
- [211] BARRY HORWITZ. % bf The elusive concept of brain connectivity. *Neuroimage*, **19(2)**:466–470, 2003. 101, 151
- [212] STEFAN HAUFE, VADIM V. NIKULIN, KLAUS-ROBERT MÜLLER, AND GUIDO NOLTE. **A critical assessment of connectivity measures for EEG data: a simulation study.** *Neuroimage*, **64**:120–133, Jan 2013. 101, 154, 162, 167
- [213] R. E. GREENBLATT, M. E. PFLIEGER, AND A. E. OSSADTCHI. **Connectivity measures applied to human brain electrophysiological data.** *J Neurosci Methods*, **207(1)**:1–16, May 2012. 101, 152, 162
- [214] CHRISTIAN GREFKES, DENNIS A. NOWAK, SIMON B. EICKHOFF, MANUEL DAFOTAKIS, JUTTA KÜST, HANS KARBE, AND GEREON R. FINK. **Cortical connectivity after subcortical stroke assessed with functional magnetic resonance imaging.** *Ann Neurol*, **63(2)**:236–246, Feb 2008. 102, 103
- [215] FABRIZIO DE VICO FALLANI, LAURA ASTOLFI, FEBO CINCOTTI, DONATELLA MATTIA, DARIA LA ROCCA, ELIRA MAK-SUTI, SERENELLA SALINARI, FABIO BABILONI, BALAZS VEGSO, GYORGY KOZMANN, AND ZOLTAN NAGY. **Evaluation of the brain network organization from EEG signals: a preliminary evidence in stroke patient.** *Anat Rec (Hoboken)*, **292(12)**:2023–2031, Dec 2009. 102
- [216] CHRISTIAN GERLOFF, KHALAF BUSHARA, ALEXANDRA SAILER, ERIC M. WASSERMANN, ROBERT CHEN, TAKAHIRO MATSUOKA, DANIEL WALDVOGEL, GEORGE F. WITTENBERG, KENJI ISHII, LEONARDO G. COHEN, AND MARK HALLETT. **Multimodal imaging of brain reorganization in motor areas of the contralesional hemisphere of well recovered patients after capsular stroke.** *Brain*, **129(Pt 3)**:791–808, Mar 2006. 103
- [217] CHRISTIAN GREFKES AND GEREON R. FINK. **Reorganization of cerebral networks after stroke: new insights from neuroimaging with connectivity approaches.** *Brain*, **134(Pt 5)**:1264–1276, May 2011. 103
- [218] LIANG WANG, CHUNSHUI YU, HAI CHEN, WEN QIN, YONG HE, FENGMEI FAN, YUJIN ZHANG, MOLI WANG, KUNCHENG LI, YUFENG ZANG, TODD S. WOODWARD, AND CHAOZHE ZHU. **Dynamic functional reorganization of the motor execution network after stroke.** *Brain*, **133(Pt 4)**:1224–1238, Apr 2010. 103
- [219] ALEX R. CARTER, SERGUEI V. ASTAFIEV, CATHERINE E. LANG, LISA T. CONNOR, JENNIFER RENGACHARY, MICHAEL J. STRUBE, DANIEL L. W. POPE, GORDON L. SHULMAN, AND MAURIZIO CORBETTA. **Resting interhemispheric functional magnetic resonance imaging connectivity predicts performance after stroke.** *Ann Neurol*, **67(3)**:365–375, Mar 2010. 103
- [220] NIKHIL SHARMA, JEAN-CLAUDE BARON, AND JAMES B. ROWE. **Motor imagery after stroke: relating outcome to motor network connectivity.** *Ann Neurol*, **66(5)**:604–616, Nov 2009. 103
- [221] DIONYSIOS MINTZPOULOS, LOUKAS G. ASTRAKAS, AZADEH KHANICHEH, ANGELOS A. KONSTAS, ANEESH SINGHAL, MICHAEL A. MOSKOWITZ, BRUCE R. ROSEN, AND A ARIA TZIKA. **Connectivity alterations assessed by combining fMRI and MR-compatible hand robots in chronic stroke.** *Neuroimage*, **47 Suppl 2**:T90–T97, Aug 2009. 103
- [222] A KAPANDJI. **Clinical test of apposition and counter-apposition of the thumb.** *Annales de chirurgie de la main organe officiel des societes de chirurgie de la main*, **5(1)**:67–73, 1986. 105
- [223] SWARTZ CENTER FOR COMPUTATIONAL NEUROSCIENCE (SCCN). **EEGLAB v9.0.2.3.** <http://sccn.ucsd.edu/eeglab/>. 109
- [224] MATLAB. *version 7.11.0 (R2010b)*. The MathWorks Inc., Natick, Massachusetts, 2010. 109, 122, 154
- [225] CLAUDE ELWOOD SHANNON. **Communication in the presence of noise.** *Proceedings of the IRE*, **37(1)**:10–21, 1949. 110
- [226] SEUNGJIN CHOI, ANDRZEJ CICHOCKI, HYUNG-MIN PARK, AND SOO-YOUNG LEE. **Blind source separation and independent component analysis: A review.** *Neural Information Processing-Letters and Reviews*, **6(1)**:1–57, 2005. 110, 112
- [227] CHRISTOPHER J JAMES AND CHRISTIAN W HESSE. **Independent component analysis for biomedical signals.** *Physiological measurement*, **26(1)**:R15, 2005. 112
- [228] A. HYVARINEN. **Fast and robust fixed-point algorithms for independent component analysis.** *Neural networks*, **10(3)**:626–634, 1999. 112
- [229] AAPO HYVÄRINEN AND ERKKI OJA. **Independent component analysis: algorithms and applications.** *Neural networks*, **13(4)**:411–430, 2000. 112
- [230] KAI KENG ANG, ZHENG YANG CHIN, HAIHONG ZHANG, AND CUNTAI GUAN. **Filter Bank Common Spatial Pattern (FBCSP).** pages 2390–2397, 2008. 122, 130

REFERENCES

- [231] KAI KENG ANG, ZHENG YANG CHIN, HAIHONG ZHANG, AND CUNTAI GUAN. **Filter bank common spatial pattern (FBCSP) in brain-computer interface.** In *Neural Networks, 2008. IJCNN 2008. (IEEE World Congress on Computational Intelligence). IEEE International Joint Conference on*, pages 2390–2397. IEEE, 2008. 122
- [232] ARNAUD DELORME AND SCOTT MAKEIG. **EEGLAB: an open source toolbox for analysis of single-trial EEG dynamics including independent component analysis.** *J Neurosci Methods*, **134**(1):9–21, Mar 2004. 122, 154
- [233] H RAMOSER, J MULLER-GERKING, AND G PFURTSCHELLER. **Optimal spatial filtering of single trial EEG during imagined hand movement,** 2000. 122, 124, 171
- [234] KEINOSUKE FUKUNAGA. *Introduction to statistical pattern recognition.* Academic press, 1990. 124, 125
- [235] Z. J. KOLES. **The quantitative extraction and topographic mapping of the abnormal components in the clinical EEG.** *Electroencephalogr Clin Neurophysiol*, **79**(6):440–447, Dec 1991. 124
- [236] BENJAMIN BLANKERTZ, RYOTA TOMIOKA, STEVEN LEMM, MOTOAKI KAWANABE, AND KLAUS-ROBERT MÜLLER. **Optimizing spatial filters for robust EEG single-trial analysis.** *IEEE Signal Processing Magazine*, **25**(1):41–56, 2008. 124, 171
- [237] SANDRINE DUDOIT, JANE FRIDLYAND, AND TERENCE P SPEED. **Comparison of Discrimination Methods for the Classification of Tumors Using Gene Expression Data.** *Journal of the American Statistical Association*, **97**(457):77–87, 2002. 129
- [238] C. K. I. WILLIAMS AND D. BARBER. **Bayesian classification with Gaussian processes.** *IEEE Transactions on Pattern Analysis and Machine Intelligence*, **20**(12):1342–1351, 1998. 130
- [239] J. KOČIJAN AND N. HVALA. **Sequencing batch-reactor control using Gaussian-process models.** *Biore-source Technology*, **137**:340–348, 2013. 130
- [240] VERA KAISER, ALEX KREILINGER, GERNOT R MÜLLER-PUTZ, AND CHRISTA NEUPER. **First Steps Toward a Motor Imagery Based Stroke BCI: New Strategy to Set up a Classifier.** *Front Neurosci*, **5**:86, 2011. 146
- [241] MAHNAZ ARVANEH, CUNTAI GUAN, KAI KENG ANG, AND CHAI QUEK. % bf Optimizing the channel selection and classification accuracy in EEG-based BCI. *IEEE Transactions on Biomedical Engineering*, **58**(6):1865–1873, 2011. 146
- [242] KJ FRISTON, CD FRITH, AND RSJ FRACKOWIAK. **Time-dependent changes in effective connectivity measured with PET.** *Human Brain Mapping*, **1**(1):69–79, 1993. 151
- [243] ALAN S GEVINS, NELSON H MORGAN, STEVEN L BRESSLER, BRIAN A CUTILLO, ROSEANN M WHITE, JUDY ILLES, DOUGLAS S GREER, JOSEPH C DOYLE, AND GERALD M ZEITLIN. **Human neuroelectric patterns predict performance accuracy.** *Science*, **235**(4788):580–585, 1987. 152
- [244] ELENA RYKHEVSKAIA, MONICA FABIANI, AND GABRIELE GRATTON. % bf Lagged covariance structure models for studying functional connectivity in the brain. *Neuroimage*, **30**(4):1203–1218, 2006. 152
- [245] NORBERT WIENER. **The theory of prediction,** 1956. 152
- [246] CLIVE WJ GRANGER. **Investigating causal relations by econometric models and cross-spectral methods.** *Econometrica: Journal of the Econometric Society*, pages 424–438, 1969. 152
- [247] ME PFLEGER AND RE GREENBLATT. **Using conditional mutual information to approximate causality for multivariate physiological time series.** *Int. J. Bioelectromagnetism*, **7**:285–288, 2005. 152
- [248] IGNACIO SANTAMARÍA, PUSKAL P POKHAREL, AND JOSÉ CARLOS PRINCIPE. % bf Generalized correlation function: definition, properties, and application to blind equalization. *Signal Processing, IEEE Transactions on*, **54**(6):2187–2197, 2006. 152
- [249] GUIDO NOLTE, ANDREAS ZIEHE, VADIM V. NIKULIN, ALOIS SCHLÖGL, NICOLE KRÄMER, TOM BRISMAR, AND KLAUS-ROBERT MÜLLER. **Robustly estimating the flow direction of information in complex physical systems.** *Phys Rev Lett*, **100**(23):234101, Jun 2008. 153
- [250] GUIDO NOLTE, OU BAI, LEWIS WHEATON, ZOLTAN MARI, SHERRY VORBACH, AND MARK HALLETT. **Identifying true brain interaction from EEG data using the imaginary part of coherency.** *Clin Neurophysiol*, **115**(10):2292–2307, Oct 2004. 154
- [251] GUIDO NOLTE, FRANK C. MEINECKE, ANDREAS ZIEHE, AND KLAUS-ROBERT MÜLLER. **Identifying interactions in mixed and noisy complex systems.** *Phys Rev E Stat Nonlin Soft Matter Phys*, **73**(5 Pt 1):051913, May 2006. 154
- [252] P. E. ROLAND, B. LARSEN, N. A. LASSEN, AND E. SKINHOJ. **Supplementary motor area and other cortical areas in organization of voluntary movements in man.** *J Neurophysiol*, **43**(1):118–136, Jan 1980. 156

REFERENCES

- [253] G. FEIN, J. RAZ, F. F. BROWN, AND E. L. MERRIN. **Common reference coherence data are confounded by power and phase effects.** *Electroencephalogr Clin Neurophysiol*, **69**(6):581–584, Jun 1988. 161
- [254] RAMÓN GUEVARA, JOSÉ LUIS PÉREZ VELAZQUEZ, VERA NENADOVIC, RICHARD WENBERG, GORAN SENJANOVIĆ, AND LUÍS GARCIA DOMINGUEZ. **Phase synchronization measurements using electroencephalographic recordings.** *Neuroinformatics*, **3**(4):301–313, 2005. 161
- [255] C. TANDONNET, B. BURLE, T. HASBROUCQ, AND F. VIDAL. **Spatial enhancement of EEG traces by surface Laplacian estimation: comparison between local and global methods.** *Clin Neurophysiol*, **116**(1):18–24, Jan 2005. 162
- [256] STEFAN HAUFE, RYOTA TOMIOKA, THORSTEN DICKHAUS, CLAUDIA SANNELLI, BENJAMIN BLANKERTZ, GUIDO NOLTE, AND KLAUS-ROBERT MÜLLER. **Large-scale EEG/MEG source localization with spatial flexibility.** *NeuroImage*, **54**(2):851–859, 2011. 167
- [257] ZEYNEP AKALIN ACAR AND SCOTT MAKEIG. **Effects of forward model errors on EEG source localization.** *Brain topography*, **26**(3):378–396, 2013. 167
- [258] ANTHONY H LEQUERICA, CATHY S DONNELL, AND DENISE G TATE. **Patient engagement in rehabilitation therapy: Physical and occupational therapist impressions.** *Disability & Rehabilitation*, **31**(9):753–760, 2009. 168
- [259] ALBERT RIZZO AND GERARD KIM. **A SWOT analysis of the field of virtual reality rehabilitation and therapy.** *Presence*, **14**(2):119–146, 2005. 168
- [260] JAMES WILLIAM BURKE, MDJ MCNEILL, DARRYL K CHARLES, PHILIP J MORROW, JACQUI H CROSBIE, AND SUZANNE M MCDONOUGH. **Optimising engagement for stroke rehabilitation using serious games.** *The Visual Computer*, **25**(12):1085–1099, 2009. 168
- [261] OUTPATIENT SERVICE TRIALISTS. **% of Rehabilitation therapy services for stroke patients living at home: systematic review of randomised trials.** *The Lancet*, **363**(9406):352–356, 2004. 168
- [262] C. ANDERSON, S. RUBENACH, C. N. MHURCHU, M. CLARK, C. SPENCER, AND A. WINSOR. **Home or hospital for stroke rehabilitation? results of a randomized controlled trial : I: health outcomes at 6 months.** *Stroke*, **31**(5):1024–1031, May 2000. 168
- [263] O. LAMBERCY, L. DOVAT, R. GASSERT, E. BURDET, CHEE LEONG TEO, AND T. MILNER. **A Haptic Knob for Rehabilitation of Hand Function.** **15**(3):356–366, 2007. 168
- [264] O. LAMBERCY, L. DOVAT, V. JOHNSON, B. SALMAN, S. WONG, R. GASSERT, T. MILNER, T.C. LEONG, AND E. BURDET. **Development of a Robot-Assisted Rehabilitation Therapy to train Hand Function for Activities of Daily Living.** In *Rehabilitation Robotics, 2007. ICORR 2007. IEEE 10th International Conference on*, pages 678–682, 2007. 168
- [265] CHUANCHU WANG, KOK SOON PHUA, KAI KENG ANG, CUNTAI GUAN, HAIHONG ZHANG, BENG TI ANG, AND CHRISTOPHER WEE KEONG KUAH. **A feasibility study of non-invasive motor-imagery BCI-based robotic rehabilitation for Stroke patients.** *4th International IEEEEMBS Conference on Neural Engineering (2008)*, pages 271–274, 2009. 168
- [266] O. LAMBERCY, L. DOVAT, HONG YUN, SENG KWEE WEE, C. KUAH, K. CHUA, R. GASSERT, T. MILNER, CHEE LEONG TEO, AND E. BURDET. **Rehabilitation of grasping and forearm pronation/supination with the Haptic Knob.** In *Rehabilitation Robotics, 2009. ICORR 2009. IEEE International Conference on*, pages 22–27, 2009. 168
- [267] MINE SARAC, ELA KOYAS, AHMETCAN ERDOGAN, MUJDAT CETIN, AND VOLKAN PATOGLU. **Brain Computer Interface based robotic rehabilitation with online modification of task speed.** *IEEE Int Conf Rehabil Robot*, **2013**:6650423, Jun 2013. 168
- [268] LAURI CONNELLY, MARY ELLEN STOYKOV, YICHENG JIA, MARIA L. TORO, ROBERT V. KENYON, AND DEREK G. KAMPER. **Use of a pneumatic glove for hand rehabilitation following stroke.** *Conf Proc IEEE Eng Med Biol Soc*, **2009**:2434–2437, 2009. 169
- [269] LAURI CONNELLY, YICHENG JIA, MARIA L. TORO, MARY ELLEN STOYKOV, ROBERT V. KENYON, AND DEREK G. KAMPER. **A pneumatic glove and immersive virtual reality environment for hand rehabilitative training after stroke.** *IEEE Trans Neural Syst Rehabil Eng*, **18**(5):551–559, Oct 2010. 169
- [270] **g.tec CSP BCI Tutorial Web-page.** <http://www.gtec.at/Download/Tutorials/Common-Spatial-Patterns-CSP-BCI-with-g-USBamp-and-Simulink-Two-Classes>. 171
- [271] **g.tec g.BSAnalyze.** <http://www.gtec.at/Products/Software/g.BSAnalyze-Specs-Features>. 171
- [272] SIAMAC FAZLI, JAN MEHNERT, JENS STEINBRINK, GABRIEL CURIO, ARNO VILLRINGER, KLAUS-ROBERT MÜLLER, AND BENJAMIN BLANKERTZ. **% of Enhanced performance by a hybrid NIRS–EEG brain computer interface.** *Neuroimage*, **59**(1):519–529, 2012. 178

REFERENCES

- [273] GERT PFURTSCHELLER, BRENDAN Z. ALLISON, CLEMENS BRUNNER, GUNTHER BAUERNFEIND, TEODORO SOLIS-ESCALANTE, REINHOLD SCHERER, THORSTEN O. ZANDER, GERNOT MUELLER-PUTZ, CHRISTA NEUPER, AND NIELS BIRBAUMER. **The hybrid BCI.** *Front Neurosci*, **4**:30, 2010. 178
- [274] FRIEDHELM C HUMMEL AND LEONARDO G COHEN. **Non-invasive brain stimulation: a new strategy to improve neurorehabilitation after stroke?** *The Lancet Neurology*, **5**(8):708–712, 2006. 180
- [275] MITRA AMELI, CHRISTIAN GREFKES, FRIEDRIKE KEMPER, FLORIAN P. RIEGG, ANNE K. REHME, HANS KARBE, GEREON R. FINK, AND DENNIS A. NOWAK. **Differential effects of high-frequency repetitive transcranial magnetic stimulation over ipsilesional primary motor cortex in cortical and subcortical middle cerebral artery stroke.** *Ann Neurol*, **66**(3):298–309, Sep 2009. 180
- [276] CHARLOTTE J. STAGG AND MICHAEL A. NITSCHKE. **Physiological basis of transcranial direct current stimulation.** *Neuroscientist*, **17**(1):37–53, Feb 2011. 180
- [277] BERNHARD ELSNER, JOACHIM KUGLER, MARCUS POHL, AND JAN MEHRHOLZ. **Transcranial direct current stimulation (tDCS) for improving function and activities of daily living in patients after stroke.** *The Cochrane Library*, 2013. 180
- [278] FEI MENG, KAI-YU TONG, SUK-TAK CHAN, WAN-WA WONG, KAHIM LUI, KWOK-WING TANG, XIAORONG GAO, AND SHANGKAI GAO. **BCI-FES training system design and implementation for rehabilitation of stroke patients.** In *Neural Networks, 2008. IJCNN 2008. (IEEE World Congress on Computational Intelligence). IEEE International Joint Conference on*, pages 4103–4106. IEEE, 2008. 180
- [279] JANIS J DALY, ROGER CHENG, JEAN ROGERS, KRISANNE LITINAS, KENNETH HROVAT, AND MARK DOHRING. **Feasibility of a new application of noninvasive brain computer interface (BCI): a case study of training for recovery of volitional motor control after stroke.** *Journal of Neurologic Physical Therapy*, **33**(4):203–211, 2009. 180